THE APPLICATION OF THE SURFACE ENERGY BALANCE SYSTEM MODEL TO ESTIMATE EVAPOTRANSPIRATION IN SOUTH AFRICA

Lesley Anne Gibson

Thesis Presented for the Degree of

DOCTOR OF PHILOSOPHY

in the Department of Environmental and Geographical Science,

Faculty of Science

UNIVERSITY OF CAPE TOWN

May 2013

DECLARATION

I, the undersigned, hereby declare that the work contained in this thesis is my own original work and that this has not been previously in its entirety or in part submitted at any university for a degree.

.

---------- ----------

Signature Date

ABSTRACT

In a water scarce country like South Africa with a number of large consumers of water, it is important to estimate evapotranspiration (*ET*) with a high degree of accuracy. This is especially important in the semi-arid regions where there is an increasing demand for water and a scarce supply thereof. *ET* varies regionally and seasonally, so knowledge about *ET* is fundamental to save and secure water for different uses, and to guarantee that water is distributed to water consumers in a sustainable manner.

Models to estimate *ET* have been developed using a combination of meteorological and remote sensing data inputs. In this study, the pre-packaged Surface Energy Balance System (SEBS) model was used for the first time in the South African environment alongside MODerate Resolution Imaging Spectroradiometer (MODIS) satellite data and validated with eddy covariance data measured in a large apple orchard (11 ha), in the Piketberg area of the Western Cape. Due to the relative infancy of research in this field in South Africa, SEBS is an attractive model choice as it is available as open-source freeware.

The model was found to underestimate the sensible heat flux through setting it at the wet limit. Daily *ET* measured by the eddy covariance system represented 55 to 96% of the SEBS estimate, an overestimation of daily *ET*. The consistent underestimation of the sensible heat flux was ascribed to sensitivities to the land surface air temperature gradient, the choice of fractional vegetation cover formula as well as the height of the vegetation canopy (3.2 m) relative to weather station reference height (2 m). The methodology was adapted based on the above findings and was applied to a second study area (quaternary catchment P10A, near Grahamstown, Eastern Cape) where two different approaches for deriving surface roughness are applied. It was again demonstrated that the sensible heat flux is sensitive to surface roughness in combination with land surface air temperature gradient and again, the overestimation of daily *ET* persisted (actual *ET* being greater than reference *ET*). It was concluded that in complex environments, at coarse resolution, it is not possible to adequately describe the remote sensing derived input parameters at the correct level of accuracy and at the spatial resolution required for the accurate estimation of the sensible heat flux.

ACKNOWLEDGEMENTS

I could not completed this thesis without the support of many individuals and organisations. I would like to thank:

Water Research Commission for funding research projects over the years, particularly Dr Kevin Pietersen, Dr Shafick Adams and most recently Wandile Nomquphu.

The Agricultural Research Council, my employer for the majority of this research.

Eric and Michelle Starke and Wikus Nel at Mouton's Valley farm for allowing me to conduct research on their property and for supplying me with weather data.

The South African Weather Service and EnviroMon Weather Service for providing weather data.

Dr Anthony Palmer (ARC-API) and Prof Tally Palmer (Rhodes University), for their support and encouragement.

Colleagues at ARC-ISCW: Pieter Haasbroek, Dr Thomas Fyfield, Dawie van Zyl, Terry Newby and Dudley Rowswell

My colleagues at GEOSS for encouragement.

Lichun Wang of ITC in the Netherlands for help with SEBS in ILWIS.

Zahn Münch (University of Stellenbosch) for support and encouragement,

My supervisors Dr Frank Eckardt, UCT, Dr Caren Jarmain, UKZN and Prof Bob (Z) Su, ITC.

To my parents for raising me to value education, to have an enquiring mind and to not be afraid of a challenge.

And Michael, Angus and Nina.

TABLE OF CONTENTS

LIST OF FIGURES

LIST OF TABLES

APPENDIX 1

LIST OF SYMBOLS

α	Surface albedo	-
a_1	Constant lapse rate of moist air	0.0065 $K.m^{-1}$
B^{-1}	Inverse Stanton number	-
C_d	Drag coefficient of the foliage elements	-
C_p	Specific heat capacity of air at constant pressure	$J.g^{-1}.K^{-1}$
C_t^*	Heat transfer coefficient of the soil	-
d_0	Displacement height	m
E	Water vapour flux density	$J \cdot m^{-2} \cdot s^{-1}$
ε	Surface emissivity	-
e_a	Actual vapour pressure	$kg \cdot m^{-1} \cdot s^{-2}$
e_s	Saturated vapour pressure	$kg \cdot m^{-1} \cdot s^{-2}$
f_c	Fractional vegetation cover	-
f_s	Complement of fractional vegetation cover	-
g	Acceleration due to gravity	$m.s^{-2}$
G_0	Soil heat flux	$W.m^{-2}$
H	Sensible heat flux	$W.m^{-2}$
h_0	Height of the vegetation	m
H_{dry}	Sensible heat flux at the dry limit	$W.m^{-2}$
h_s	Roughness height of the soil	m
H_{wet}	Sensible heat flux at the wet limit	$W.m^{-2}$
k	von Karman's constant	-
$K\downarrow_{day}$	Daily incoming shortwave radiation	$W.m^{-2}$
L	Obukhov length	m
L_{day}	Daily longwave radiation	$W.m^{-2}$
N	Number of sides of the leaf to participate in heat exchange	-
n_{ec}	Within canopy wind speed profile extinction coefficient	-
p	Ambient pressure	kPa
P	Atmospheric pressure at elevation z	kPa
P_0	Atmospheric pressure at sea level	kPa
Pr	Prandtl number	-
P_v	Proportional vegetation cover	-
R	Specific gas constant	-
Re^*	Reynolds number	-

r_{ew}	External resistance at the wet limit	Ω
R_{lwd}	Downward longwave radiation	$W.m^{-2}$
R_n	Net radiation	$W.m^{-2}$
R_{swd}	Incident shortwave radiation	$W.m^{-2}$
T	Ambient temperature	K
T_0	Land surface temperature	K
T_a	Air temperature	K
T_{K0}	Reference temperature (K) at elevation z	K
u	Wind speed	$m.s^{-1}$
$u(h)$	Horizontal wind speed at the canopy top	$m.s^{-1}$
$u*$	Friction velocity	$m.s^{-1}$
V	Kinematic viscosity of the air	$m^2.s^{-1}$
Z	Height above the surface	m
z_0	Surface roughness	m
z_{0h}	Scalar height for heat transfer	-
z_{0m}	Roughness height for momentum transfer	m
Γ	Psychrometric constant	-
Γc	Soil heat flux ratios for full vegetation canopy	-
Γs	Soil heat flux ratios for bare soil	-
Δ	Rate of change of saturation vapour pressure with	$kPa\ °C^{-1}$
θ_0	Potential temperature at the surface	K
θ_a	Potential air temperature at height z	K
θ_v	Potential virtual temperature near the surface	K
Λ	Latent heat of vaporization	$W.m^{-2}$
Λ	Evaporative fraction	-
Λ_r	Relative evaporation	-
λE	Latent heat flux	$W.m^{-2}$
λE_{wet}	Latent heat flux at the wet limit	$W.m^{-2}$
P	Density of air	$kg.m^{-3}$
ρ_w	Density of water	$kg.m^{-3}$
Σ	Stephan–Boltzman constant	-
Ψ_h	Stability correction functions for sensible heat	
Ψ_m	Stability correction functions for momentum	
$\overline{R_n}$	Daily net radiation	$W.m^{-2}$

LIST OF ABBREVIATIONS

ARC	Agricultural Research Council
ARC-ISCW	Agricultural Research Council - Institute for Soil, Climate and Water
ASTER	Advanced Spaceborne Thermal Emission and Reflection Radiometer
AWS	Automatic weather stations
CSIR	Council for Scientific and Industrial Research
DEM	Digital elevation model
DOY	Day of year
EF	Evaporative fraction
EMR	Electromagnetic radiation
EOS	Earth Observing System
ET	Evapotranspiration
ILWIS	Integrated Land and Water Information System
LAI	Leaf area index
LST	Land surface temperature
METRIC	Mapping EvapoTranspiration with high Resolution and Internalised Calibration
MODIS	MODerate Resolution Imaging Spectroradiometer
MSG	Meteosat Second Generation
MST	MODIS Swath Tool
NDVI	Normalised Difference Vegetation Index
NPOESS	National Polar-orbiting Operational Environmental Satellite System
NPP	NPOESS Preparatory Project
PELCOM	Pan-European Land Use and Land Cover Monitoring
SAWS	South African Weather Service
SEBAL	Surface Energy Balance Algorithm over Land
SEBI	Surface Energy Balance Index
SEBS	Surface Energy Balance System
SEVIRI	Spinning Enhanced Visible and InfraRed Imager
SMAC	Simplified method for atmospheric correction
SNR	Signal-to-noise ratio
SRTM	Shuttle Radar Topography Mission
SWIR	Shortwave infrared
TOA	Top of atmosphere
UT	Universal Time
VITT	Vegetation Index/Temperature Trapezoid
WetSpass	Water and Energy Transfer between Soil, Plants and Atmosphere under quasi
WGS84	World Geodetic System 1984
WRC	Water Research Commission

1. INTRODUCTION

With an average rainfall of less than 500mm per annum and much of the land considered semi-arid, South Africa is a water stressed country. The country has various climatic zones from semi-desert to tropical and is prone to erratic, unpredictable extremes in the form of droughts and floods. The average potential evaporation is higher than the rainfall in all but a few isolated areas where rainfall exceeds 1400mm per year (Burger, 2003). This low precipitation / high evaporation rate results in low runoff with only 8.6% of the rainfall being available as surface water. Furthermore, owing to the uneven spatial distribution of rainfall across the country, the natural availability of water is also highly uneven with nearly two-thirds of the country receiving less than the national average.

South Africa has well-developed commercial agriculture with the agro-industrial sector comprising 15% of the country's gross domestic product (Burger, 2005). Subsistence farming is also practised resulting in a dual agricultural economy. Only about 13% of South Africa's land surface can be used for crop production with high-potential arable land comprising only 22% of the total arable land. For dryland agriculture to be successfully practised, 500mm of rainfall per annum is required (Turton *et al.*, in NASA, 2005) so one of the limiting factor in crop production is the availability of water. The consequence of this, coupled with the erratic nature of the country's rainfall, is that many farmers in South Africa rely on irrigation in order to be commercially successful. Irrigated agriculture is by far the biggest single user of run-off water in South Africa and contributes more than 30% of the gross value of the country's crop production with about 90% of the country's fruit, vegetables and grapes being produced under irrigation (Burger, 2011).

Given this water scarce scenario, it is important for managers to have accurate information of all aspects of water resource management including water use by crops and natural vegetation in a catchment. Evapotranspiration (ET[1]) is the sum of water lost to the atmosphere from the soil surface (including intercepted water) through evaporation and from plant tissues via transpiration and is a vital component of the water cycle, which includes precipitation, runoff, stream flow, soil water storage

[1] *ET* throughout this text refers to actual evapotranspiration unless specific reference is made to reference evapotranspiration in which case the abbreviation will be ET_0

and *ET* (Mu *et al.*, 2007). This combined process whereby water is lost from the soil surface by evaporation and from the plant by transpiration occurs simultaneously and it is difficult to distinguish between the two processes. With the exclusion of water availability, evaporation is mainly a function of the fraction of solar radiation reaching the soil surface and this is largely determined by plant canopy (Allen *et al*., 1998). Water loss during transpiration through the stomata on the leaf is dependent on the genetics and stage in growth of the plant as well as external factors such as radiation, air temperature and humidity, and wind.

The dependency of the physical process of evaporation, whereby a liquid (water) is transformed to a gas (water vapour), on water availability and incoming solar radiation, reflects the interactions between surface water processes and climate (Sobrino *et al*., 2007). In meteorology, evaporation is usually restricted to the change of a liquid to gas without a change in temperature. Sensible heat is that part of the energy flux from a surface which produces a temperature change and this must be distinguished from latent energy which is used to describe the evaporation process. Evaporation is a cooling process since there is a removal of energy when water evaporates from a surface. Part of this energy remains latent in the atmosphere and is released when water vapour condenses. Water vapour is therefore an energy carrier and energy must be available to allow the water to evaporate (Savage *et al.*, 2004).

Accurate knowledge of temporal and spatial variations in precipitation and *ET* is critical for improved understanding of the interactions between land surfaces and the atmosphere (Mu *et al*., 2007), and owing to increasing human consumption, climate impacts and decreasing availability, methods for monitoring the water balance at both fine and regional scales are important in order to preserve and manage water resources (Melesse *et al*., 2006). However, precipitation and *ET* are the most problematic components of the water cycle to estimate accurately because of the heterogeneity of the landscape and the large number of controlling factors involved, including climate, plant biophysics, soil properties, and topography (Mu *et al*., 2007).

The accurate estimation of *ET* remains a challenge to researchers in the field of micrometeorology and hydrology as well as for water resources managers and planners (Jarmain *et al*., 2009). *ET* can be measured or estimated using empirical formulae from taking measurements in the field or more indirectly rather than as a result of a specific evapotranspiration experiment. The field based

measurements are generally point based and therefore not practical over a large area. Internationally it is now recognised that remote sensing based models hold great potential for the spatial estimation of *ET* at both field and catchment scale and earth observation data can be used in *ET* estimation methods to extend point measurement of *ET* to much larger areas, even areas where measured meteorological data may be sparse (Jarmain *et al.,* 2009).

One method used to estimate *ET* is as residual in the surface energy balance. The net incoming solar radiation at any location is converted into heat energy, heating the air above the soil surface, the plant canopy and the soil itself, and into latent heat of evapotranspiration from the soil surface and plant canopy. If the net incoming radiation and the energy consumed in heating the air and the soil can be measured, then the latent heat of evaporation from the soil can be estimated and the rate of evaporation of water deduced (Blight, 2002). These exchanges of energy or heat are called fluxes. The estimation of these fluxes at the land surface has long been recognized as the most important process in the determination of the exchanges of energy and mass among hydrosphere, atmosphere and biosphere (Su, 2002).

The sources of energy in the soil-plant-atmosphere system include:

- Solar energy during the day and terrestrial radiant energy at night;
- Heat energy carried into the area by wind (advected energy);
- Heat energy stored by vegetation and in land masses;
- Heat energy stored in water bodies.

The most important of these energy sources is usually solar energy which is why the energy balance used in this research is referred to as the simplified energy balance i.e. advected energy is excluded but advected energy may on occasion be considerable. However, due to its complex nature, advected energy is not routinely accounted for when using methods to estimate surface sensible heat and latent energy flux densities (Savage *et al.*, 2004).

In the energy balance approach, the simplified energy balance equation is used to calculate *ET* (FIGURE 1).

$$\lambda E = R_n - G_0 - H \qquad [1]$$

where λE is the turbulent latent heat flux (λ is the latent heat of vaporization and E is water vapour flux density), R_n is net radiation, G_0 is the soil heat flux and H is the sensible heat flux (Su, 2002).

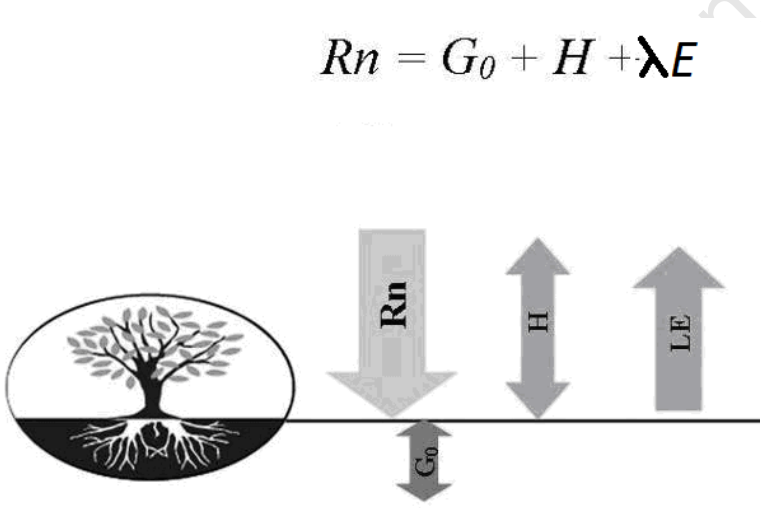

Figure 1: A graphical representation of the simplified surface energy balance, simplified from Su (2006).

In contrast to the traditional methods of estimating *ET*, such as Bowen ratio, and eddy covariance which are costly, time consuming, and require elaborate and sensitive measurement equipment, remote sensing based energy balance models have the capacity to estimate *ET* across larger areas, different land covers and across catchment boundaries. However limitations of individual models should be acknowledged. Since satellite imagery provides spatially explicit as well as multi-temporal information on reflected or emitted electromagnetic radiation (EMR) from the earth's surface (Verstraeten *et al.*, 2008), techniques to assess area *ET* using earth observation have been developed for large areas and at varying spatial scales. Data in multiple EMR wavebands allow for the extraction of land cover, vegetation cover, emissivity, albedo, surface temperature and energy flux information, and data at

regional scales allow for greater spatial coverage than is possible with *in situ* methods (Melesse *et al*., 2006). However, multiple datasets such as the abovementioned albedo, emissivity etc. must be available or able to be generated, at appropriate spatial and temporal scales, in order to run a model based on this approach.

Recent developments in remote sensing technologies have led to the possibility of obtaining land surface information at spatial resolutions from 0.5m – 5km, with frequent revisit times (up to every 15 minutes). The degree of success and accuracy of that information varies; however some authors (Bastiaanssen *et al*., 2006; Bastiaanssen & Bos, 1999) report that remote sensing has many advantages such as the objectivity and repeatability of the measurements, the synoptic nature of data, and spatial representivity of the data. With these recent advances in remote sensing have come many different approaches and techniques for estimating evaporation using earth observation data. Some of these approaches will be discussed in Chapter 2 in the literature review.

1.1. BACKGROUND TO RESEARCH

Accurate estimates of temporal and spatial variations in precipitation and evapotranspiration (*ET*) are critical for improved understanding of the interactions between land surfaces and the atmosphere (Mu *et al*., 2007). Methods for monitoring the water balance at both local and regional scales are required to preserve and manage water resources (Melesse *et al*., 2006). In a water scarce country like South Africa with a number of large consumers of water, it is important to estimate *ET* with a high degree of accuracy. This is especially important in the semi-arid regions where there is an increasing demand for water and a scarce supply thereof. *ET* varies regionally and seasonally, so knowledge of *ET* is fundamental to save and secure water for different uses, and to guarantee that water is distributed to water consumers in a sustainable manner.

The South African National Water Act of 1998, undertaking "some for all for always" and legislating that ecological reserves be calculated before new water licences be granted for other uses, is aimed at allowing for equitable distribution of water resources, including an allocation to the environment. In order to manage this allocation process, managers and decision makers require information. Remote

sensing technology holds great promise in this regard (Jha & Chowdary, 2006) as it can cost-effectively provide frequent data on a relatively large scale that allow specific water resource situations to be monitored on a long-term basis.

In the South African context, in irrigated areas, actual *ET* can be equated to the water usage of a crop. By using remote sensing techniques to estimate *ET*, it is possible to acquire spatial estimates of actual water use across large areas. In terms of the National Water Act this information can be used in the validation and verification of existing lawful water use and can aid in the issuing of new licences, since the water use at catchment scale may be estimated. Further to this, farmers may use this water use information to analyse the water use between crops and even within fields to identify areas of high water consumption and to better manage their water usage and irrigation efficiency.

The water use between biomes and different natural vegetation types can be assessed using spatial estimates of *ET*. Catchment managers may find it useful to understand water use variation of natural vegetation within a catchment and between, for example, indigenous vegetation and invasive alien plant species (IAPs). This can guide planning for the removal of IAPs in terms of determining priority areas and time frames.

Spatial estimates of *ET* may be used to complement the results of, or be used as input into, hydrological models to help better understand the hydrological or geohydrological regime in an area (Münch *et al*, 2013). Finally the change in *ET* over time can be used to assess the change in water availability in a region. This information may be useful in climate change studies and help analyse drought length and intensity.

Given that, in South Africa, research into remote sensing *ET* estimation is in its infancy, together with the legislative framework (National Water Act of 1998), it is logical that preliminary research efforts should focus on the evaluation of existing models rather than the development of new models. Should an existing model be found to yield accurate estimates of *ET*, the assimilation of these estimates into existing monitoring programmes such as the drought monitoring programme (http://www.amesd.org/sadc.html) will have been expedited.

This research arose from a Water Research Commission (WRC) funded project (Gibson *et al.,* 2009) where earth observation data were used to determine various water fluxes. The Surface Energy Balance System (SEBS) model was used to calculate annual *ET* with MODerate Resolution Imaging Spectroradiometer (MODIS) satellite data for a quaternary catchment in the Piketberg area (Western Cape). Through a simplified water balance (with annual *ET* as one of the input) the legal compliance of water users to water use legislation was assessed. The results of the study were inconclusive as the estimated annual catchment *ET* significantly exceeded the estimated annual catchment rainfall. Gibson *et al.* (2009) proposed that the inaccuracies in the water use results were due to many uncertainties and limitations with both the input data and the methodology associated with the estimation of all water fluxes. However the largest uncertainty was attached to the *ET* estimate.

The lack of confidence in the annual *ET* estimate by Gibson *et al.* (2009) was due to the estimated catchment *ET* from the SEBS model for the study period (a hydrological year) being nearly twice the estimated rainfall for the same catchment for the same period. This assumed overestimation of SEBS estimated *ET* was further highlighted when the results of an alternative model (Batelaan & De Smedt, 2001), Water and Energy Transfer between Soil, Plants and Atmosphere under quasi Steady State (WetSpass), were analyzed. In the SEBS model, the amount of *ET* is constrained by the available energy with available moisture being inferred from parameters such as vegetation cover and the differences between the land surface and air temperature. The *ET* estimated by the WetSpass model is constrained by the amount of precipitation which fell in the catchment and since it is based on a water balance, the amount of *ET* may not exceed the amount of precipitation. Interestingly, the results of both methods across a hydrological year in the Gibson *et al.* (2009) study reflected the constraining factor of their approaches respectively. Using the WetSpass model resulted in higher estimated *ET* in the winter months where there was high water availability and using the SEBS model resulted in higher *ET* in the summer months when there is high energy availability. Although it may be possible for annual *ET* to exceed annual precipitation in certain instances, such as where large-scale irrigation from upstream or groundwater resources is practised, it is believed that *ET* was overestimated as evidence pointed towards there being limited water availability during the hot, dry summer months. Since irrigated agriculture formed a small portion of the catchment (2.4%) in comparison to natural vegetation (29.7%) and dryland agricultural (66.5%), the higher *ET* than precipitation at catchment scale could not be ascribed to evaporative losses due to irrigation.

Arising from Gibson *et al*. (2009) was the need to fully validate and analyse the *ET* results from the SEBS model within a South African environment. Due to the complexity of the model, there are therefore many opportunities for errors and uncertainties to be introduced. This needs to be analysed, tested and documented in the South African environment. This research seeks to address this need. Should it be possible to accurately model spatial estimates of *ET* across large areas using free software and data, then the operational monitoring of water use for many aspect of water resource management will be feasible.

Since the field validation funding was tied to the WRC research project by Gibson *et al*. (2009), the field validation had to take place within the study area and more specifically the pilot study area selected by Gibson *et al*. (2009). Furthermore, since the research has been partially funded by the Agricultural Research Council, the validation site was required to have an agricultural land use. A large apple orchard (11 ha) on the farm Mouton's Valley, within the pilot study area of Gibson *et al*. (2009), was chosen as the site for the field validation. This site was selected due to size of the orchard and the location of an automatic weather station situated just outside the orchard.

The most valuable lesson learnt has been around the complexity of the *ET* estimation using the SEBS model. The SEBS model is available as open-source freeware and it can be used by practitioners with remote sensing knowledge who may not necessarily have the micrometeorological expertise to develop a model themselves. However, the derivation of *ET* using the SEBS model is a complex process requiring several sources of input data and numerous processing steps to derive intermediate output products. The intermediate products are then combined through additional processing algorithms to derive the final daily *ET* product. Whilst the open-source format of SEBS is very useful and can speed up the research process, there are some instances where specialist knowledge is required to implement the model correctly to derive the most accurate results. Finally, the SEBS model was initially developed for agricultural applications and although it has been applied across many land covers (as will be shown in Chapter 2.2), it may be that less accurate results are produced in areas of natural veld or dryland agriculture.

1.2. AIMS

The broad aim of this research is to implement the pre-packaged SEBS model in ILWIS in the South African environment with MODIS TERRA and AQUA data. As a pre-packaged software is accessible to remote sensing practitioners who may not have specific energy balance expertize, it is important for the pre-packaged version of SEBS to be tested before large scale roll-out (for operational, research or monitoring purposes) is implemented. Therefore the aim is to compare, analyse and validate the results with field measured eddy covariance data, elucidate model sensitivities and make recommendations on the future use of the pre-packaged SEBS model.

The specific objectives of this research are to:

1. Apply the pre-packaged SEBS model in ILWIS to the field validation site.
2. Compare and analyse results obtained from daily MODIS TERRA (MOD 02) and MODIS AQUA (MYD 02) data for:
    a. the calculated remotely sensed parameters (albedo, vegetation parameters, emissivity and land surface temperature) which are required as input into the SEBS model;
    b. the energy balance and *ET* calculations using the pre-package SEBS model in ILWIS;
3. Validate the energy balance and evapotranspiration results with field measured data;
4. Analyse and explain the results and identify potential sources of error or model sensitivities.

The above objectives are met through the course of this research. Conclusions and recommendations regarding the future use of the pre-packaged SEBS model in South Africa are made.

1.3. THESIS STRUCTURE

The structure of the thesis is built around fulfilling the objectives of the research. Firstly, a literature review to set the scene and explain key concepts is set out in Chapter 2. Particular reference is made to the current status of remote sensing *ET* estimation in South Africa (Chapter 2.1), SEBS references in the literature (Chapter 2.2) and the formulation from literature of the SEBS model (Chapter 2.3).

Chapter 3 describes the validation site and methodology - conducted by the CSIR (Jarmain & Mengistu, 2011)- used to validate the results of this research.

In fulfillment of Objective 1, Chapter 4 provides a detailed method and the materials used focussing on the remote sensing aspects, (Chapter 4.1), the meteorological requirements (Chapter 4.2) and finally the SEBS calculations (Chapter 4.3).

In Chapter 5, the first results of the research are presented. Chapter 5.1 presents the results of required meteorological calculations, Chapter 5.2 fulfils Objective 2a by presenting the results of the remote sensing input parameters such as albedo, vegetation inputs and land surface temperature. Objective 2b and Objective 3 are met in the energy balance and *ET* results presented in Chapter 5.3.

Objective 4 is met in Chapters 6 -8 where the sensitivity of the SEBS model to various input parameters is explored. Chapter 6 primarily consists of a paper (published in Hydrological and Earth Systems Sciences) where model uncertainties and sensitivities are explored. This paper has been edited in this thesis to improve it. Chapter 7 accounts for model sensitivities by describing adaptions to the methodology and the results when the SEBS model was applied to a different catchment in the Eastern Cape. The study area for Chapter 7 is different to the rest of the thesis as it was important to test the SEBS model under different environmental conditions in light of the model uncertainties and sensitivities which are uncovered.

To bring the research to a close, the factors which may affect the accuracy of the results are taken into account and the original research methodology is adapted and applied back to the field validation site at Mouton's Valley. The results of the adapted methodology are presented in Chapter 8 where it is shown that despite the changes in the methodology, the estimated *ET* remains higher than the field validation measurements.

The thesis is concluded in Chapter 9 with a summary of research finding (Chapter 9.1), conclusions (Chapter 9.2) and recommendations for the use of SEBS and *ET* estimation in South Africa (Chapter 9.3).

2. LITERATURE REVIEW

For the past few years, there has been interest in the scientific community in estimating *ET* by remote sensing, since it is a unique way to retrieve *ET* at several temporal and spatial scales (Sobrino *et al.*, 2007). There have been many techniques published but this review will focus on the techniques used in this research, that is, the energy balance approach and specifically the Surface Energy Balance System. However reference is made to various review papers (Courault *et al*., 2005; Overgaard *et al*., 2006; Gowda *et al*., 2007; Kalma *et al*., 2008; Verstraeten *et al*., 2008; Petropoulos *et al*. 2009) where the status of earth observation *ET* models and broad descriptions of the various techniques are given.

Courault *et al*. (2005) provide an overview of work done in the international community over the last 25 years related to evapotranspiration estimation from earth observation data; Overgaard *et al*. (2006) review the different types of energy-based land-surface models and the potential of linking these to distributed hydrological models; Kalma *et al*. (2008) focus on the use of remotely sensed surface temperatures in *ET* estimation; Petropoulos *et al.* (2009) examine surface temperature/ vegetation indices methods in retrieving land surface energy fluxes; and Verstraeten *et al.* (2008) assess evaporation methods across different scales of observation, from leaf scale (e.g. porometry) or point scale (e.g. lysimetry), to field scale (e.g. eddy covariance and scintillometry), landscape/ catchment scale (e.g. mass water balance and energy balance) and finally continental scale where only the earth observation energy / mass water balance is possible.

ET estimation methods based on earth observation techniques can be classified according to the concept on which they are based. Verstraeten *et al*. (2008) identify four concepts and classify the various models (Table 1) according to these concepts which are identified as:

(i) the parameterization of the surface energy balance;

(ii) the Penman-Monteith equation;

(iii) the water balance approach, or;

(iv) relationships between vegetation indices and land surface temperature assessed with earth observation data.

Table 1: A list of selected *ET* assessment methods based on earth observation techniques simplified from Verstraeten *et al*. (2008).

Concept	Method	Parameters		Selected references
		EO	Other	
Parameterisation of the energy balance	SEBAL (Surface Energy Balance Algorithm for Land)	T_0, α, *NDVI*	T_a, *u*, ε, *RH*, z_0	Bastiaanssen *et al*, (1998), Bandara (2006), Timmermans *et al*. (2007)
	SEBS (Surface Energy Balance System)	T_0, α, *NDVI*	T_a, *u*, ε, *LAI*, e_a & e_{sat}, z_0	Su (2002), Jia *et al* (2003)
	S-SEBI (Simplified- Surface Energy Balance Index) iNOAA (ET of European forests from NOAA-imagery)	T_0, α, *NDVI*	T_a, ε, *(RH)*	Roerink *et al*. (2000)
Penman-Monteith (PM) based	Trapezoidal Shape (Relationship between land surface temperature and vegetation indices used to estimate ET)	T_0, *SAVI*	Ta, ε, vpd, *LAI*	Moran *et al*. (1994), Moran *et al*. (1997)
	Wang (Combination of day and night land surface temperatures with *NDVI*)	T_0, α, *VI*	Meteorological data	Wang *et al*. (2006)
	Cleugh (remote sensing inputs into PM equation)	α, *VI*	Meteorological data	Cleugh *et al*. (2007)
Water balance based	SWAP (Soil, water, atmosphere, plant)	α, *VI*	Meteorological, soil, groundwater table data	Santhi *et al*. (2005), Kaur *et al*. (2003)
VI/LST based	Jackson (Relationship between VI and Land surface temperature)	T_0, *VI*	T_a, *u*, calibration coeff.	Jackson *et al* (1977) (In Verstraeten *et al*. (2008)

According to Verstraeten *et al*. (2008), with the exception of the parameterization of the surface energy balance which is based entirely on earth observation derived parameters and meteorological data, other approaches are based on a combination of the water balance approach, remotely sensed surface temperature and vegetation indices. In Table 1, the classification method of Verstraeten *et al*. (2008) is used to identify remote sensing *ET* techniques and the data input requirements of each method.

In terms of the accuracies of the methods, Verstraeten *et al*. (2008) state that factors (e.g. data requirements, complexity of data assimilation, temporal and spatial scale effects) other than the *ET* estimates must be considered before drawing conclusions since these factors may affect the accuracy assessments.

In Su (2006), it is stated that from a remote sensing perspective, there are two principles which need to be considered when attempting to calculate *ET*: the conservation of energy, and the effect of turbulent transport. The conservation of energy states that *ET* is a change in state of water by demanding a supply of energy for vaporisation and if all sources and sinks for energy can be determined, *ET* will remain the only unknown. The effect of turbulent transport acknowledges the role of the wind in transporting vapour away from an evaporating surface (Su, 2006). This is the basis of the energy balance approach in the estimation of evaporation using earth observation data.

Different methods have been developed recently to derive surface fluxes from remote sensing observations in order to estimate *ET*. Remote sensing energy balance methods use empirical relationships and physical modules from remotely sensed and meteorological data. The Surface Energy Balance Index (SEBI) model (Menenti & Choudhury, 1993) was the foundation for the remote sensing based surface energy balance approach (Badola, 2009). Models such as Surface Energy Balance Algorithm over Land (SEBAL) (Bastiaanssen *et al.*, 1998) and SEBS (Su, 2002) use earth observation data directly to estimate input parameters and *ET*. Badola (2009) points out that each algorithm developed for energy balance closure over land has its own advantages and disadvantages. The SEBAL model, which is probably the widely published remote sensing *ET* model uses surface temperature, surface reflectance and Normalised Difference Vegetation Index (*NDVI)* together with their interrelationships to deduce surface fluxes (Bastiaanssen *et al.*, 1998). Threshold values are extracted from wet and dry surfaces on the studied area. The sensible heat flux is computed by inverting the sensible heat flux expression over both dry ($\lambda E = 0$) and wet ($H = 0$) land with latent heat flux being

computed as the residual of the energy balance. The major advantage of SEBAL is that it demands few input variables but it can only be applied to areas which have both wet and dry land pixels available (Bastiaansen *et al.*, 1998). SEBAL is protected by intellectual property and may not be used without the developer's permission, however the original algorithms were presented in the formulation publication (Bastiaansen *et al*., 1998) so it is possible to reconstruct the original model. However subsequent improvements to the model remain largely unpublished.

In contrast to SEBAL, SEBS is available as part of the free open-source software ILWIS. SEBS is scale independent in that the wet and dry limits are not set by the range of conditions present across a scene. SEBS was proposed by Su (2002) for the estimation of atmospheric turbulent fluxes and evaporative fraction[2] using satellite earth observation data, in combination with meteorological information. Reflectance and radiance measured by the satellite are used to calculate land surface parameters - albedo, emissivity, surface temperature, fractional vegetation cover and leaf area index (*LAI*). Other inputs are temperature, air pressure, humidity and wind speed at reference height which are obtained from a weather station. The third input is the radiation component which can be measured directly or can be modelled. The instantaneous values are used to calculate the daily value because evaporative fraction tends to be constant during daytime hours, although the H and λE fluxes vary considerably (Ahmad *et al.*, 2005).

Although there are many potential advantages to using remote sensing techniques to estimate ET, there are some limitations. The shortcomings of using remote sensing based *ET* models are succinctly presented by Jarmain *et al.* (2009) as being the limited availability of high resolution thermal infrared imagery which is essential when using an energy balance approach, the scattering and absorption of radiation by clouds, and insufficient attention given to the spatial interpolation of weather station data across a larger area. The limited availability of high spatial and temporal resolution thermal infrared imagery persists (Table 1). Further, the temporal and spatial scales, in combination, of earth observation data from the existing set of earth observing satellite platforms are not sufficiently high for use in the estimation of spatially distributed *ET* for on-farm irrigation management purposes (Gowda *et al.*, 2008).

[2] The evaporative fraction is the proportion of energy available to evaporate water. It is considered an instantaneous estimation. Evaporative fraction is estimated as a function of the other components of the simplified energy balance and the equation used to calculate this is given in Equation 17

Table 2: Spatial, spectral and temporal characteristics of satellite sensors

SENSOR	SPATIAL & SPECTRAL CHARACTERISTICS			TEMPORAL RESOLUTION
	V & NIR	SWIR	TIR	
Landsat TM	4 bands, 30 m	2 bands, 30 m	1 band, 120 m	16 days
[3]Landsat ETM+	4 bands, 30 m	2 bands, 30m	1 band, 60 m	16 days
SPOT V	4 bands, 30 m	-	-	2 – 3 days
MODIS	2 bands at 250 m, 14 bands at 500 m	3 bands at 500 m, 10 band at 1 000 m	6 bands at 1 000 m	Daily
ASTER	3 bands, 15 m	[4]5 bands, 30 m	5 bands, 90m	[5]Variable

Lower resolution imagery such as MODIS with a nominal 1km resolution is often too coarse for many applications although the high temporal (daily) resolution is advantageous. Conversely, high spatial resolution imagery such as Landsat or ASTER does not provide adequate temporal resolution for certain applications such as irrigation scheduling where daily data is desirable. These resolution issues will be further magnified if the thermal sensors on future Landsat satellites are abandoned (Gowda *et al.*, 2007). Thermal infrared images from the current Landsat suite are no longer viable due to the scan-line correction problem experienced by Landsat ETM+ (Jarmain *et al.*, 2009) and the current limited image acquisition of Landsat TM contribute to difficulties in conducting contemporary studies with this dataset, however this remains an option for historic studies.

Kalma *et al.* (2008) report that errors associated with using surface temperatures to estimate sensible heat flux are significant due to 1) significant inaccuracies in radiometric temperature estimation and the inequality between radiometric and aerodynamic surface temperature, 2) the temporal and spatial

[3] On May 31, 2003, the Scan Line Corrector (SLC), which compensates for the forward motion of Landsat 7, failed. Subsequent efforts to recover the SLC were not successful, and the failure appears to be permanent. Without an operating SLC, the Enhanced Thematic Mapper Plus (ETM+) line of sight now traces a zig-zag pattern along the satellite ground track. As a result, imaged area is duplicated, with width that increases toward the scene (USGS, 2007).

[4] ASTER shortwave infrared data acquired since April 2008 are not useable, and show saturation of values and severe striping (JPL, 2009)

[5] ASTER is not routinely acquired in the same way as other imagery. However, data acquisition requests can be submitted and if successful, images will be supplied. Each day the ASTER Ground Data System (GDS) in Japan analyzes the database of requests for ASTER data acquisitions and develops a schedule for 27 hours of observations (NASA, 2007).

variability in the difference between land surface and air temperature, 3) errors in estimating the available energy, 4) errors in ground based meteorological data and finally 5) errors in model assumptions.

Data continuity is an important consideration when contemplating studies where long data records are required. Landsat with a 30 year history is a particularly valuable image source. The Landsat Data Continuity Mission was launched in late 2012 (http://landsat.usgs.gov/about_project_descriptions.php) and this will allow for the continued collection of data at high (30 m) resolution and will include two thermal infrared bands (http://landsat.usgs.gov/LDCM_DataProduct.php). The MODIS TERRA sensor has been operating for over a decade and data continuity for MODIS data is also a concern. However the National Polar-orbiting Operational Environmental Satellite System (NPOESS) is the next generation of low earth orbiting environmental satellites (http://www.ipo.noaa.gov/index.php) due to be launched in 2013 which should provide continuous MODIS equivalent data. Furthermore the NPOESS Preparatory Project (NPP), was due to be launched[6] in October 2011 in order to extend the TERRA and AQUA measurement series by providing a bridge between NASA's EOS missions and NPOESS.

The irregular, non-systematic capture of ASTER imagery makes on-going *ET* estimates with this image source highly problematic and historic studies are unlikely to be possible due to large temporal gaps in image acquisitions over most areas, as was reported by Gibson *et al*. (2009). Furthermore, the problems experienced by ASTER with saturated values in the shortwave infrared wavelengths (http://asterweb.jpl.nasa.gov/swir-alert.asp) add to these challenges when using this particular image source.

When remote sensing based estimates are compared with ground based measurements of *ET*, from approximately 30 validation studies, Kalma *et al.* (2008) note that the more complex physical and analytical methods are not necessarily more accurate than statistical or empirical methods. However the availability of training data for some of the empirical methods may be a limitation. However it was observed that ground based measurements of *ET* have reported uncertainties of 10–15% whereas the

[6] The Obama Administration has since terminated the NPOESS program. A new Joint Polar Satellite System (JPSS), jointly developed by NASA and NOAA has become the new focus of climate-related remote-sensing observations (http://www.climatesciencewatch.org/2012/07/10/jpss-satellite-delays-risk-loss-of-global-climate-data-continuity/).

uncertainties associated with various earth observation techniques are 15–30% (Kalma *et al*., 2008). However if the available energy (R_n - G_0) is taken from ground based observations, the earth observation techniques improve in accuracy with a decrease in the relative error from 30% down to 17% (Kalma *et al*., 2008).

Land surface temperature is a key parameter in energy budget models, *ET* models, estimating soil moisture, forest detection and forecasting, monitoring the state of the crops, studying land and sea breezes and nocturnal cooling (Batatia & Bessaih, 2009). It has been reported in the literature that *ET* estimation has been achieved using high spatial but low temporal resolution satellite data such as that obtained from the Landsat and ASTER sensors. These sensors provide data relevant for field scale estimation of *ET* (Kustas *et al*., 2004) however the temporal resolution of this data does not allow for operational *ET* estimation. Contrary to this, *ET* can be routinely estimated using coarse resolution satellite data such as that from the MODIS and AVHRR sensors. However due to the resolution of especially the thermal bands, the spatial scale at which these estimations can occur are not always useful (Table 2). Referring to MODIS data specifically, the resolution in the reflective bands ranges from 250 – 500m with it being possible to calculate *NDVI* at 250m resolution. If the higher resolution of the reflective bands could be used to downscale the radiometric surface temperature (derived from the thermal infrared bands), then it may be possible for routine *ET* estimates to be carried out daily to every second day at a spatial scale that is useful for assessing water use at catchment scale. The functional relationship between the radiometric surface temperature (*TR*) and vegetation indices (generally available at higher spatial resolutions than thermal band data) is reported in the literature (Agam *et al*., 2007) where empirically derived *NDVI-TR* relationships are used to disaggregate *TR* to the vegetation index resolution. Successful application of such a technique allows for high temporal and spatial resolution *ET* estimates from satellite.

Before highlighting remote sensing *ET* research in South Africa, it is of interest to briefly focus on the current state of research in Australia. Like South Africa, Australia has a higher potential evaporation than precipitation in most areas (Glenn *et al.*, 2011) and the two countries face similar challenges on competing uses of water (Adreen, 2011). Furthermore, remote sensing technologies are particularly suited to both the South African and the Australian landscape due to the vast scale, diverse landscapes and the favourable climate (with the absence of cloud a necessity for optical remote sensing applications). In addition, water legislation in South Africa and Australia is similar in that both the South African National Water Act (1998) and Australia's Commonwealth Water Act (2007) attempt to balance

human and environmental demands for water (Adreen, 2011). Finally, given the advancement of remote sensing *ET* research in Australia, it would be prudent to briefly take cognisance of what is taking place in the Australian research arena.

A review paper by Glenn *et al*. (2011) on the status of Australian ground based and remote sensing estimates of *ET* describes advances in the Australian research scene. According to Glenn *et al.* (2011) reflective-band remote sensing and ground data have been combined to project *ET* at the regional and continental scales in Australia for nearly 20 years. The early studies were based on vegetation indices obtained from satellite imagery which were then combined with meteorological data and biogeochemical modelling to arrive at *ET*. The availability of MODIS data in 1999 and 2002 with the successful launch of the TERRA and AQUA satellites respectively meant that remote sensing applications for *ET* began to take a new direction.

The 2007 legislation resulted in the Bureau of Meteorology being delegated the mandate to develop a range of up-to-date water information services. This legislation appears to have created momentum for the development of remote sensing *ET* methods in Australia with Cleugh *et al*. (2007) developing a vegetation index model for predicting *ET* using MODIS remote sensing data and ground meteorological (through the Penman-Monteith) data (Glenn *et al*., 2011). Cleugh *et al*. (2007) report that an aerodynamic resistance-surface energy balance approach failed because small errors in the surface temperature resulted in large errors in the sensible heat flux. Glenn *et al*. (2011) describe the alternative approach taken by Cleugh *et al*. (2007) as setting a fixed daily value for leaf-level stomatal conductance, derived from tower data, and, if leaf-level stomatal conductance is known, *ET* can be calculated from a combination of *LAI* (derived from MODIS) and potential evapotranspiration equation from meteorological data. Similar approaches - in that they use potential evapotranspiration derived from meteorological data combined with a satellite derived vegetation index of some description - have been proposed by Leuning *et al*. (2008), Zhang *et al*. (2008) and Guerschman *et al*. (2009). Mu *et al*. (2011) have improved on the Cleugh *et al*. (2007) model.

2.1. EARTH OBSERVATION ET STUDIES IN SOUTH AFRICA

Reviews in the South African literature on remote sensing *ET* techniques have been carried out by Gibson *et al*. (2009) and Jarmain *et al*. (2009). Jarmain *et al*. (2009) present the algorithms for four remote sensing *ET* models: Surface Energy Balance Algorithm for Land (SEBAL) model (Bastiaanssen *et al*., 1998), Surface Energy Balance System (SEBS) model (Su, 2002), Mapping EvapoTranspiration with high Resolution and Internalised Calibration ($METRIC_{tm}$) model (Allen *et al.,* 2007) and Vegetation Index/Temperature Trapezoid (VITT) model based on Moran *et al.* (1994). Furthermore, a number of studies have been conducted in South Africa where *ET* has been estimated from earth observation data.

The differing spatial scales at which remote sensing estimation of *ET* has been carried out in South Africa from field scale through to catchment and regional scale are categorized (Table 3). Further to the review by Jarmain *et al*. (2009), field-scale studies assessing the application of remote sensing data to water use efficiency have been carried out using the SEBAL model with high resolution (predominantly Landsat) imagery (Klaasse *et al*., 2008; Klaasse *et al*., 2011; Jarmain *et al*., 2011a; Jarmain *et al*., 2011b; Hellegers *et al*., 2011; Jarmain and Klaasse, 2012; WE Consult, 2011). A benefit of conducting field-scale studies is that in situ validation, although expensive, is achievable and was indeed achieved for a number of the aforementioned projects.

Various remote sensing data applications at catchment scale (Table 3) have been investigated for catchment hydrology (Kongo & Jewitt, 2006), water use estimation (Gibson *et al*., 2009; Hellegers *et al*., 2011) and most recently operational water planning and allocation purposes (WE Consult, 2012). Kongo & Jewitt (2006) investigate the use of remote sensing data to estimate *ET* in South Africa at catchment level, investigating a catchment's response to rainwater harvesting. Proper validation was lacking but on comparing *ET* for a pixel with *ET* calculated from the pixel containing the weather station, it was found that for that day, SEBAL overestimated *ET* by 1.3mm.

Table 3: Summary of studies conducted in South Africa. Different methods for estimating *ET* were assessed and their usefulness in various water resources applications and across various spatial and temporal scales were assessed in historical and operational mode.

Type	Study focus	Parameters	Temporal scale	Spatial scale / resolution	Reference
Review	Methodology	ET, Energy balance	Instantaneous, day, week, month	Field / 30 m	Jarmain *et al.* (2009)
Historic	Catchment Water use	ET, Rain, Runoff, Groundwater recharge	Day, month, year for 1 year	Catchment / 1 km	Gibson *et al.* (2009)
Historic	Catchment Water use efficiency	ET	Day, two-weekly for 3 years	Field, catchment / 250 m	Hellegers *et al.* (2011)
Historic	Natural veld Water use	ET	Day, season, annual	Regional / 1 km	Palmer & Weideman (2011)**
Historic	IAP, Natural veld Water use	ET, Rain, Rain-ET	Day, two-weekly for 3 years	Provincial / 250 m	Jarmain & Meijninger (2012)
Historic	Catchment hydrology	ET, Energy balance	90 days	Catchment / 250 m	Kongo & Jewitt (2006)
Historic	Agricultural Water use efficiency	ET	3 years	Field, regional / 30 m	Klaasse *et al.* (2008)
Operational	Agricultural Water use efficiency	ET, Soil moisture, Energy balance	Weekly, 8 months (grape growing season)	Field, regional / 30 m	Klaasse *et al.* (2011); Jarmain *et al.* (2011a)
Operational	Agricultural Water use efficiency	ET, Energy balance	Weekly, for a period of 12 months	Field, farm, region / 30 m	Jarmain *et al.* (2011b)
Operational	Agricultural water management	ET, Soil moisture, Energy balance	Weekly, 8 months (grape growing season)	Field, regional / 30 m	Jarmain & Klaasse (2012)
Operational	Catchment scale Planning and water allocation	ET, Rain, Rain-ET	Weekly for a period of 12 months	Field, catchment, region / 30 m	WE Consult (2011)

**This study did not apply the energy balance approach for estimating *ET*.

Gibson *et al*. (2009) use the SEBS model to calculate annual *ET* for a quaternary catchment in the Western Cape, to assess the compliance of water users to water use legislation. The results of the study are inconclusive as the estimated annual catchment *ET* significantly exceeds the estimated annual catchment rainfall. Finally, Hellegers *et al*. (2011) use SEBAL estimates of *ET* to assist in assessing competing claims on water resources in the transboundary Incomati catchment shared between South Africa, Swaziland and Mozambique.

At a provincial scale, Jarmain & Meijninger (2012), using SEBAL, assess the impact of Invasive Alien Plant species (IAPs) and the clearing thereof by the Working for Water (WfW) programme, on *ET* and the availability of water resources in the Western Cape and KwaZulu-Natal provinces. They conclude that this approach (combining spatial *ET* data with information on land use) can be used to determine the *ET* of IAPs. Although the 250m resolution SEBAL data can be used, higher resolution data (<30m) would better assess the impact of IAPs on *ET* across a wider range of invasion densities and water regimes including riparian zones. Suited to regional *ET* estimation but differing from the energy balance methods, a parsimonious spatial *ET* method based on leaf area index (*LAI*) and the Penman-Monteith equation (Palmer & Weideman, 2011) has been used with good success in several areas in South Africa. This method uses the MODIS *LAI* to convert reference evapotranspiration (ET_0) from the Penman-Monteith equation to actual *ET* for each pixel. A *LAI* ratio is calculated by dividing the *LAI* of a pixel by the maximum *LAI* retrieved at the site over 10 consecutive years of MODIS data and this is in turn multiplied by an optimized scaling factor which relates leaf-level conductance to canopy conductance This method has been found to be particularly suited to natural vegetation with specific application to determining the water use efficiency (WUE) of rangelands.

The methods having proved their usefulness in historic studies have evolved into operational applications in a number of instances (Table 3). Two SEBAL studies (Klaasse *et al*., 2008) using high resolution Landsat imagery, determined the *ET*, biomass production and biomass WUE of table and wine grapes in the main production areas of the Western Cape for three grape seasons. The interest generated by this study led to the initiation of an operational project where remote sensing-based data maps and other information were made available at a weekly timestep via a GrapeLook website (Klaasse *et al*., 2011) for table and wine grape producing areas of the Western Cape. Grapelook was the first African example where *ET* and related data maps (biomass, WUE, nitrogen content) as well as satellite data-derived irrigation advice were determined and made available to users. This approach was subsequently extended to include deciduous fruit producing areas of the Western Cape (Jarmain and Klaasse, 2012) for the growing season of 2011-12. This operational approach is being replicated in two studies to assess the WUE of sugarcane and grain crops. Weekly data maps are disseminated though the website viewers SugarcaneLook (Jarmain *et al*., 2011b) and GrainLook (Jarmain *et al*., 2013). Following on from the study conducted in the Incomati catchment (Hellegers *et al*., 2011), the European Union-funded project WATPLAN was launched. WATPLAN aims to develop a web-based, operational tool (www.watplan.com) where water balance information (rainfall, *ET*, Rain-*ET*) for the entire Incomati catchment is disseminated weekly. Information provided through WATPLAN will be

integrated with the operational water resources management system of the Incomati catchment management agency (CMA).

Arising from past and current operational projects, has been the realisation that field validation of remotely sensed *ET* estimates is a necessary component of these operations to allow for data products to be used with confidence. In addition, the need to find further users of and uses for the data products has become apparent. The presentation of the end product and its usability differs from historic studies where a map may be an acceptable deliverable. For operational applications of remote sensed *ET* estimates to be adopted, there is a need to integrate the *ET* data products into other systems such as irrigation scheduling, allowing for ease of use and interpretation.

In terms of the chronology, Kongo & Jewitt (2006) were the first to use remote sensing to estimate *ET* in South Africa. In 2009, besides the WRC report published by Gibson *et al.* (2009) which has already been discussed in Chapter 1.1, a number of publications with different applications appeared. Jarmain *et al.* (2009) evaluated the accuracy of models that estimate evaporation spatially using earth observation data in a variety of environments including an open water surface, forestry plantation, wetlands, and native vegetation under semi-arid environments varying in vegetative cover. The models evaluated include the Surface Energy Balance Algorithm for Land (SEBAL), Mapping EvapoTranspiration with High Resolution and Internalized Calibration (METRIC), Vegetation Index / Temperature Trapezoid (VITT) and Surface Energy Balance System (SEBS) models. Jarmain *et al*. (2009) reported that SEBAL, METRIC and SEBS quite easily simulated net radiation accurately, but the accuracy of soil heat flux and heat storage of a water body was more variable. Similarly, for the sensible heat flux density (*H*) at the time of satellite overpass for various land uses and with different models, accurate estimates of simulated *H* were not always achieved. Evaporative fraction (*EF*) estimates were simulated accurately in many cases. The VITT model generally yielded the least accurate evaporation estimates.

In 2010, a technique to determine reference crop evapotranspiration based on a modification of the FAO56 reference crop evapotranspiration as part of a soil moisture modelling process was developed

(Sinclair & Pegram, 2010). ET_0[7] was computed using forecast field meteorological variables from the Unified Model runs done by the South African Weather Service (SAWS) with Meteosat data being used to estimate hourly radiation data. Once ET_0 has been calculated, MODIS *NDVI,* together with the TOPKAPI (Todini & Ciarapica, 2001) distributed hydrological model are used to calculate a water stress and a crop factor which are used to model *ET* from ET_0.

In 2011, a spatial *ET* method was developed based on *LAI*, particularly suited to natural vegetation, with specific application to determining the water efficiency of rangelands (Palmer & Weideman, 2011). In the latest publication of remote sensing *ET* in South Africa, Münch *et al*. (in press) use the results of the Palmer & Weideman (2011) model and the MOD16 data product to successfully contextualize the hydrogeology of a catchment in the Sandveld.

Finally, it should also be mentioned that a number of freely downloadable *ET* data products exist, for example the Landsaf data and MODIS 16 *ET* product. Jarmain *et al*. (2009) refer to a number of others. The MOD16 *ET* product specifically has generated interest. The MODIS Science Team, in 2011, released a MODIS *ET* data product (MOD16) available freely for download. The MOD16 *ET* products are regular 1-km2 global land surface *ET* datasets for vegetated land areas at 8-day and monthly intervals (Mu *et al*., 2011). The MOD16 *ET* product is created using MODIS global land cover (MOD12Q1), a daily meteorological reanalysis dataset from NASA's Global Modelling and Assimilation Office, and MODIS biophysical parameters (albedo, Leaf Area Index and Enhanced Vegetation Index) as input into the Penman-Monteith equation. The algorithm performance has been validated against 46 flux tower measurements across seven biomes but validation in Africa has not been published to date.

Besides Jarmain *et al.* (2009) and Gibson *et al*. (2009), the use of the SEBS model in South Africa has been limited.

[7] ET_0 being reference crop evapotranspiration where: the reference surface is a hypothetical grass reference crop with an assumed height of 0.12m, a fixed surface resistance of 70 s m^{-1} and an albedo of 0.23. The reference surface closely resembles an extensive surface of green well-watered grass of uniform height, actively growing and shading the ground. It should be noted that ET_0 is thus not the same as actual *ET*.

2.2. SEBS IN THE LITERATURE

The SEBS model was developed by Prof Z. Su, at the ITC in the Netherlands, and the formulation publication (Su, 2002) describes the model and provides the required equations. The environments in which the SEBS model has been applied range from forests (Badola, 2009) to wetlands (Alvarez, 2007), irrigated agriculture (Jia *et al*., 2003) to sparsely vegetated and barren land (Xin, 2006). SEBS publications outside of South Africa by: type of publication, study area, scale, environments, purpose of research and the sensors used, are summarized in Table 4. and SEBS publications by: source of information on land surface physical parameters, fractional vegetation cover method, the validation method and reported accuracies are summarized in Table 5.

It is difficult to properly assess the accuracy of the results from the SEBS model from the literature as there does not appear to be a standard method for presenting the results and validation methods and their associated accuracies vary from study to study. Published results of the SEBS model have been validated with a variety of field and/or complementary methodologies such as the lysimeter (Lin, 2006), flux tower measurements using eddy covariance or Bowen Ratio methods (Su, 2002; Su *et al*., 2005; Timmermans *et al*., 2005; McCabe & Wood, 2006; Badola, 2009; van der Kwast *et al*., 2009) and the large aperture scintillometer (Jia *et al*., 2003; Timmermans *et al*., 2005). Additionally, results have been compared to hydro-meteorological equations (Hailegiorgis, 2006; Lin, 2006; Gebreyesus, 2009) and the water balance or by examining hydrological consistency with other datasets (Su & Roerink, 2004; Alvarez, 2007; McCabe *et al*., 2008; Pan *et al*., 2008).

The accuracies in the evapotranspiration and energy flux estimates as determined using the SEBS model are comparable with validation measurements as shown by Alvarez (2007), Gebreyesus (2009), Hailegiorgis (2006), Jia *et al*. (2003), Lin (2006), McCabe & Wood (2006), McCabe *et al.* (2008), Su (2002), Su *et al*. (2005), Timmermans *et al*. (2005) and Van der Kwast *et al*. (2009). Reported inaccuracies are in the overestimation of the latent heat flux such as was found in the studies by McCabe & Wood (2006) and Su & Roerink (2004). Prior to 2011, the only author to report extreme inaccuracies is Badola (2009) who found that latent heat flux was severely overestimated and sensible heat flux severely underestimated in a forested area. Since the SEBS model was originally developed for agriculture, the inference may be that the inaccuracies were due to the model being applied to non-agricultural land

Table 4: Chronological summary of SEBS publications.

Author	***Type of publication***	***Study area***	***Description of spatial and temporal scale***	***Environments***	***Purpose of research***	***Sensors used for SEBS calculation***
Su**(2002)**	Journal	Barrax, Spain	Field scale	Shrub, cotton, grass	Formulation of the model	TMS-NS001
Jia *et al.* **(2003)**	Journal	3 locations in Spain	Local scale: across 2 – 6 1000m resolution pixels 3 – 5 ATSR images per location.	Dry vineyard surface. Irrigated fruit trees and alfalfa. Various irrigated crops	Validation and improvement of SEBS model	ATSR
Su *et al.* **(2005)**	Journal	Iowa, USA	Field scale and regional scale Single date Landsat	Corn and soybeans	Determine the accuracy of SEBS at the field scale and at catchment scale	Landsat GOESS MODIS
Timmermans *et al.* **(2005)**	Conference proceedings	Barrax, Spain	Field scale Single date ASTER image	Forest nursery, wheat stubble, vineyard, sunflower, corn	Comparison of results from one-source (SEBS & SEBAL) and two-source (TSEB) for net radiation, soil heat flux and sensible heat flux	ASTER
Hailegiorgis **(2006)**	M. Sc thesis	Regge and Dinkel, The Netherlands	Regional: catchment 8 Landsat images	Heath lands, grasses, forests and crops (maize)	Assessment of summer time ETa	Landsat
Lin **(2006)**	M. Sc thesis	Hebei Plain, Northeastern China	Regional 6 MODIS images	Predominantly croplands	Eta estimation and spatial-temporal distribution patterns. Tests of sensitivity of SEBS to inputs	MODIS TERRA
McCabe & Wood **(2006)**	Journal	Iowa, USA	Field and catchment scale Single date ASTER, Landsat and MODIS images	Corn and soybeans	Scale influences on remote sensing estimation of evapotranspiration	ASTER, Landsat, MODIS TERRA
Alvarez **(2007)**	M. Sc thesis	Costa Rica	Regional 3 ASTER images 17 MODIS images	Wetlands	Define effects of vegetation removal on *ET* in a wetland	ASTER MODIS TERRA
Pan *et al.* **(2008)**	Journal	Red-Arkansas River Basin, USA	Regional 3 MODIS images	Varied Forest, wooded grassland, cropland, open shrubland	Remote sensing data to estimate regional scale terrestrial water cycle	MODIS TERRA MODIS AQUA
Xin **(2007)**	M. Sc thesis	Northwest China	Regional 4 MODIS images	Varied: predominantly barren or sparsely vegetated land	Analysis of spatial and temporal Eta in Heihe River Basin using SEBS	MODIS TERRA
McCabe *et al.* **(2008)**	Journal	Arizona, USA	Regional 6 MODIS images	#	Sensible heat flux for hydrological consistency	MODIS TERRA MODIS AQUA
Badola **(2009)**	M. Sc thesis	Central Netherlands	Field scale Single ASTER image	Forests	Test SEBS over forested area and investigate sensitivity to parameters derived from remotely sensed data	ASTER
Gebreyesus **(2009)**	M. Sc thesis	Salamanca, Spain	Local scale. Sub-catchment 13 MODIS images	Dryland agriculture Some irrigated crops	Validation of remote sensing estimation of soil moisture and energy fluxes	MODIS TERRA
Jia *et al.* **(2009)**	Journal	Yellow River Delta, China	Regional 67 MODIS images over a year	Wetland	Extrapolating daily to annual *ET* across a region	MODIS TERRA
Rwasoka *et al.* **(2011)**	Journal	Upper Manyame Catchment, Zimbabwe	Regional 9 MODIS images over three years	Grasslands Urban	Water resource and environmental management and planning	MODIS
Gibson *et al.* **(2011b)**	Journal	Western Cape, South Africa	Local scale, 1 MODIS image, 1 ASTER image	Agricultural – apple orchard, dryland agriculture	Water use determination	MODIS TERRA MODIS AQUA
Gokmen *et al.* **(2012)**	Journal	Konya Basin, Central Anatolia, Turkey	Regional 42 MODIS images over 6 months	Sparse steppe vegetation, crops, wetland	Adapting the SEBS model	MODIS
Lu *et al.* **(2012)**	Journal	Jiangxi province, southern China	Local 96 MODIS images over a year	Evergreen coniferous trees	Assess results in heterogeneous land surfaces	MODIS TERRA MODIS AQUA

Table 5: Validation, reported accuracies and SEBS model sensitivities.

Authors	***Source of information on land surface physical parameters***	***Method used to calculate fractional vegetation cover***	***Validation method***	***Reported accuracies***
Alvarez **(2007)**	LIDAR and derived from ASTER	Choudhary *et al*., 1994	Compared to measured water levels	Within 10% of *ET* (from water level determination of storage)
Badola **(2009)**	Empirically derived from ASTER data	Baret *et al*., 1995; Carlson & Ripley, 1997; Gutman & Ignatov, 1998 & Jiang *et al*., 2006.	Three flux towers	Severe overestimation of latent heat flux and underestimation of sensible heat flux in forested areas.
Gebreyesus **(2009)**	Land cover classifications	SEBS in ILWIS- assumed Carlson & Ripley, 1997	Crop coefficients and ET_0	r^2 of 0.86 and 0.91 when compared with complimentary approach
Gokmen *et al.* **(2012)**	Empirically derived from MODIS data	Not specified	Bowen ratio	For H: RMSE of 142.7 prior to algorithm adjustment, RMSE of 103.9 post algorithm adjustment
Hailegiorgis **(2006)**	Empirically derived from Landsat data	Choudhary *et al*., 1994	Compared to results of hydrometeorological equations over grassland	ETa reported to be satisfactory when compared with ET_0
Jia *et al.* **(2003)**	Empirically derived from ATSR data	Baret *et al*., 1995	Large aperture scintillometer	RMSD for dry vineyard = 24.2 $W.m^{-2}$, Irrigated fruit trees and alfalfa = 36.5$W.m^{-2}$, Mixed irrigated crops = 8.5 $W.m^{-2}$
Jia *et al.* **(2009)**	Land cover classification, MODIS LAI, field measurements	Not specified	ET_0 (ETa for a wetland should be very close to ET_0)	ETa reported to be acceptable when compared with ET0 RMSE for "Suaeda heteroptera" = 0.88mm "reed swamp" = 1.3mm
Lin **(2006)**	Empirically derived from MODIS data	Gutman & Ignatov, 1998	Lysimeter Pan evaporation, Crop *ET* (ETc)	Good agreement reported between SEBS ETa and lysimeter values
Lu *et al.* **(2012)**	Empirically derived from MODIS data	Pridhodko & Goward, 1997	Eddy covariance flux measurements	For evaporative fraction, r^2 of between 0.552 and 0.557
McCabe & Wood **(2006)**	Empirically derived from ASTER and Landsat and Landsat land cover classifications	Baret *et al*., 1995	Eddy covariance flux measurements	Tendency for over prediction with SEBS but good correlation to field measured values: r^2 = 0.71 for ASTER and r^2 = 0.74 for Landsat.
McCabe *et al.* **(2008)**	MODIS data products and land classifications	Xavier & Vettorazzi, 2004	Hydrological consistency with other remote sensed variables	For soil moisture anomalies from AMSR-E there is considerable agreement with available sensible heat flux predictions
Pan *et al.* **(2008)**	MODIS data products and land classifications	Not specified	Hydrological consistency with other remote sensed variables	SEBS retrieved *ET* values are higher than Variable Infiltration Capacity based predictions
Rwasoka *et al.* **(2011)**	Empirically derived from MODIS data	Sobrino & Raissouni, 2000	Advection-aridity *ET* and ET_0	Urban: between -1.5 and 0.4 $mm.d^{-1}$ Grassland: between 0.6 and 3.8 $mm.d^{-1}$
Su **(2002)**	Empirically derived from TMS data	Not specified	Flux towers: eddy covariance and Bowen ratio	Mean error of SEBS is estimated to be around 20% relative to the mean sensible heat flux.
Su & Roerink **(2004)**	Not specified	Not specified	Flux towers: eddy covariance and Bowen ratio	Overestimation of Rn and LE. G_0 and H results are better. Too few observations to draw conclusions
Su *et al.* **(2005)**	Field measured and empirically derived from Landsat data	Chen & Cihlar, 1995	Ten flux towers: eddy covariance	Five corn sites: relative root-mean-square error = 13.32% and root mean absolute error = 9.73% 3 soybean sites root-mean-square error = 14.02% root mean absolute error = 10.72%
Timmermans *et al.* **(2005)**	Empirically derived from ASTER data	Choudhary *et al*., 1994	Flux towers: eddy covariance. Large aperture scintillometer, TSEB & SEBAL	Slight underestimation of Rn, G0 slightly underestimated for low vegetation cover, underestimated H of up to 140 $W.m^{-2}$
Van der Kwast *et al.* **(2009)**	Empirically derived from ASTER data and field observations	Not specified	Flux towers: eddy covariance. Large aperture scintillometer	Standard deviations of SEBS estimated H similar to field measured values. SEBS estimated H good when the footprint of the measurements covers only one land cover type.
Xin **(2007)**	MODIS land cover product	Choudhary *et al*., 1994	#	#

covers. However authors of other studies outside of irrigated agriculture have not reported the same inaccuracies.

When looking at the use of different resolution sensors at a smaller scale or catchment scale, there tends to be good agreement between the results obtained by using high and coarse resolution sensors. For a wetland, Alvarez (2007) finds that the *ET* estimates from MODIS are within 5% of the results obtained from ASTER with better results being obtained where the vegetation is less fragmented. Similarly McCabe & Woods (2006) find that at field scale, the ASTER values are not regularly within 10% of MODIS values but at a catchment scale, results for ASTER, Landsat and MODIS are within 10% of each other. From the literature it is therefore clear that the SEBS model has been used with varied success to model energy fluxes and *ET* in a range of environments with an emphasis on agriculture and with a variety of sensors.

Several authors attribute the sensitivity of the SEBS model to various input parameters including: roughness length (Lin, 2006; Alvarez, 2007; Van der Kwast *et al*., 2009, Gebreyesus, 2009), zero plane displacement height (Lin, 2006), land surface temperature (Badola, 2009; Van der Kwast *et al.*, 2009), wind speed and wind direction (Van der Kwast *et al.*, 2009), fractional vegetation cover (Badola, 2009; Lin, 2006), surface emissivity (Badola, 2009; Van der Kwast *et al.*, 2009; Lin, 2006), albedo (Badola, 2009; Van der Kwast *et al.*, 2009), *NDVI* (Badola, 2009; Van der Kwast *et al.*, 2009), shortwave incoming radiation (Van der Kwast *et al*., 2009) and the height of the planetary boundary layer (Van der Kwast *et al*., 2009).

In the formulation publication of SEBS (Su, 2002), the sensitivity of the sensible heat flux to parameters[8] used in its calculation are found to be around 40 $W.m^{-2}$ when the various terms are assumed independent of each other. Since in reality at least some of the terms are correlated, the expected sensitivity can then be estimated in the order of 20 $W.m^{-2}$, which is around 20% relative to the mean sensible heat flux (Su, 2002). Of the reported sensitivities since the work of Su (2002), Badola (2009) and Van der Kwast *et al.* (2009) report SEBS to be most sensitive to land surface temperature. However, Lin (2006) reports that the SEBS model is most sensitive to roughness length and according to Van der

[8] land surface temperature and air temperature gradient, friction velocity, excess resistance to heat transfer, and stability correction function for heat transfer.

Kwast *et al.* (2009), sensitivity to aerodynamic parameters (roughness length, zero plane displacement height and canopy height) and the method used to derive these parameters should be considered depending on the heterogeneity of the image footprint.

Lin (2006) demonstrates the sensitivity of the SEBS model to zero plane displacement height especially at high zero plane displacement heights and high *NDVI*. SEBS modelled evaporative fraction decreases slightly with increasing displacement height at lower *NDVI*, but when the zero plane displacement height reaches a certain threshold, the evaporative fraction begins to decrease rapidly with increasing displacement height. Lin (2006) concludes that evaporative fraction is a function of not only displacement height but also of *NDVI*. Areas that have high green leaf biomass (and therefore high *NDVI*) normally have a relatively lower evaporative fraction but are more sensitive to the displacement height (Lin, 2006).

Lin (2006) further demonstrates the sensitivity of evaporative fraction to aerodynamic roughness length particularly at lower *NDVI* and concludes that the larger the *NDVI*, the more *ET* will take place and the less sensitive the outputs will be to aerodynamic roughness height changes. It was also illustrated that at *NDVI* of around 0.6, the SEBS model is most sensitive to change in aerodynamic roughness.

Lin (2006) and Badola (2009) differ in their findings regarding the sensitivity of the SEBS model to fractional vegetation cover. Lin (2006), who uses coarse resolution MODIS imagery, reports the SEBS model to be relatively insensitive to change in fractional vegetation cover whereas Badola (2009), using high resolution ASTER imagery finds a great sensitivity of sensible heat flux to change in fractional vegetation cover. Badola (2009) motivates this sensitivity by the use of the fractional vegetation cover and its complement in the calculation of the sensible heat flux (see Equations [12], [13] and Equations [6], [7] & [8] in Chapter 2.3). The differing land covers under study by Lin (2006) and Badola (2009) should be noted, in that the former's object of study is predominantly cropland whereas the latter's object of study is forested areas with tall canopies.

In criticism of the literature around the application of the SEBS model, prior to 2010 much of the available literature was published in the so-called grey literature with a limited peer review process.

Due to this limitation, it would be specious to draw firm conclusions around the reported accuracies. However, post 2010; journal papers (Gibson *et al*., 2011b; Rwasoka *et al*., 2011; Gokmen *et al*., 2011; Lu *et al*., 2011) on the application of the SEBS model have been more critical in establishing the accuracy of the model. Rwasoka et al. (2011) report an overestimation of *ET* at a grassland site which they ascribe to the heterogeneity of the landscape. Heterogeneity is further put forward as a reason for inaccuracies by Gibson *et al*. (2011b) Lu *et al*. (2012) and Gokmen *et al*. (2012). Further, Lu *et al*. (2011) state that lack of energy balance closure leads to inaccuracies in results.

2.3. SEBS FORMULATION

According to Su (2006), it is possible to estimate the latent heat flux as a residual of the surface energy balance algorithm after the sensible heat flux has been derived (Equation 1). However, because the sensible heat flux is not constrained by the available energy but is determined solely by surface temperature and the meteorological conditions at the reference height, there is an associated uncertainty in the derived latent heat flux and therefore also in the evaporative fraction. However, in SEBS this uncertainty is limited by considering the sensible heat flux at both the wet and dry limit and the actual sensible heat flux is constrained to this range. The sensible heat flux at the wet limit is derived from a combination equation and the sensible heat flux at the dry limit is set by the available energy. In SEBS, the daily *ET* is determined from the total daily available energy by assuming the evaporative fraction is constant throughout the day.

Instantaneous net radiation is estimated based on radiative energy balance:

$$R_n = (1-\alpha)R_{swd} + \varepsilon \cdot R_{lwd} - \varepsilon \cdot \sigma \cdot T_0^4 \qquad [2]$$

where α is broadband albedo in the visible and near-infrared band; ε is broadband emissivity in the thermal infrared band; R_{swd} is incident shortwave radiation; R_{lwd} is downward longwave radiation; T_0 is surface temperature and σ is Stephan–Boltzman constant (Su *et al*., 2005).

The other component comprising the available energy is the soil heat flux. In the absence of observed soil heat flux measurements, as in satellite applications, empirical formulations of the soil heat flux based on net radiation and the vegetation fraction are used to estimate the total soil heat flux for the area.

$$G_o = R_n \cdot \left[\Gamma_c + (1 - fc) \cdot (\Gamma_s - \Gamma_c)\right] \quad [3]$$

where Γ*c* (0.05) (Monteith, 1973 in Su, 2002) and Γ*s* (0.315) (Kustas & Daughtry, 1989 in Su, 2002) are the soil heat flux ratios for full vegetation canopy and for bare soil respectively and f_c is the fractional vegetation cover (Su *et al*., 2005).

At the wet and dry limits, the equations used to calculate the sensible heat flux (Equations [4] & [5] respectively) differ from the sensible heat flux equations which are used when the wet or dry limit has not been reached (Equations [6], [7] & [8]) (Su, 2002).

$$H_{wet} = \left((R_n - G_0) - \frac{\rho C_p}{r_{ew}} \cdot \frac{e_s - e}{\gamma} \right) \Big/ \left(1 + \frac{\Delta}{\gamma} \right) \quad [4]$$

where *e* and e_s are actual and saturation vapour pressure respectively; γ is the psychrometric constant, r_{ew} is the external resistance at the wet limit and Δ is the rate of change of saturation vapour pressure with temperature.

$$H_{dry} = R_n - G_0 \quad [5]$$

$$u = \frac{u_*}{k}\left[\ln\left(\frac{z-d_0}{z_{0m}}\right) - \Psi_m\left(\frac{z-d_0}{L}\right) + \Psi_m\left(\frac{z_{0m}}{L}\right)\right] \quad [6]$$

$$\theta_0 - \theta_a = \frac{H}{k u_* \rho C_p}\left[\ln\left(\frac{z-d_0}{z_{0h}}\right) - \Psi_h\left(\frac{z-d_0}{L}\right) + \Psi_h\left(\frac{z_{0h}}{L}\right)\right] \quad [7]$$

$$L = \frac{\rho C_p u_*^3 \theta_v}{kgH} \quad [8]$$

where z is the height above the surface, u_* is the friction velocity, k = 0.4 is von Karman's constant, d_0 is zero plane displacement height, z_{0m} is the roughness height for momentum transfer, θ_0 is the potential temperature at the surface, θ_a is the potential air temperature at height z, z_{0h} is the scalar height for heat transfer, Ψ_m and Ψ_h are the stability correction functions for momentum and sensible heat respectively, L is the Obukhov length, C_p is the specific heat capacity of air at constant pressure, g is acceleration due to gravity and θ_v is the potential virtual temperature near the surface (Su, 2002). The friction velocity, the sensible heat flux and the Obukhov stability length are obtained by solving the system of non-linear Equations [6], [7] and [8] using the method of Broyden (Press *et al*., 1997 in Su, (2002)). Derivation of the sensible heat flux therefore requires only the wind speed and temperature at the reference height as well as the surface temperature and is independent of other surface energy balance terms.

If H calculated from Equations [6], [7] and [8] exceeds H_{dry} calculated from Equation [5], then the dry limit is said to have been reached and Equation [5] is used to determine H. If H_{wet} calculated from Equation [4] exceeds H calculated from Equations [6], [7] and [8], then the wet limit is said to have been reached and Equation [4] is used to determine H.

In the derivation of H, aerodynamic and thermal dynamic roughness parameters are required. The aerodynamic roughness parameter can vary in space and time for two different reasons: variations in surface roughness and variations in atmospheric stability. The first is the dominant cause of variations in space (at a specific time of a satellite overpass), whereas the second is the dominant cause of

variations in time (at a specific field site) (Van der Tol *et al.*, 2009). Su (2002) advises using the within-canopy turbulence model proposed by Maasman (1997) to estimate aerodynamic parameters d_0 and z_{0m}, if near surface wind speed, the height of the vegetation (h_0) and the leaf area index are known. If only the height of the vegetation is available, the relationships proposed by Brutsaert (1982) can be used:

$$h_0 = \frac{z_{0m}}{0.136} \quad [9]$$

$$d_0 = \frac{2}{3} h_0 \quad [10]$$

If a detailed land use map is available, tabulated values for aerodynamic parameters can be used. However, the first method is recommended since the aerodynamic parameters depend not only on surface characteristics but also wind speed and direction (Su, 2002). It should be noted that estimates of aerodynamic resistance based on optical remote sensing contain a large degree of uncertainty (Van der Tol *et al.*, 2009). However if none of the above data is available, the aerodynamic parameters can be related to remote sensing vegetation inputs, and the normalized difference vegetation index (*NDVI*) is used (Su & Jacobs, 2001, in Hailegiorgis, 2006):

$$z_{0m} = 0.005 + 0.5\left(\frac{NDVI}{NDVI_{\max}}\right)^{2.5} \quad [11]$$

The roughness height for heat transfer, z_{0h}, which changes with surface characteristics, atmospheric flow and thermal dynamic state of the surface, can be derived from z_{0m}:

$$z_{0h} = \frac{z_{0m}}{\exp\left(kB^{-1}\right)} \quad [12]$$

where B^{-1} is the inverse Stanton number, a dimensionless heat transfer coefficient. For vegetated areas, an extended model is used to estimate the kB^{-1} value (Equation [13]):

$$kB^{-1} = \frac{kC_d}{4C_t \frac{u_*}{u(h)}\left(1 - e^{-n_{ec}/2}\right)} f_c^{\,2} + 2 f_c f_s \frac{k \cdot u_* / u(h) \cdot z_{0m}/h}{C_t^*} + kB^{-1} f_s^{\,2} \qquad [13]$$

Where f_c is the fractional canopy cover and f_s is its complement. C_t is the heat transfer coefficient of the leaf and in most conditions is bounded as $0.005N<C_t<0.075N$ where N is the number of sides of the leaf to participate in heat exchange. C_t^* is the heat transfer coefficient of the soil and is given by $C_t^* = Pr^{-2/3} Re^{*-1/2}$, where Pr is the Prandtl number Re^* is the roughness Reynolds number ($Re^* = h_s u_* / v$, with h_s the roughness height of the soil. The kinematic viscosity of the air is $v = 1.327 \cdot 10^{-5} (p_0/p)(T/T_0)^{1.81}$ with p and T the ambient pressure and temperature and p_0 = 101.3 kPa and T_0 = 273.15 K. n_{ec} is the within canopy wind speed profile extinction coefficient is formulated as a function of the cumulative leaf drag area at the canopy top:

$$n_{ec} = \frac{C_d \cdot LAI}{2u_*^2 / u(h)^2} \qquad [14]$$

where C_d is the drag coefficient of the foliage elements (assumed = 0.2), LAI is the one-sided leaf area index defined for the total area, $u(h)$ is the horizontal wind speed at the canopy top.

kB^{-1} required in Equation [12] is calculated using Equation [13] for vegetated areas while for bare soil the model proposed by Brutsaert (1982) is used:

$$kB^{-1} = 2.46\left(\mathrm{Re}_*\right)^{1/4} - \ln[7.4] \qquad [15]$$

According to formulations by Su (2002), the relative evaporation is derived from the sensible heat flux and the sensible heat flux calculated at the wet and dry limits.

$$\Lambda_r = 1 - \frac{H - H_{wet}}{H_{dry} - H_{wet}} \quad [16]$$

where Λ_r is relative evaporation, H is the sensible heat flux and H_{wet} and H_{dry} are the sensible heat flux at the wet and dry limits respectively. The relative evaporation is, in turn, used together with R_n, G_0 and the latent heat flux at the wet limit to estimate the evaporative fraction:

$$\Lambda = \frac{\lambda E}{R_n - G_0} = \frac{\Lambda_r \cdot \lambda E_{wet}}{R_n - G_0} \quad [17]$$

where Λ is the evaporative fraction and λE and λE_{wet} are the latent heat flux and the latent heat flux at the wet limit respectively.

In SEBS it is assumed that the daily value of evaporative fraction is approximately equal to the instantaneous value, since the difference between the instantaneous evaporative fraction at satellite overpass and the evaporative fraction derived from the 24-hour integrated energy balance is marginal and may be neglected (Ahmad *et al*. 2005) as the evaporative fraction generally remains constant throughout the day. From this, the daily *ET* can be determined as:

$$ET = 8.64 \times 10^7 \times \frac{\Lambda \cdot \overline{R_n}}{\lambda \rho_w} \quad [18]$$

where *ET* is the actual evaporation on daily basis (mm.d^{-1}), λ is the latent heat of vaporization (J.kg), ρ_w is the density of water (kg.m^{-3}) and $\overline{R_n}$ is the daily net radiation flux (Lin *et al.*, 2008):

$$\overline{R_n} = (1 - c_1) \cdot \alpha \cdot K\downarrow_{day} + L_{day} \quad [19]$$

where c_1 is a conversion factor of 1.1 for instantaneous to broad band albedo, α is broad band albedo and used in the instantaneous net radiation flux calculation in SEBS, $K\downarrow_{day}$ is incoming shortwave radiation (measured or modelled) and L_{day} is daily longwave radiation (Hailegiorgis, 2006). It is clear from Equations [18] and [19] that aside from evaporative fraction itself, albedo is the sole remote sensing derived variable used in the upscaling from instantaneous evaporative to daily ET.

3. VALIDATION SITE

The Mouton's Valley farm is situated in the Bo-Piketberg (Figure 2). The Bo-Piketberg is an elevated mountainous area which lies approximately 10 kilometres to the west and the northwest of Piketberg in the Western Cape Province. It lies within the Berg River Water Management Area, and is drained by the Platkloof and Boesmans Rivers which feed the Berg River to the south at the foot of the mountain. Annual rainfall averages at over 800mm per annum making it a relatively high rainfall region with most of the precipitation falling in the winter months as a result of cold front systems.

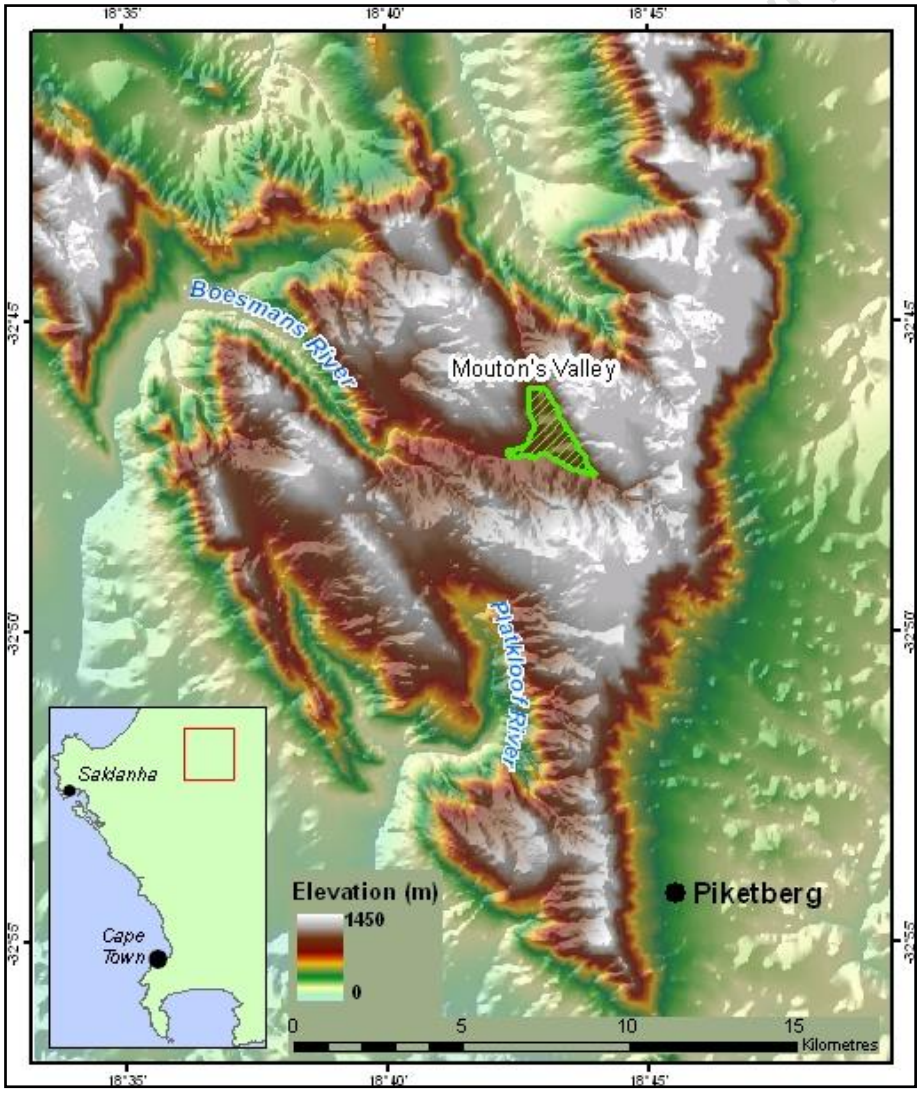

Figure 2: Location of the study area.

The Bo-Piketberg is made up of a variable thickness of the Table Mountain Group rocks, which are dominated (73%) by quartzose sandstone (quartz arenite). In the study area, the Peninsula Formation is the most represented formation consisting of thickly bedded quartzitic sandstone with the Nardouw Formation also having a significant presence. Basement rock of the Malmesbury Group appears in the southeast of the study area at the base of the mountain and Quaternary alluvial deposits are found in the southwest.

The land use is predominantly farming (fruit – deciduous and citrus, flowers and buchu) while the steeper terrain is undeveloped and uncultivated consisting of natural vegetation however, encroachment by invasive alien vegetation species is a reported problem. Cultivated land is irrigated mainly using surface water from farm dams but boreholes do exist and are in operation.

The farm Mouton's Valley is situated in the Mouton's Valley with the cultivated fields being nestled between the north bank of the Boesmans River, the large dam at The Hermitage to the north, and steep mountain slopes to the east (Levant Hill, 1146 m) and the west (790 m). The cultivated land on the farm Mouton's Valley covers an area of approximately 150 ha and has an elevation of between 500 and 540 m above sea level (Figure 2). Mouton's Valley is a fruit farm with both deciduous (apples, nectarines, persimmons, peaches and pears) and citrus fruits (oranges and lemons) being grown (Figure 3). Irrigation is predominantly from the large dam at The Hermitage and the owners report that this contains sufficient water for their irrigation requirements. There is an Enviromon agroclimatology weather station situated on the farm and rainfall, temperature, relative humidity, solar radiation, sun hours and leaf wetness are recorded at hourly intervals.

The field validation took place in an apple orchard (11 ha) which was made up of three different apple cultivars – 11 rows of Braestarr, 16 rows of Royal Gala and 15 rows of Redchief. At the time of the energy balance and total evaporation measurements from 7 November to 1 December 2008 (DOY 315 – 326), the average canopy height was 3.2 m. The apple trees did not cover the soil surface completely, rather by about 75 %. The inter-row areas were planted with grass (Jarmain & Mengistu, 2011). Good quality data was available from 10 to 21 November 2008 (Day of year (DOY) 315 to 326) and this is the time period studied in this research.

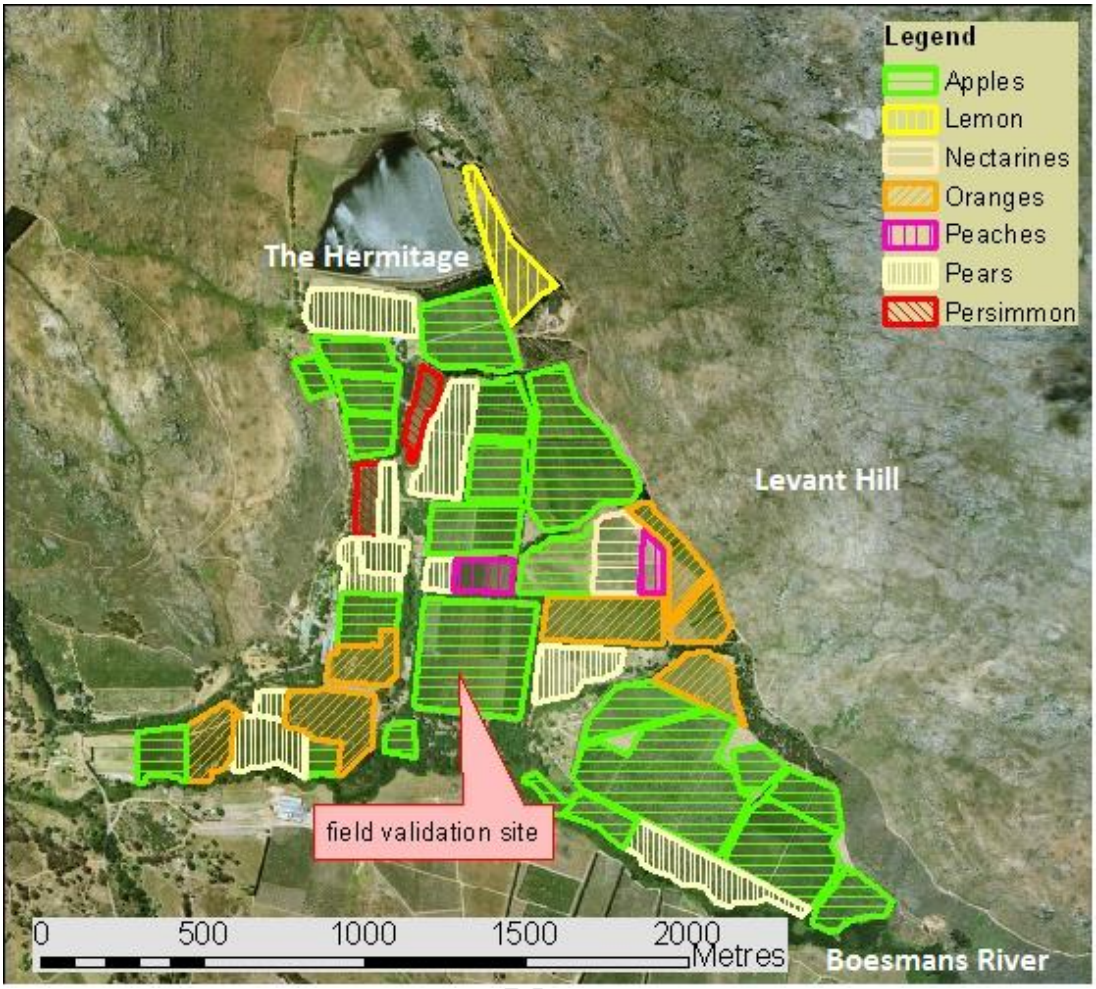

Figure 3: Crops grown on Mouton's Valley farm and the location of the field validation site shown on a colour aerial photograph with field boundaries digitized from the photograph and crop information obtained from the Mouton's Valley farm manager.

Rain was recorded on DOY 316 and 317 with up to 14mm falling in one hour on DOY 317, and cloud cover on DOY 316 – 319 can be seen in the decrease in measured radiation Figure 4a). The inverse relationship of relative humidity to temperature is observed (Figure 4b) with very high humidity recorded during and after the rainfall event and low humidity recorded on the hottest days. The lowest minimum temperature (15°C) was recorded at the beginning of the study period on DOY 315 and the highest maximum temperature (35°C) was recorded at the end of the study period on DOY 325. The wind speed generally increases during the course of the day and generally dies by early morning (Figure 4c). However there are exceptions.

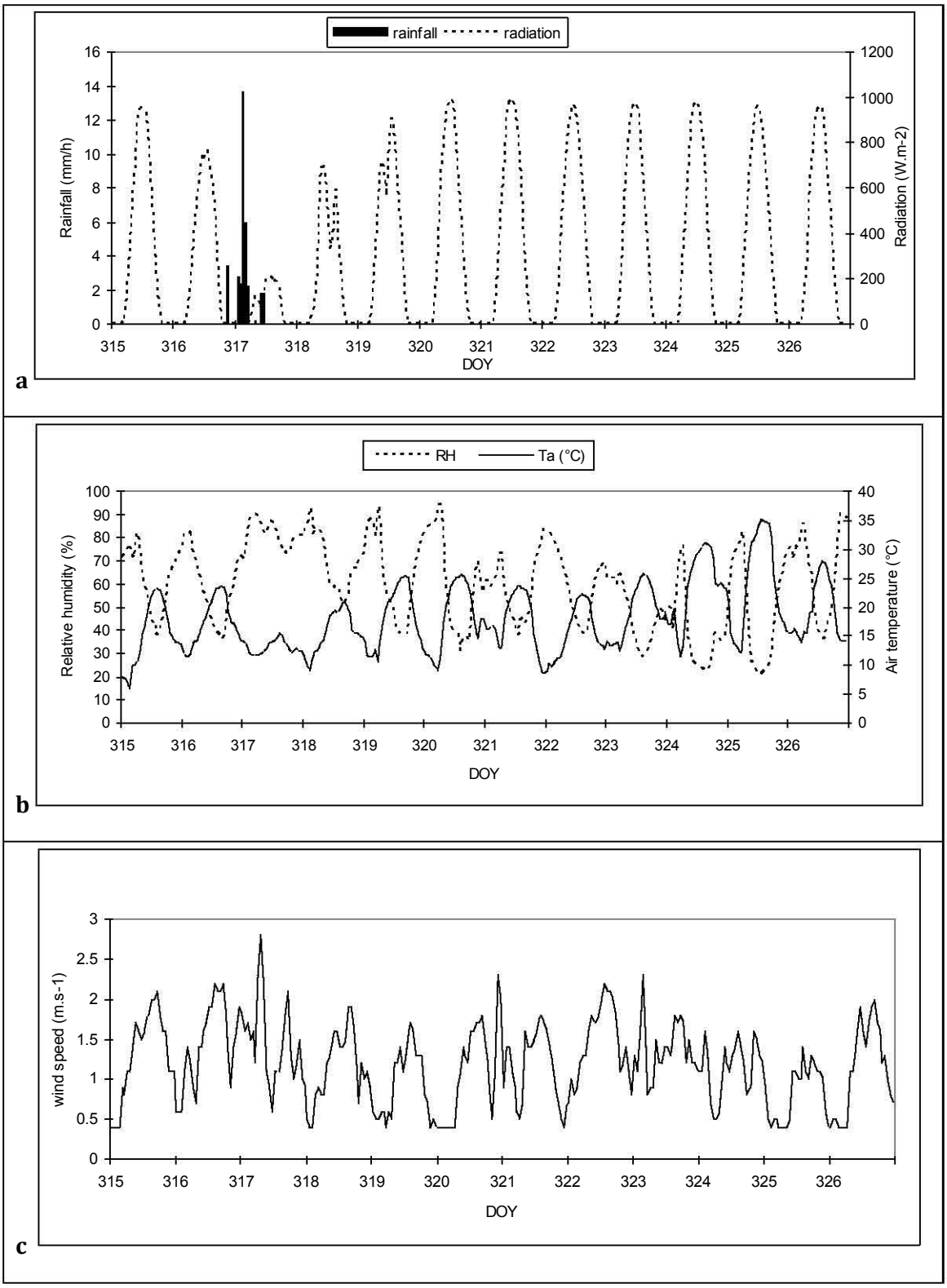

Figure 4: Recorded meteorological data for the field campaign period: a) rainfall and radiation, b) relative humidity and air temperature and c) wind speed.

Irrigation data is not available for the study period but soil water content was measured as part of the field campaign (Figure 5). A sudden increase in soil water content in this study area will either be as a result of irrigation or a rainfall event. By examining Figure 5 in conjunction with the meteorological data presented (Figure 4), it can be surmised that the increase in soil water content on DOY 317 was due to rainfall on that day and on DOY 325, after a number of hot dry days with declining soil water content, the orchard was irrigated in anticipation of the following day's maximum temperature of 35°.

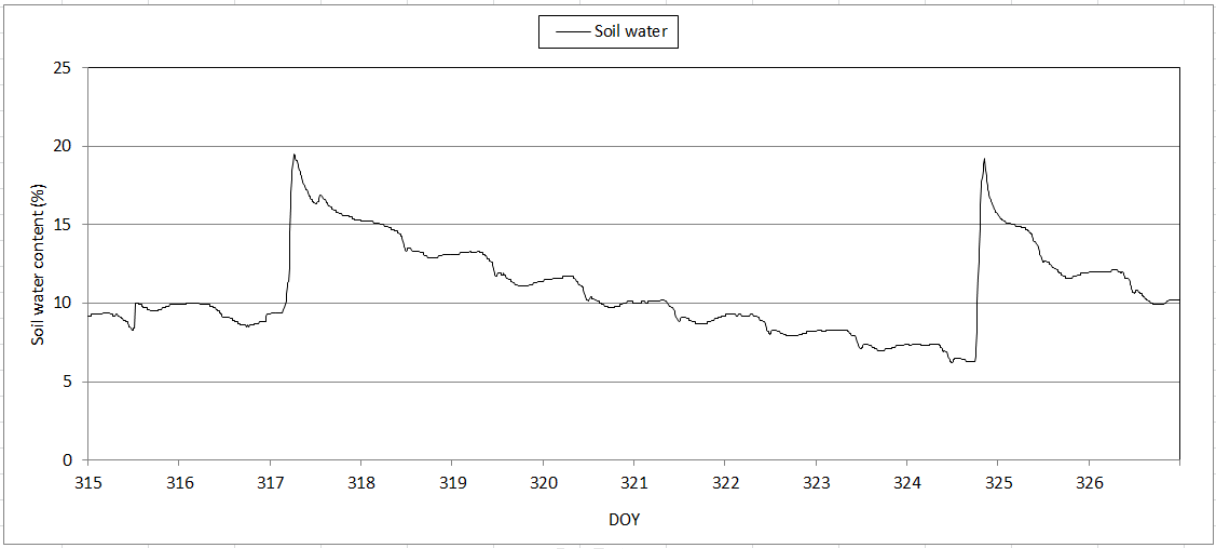

Figure 5: Soil water content measured at depth of 8 cm during the field campaign.

Energy balance and evapotranspiration field validation data was captured by the CSIR (Jarmain & Mengistu, 2011) from 7 November to 1 December 2008. A one-sensor eddy covariance system was used for the estimation of the sensible heat flux density. The one-sensor system utilizes the simplified energy balance and as such, the latent heat flux is solved as residual and therefore no closure term is used. The instrumentation was installed in the middle of an apple orchard selected on the Mouton's Valley farm, in a section planted with Royal Gala trees. An RM Young three-dimensional ultrasonic anemometer (model 81000, Traverse city, Michigan, USA – path length of 150 mm) was used to estimate sensible heat flux density. Two net radiometers were used to measure the net radiation above the apple orchard. One REBS Q*6 net radiometer was installed above the apple tree row, and one NR-Lite net radiometer (Model 240-110, Kipp & Zonen) was installed above the inter-row area (Figure 6). The average value of these two sensors was used in the calculations. Soil temperature (using type-E soil averaging thermocouples) and soil heat fluxes (REBS heat flux plates) were measured at four different positions between the tree rows and the data was used to estimate the soil heat flux density. Using the

estimates of sensible heat flux density and that of net irradiance and soil heat flux density, the latent energy flux density was subsequently calculated using the shortened energy balance equation. Since problems were experienced with the RM Young sonic anemometer, some data was lost especially during the latter part of the measurement period. More information on the field validation campaign including the installation of the equipment is reported in Jarmain & Mengistu (2011).

Figure 6: Instrumentation installed at the apple orchard, a) the sonic anemometer and net radiometers clearly visible above the apple trees, b) the apple orchard from above and c) the apple orchard showing the inter-rows planted with grass and d) and e) the Moutons Valley automatic weather station (photos a-c from Jarmain & Mengistu, 2011).

The data from the one-sensor type eddy covariance system was used to validate the energy balance results from the SEBS model. The SEBS energy balance results are "instantaneous" and relate to average values for the hour during which the satellite image was captured, whereas the eddy covariance flux data is recorded at 30 minute intervals. The instantaneous energy balance data (net radiation, soil heat flux, sensible heat flux, latent energy flux) and the evaporative fraction calculated using the SEBS model are validated against 30 minute field measured values and the SEBS calculated daily *ET* results are validated against the field measured half-hourly data summed to a 24 hour total.

It should be stated that the resolution of the MODIS imagery in relation to the field validation site is problematic as it is shown in Figure 7a that the MODIS footprint exceeds the size of the apple orchard and multiple land covers are included in the MODIS pixel used to validate the field results. It can also be seen in Figure 7b that the ASTER data would have adequately captured the heterogeneity of the scene and although the mixed pixel effect may have come into play along field boundaries, for land patches the size of the apple orchard under study, it is ideal.

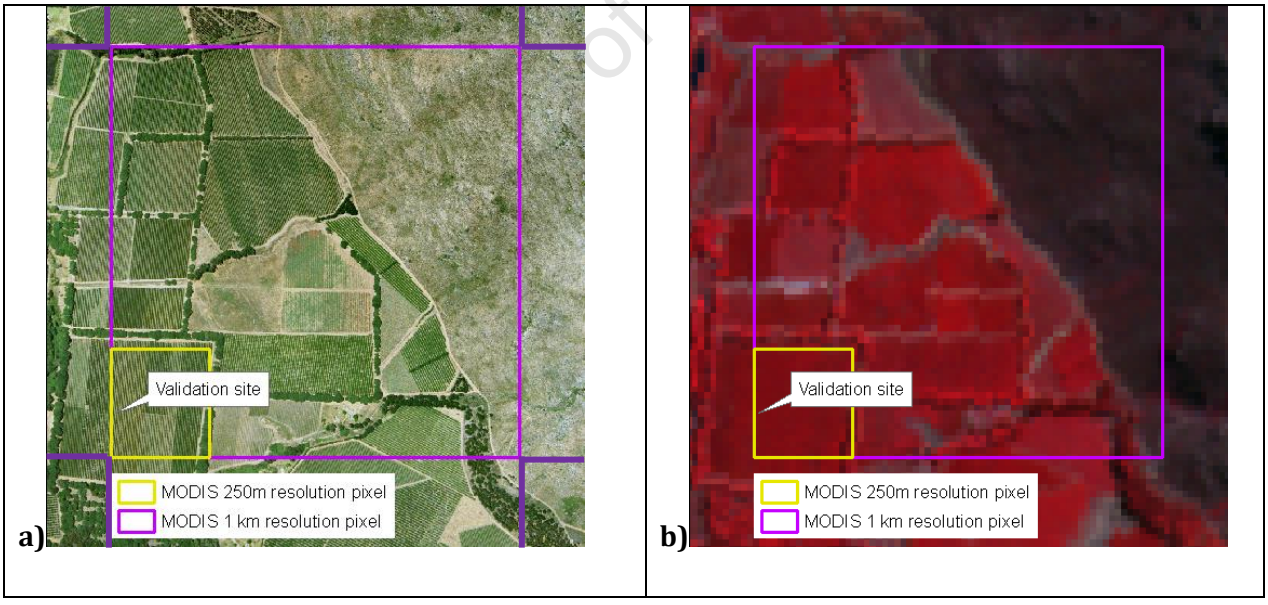

Figure 7: MODIS pixel footprints shown on a) an aerial photograph and b) an ASTER 321 image (22 March 2008) of the study area.

4. MATERIALS & METHOD

The SEBS model methodology will be discussed under the headings: *Remote sensing preprocessing* (Chapter 4.1), *Meteorological calculations* (Chapter 4.2) and *SEBS calculations* (Chapter 4.3). *Remote sensing preprocessing* includes data selection (Chapter 4.1.1), acquisition (Chapter 4.1.2), transformation (Chapter 4.1.3), converting to radiance or reflectance (Chapter 4.1.4) and atmospheric correction (Chapter 4.1.5). *Meteorological calculations* (Chapter 4.2) pertain to the meteorological data and calculations required for the SEBS model. *SEBS calculations* section (Chapter 4.3) details the calculation of the remote sensing derived input parameters required which are albedo (Chapter 4.3.1), vegetation parameters (Chapter 4.3.2), surface emissivity (Chapter 4.3.3) and land surface temperature (Chapter 4.3.4) Ultimately under SEBS calculations, the energy fluxes and evapotranspiration within the SEBS model (Chapter 4.3.5) is described. The general flow and the complexity of some of the SEBS methodology is illustrated in Figure 8 which shows the input data, processing stages and tools which are used in this research using MOD 02 data by way of example..

4.1. REMOTE SENSING PREPROCESSING

The SEBS model will be used to estimate evapotranspiration and energy balance components using data from two sensors MODIS TERRA & MODIS AQUA. The methodology is identical for both TERRA and AQUA data, however, for simplicity in the text, only MODIS TERRA will be referred to unless the reference is specific to MODIS AQUA. Note that the prefix MOD refers to MODIS TERRA and the prefix MYD refers to MODIS AQUA. A flowchart of the preprocessing methodology is shown in Figure 9.

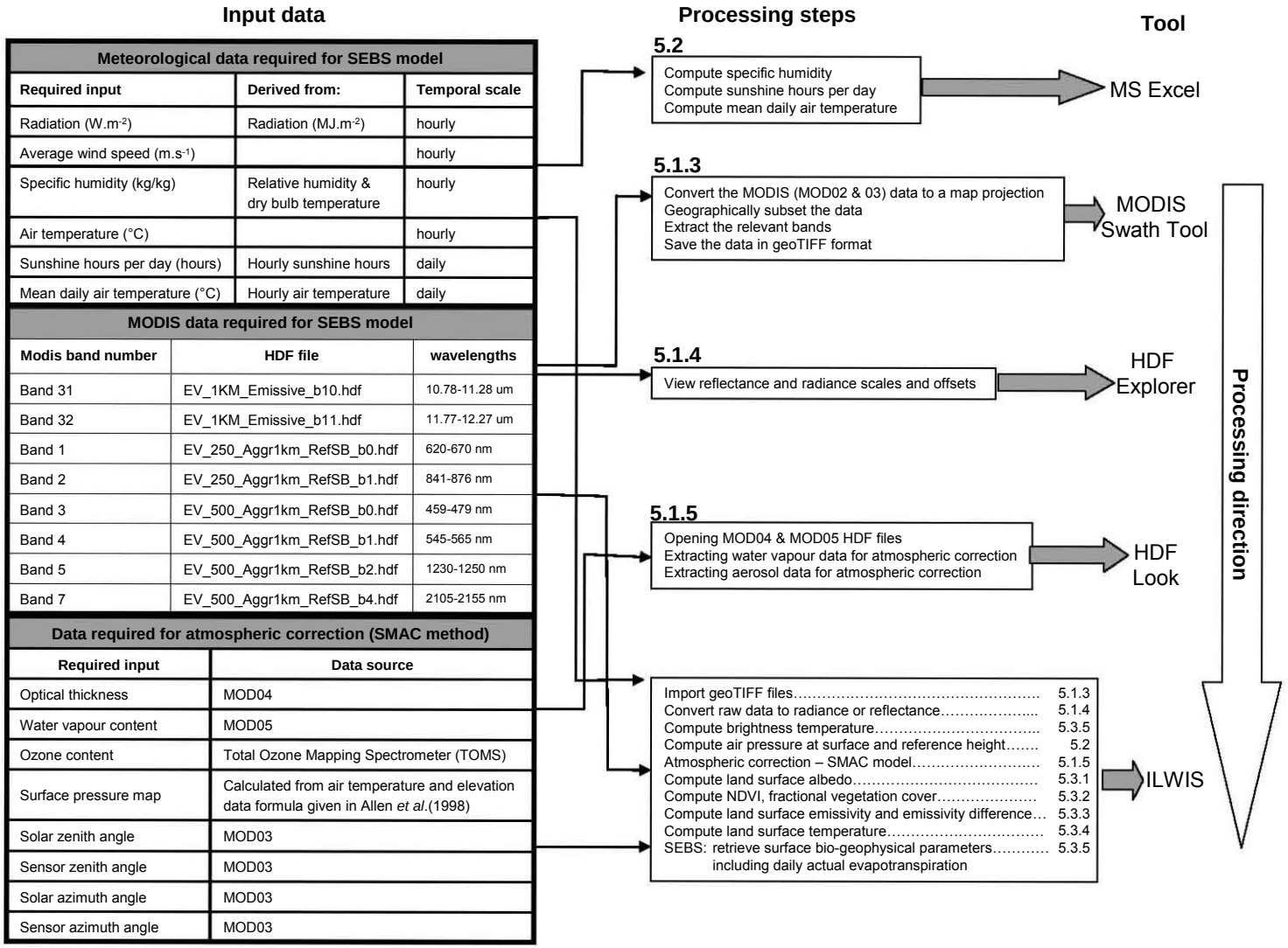

Figure 8: Input data, processing stages and tools required when using MOD 02 data in the SEBS model in ILWIS.

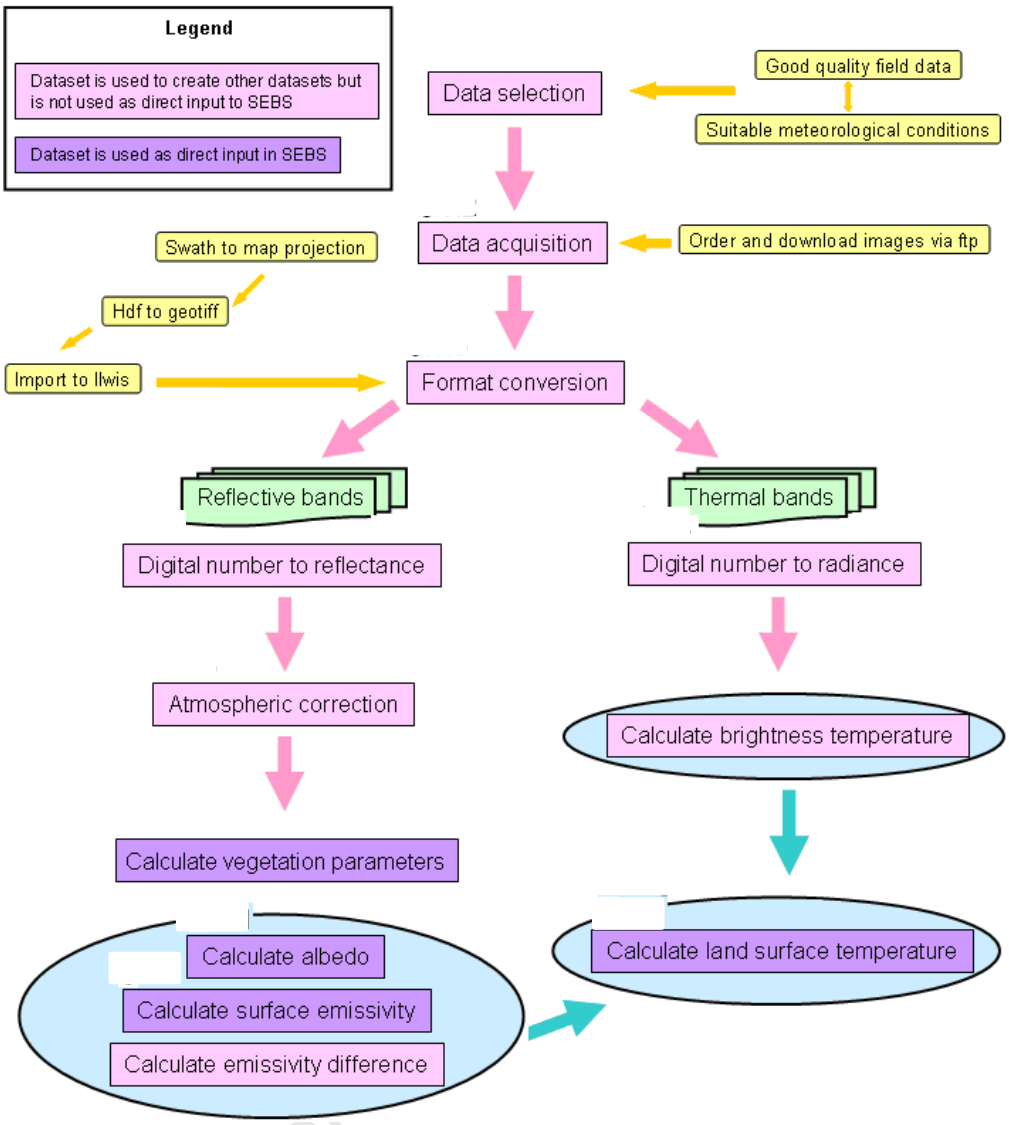

Figure 9: Flow diagram of remote sensing preprocessing steps when using MOD 02 data with numbers corresponding with section number in the text.

4.1.1. DATA SELECTION

Many of the methods (including SEBS) for estimating *ET* using remote sensing data rely on the use of land surface temperature derived from thermal infrared satellite data. Land surface temperature is the result of the equilibrium thermodynamic state dictated by the energy balance between the atmosphere, surface and subsurface soil and the efficiency by which the surface transmits radiant energy into the atmosphere (surface emissivity) (Schmugge *et al.*, 2002). Additionally, the reflectances measured by the

satellite are used to calculate other land surface parameters i.e. albedo and *NDVI* which are then used to respectively: empirically derive net radiation, and estimate other inputs for the calculation of the soil heat flux and the sensible heat flux. For this reason, a satellite sensor which captures electromagnetic radiation in the visible, near infrared and thermal infrared is critical in order to use a model such as SEBS.

A caveat in the research should be stated upfront. It was originally proposed that high resolution ASTER imagery would be used in combination with MODIS imagery. Due to cloud cover during the field validation period and in field instrument failure, only one ASTER image was available for the field validation period. Since there would be little value in using a single ASTER image, MODIS data alone was selected to correspond with the field validation period. With the benefit of hindsight it became apparent that due to study area heterogeneity and the coarse resolution of the MODIS pixel, despite the large size of the orchard, the SEBS results from the MODIS data represent a mixed pixel effect and not only the fluxes from the apple orchard itself. Despite the limitations to the research, it was still possible to obtain valuable insight into the workings of the SEBS model. The field validation data allowed the results from the SEBS model to be benchmarked if not directly compared and important conclusions and recommendations could be made regarding the use of the SEBS model in South Africa.

MODIS is a key instrument aboard both the TERRA (EOS AM) and AQUA (EOS PM) satellites, in orbit at 705 km above the earth. TERRA successfully launched on 18 December 1999 while AQUA was successfully launched on 4 May 2002 (http://modis.gsfc.nasa.gov/about/design.php). The direction of the satellites differ in that TERRA orbits the Earth, north to south, and it is timed to pass over the equator in the morning (10:30 am). AQUA orbits the Earth, south to north, and it is timed to pass over the equator in the afternoon (1:30 pm). Together, TERRA MODIS and AQUA MODIS view the entire Earth's surface every 1 to 2 days, acquiring data in 36 spectral bands (http://modis.gsfc.nasa.gov/about/). Further information on the MODIS instrument is given in Appendix 1.

During a field campaign conducted in the study area, the energy fluxes and total evaporation of an apple orchard were measured by the Council for Scientific and Industrial Research (Jarmain & Mengistu, 2011). A one-sensor type eddy covariance system was used to collect the data from 7 November to 1 December 2008. Due to sensor problems, good quality data was only available from 10 to 21 November

2008 (day of year (DOY) 315 to 326) (Jarmain & Mengistu, 2011). It is unfortunate that some of the days for which good quality field data was captured were cloudy and rainy thereby reducing the number of days that could be used to validate the results of this research. This is shown in Figure 10 and Figure 11 where true colour MODIS TERRA and AQUA images are displayed illustrating the extent of the cloud cover over the period for which good quality field data was obtained. The days with favourable meteorological conditions for this research which corresponded to days where good quality field data was captured were reduced to only nine days (DOY 315, 319 – 326) out of the anticipated one month and are indicated in Figure 10 and Figure 11 by the green box around the day of year (DOY). The dates for MODIS data selection therefore corresponded days with clear sky conditions where good quality field data was obtained.

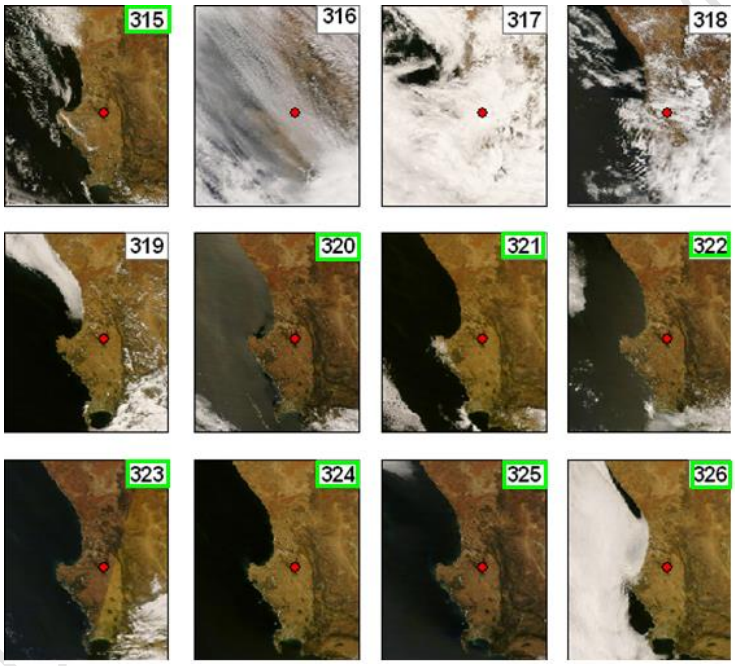

Figure 10: MODIS TERRA true colour images for the dates corresponding to good quality field data. Day of year and the location of the field validation site are shown in each image[9].

[9] Data available at: http://rapidfire.sci.gsfc.nasa.gov/subsets/?subset=SBenguela

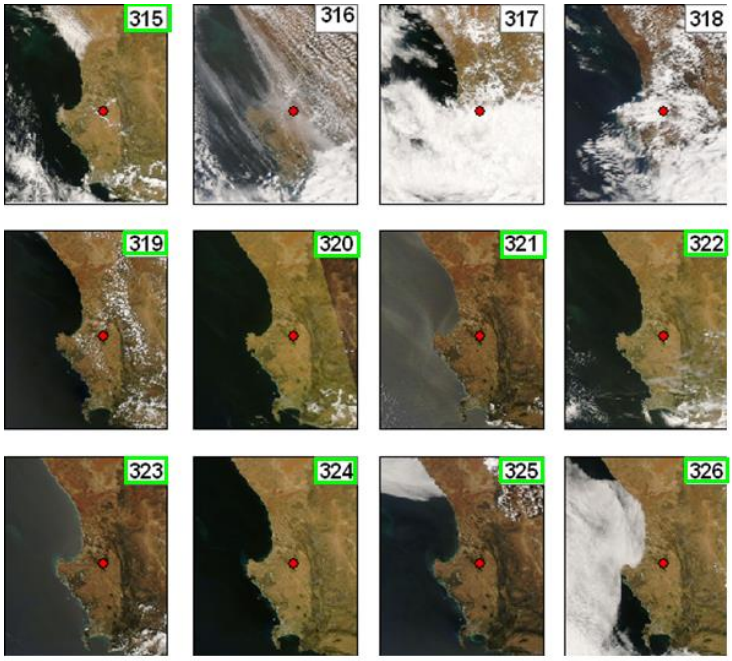

Figure 11: MODIS AQUA true colour images for the dates corresponding to good quality field data. Day of year and the location of the field validation site are shown in each image[8].

4.1.2. DATA ACQUISITION

MODIS reflectance and radiance bands are required for the SEBS model and were selected for clear sky days which corresponded to dates for which field validation data was available. The required data, the scientific data contained within each dataset and where they are used in the methodology are illustrated in the flow diagram in Figure 8. Further information on the datasets is contained in Appendix 1, including the MOD 02 and MYD 02 files which were selected and downloaded.

4.1.3. DATA TRANSFORMATION

The MODIS Swath Tool (MST) is used to process the MOD 02 and MOD 03 hdf files. First of all the images were converted to a map projection, then to geographically subset the image, extract the relevant bands and finally save the image in geoTIFF format (further information is given in Appendix 1). Not all 86 bands contained within the hdf are required for evapotranspiration estimation

so the MST is used to extract the relevant eight bands (Table 6). The data is finally imported into ILWIS and saved in the ILWIS file format. All processing from this point on is carried out in ILWIS using functions, the command line or scripts.

Table 6: MODIS bands required for evapotranspiration estimation.

Band name in hdf format	**MODIS band number**
EV_1KM_Emissive_b10	B31
EV_1KM_Emissive_b11	B32
EV_250_Aggr1km_RefSB_b0	B1
EV_250_Aggr1km_RefSB_b1	B2
EV_500_Aggr1km_RefSB_b0	B3
EV_500_Aggr1km_RefSB_b1	B4
EV_500_Aggr1km_RefSB_b2	B5
EV_500_Aggr1km_RefSB_b4	B7

4.1.4. CONVERTING TO RADIANCE AND REFLECTANCE

The data in the original hdf is recorded in digital numbers (DN). The data for each band must be converted to reflectance (bands 1 -5, 7) or radiance (bands 31 & 32) in order to be of use in quantitative remote sensing studies. For MODIS Level 1B data, the reflectance scales and reflectance offsets are computed from the calibration parameters in such a way that the reflectance product can be found directly from the digital numbers (Toller & Isaacman, 2002).

$$\text{Re}\,flec\,\text{tan}ce = reflec\,\text{tan}ce\_scale\left(DN - reflec\,\text{tan}ce\_offset\right) \quad [20]$$

Similarly, reflectance values can be calculated for the thermal bands using radiance scale and offset values.

$$Radiance = radiance\_scale(DN - radiance\_offset) \quad [21]$$

4.1.5. ATMOSPHERIC CORRECTION

The accurate retrieval of surface reflectance and temperature is very important in deriving land surface biophysical parameters and in determination of fluxes. In mapping the surface physical properties, the surface information is highly affected by atmospheric components (scattering by aerosols and absorption by gases, such as oxygen, water vapour and ozone) and their magnitude (Hailegiorgis, 2006). The simplified method for atmospheric correction (SMAC) proposed by Rahman & Dedieu (1994) has been programmed into ILWIS to correct for the effects of the atmosphere on MODIS visible, near infrared and shortwave infrared data. SMAC is a radiative transfer model and therefore requires a description of the components in the atmospheric profile in order to correct for these effects. The required inputs into SMAC are shown in Table 7 along with the unit of measurement, the valid range and the source of the data.

Table 7: Inputs required for SMAC.

General Requirement	**Specific requirement**	**Source**
Band-by-band top of atmospheric reflectance	Each spectral band measured in reflectance	MOD 02 with digital numbers converted to reflectance
Coefficient file for the sensor	MODIS file	http://www.cesbio.ups-tlse.fr/fr/serveurs4.htm and loaded in Ilwis
Atmospheric parameters:	optical thickness (nm)	MOD 04 http://ladsweb.nascom.nasa.gov/data/search.html.
	Water vapour content ($g.cm^{-2}$)	MOD 05 http://ladsweb.nascom.nasa.gov/data/search.html.
	Ozone content (g.atm.cm)	Total Ozone Mapping Spectrometer (TOMS) http://toms.gsfc.nasa.gov/
Surface pressure	(hPa)	Empirical formula (Allen, 1998) and DEM from MOD 03
Sun/satellite angle data:	Solar zenith angle (degrees)	MOD 03 scaled using 0.01 scale factor
	Solar azimuth angle (degrees)	MOD 03 scaled using 0.01 scale factor
	Sensor zenith angle (degrees)	MOD 03 scaled using 0.01 scale factor
	Sensor azimuth angle (degrees)	MOD 03 scaled using 0.01 scale factor

Each of the reflective bands (bands 1- 5, 7) is atmospherically corrected using SMAC. There are many pixels of missing data in the MOD 04 and MOD 05 products so to overcome this, mean values across the

study area are used for MOD 05. A default optical depth value of 0.05 was used for each image based on the findings of Gibson *et al*. (2009), where for the same study area, over an entire year (30 images), the mean aerosol optical depth from MOD 04, exceeded 0.05 on only three occasions.

4.2. METEOROLOGICAL CALCULATIONS

It has already been stated in Chapter 2 that SEBS is a scale independent model proposed by Su (2002) for the estimation of atmospheric turbulent fluxes and evaporative fraction using satellite earth observation data in combination with meteorological information. The meteorological inputs required in SEBS are radiation[10] ($W.m^{-2}$), temperature[10 & 11] (°C), air pressure[10] (Pa) at surface and at reference height, specific humidity[10] ($kg.kg^{-1}$) wind speed[10] ($m.s^{-1}$) at reference height and sunshine duration[10] (hours). This data can all be obtained directly from automatic weather stations (AWS) or indirectly using empirical formulae and data from the AWS. Hourly recordings from the Mouton's Valley AWS (ideal because of its on site location) were made available for this research.

The satellite images were not all captured at exactly the same time every day. The time had to be converted from Universal Time (UT) to local time by adding 2 hours. The local time was used to select the appropriate meteorological record by using the data that was collected at the same time as the satellite image was captured. For example, if an image was captured at 10:30 am local time, the meteorological data recorded at 11 am will be used as that is most representative of the weather conditions at the time of satellite image capture since it is the average weather conditions of the previous hour which is recorded at the weather station.

The units which are recorded at the AWS are not necessarily in the units which are required in the SEBS model and the following data conversions are performed:

1) Radiation data from MJ to $W.m^{-2}$ using: MJ = 277.777 $W.m^{-2}$

[10] Instantaneous i.e. hourly average at time of satellite overpass

[11] Daily average

2) Average daily temperature (°C) by summing the hourly values for the 24 hour period (calendar date) and averaging for the day.

3) Air pressure (P) at the surface and reference height (height of the AWS) using dry bulb temperature, elevation and the formula given by Burman *et al.* (1987) cited in Allen *et al.* (1998)

$$P = P_0\left(\frac{T_{Ko} - \alpha_1(z - z_0)}{T_{K0}}\right)^{\alpha_1 R} \quad [22]$$

where P is atmospheric pressure at elevation z (kPa), P_0 is atmospheric pressure at sea level (101.3 kPa), z is elevation (m), z_0 elevation at reference level (m), g is gravitational acceleration = 9.807 (m.s^{-2}), R is the specific gas constant (287 J.kg^{-1}.K^{-1}), a_1 is the constant lapse rate moist air (0.0065 K.m^{-1}), T_{K0} is the reference temperature (K) at elevation z_0 given by T_{K0} = 273.16 + T where T is the mean air temperature for the time period of calculation (°C)

4) Specific humidity (kg.kg^{-1} using a conversion formula (courtesy ARC-ISCW) with dry bulb temperature and relative humidity as inputs.

5) Daily sunshine duration (hours) by summing the hourly values for the 24 hour period (calendar date).

4.3. SEBS CALCULATIONS

The remote sensing inputs for the SEBS model will be described followed by the energy flux and *ET* calculations within the SEBS model. Remote sensing inputs to the SEBS model are calculated from MODIS reflectance bands and the flow of the methodology can be tracked using Figure 8 and Figure 9 as a guide: albedo (Chapter 4.3.1), vegetation parameters (Chapter 4.3.2) and emissivity (Chapter 4.3.2), and thermal bands: land surface temperature (Chapter 4.3.4).

4.3.1. ALBEDO

Land surface albedo (α) is determined using the narrow to broadband albedo MODIS specific calculation formulated by Liang (2001).

$$\alpha = 0.160\alpha_1 + 0.291\alpha_2 + 0.243\alpha_3 + 0.116\alpha_4 + 0.112\alpha_5 + 0.081\alpha_7 - 0.0015 \quad [23]$$

where α_1, α_2, α_3, α_4, α_5 and α_7 are surface reflectance derived from MODIS bands 1- 5 & 7.

4.3.2. VEGETATION PARAMETERS

The required vegetation parameters for SEBS are the *NDVI*, proportion of vegetation (used to assign surface emissivity values) and fractional vegetation cover. The *NDVI* is defined as:

$$NDVI = \frac{NIR - R}{NIR + R} \quad [24]$$

where *NIR* is the near infrared reflectance and *R* is the visible red reflectance (Mather, 1999).

In the version of the SEBS model used in this research, when using MODIS data, proportional vegetation cover is calculated according to the formula which Sobrino & El Kharraz (2003) derived from Carlson & Ripley's (1997) fractional vegetation cover formula.

$$P_v = \frac{(NDVI - NDVI_{\min})^2}{(NDVI_{\max} - NDVI_{\min})^2} \quad [25]$$

where $NDVI_{min}$ is taken to be 0.2 and $NDVI_{max}$ is taken to be 0.5.

$$f_c = \frac{(NDVI - NDVI_{\min})^2}{(NDVI_{\max} - NDVI_{\min})^2} \quad [26]$$

where $NDVI_{min}$ is taken to be 0.2 and $NDVI_{max}$ is taken to be the lowest NDVI value calculated for field validation site for the study period. The apple orchard is reported as having 75% canopy cover in the form of apple trees and the inter-row areas are planted with grass (Jarmain & Mengistu, 2011). This should equate to a full vegetation cover and hence the assignment of the lowest *NDVI* value for the study period to equal $NDVI_{max}$., in order to force the fractional vegetation cover to equal 1. [12]

4.3.3. SURFACE EMISSIVITY

The land surface emissivity and the emissivity difference are calculated by considering the NDVI value for individual pixels. The *NDVI* value is used to distinguish between bare soil pixels, mixed pixels and vegetated pixels and emissivity is calculated accordingly (Sobrino & El Kharraz, 2003). Albedo of less than 0.035 is used to identify water pixels and a constant emissivity of 0.995 is assigned.

1. Bare soil pixels are identified where *NDVI* < 0.2, then

$$Emissivity = 0.9825 - 0.051 * \alpha_1$$

$$Emissivitydifference = -0.0001 - 0.041 * \alpha_{red}$$

[12] The calculation of f_c is explored later in the thesis (Chapter 6.3.2),

2. Vegetation pixels are identified where *NDVI* > 0.5

   Emissivity = 0.990

   Emissivity difference = 0

3. Mixed pixels are identified where 0.2 =< *NDVI* <= 0.5

$$Emissivity = 0.997 - 0.018 * Pv$$

$$Emissivitydifference = 0.006 * (1 - Pv)) \quad [27]$$

4.3.4. LAND SURFACE TEMPERATURE

The brightness (blackbody) temperatures of bands 31 & 32 are one of the inputs needed in the calculation of land surface temperature. The radiance values of bands 31 & 32 are converted to brightness temperature by applying Plank's equation.

The land surface temperature (T_0) is calculated with brightness temperatures, surface emissivity, emissivity difference, and water vapour content using a split window method (Sobrino & Raissouni, 2000) in application to MODIS data in the SEBS model. The split window method makes use of the observation that the transmission of a path through a moist atmosphere at one wavelength is closely correlated with the transmission through the same path at a second nearby wavelength (Batatia & Bessaih, 2009).

$$T_0 = btm_2 + (1.97 + 0.2 * W) * (btm_2 - btm_1) - (0.26 - 0.08 * W) * \sqrt{btm_2 - btm_1} + (0.2 - 0.67 * W) + (64.5 - 7.35 * W) * (1 - \varepsilon) - (110 - 20.4 * W) * d\varepsilon \quad [28]$$

where btm_1 is brightness temperature for MODIS band 31, btm_2 is brightness temperature for MODIS band 32, W is water vapour content, ε is surface emissivity and $d\varepsilon$ is surface emissivity difference. If the water vapour content of the atmosphere is not known, it can be estimated using the formula by Li *et al.* (2003).

$$W = 13.73 - 13.66 \tau_{12} / \tau_{11} \qquad [29]$$

where τ_{12}/τ_{11} is the ratio of the two split-window channel transmittance from bands 31 and 32 respectively in the case of MODIS (Mao *et al.*, 2005).

4.3.5. ENERGY FLUX AND ET CALCULATIONS

Following the data preparation and preprocessing, the data is input into the SEBS model (Figure 12) and run for each MODIS dataset. For this research, this entailed repeating the process 18 times (nine times for MOD02 and nine times for MYD 02). It can be seen in Figure 12 that it is possible to include land use maps with associated surface roughness, canopy height and displacement height but where these data sets are not available these parameters can be modelled within the SEBS algorithm using Equations [9], [10] & [11]. This approach was taken in this research.

The instantaneous energy fluxes calculated in the SEBS model include: the soil heat flux (Equation [3]), sensible heat flux at the wet limit (Equation [4]), sensible heat flux at the dry limit (Equation [5]), sensible heat flux (Equations [4] – [8]), latent energy flux (Equation [17]), net radiation (Equation [2]), evaporative fraction (Equation [17]) and relative evaporation (Equation [16]). The single daily flux output is daily actual evaporation (Equation [18]).

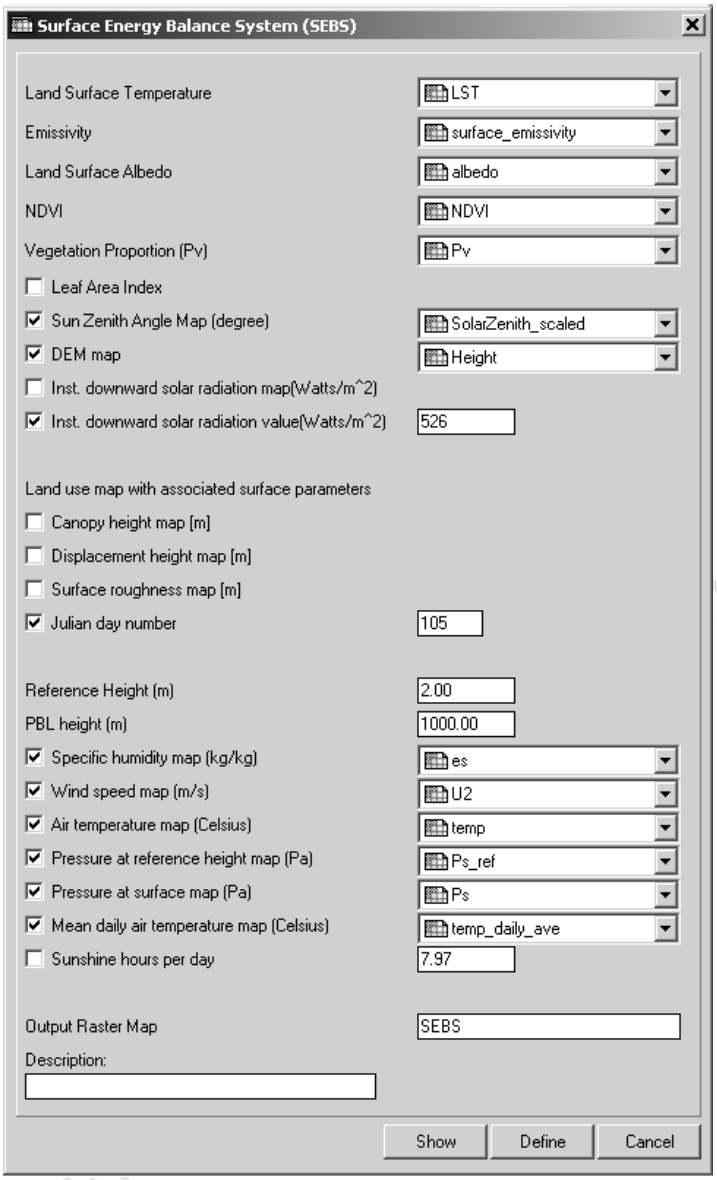

Figure 12: Example of the SEBS form in ILWIS showing all the required input data.

5. RESULTS

The meteorological conditions and calculated meteorological input parameters required for the SEBS model will be briefly presented (Chapter 5.1). This will be followed by the results of the remote sensing input parameters (Chapter 5.2) which are: albedo (Chapter 5.2.1), vegetation parameters (Chapter 5.2.2) and land surface temperature (Chapter 5.2.3). Finally the results of the energy balance and daily actual evaporation will be presented (Chapter 5.3) – net radiation (Chapter 5.3.1), soil heat flux (Chapter 5.3.2), sensible heat flux (Chapter 5.3.3), and latent heat flux (Chapter 5.3.4)

5.1. METEOROLOGY

The meteorological data was selected according to the criteria specified in the methodology, the conversions to appropriate units were carried out and the required daily calculations were done. This was done to correspond with each image capture and the results of these calculations and all meteorological data used in this research are tabulated in Table 8.

It can be seen in Figure 13a that downward shortwave radiation is higher for TERRA overpass than for AQUA overpass which can be attributed to the fact that the TERRA images are captured closer to solar noon than the AQUA images (Figure 13b). The marked fluctuation within the TERRA overpass and within the AQUA overpass radiation results is due to the fluctuation in image capture time as is shown in Figure 13b. As expected, the air temperature is higher at AQUA overpass than at TERRA overpass (Figure 13c) due to the lag effect. Also, the wind speed is higher in the afternoon than in the morning so at AQUA overpass higher wind speeds are recorded than at TERRA overpass (Figure 13d). The relative humidity is higher at TERRA overpass than at AQUA overpass (Figure 13e), however when specific humidity is examined (Figure 13f), it can be seen that the results at TERRA and AQUA overpass times are similar. This is due to air temperature being used in the specific humidity calculation and since the air temperature is higher at AQUA overpass than TERRA overpass this results in similar specific humidity despite the differences in relative humidity.

Table 8: Meteorological recordings and calculations at image capture time.

DOY	*Sensor overhead*	*Local Time*	*Radiation W.m^{-2}*	*Temperature °C*	*Windspeed m.s^{-1}*	*Specific humidity*	*Daily average temperature °C*	*Daily sunshine*
315	*TERRA*	11:00	866.66	19.45	1.6	0.009	15.27	10.6
	AQUA	16:00	550	22.94	2	0.008		
319	*AQUA*	15:00	816.66	24.91	1.7	0.009	18.17	9.61
320	*TERRA*	12:00	961.11	24.35	1.2	0.009	18.26	10.7
	AQUA	16:00	625	25.45	1.7	0.009		
321	*TERRA*	11:00	886.11	22.09	1.4	0.009	17.68	10.9
	AQUA	15:00	800	23.25	1.8	0.009		
322	*TERRA*	11:00	863.89	18.46	1.7	0.008	15.66	10.6
	AQUA	16:00	619	22.12	2.1	0.008		
323	*TERRA*	12:00	955.55	22.66	1.4	0.008	19.14	10.8
	AQUA	15:00	791.66	25.97	1.4	0.007		
324	*TERRA*	11:00	877.78	27.66	1.2	0.007	23.62	10.9
	AQUA	16:00	633.33	31.02	1.4	0.008		
325	*TERRA*	12:00	950	33.16	1.1	0.008	23.83	10.8
	AQUA	15:00	780.55	35.02	1.4	0.009		
326	*TERRA*	11:00	855.55	23.15	1.6	0.011	19.07	10.6
	AQUA	15:00	800	27.76	1.7	0.010		

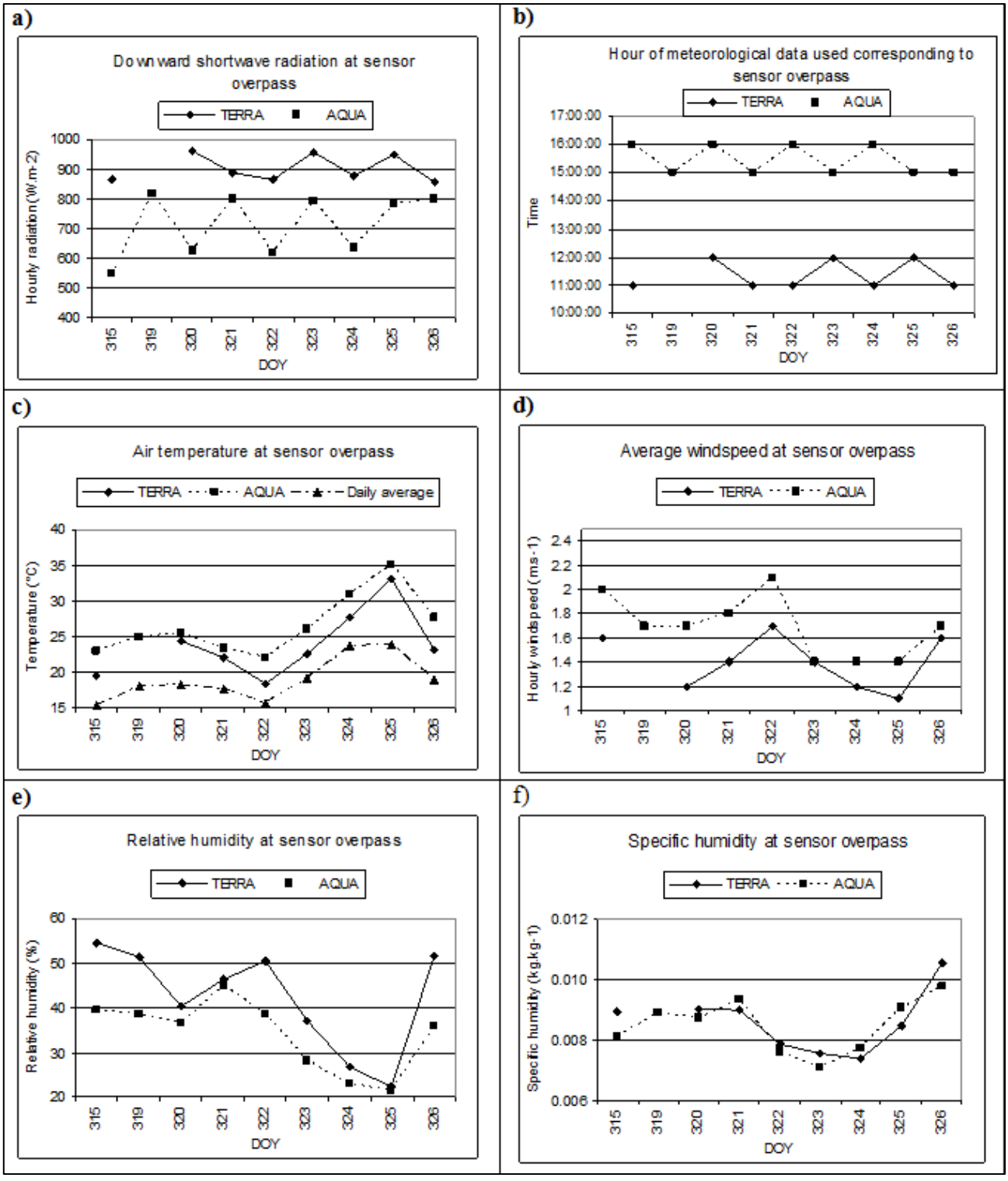

Figure 13: Comparison of meteorological measurements and calculations at image capture time.

At 1km resolution, no single complete pixel was contained within the apple orchard where the field validation took place but rather four pixels were partially contained within the orchard. The pixel value used for the validation was the pixel with the largest proportion contained within the orchard and also directly on the site of the field validation equipment. It was shown in Figure 7 that the pixel footprint of a MODIS scene for this area at 1 km resolution exceeds the boundaries of the orchard in which the field validation is taking place, Multiple tree crops (apples, oranges, peaches, nectarines and pears, (Figure 3) and the west facing slope of Levant Hill with natural vegetation all are contained within the 1 km pixel resolution. For this reason, it is expected that the results obtained from the SEBS model will represent this multitude of land covers and not exclusively represent the evapotranspiration of the apple orchard where the field validation was conducted. The parameters required for SEBS were calculated from each of the TERRA and AQUA datasets as per the prescribed methodology. The results of these calculations extracted for the field validation site are shown in Table 9.

Table 9: MODIS TERRA and AQUA pre-processing results.

DOY	SENSOR	LOCAL TIME	SOLAR ZENITH	SENSOR ZENITH	ALBEDO	EMISSIVITY	NDVI	fc	T_0 (K)
315	TERRA	10:50	27	3	0.11	0.99	0.54	1	301.1
	AQUA	15:10	40	46	0.11	0.99	0.53	1	302.6
319	AQUA	14:45	34	7	0.08	0.99	0.60	1	300.2
320	TERRA	11:10	23	32	0.08	0.99	0.60	1	299.7
	AQUA	15:30	43	62	0.10	0.99	0.63	1	299.6
321	TERRA	10:15	33	56	0.11	0.99	0.59	1	299.3
	AQUA	14:35	31	18	0.08	0.99	0.59	1	302.2
322	TERRA	10:55	25	10	0.11	0.99	0.53	1	297.9
	AQUA	15:15	40	52	0.12	0.99	0.57	1	298.1
323	TERRA	11:40	17	64	0.08	0.99	0.63	1	295.4
	AQUA	14:20	28	38	0.07	0.99	0.62	1	301.7
324	TERRA	10:45	27	15	0.12	0.99	0.56	1	304.9
	AQUA	15:05	37	38	0.11	0.99	0.60	1	307.3
325	TERRA	11:25	19	54	0.08	0.99	0.57	1	303.9
	AQUA	14:10	26	53	0.08	0.99	0.63	1	305.8
326	TERRA	10:30	29	36	0.12	0.99	0.58	1	302.4
	AQUA	14:50	34	19	0.09	0.99	0.53	1	306.8

By examining results in Table 9, a number of observations can be made and the results for each remote sensing parameter will be discussed further under the appropriate section:

1 There is a high variation in sensor zenith angle (from 3 to 64°) and to a lesser extent in solar zenith angle (from 17 to 43°)

2 There is a fluctuation in albedo from 0.07 to 0.12

3 NDVI ranges from 0.53 to 0.63

4 Fractional vegetation cover remains a constant 1

5 Emissivity remains a constant 0.99

6 Land surface temperature a) T_0 fluctuates from 295.4K – 307.3K, a range of 11.9K b) T_0 almost always higher in afternoon than in the morning and c) the fluctuation in T_0 from TERRA overpass to AQUA overpass ranges from -0.1 to 4.4 K

It is usual to consider the sensor zenith angle when selecting appropriate satellite images with low sensor zenith angles recommended. For example, Tasumi *et al.* (2008) noted that images having large view angles cause substantial smearing of the final product (with reference to the 16-day MODIS albedo product) so that the effective resolution increases from the assumed 1 km pixel resolution to around 2 – 3 km in reality. However due to the short period for which field validation data was available, this was not considered and all cloud free images corresponding to good quality field data were used in this research. It can be seen in Figure 14a that the sensor zenith angle for the field validation site ranges from 3 to 64° for TERRA and from 7 to 62° for AQUA; with TERRA generally having lower sensor zenith angles for the period of the field campaign. The solar zenith angle (Figure 14b) is directly dependent on the time at which the image was captured and since TERRA overpass is generally closer to solar noon, the solar zenith angles reflect this.

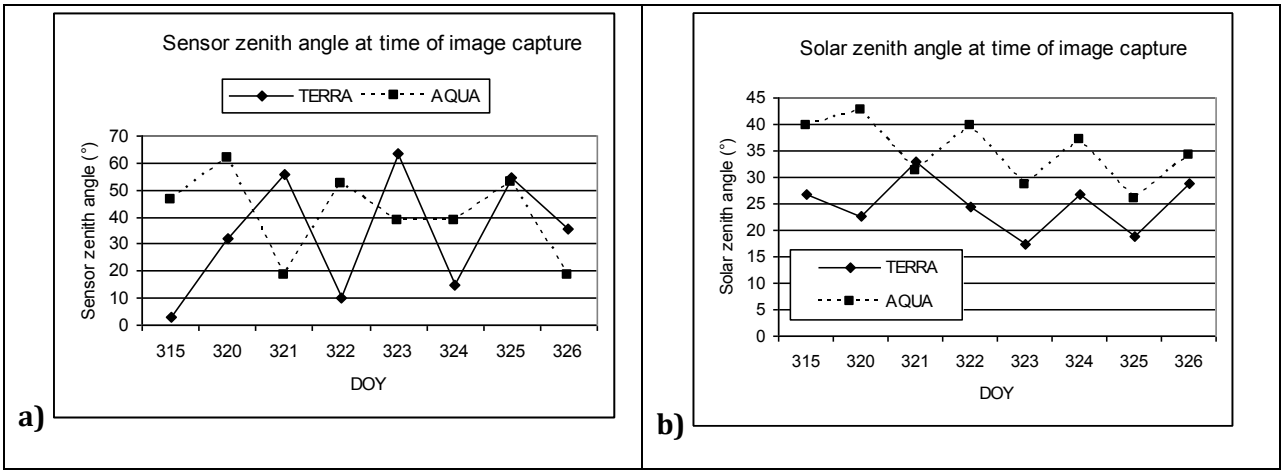

Figure 14: Sensor (a) and solar (b) zenith angles at time of image capture.

5.2.1. ALBEDO

The calculated albedo for the period ranged from 0.07 to 0.12 which is lower than anticipated when compared with literature values and it can be seen from Figure 15a and Figure 15b that sensor zenith angle alone does not influence the fluctuation in albedo calculation.

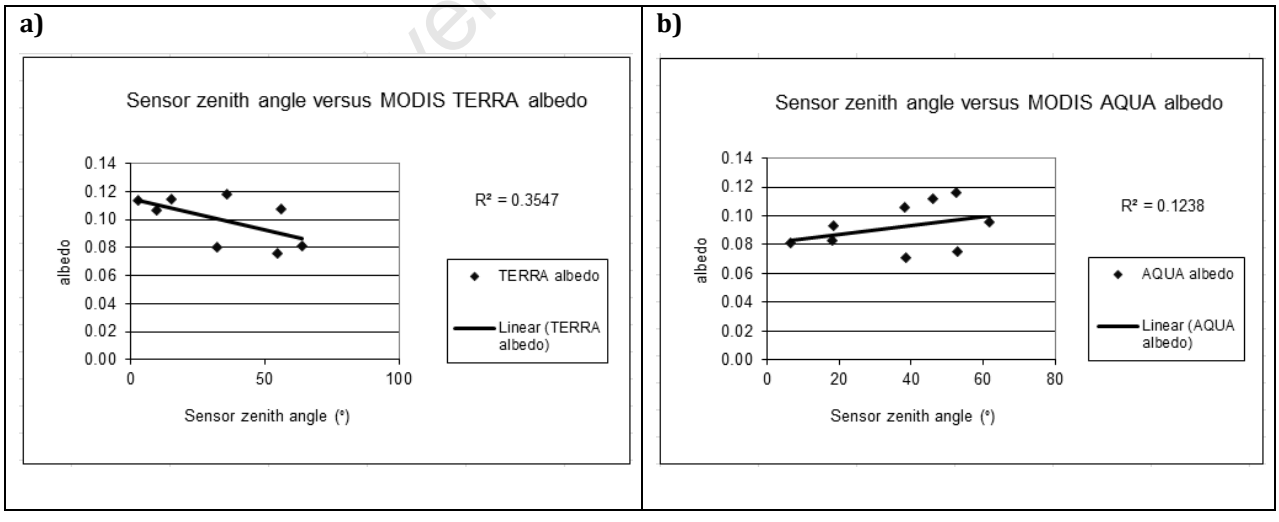

Figure 15: Sensor zenith angles against calculated albedo for a) TERRA results and b) AQUA results.

From Table 10 (Brutsaert, 1982) one would expect albedo values for the study area to be higher than 0.07 with possibly the highest value of 0.12 entering into the lower limit of expectations. It can be seen in Table 8 that albedo fluctuated from day to day and did not follow a pattern such that it decreased from beginning to end of the field campaign which may have been explained by a slight increase in canopy as the season progressed. Since the landscape can therefore be considered to have been largely unchanged for the short period of the field campaign, the solar and sensor zenith angles were investigated to see whether despite the atmospheric correction procedure, they may be influencing the albedo result.

Table 10: Selected typical albedo values (Brutsaert, 1982).

Nature of surface	**Albedo**
Deep water	0.04 – 0.08
Moist dark soils; ploughed fields	0.05 – 0.15
Gray soils; bare fields	0.15 – 0.25
Green grass and other short vegetation (e.g. alfalfa, potatoes, beets)	0.15 – 0.25
Dry grass; stubble	0.15 – 0.20
Deciduous forest	0.15 – 0.25
Fresh dry snow	0.80 -0.90

The effects of smearing in the albedo calculation (16-day MODIS albedo product) are reported to be most problematic when applied to individual agricultural fields or small land use areas (Tasumi *et al*., 2008). For this study, the effect of smearing at high sensor zenith angle will effectively increase the number of land covers which are used in the calculation of albedo and therefore decrease its accuracy although whether this will result in an increase or decrease in albedo, will be dependent on the land covers which are included.

Carrer *et al*. (2010) illustrated that in situations with vegetation above a non-bright soil, typical of many land covers, albedo decreases with the approach of local noon and then increases after local noon (Figure 16). Carrer *et al*. (2010) points out that the opposite scenario is also true where in sparse vegetation over a bright sandy soil typical of a semi-arid ecosystem; albedo creates a peak at local noon. The same trend in albedo around local noon has been observed in Figure 17a and in Figure 17b.

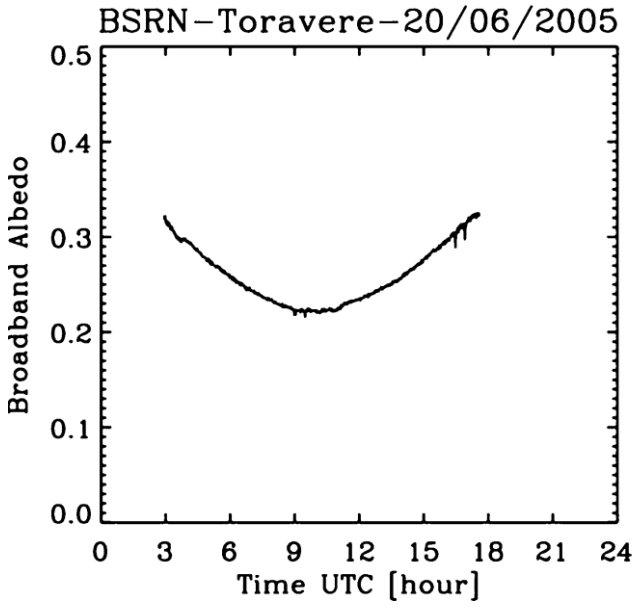

Figure 16: Fluctuation in albedo around local noon for a vegetated area over non-bright soil (Carrer *et al.*, 2010).

In Figure 17a and in Figure 17b it can be seen that solar zenith angle does appear to play a strong role in the calculation of albedo for each of the sensors individually. However, when taken together, the correlation weakens significantly (Figure 17c). This could also be because TERRA and AQUA should have opposite solar zenith angles (i.e. if TERRA is depicted as positive, then AQUA should be depicted as negative) due to be TERRA being in a descending orbit and AQUA being in an ascending orbit. However, all solar zenith angle data in MOD03 data are depicted as positive values.

The higher solar zenith angles corresponding to lower albedo particularly for TERRA images may be due to less illumination because of the steep topography of Levant Hill is only sunlit at higher solar zenith angles. This steep topography particularly to the east of the study area will have an influence on the results especially for TERRA images captured early in the day.

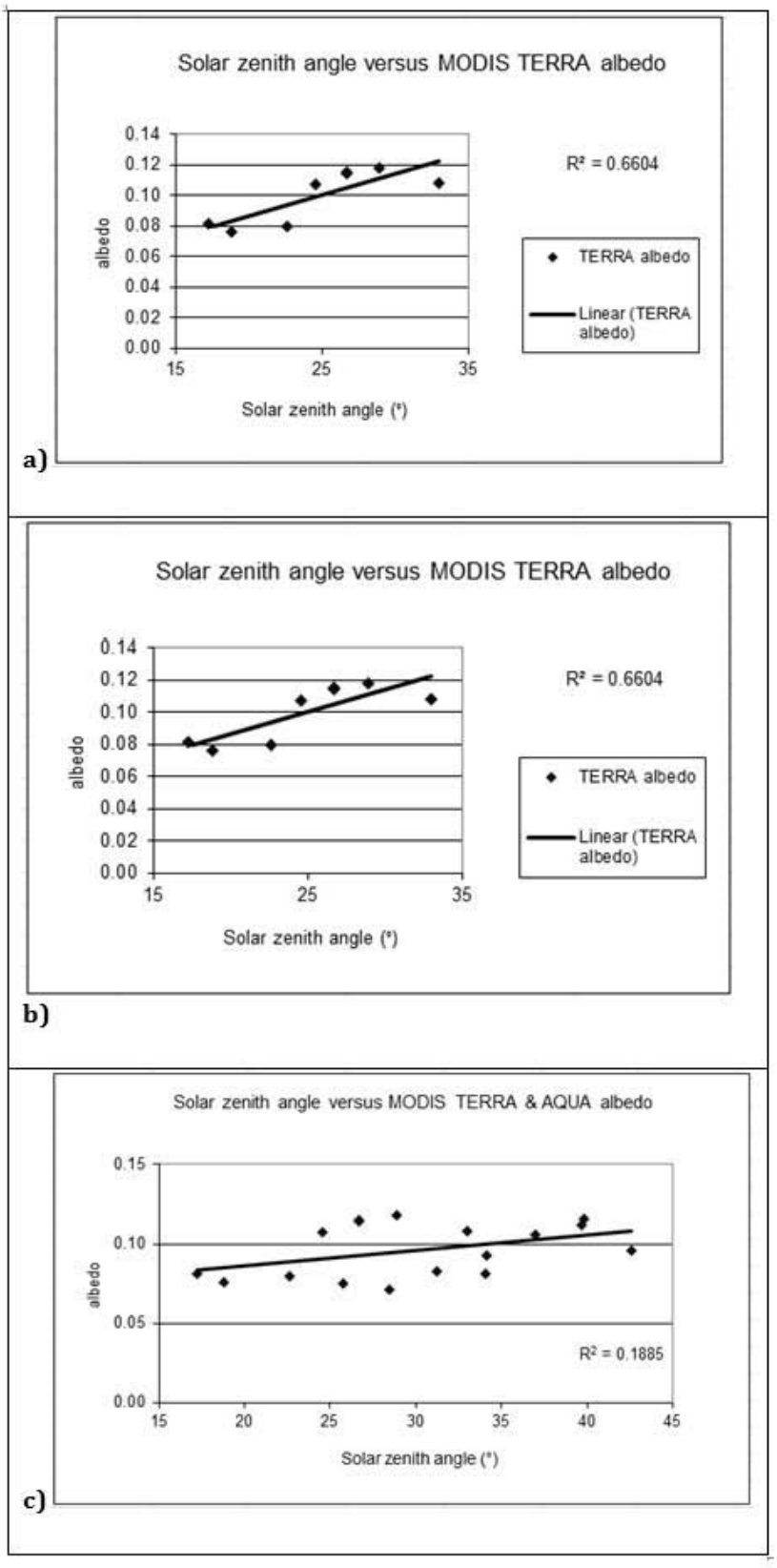

Figure 17: Solar zenith angles against calculated albedo.

Although the result of the albedo calculation does fluctuate for the study period, the question of whether or not this fluctuation is significant must be raised. The major use of albedo in the SEBS model is in the calculation of net radiation (Equation [2]). It is also used in the daily net radiation calculation (Equation [19]) and to a lesser in the estimation of surface emissivity (Equation [27]). To illustrate the sensitivity of the net radiation calculation to the fluctuation in albedo, the MODIS AQUA image for DOY 319 was used keeping all other inputs constant but changing the albedo value from between 0.07 – 0.15. It can be seen in Figure 18 that a fluctuation in albedo alone across this range can impact the calculation of instantaneous net radiation by ten percent. The effect of albedo on the daily *ET* result is shown later in Chapter 6.3.4.

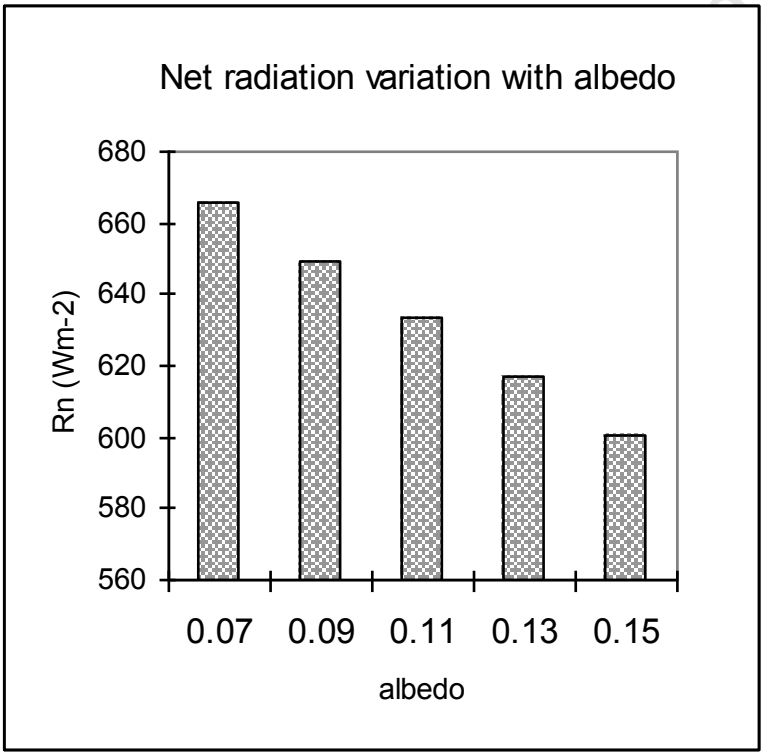

Figure 18: Net radiation calculated for DOY 319 using MODIS AQUA data keeping all variables constant but adjusting albedo values.

The sensitivity of the SEBS model to albedo with a focus specifically on the upscaling of evaporative fraction to daily *ET* is lacking in the literature as often the sensitivities to input parameters are determined by assessing the sensible heat flux results (such as Badola, 2009; Van der Kwast *et al.*, 2009).

5.2.2. VEGETATION PARAMETERS

As with albedo, the *NDVI* result (Figure 19) is neither constant for the study period nor does it show an upward trend which would reflect the end of the leaf-up period. It should be noted however that due to the short study period, a substantial variation in *NDVI* would not be expected unless a catastrophic event such as hail, disease or drought were to occur. The *NDVI* calculation typically yields lower results for TERRA data than with AQUA data. As with albedo, the reason for the fluctuation in this calculation may be due the shading effect of Levant Hill. However, the value of using a ratio such as *NDVI* is to minimize the effects of factors such as noise, topography or differences in illumination (Mather, 1999) which may be the reason why the *NDVI* fluctuations are less pronounced than the albedo calculation.

As with albedo, this fluctuation in *NDVI* may be due to uncertainties associated with the atmospheric correction process, the mixed pixel effect or smearing due to high sensor zenith angles. Although the MODIS pixels are geocorrect in that the pixels boundaries have the same location from one image to image, the instantaneous field of view will differ for each image depending on the sensor zenith angle. Therefore although the pixels have the same geolocation for each image captured, the land cover represented by that pixel will vary dependent on the view angle. The significance of this fluctuation in the SEBS model and how it will be propagated through the model should be examined. In SEBS, *NDVI* is used in the estimation of proportional vegetation (Equation [25]) fractional vegetation cover (Equation [26]) and emissivity (Equation [27]). Furthermore, if a land cover map with corresponding roughness heights is not used, then it is also used to determine these parameters (Equations [9] to [12]).

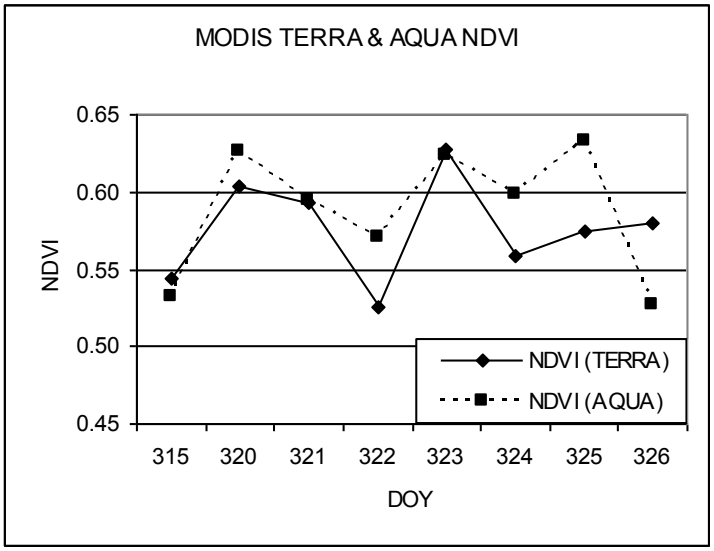

Figure 19: *NDVI* calculated using TERRA & AQUA data.

5.2.3. LAND SURFACE TEMPERATURE

The calculated T_0 for the period for the study area ranged from 295.4K – 307.3K (Table 9). T_0 is almost always calculated as being higher in the afternoon than in the morning (Figure 20) with the fluctuations in T_0 from TERRA overpass to AQUA overpass ranges from -0.1 to 4.4 K.

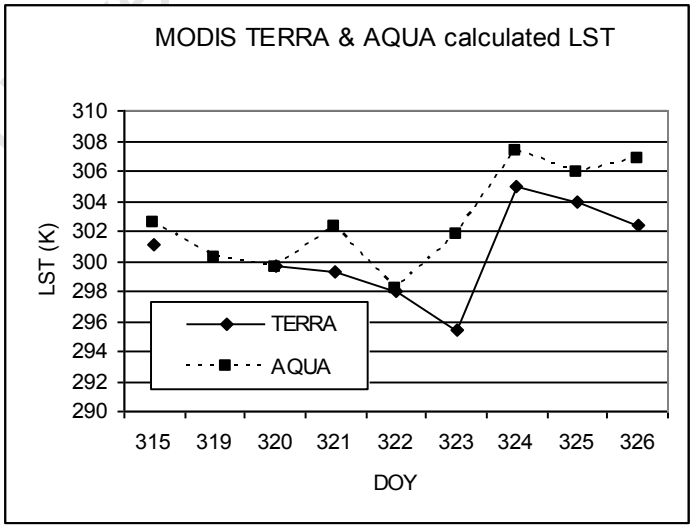

Figure 20: Land surface temperature calculated using TERRA & AQUA data.

The accuracy of the T_0 estimates in this research is difficult to assess as there is no surface validation data. However if the estimates are compared with the Meteosat SEVIRI T_0 data product corresponding to the same time of image acquisition, then a possible range in the T_0 estimates can be set. It must be noted that with a pixel resolution of approximately 3km, SEVIRI has a coarser resolution than MODIS. However, since it is geostationary, the view angle remains constant at each location and therefore comparisons from one image acquisition to the next can be made with the impact of view angle effects being excluded. The T_0 from Meteosat SEVIRI (SEVIRI/Meteosat LST Product: LSA-4 (MLST) Product version 7.2) corresponding to T_0 calculated for this research is shown in Table 11 and Figure 21.

Table 11: T_0 results from SEBS compared with the Meteosat SEVIRI T_0 product.

DOY	LOCAL TIME	SOLAR ZENITH ANGLE (°)	SENSOR ZENITH ANGLE (°)	MODIS SEBS T_0 (K)	SEVIRI T_0 (K)	T_0 DIFFERENCE (SEVIRI – MODIS) T_0 (K)
315	10:50	27	3	301.1	301.8	0.7
	15:10	40	46	302.6	304.7	2.1
319	14:45	34	7	300.2	302.9	2.7
320	11:10	23	32	299.7	304.0	4.3
	15:30	43	62	299.6	304.2	4.6
321	10:15	33	56	299.3	300.3	1.0
	14:35	31	18	302.2	305.0	2.8
322	10:55	25	10	297.9	301.3	3.4
	15:15	40	52	298.1	300.9	2.8
323	11:40	17	64	295.4	305.5	10.1
	14:20	28	38	301.7	308.8	7.1
324	10:45	27	15	304.9	311.2	6.3
	15:05	37	38	307.3	310.9	3.6
325	11:25	19	54	303.9	314.4	10.5
	14:10	26	53	305.8	316.3	10.5
326	10:30	29	36	302.4	305.9	3.5
	14:50	34	19	306.8	311.8	5.0

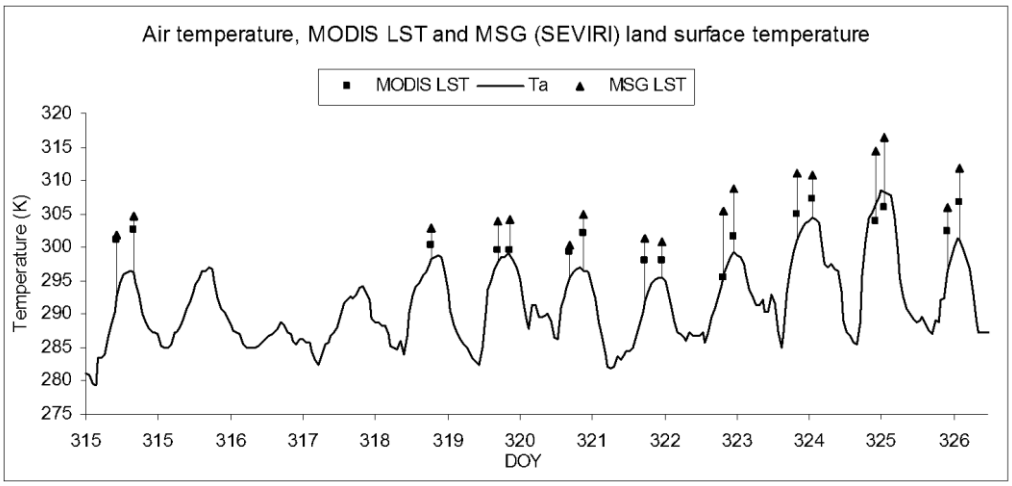

Figure 21: Air temperature (T_a) at image capture time plotted against land surface temperature (LST) obtained from MODIS and SEVIRI.

Kalma *et al*. (2008) state that atmospheric factors, surface emissivity and view angle effects lead to considerable uncertainty in the land surface temperature calculation. Madeira *et al.* (2005) reported that the best predictor of disagreement between the MODIS and SEVIRI estimates was the view angle of the MODIS data. Where there is a high MODIS view angle, Madeira *et al.* (2005) reported a high discrepancy between the MODIS and SEVIRI T_0 estimates, however, this trend is not apparent here (Figure 22). However, for MODIS level 1B data the corresponding geolocation files (MOD03) for solar and sensor zenith angle only indicate the angle from the zenith and not the direction, therefore the magnitude of the view angle is available but not the direction. This makes a true analysis of the effect of view angle difficult. If the MODIS T_0 data products are used instead of calculating the T_0 from the thermal bands using level 1B data, then the direction of the view angle is recorded such that a negative sign of the viewing angle means MODIS is viewing the grid from the east (Wan, 2006). Solar zenith angle also did not impact on the difference between the MODIS and SEVIRI estimates in this research (Figure 22). Finally, there was no notable difference between the performance of the TERRA and AQUA T_0 calculation when compared with the SEVIRI T_0 product. It is therefore surmised that, as put forward by Madiera *et al*. (2005), the resolution of the sensor instantaneous field of view together with the topography of the study area plays the largest role in the difference between the SEVIRI and MODIS results.

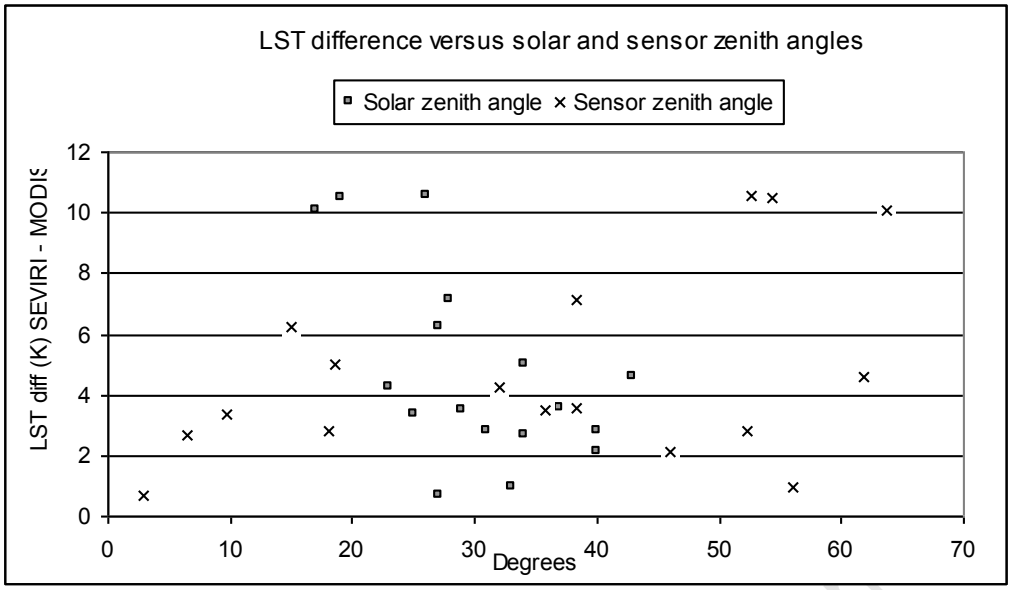

Figure 22: SEVIRI T_0 minus SEBS calculated T_0 from MODIS plotted against solar and sensor zenith angles showing no correlation between zenith angles and T_0.

5.3. ENERGY BALANCE AND EVAPOTRANSPIRATION RESULTS

The prepared meteorological and remotely sensed input data presented above was used to run the prepackaged SEBS model in ILWIS for each DOY for which TERRA and AQUA data were acquired. The results of the energy balance partitioning and the daily evapotranspiration are given in Table 12 with the field measured values given alongside for validation purposes. When examining Table 12, the following observations can be made:

1 SEBS calculated *ET* is higher than field measured values. SEBS calculated *ET* ranges from 6.0 – 8.2 mm/day whereas the field measured values range from 4.0 to 7.3 mm/day. Presented differently, the field measured values ranged from 55 – 96 % of the SEBS estimates.

2 Relative evaporation (Λ_r) is always equal to one implying that *ET* is taking place at its potential rate. The field measured daily *ET* ranged from 85 – 121 % of ET_0 and SEBS estimates of *ET* ranged from 116 – 154 % of ET_0.

3 Evaporative fraction (Λ) results differ from TERRA to AQUA. Λ is higher in the AQUA calculation by 5 – 10% when compared with the TERRA calculation and the link to the field measured value is tenuous.

4 Sensible heat flux (H) is always equal to the sensible heat flux at the wet limit (H_{wet}).

5 There is less variation in SEBS calculated G_0 than in the field measured G_0 value.

To objectively assess the results, the SEBS estimates are plotted against the field results together with lower and upper limits of 15 and 30 % error respectively (Figure 23). According to Kalma *et al* (2008) remote sensing estimates can be expected to be within 15 – 30 % of field measured values so SEBS values falling within this range can be viewed as falling within expected accuracies. From Figure 23 it can be seen that out of the 15 SEBS ET estimates, three estimates fall within the 15 % accuracy range, another three fall within the 30 % accuracy range with the remaining nine estimates falling outside the 30 % accuracy range.

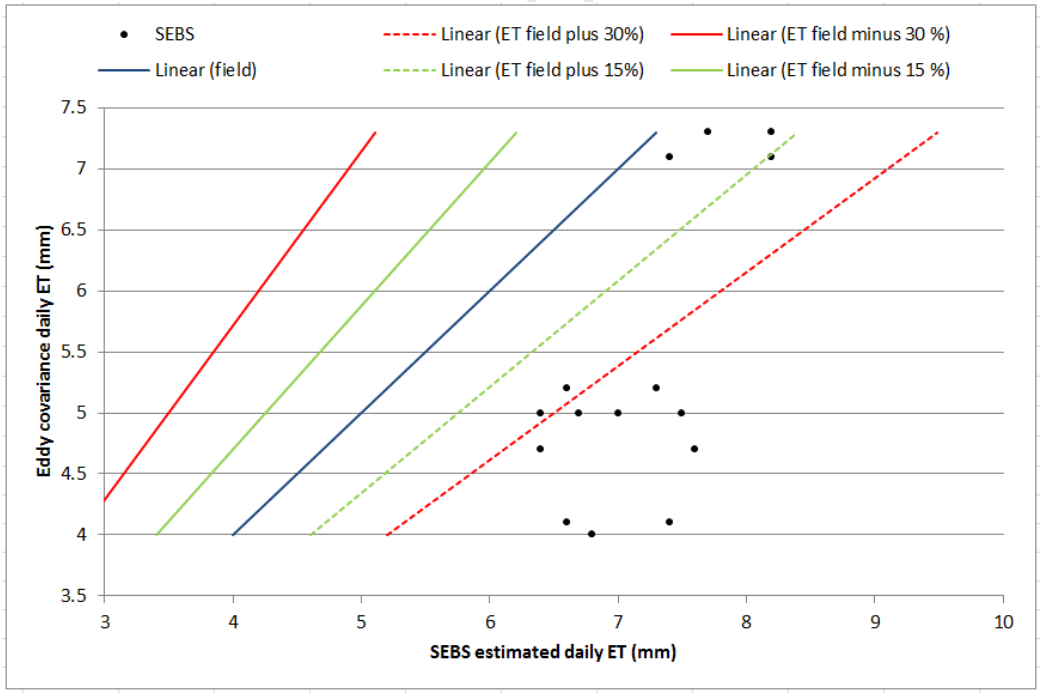

Figure 23: SEBS *ET* plotted against field measured *ET* plus and minus a 30 % error.

Table 12: MODIS AQUA & TERRA energy balance results and corresponding field measurements (# = no data).

DOY	SENSOR	R_n SEBS	R_n field	G_0 SEBS	G_0 field	H_{dry} SEBS	H SEBS	H field	H_{wet} SEBS	λE SEBS	λE field	Λ SEBS	Λ field	Λ_r SEBS	ET_{daily} SEBS	ET_{daily} field	ET0
315	TERRA	631	703	32	85	600	92	339	92	507	278	0.85	0.45	1	6.6	4.1	4.8
	AQUA	366	520	18	75	347	28	223	28	319	222	0.92	0.5	1	7.4	4.1	4.8
319	TERRA	#	#	#	#	#	#	#	#	#	#	#	#	#	#	#	
	AQUA	657	649	33	61	624	98	147	98	526	442	0.84	0.75	1	6.8	4.0	
320	TERRA	758	764	38	121	720	130	218	130	590	425	0.82	0.66	1	6.6	5.2	5.4
	AQUA	479	530	24	73	455	63	144	63	392	313	0.86	0.69	1	7.3	5.2	5.4
321	TERRA	682	673	34	97	648	120	101	120	528	476	0.81	0.82	1	6.7	5.0	5.2
	AQUA	615	617	31	48	585	75	185	75	509	383	0.87	0.67	1	7.5	5.0	5.2
322	TERRA	647	712	32	102	614	117	119	117	498	492	0.81	0.81	1	6.4	5.0	4.8
	AQUA	447	520	22	62	424	54	204	54	370	255	0.87	0.56	1	7.0	5.0	4.8
323	TERRA	796	775	40	105	756	192	#	192	565	#	0.75	#	1	6.4	4.7	5.5
	AQUA	641	681	32	27	609	91	178	91	517	476	0.85	0.73	1	7.6	4.7	5.5
324	TERRA	674	719	34	114	640	89	91	89	551	514	0.86	0.85	1	7.4	7.1	6.1
	AQUA	474	537	24	62	451	33	74	33	417	402	0.93	0.85	1	8.2	7.1	6.1
325	TERRA	826	794	41	111	784	139	-1	139	645	684	0.82	#	1	7.7	7.3	6.0
	AQUA	674	691	34	35	640	91	18	91	549	638	0.86	0.97	1	8.2	7.3	6.0
326	TERRA	635	726	32	117	603	84	-11	84	519	620	0.86	1.02	1	7.0	#	5.3
	AQUA	612	614	31	38	581	57	76	57	524	500	0.90	0.87	1	7.9	#	5.3

To unravel the results one must look at results in order that they are calculated in SEBS to better understand where errors, inaccuracies or inconsistencies may be occurring. In SEBS the first step is to calculate the available energy i.e. net radiation (R_n) (Equation [2]). From R_n, the energy is partitioned firstly into the soil heat flux (G_0) (Equation [3]) and secondly into the sensible heat flux (H) (Equations [4] to [8]). Relative evaporation (Λ_r) (Equation 16]) is then determined using H, the sensible heat flux at the wet limit (H_{wet}) (Equation [4]) and the sensible heat flux at the dry limit (H_{dry}) (Equation [5]) are subsequently calculated. The evaporative fraction (Λ) (Equation [17]) is calculated from Λ_r, R_n, G_0 and the latent heat flux at the wet limit ($\lambda E_{wet} = R_n - G_0 - H_{wet}$). Finally the latent heat flux (λE) (Equation [17]) is calculated from R_n, G_0 and Λ. The results will now be examined more closely in this order under the appropriate headings.

5.3.1. NET RADIATION

It can be seen in Figure 24 that the net radiation (R_n) for the study period follows a typical bell curve with net radiation peaking at around 13:00 local time. It can also be seen that the net radiation is typically higher at TERRA image capture time than at AQUA image capture time.

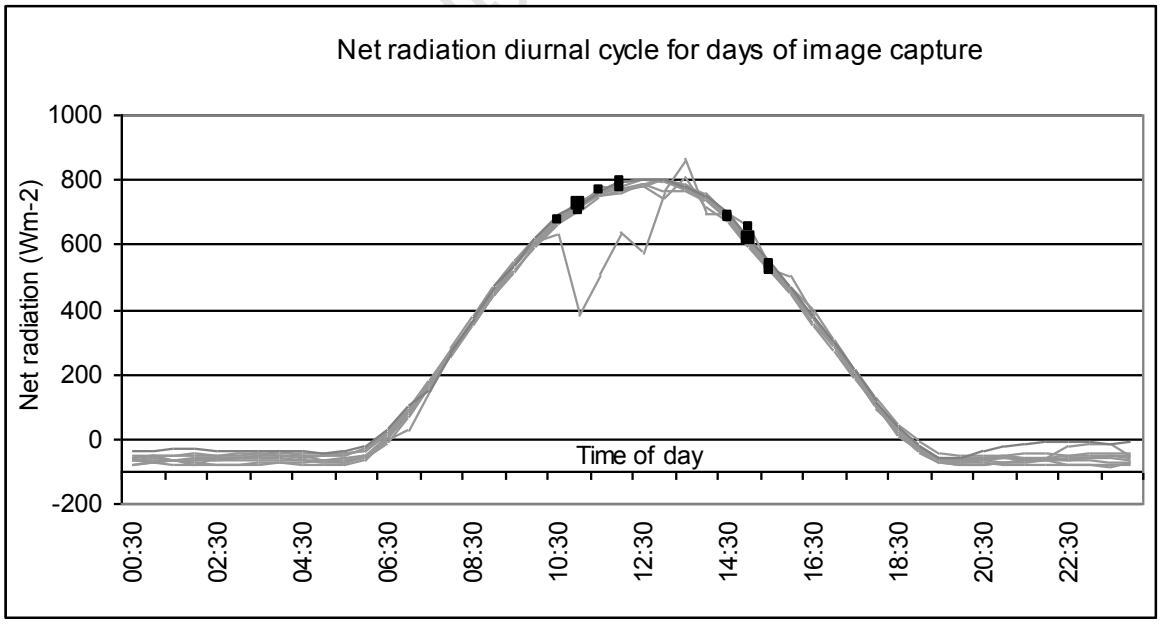

Figure 24: Net radiation as measured in the field for days of image capture (grey lines) with the time of each satellite image capture shown as a black square.

Despite the uncertainties found in T_0 and albedo which are used in the calculation of net radiation (Equation [2]), the SEBS calculated R_n compared favourably with the field measured data for both the TERRA and the AQUA data, although if Figure 25 is examined it can be seen that the results from AQUA were better than the TERRA results with r^2 being 0.89 and 0.72 respectively. It is possible that condensation on the field instrument sensors may have an impact on the recordings at the time of TERRA overpass but at AQUA overpass, any condensation will have evaporated. Alternatively, this discrepancy may be a result of the relatively small datasets which are used to formulate these correlations. However there is a strong correlation exists between SEBS R_n and the field measured values.

Concerning accuracy, despite the heterogeneity of the study area and the estimated albedo which is suspected to be too low, the SEBS R_n calculation has performed well with the calculated value falling within ten percent of the field measured value for most records (Figure 26). If Figure 25 and Figure 26 are studied concurrently, it can be seen that although the results from AQUA data are correlated more closely to the field validation results, the results from TERRA data are closer to the field measured results on more occasions than the results from the AQUA data.

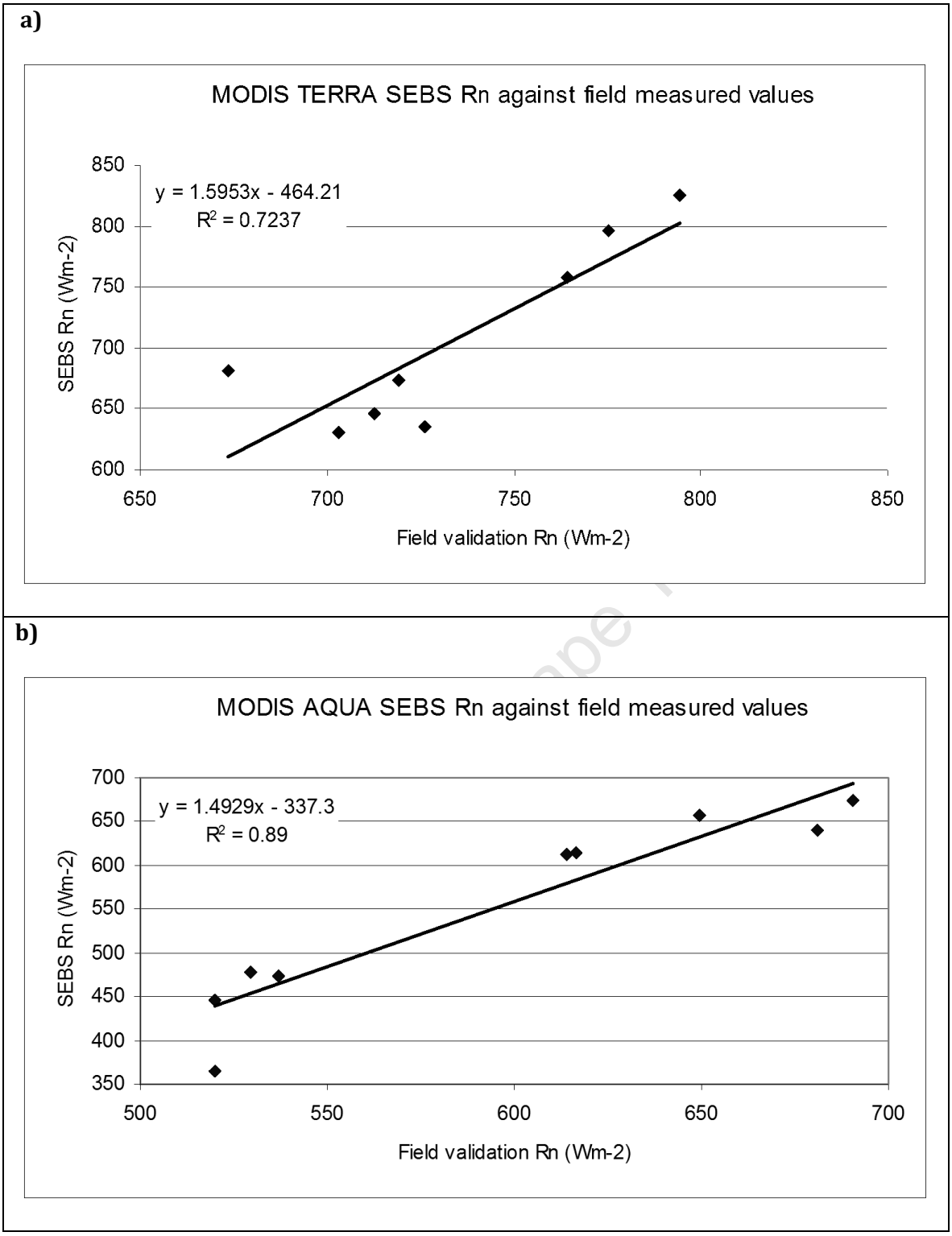

Figure 25: The MODIS TERRA (a) & AQUA (b) SEBS estimated instantaneous net radiation as a function of field measured net radiation for days on which MODIS images were acquired.

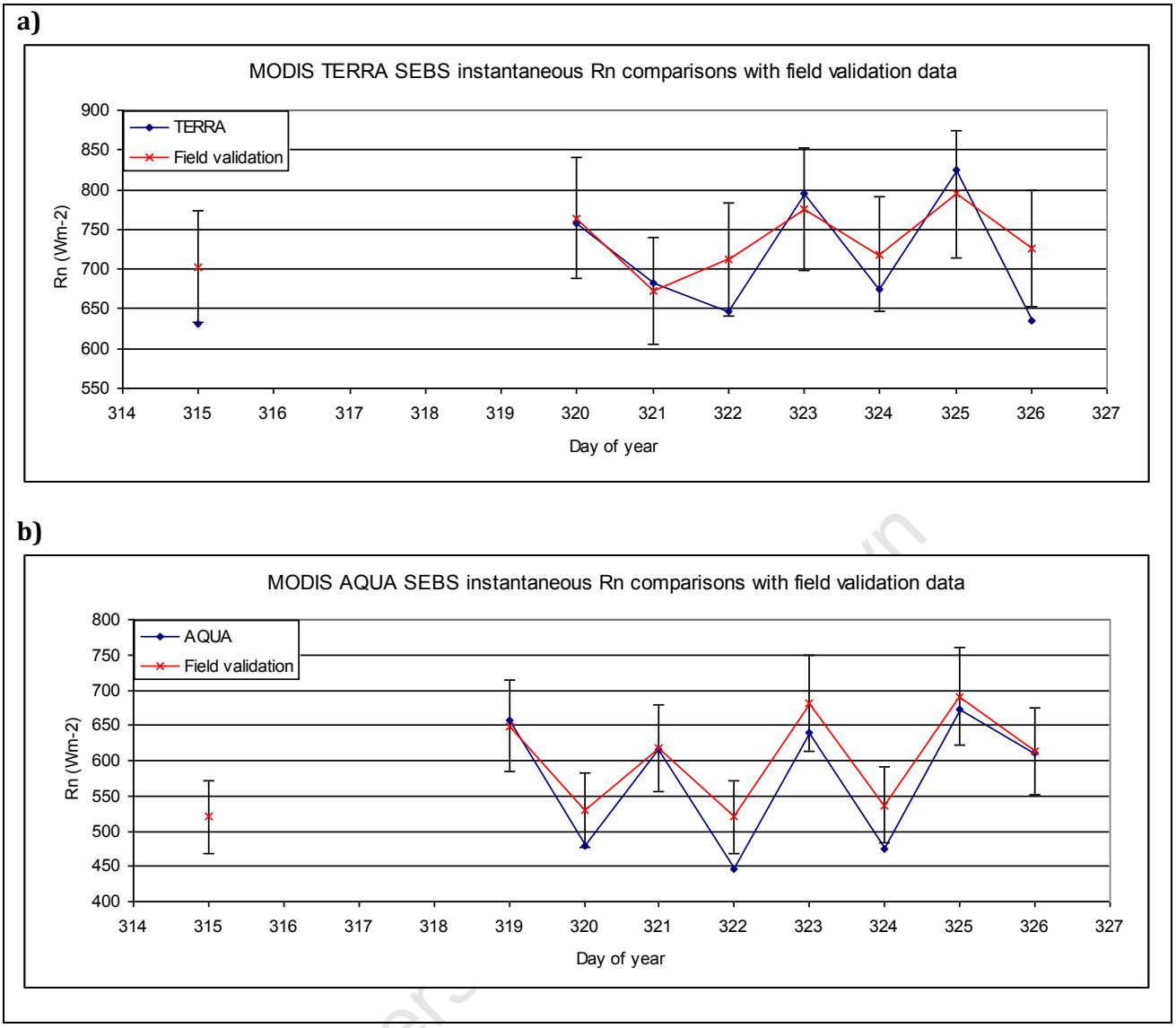

Figure 26: The MODIS TERRA (a) and AQUA (b) SEBS calculated instantaneous radiation plotted against field validation data with 10% errors bars shown on the field validation measurements.

5.3.2. SOIL HEAT FLUX

In SEBS, the soil heat flux (G_0) (Equation [3]) is calculated from net radiation using the fractional vegetation cover to determine what proportion of energy is allocated to heating the soil (Equation [26]). It was shown in TABLE 9 that for the field validation site, the fractional vegetation cover was determined to be equal to one, implying a complete vegetation cover with no bare soil. This was due to

the $NDVI_{max}$ purposefully being set to equal the minimum *NDVI* result for the field validation site for the study period (Equation [26]). It is important to consider this when assessing the results of the soil heat flux calculation as it is dependent on firstly, the accurate calculation of net radiation and secondly the correct determination of the fractional vegetation cover as any errors in these calculations will be propagated through to the calculation of the soil heat flux. The results of the SEBS calculated soil heat flux as compared with field measured values are shown in Figure 27. It can be seen that there is a much higher correlation between the results from the AQUA dataset and the field measured values ($r^2 = 0.62$) than between the results from the TERRA dataset and the field measured values ($r^2 = 0.13$).

The soil heat flux as measured in the field for each of the days of image capture is shown in Figure 28. The diurnal heat flux can be seen to peak at around 11 am at the approximate time of TERRA overpass, dip in the middle of the day, with a smaller peak later at around 4 pm just after AQUA overpass. The peak at 11 am is probably due to the structure and orientation of the orchard in which the field validation was conducted. Due to the apple trees being planted in rows running approximately from north to south, when the sun is at a lower position above the horizon, there is more direct sunlight to the soil surface than when the sun is directly overhead where the soil is being shaded by the canopy. As the solar elevation angle decreases in late afternoon, more soil surface is exposed to direct sunlight once again, explaining the second smaller peak. Since solar radiation is lower in the late afternoon than in the late morning, the peak in the late afternoon soil heat flux is lower than the late morning peak. Given the diurnal heat flux particular to this study area and the fact that the fractional vegetation cover is calculated to be equal to one, it would be expected that the results of the soil heat flux from the AQUA dataset would be more accurate than the results from the TERRA dataset since the effect of the shade as detected by the soil heat flux sensors in the late afternoon match the effect of shade which a fractional vegetation cover of one implies.

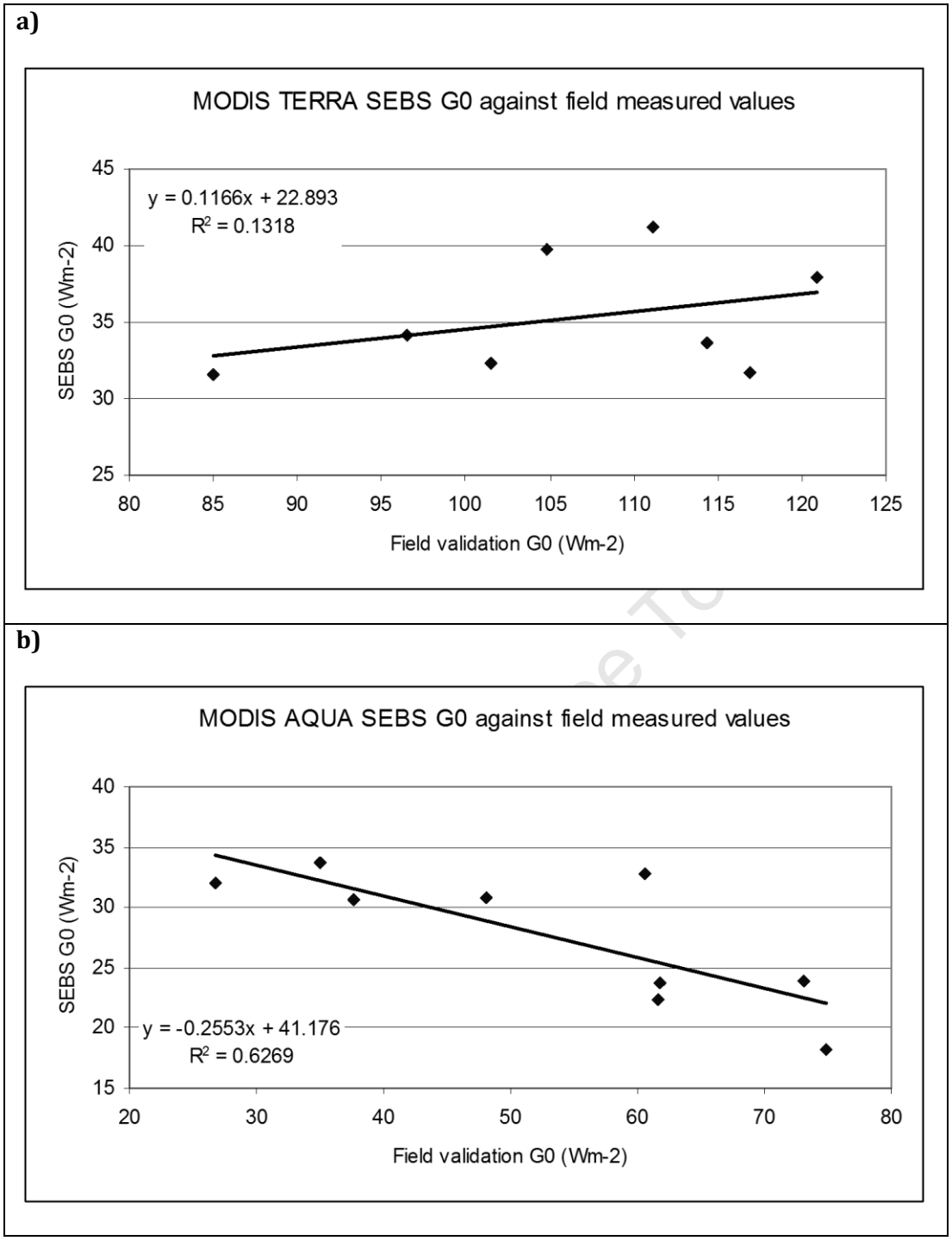

Figure 27: TERRA (a) & AQUA (b) SEBS soil heat flux (G_0) against field measured values.

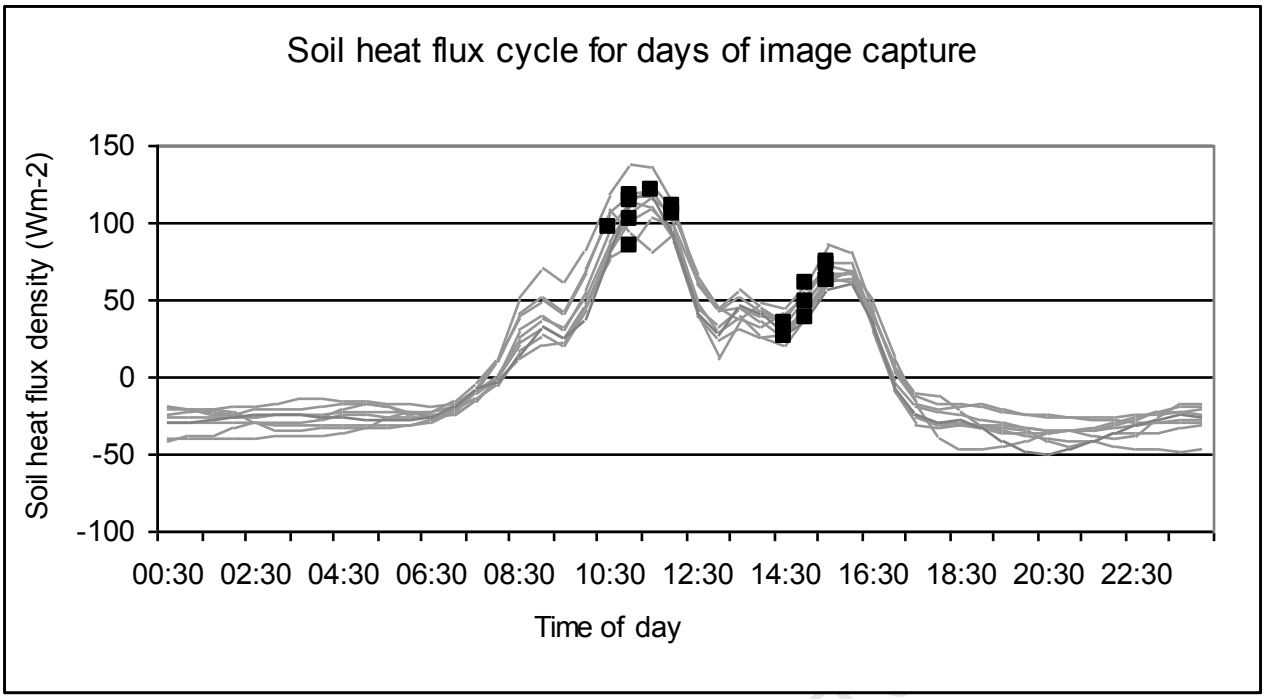

Figure 28: The soil heat flux as measured in the field for days of image capture (grey lines) with the time of each satellite image capture shown as a black square.

The results of the SEBS calculated net radiation and soil heat flux have been presented separately. However, since the sum of remaining components of the energy balance will be equal to the difference between the calculated net radiation and soil heat flux, at this point it may be useful to assess net radiation minus soil heat flux (available energy) in order to determine the highest potential accuracy that can be expected from the remaining energy balance components.

It can be seen in Figure 29 that the $R_n - G_0$ for the AQUA dataset agrees much better with the field data than the TERRA dataset for this site. With the exception of DOY 315, $R_n - G_0$ from the AQUA dataset is consistently well within ten percent of the field measured values (Figure 29b). However, Figure 29a illustrates that the results from the TERRA dataset are erratic with $R_n - G_0$ very close to the field measured values for three of the records but outside the ten percent error margin for four of the records. From the $R_n - G_0$ results, a higher accuracy in AQUA results than TERRA results for the remaining heat fluxes would be expected.

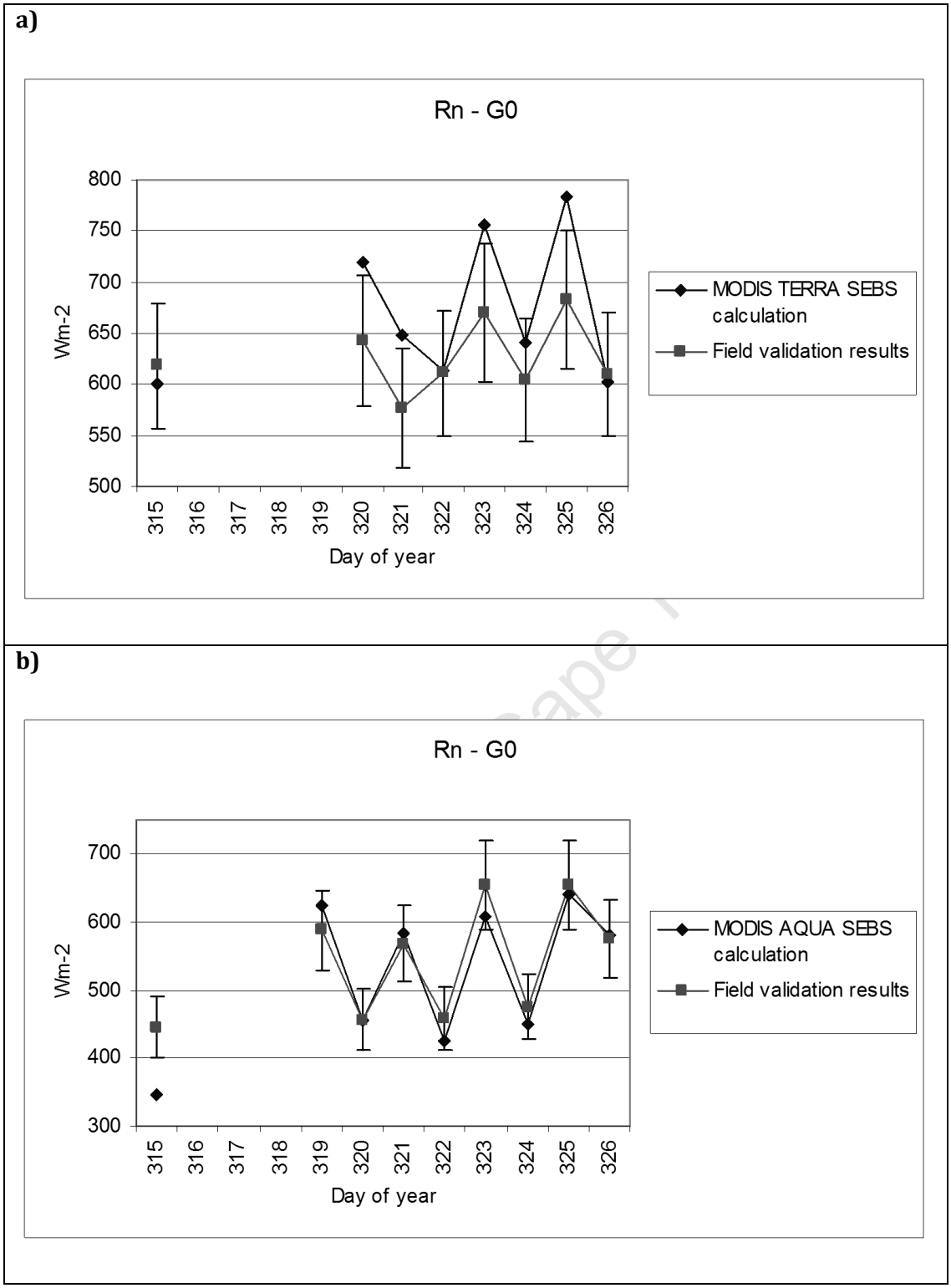

Figure 29: Net radiation minus soil heat flux as calculated using SEBS with MODIS TERRA data (a), MODIS AQUA data (b,) compared with the field validation data. Ten percent error bars are shown on the field validation calculation.

5.3.3. SENSIBLE HEAT FLUX

The sensible heat flux (H) is calculated in SEBS independently of the other surface energy balance terms by solving Equations [4] to [8] using, wind speed, temperature at reference height and at the surface, and roughness lengths for heat and momentum transfer. The roughness lengths in this research are calculated from remotely sensed vegetation indices (Equations [9] to [12]) and the advice by Su (2002) regarding this method was noted.

If the results of the field measured values of H and the SEBS calculated values for H in Table 12 are examined in conjunction with Figure 30, it can be seen that there is no agreement between the SEBS calculated values and the field measured values with r^2 values of 0.01 and 0.03 for the TERRA and AQUA dataset respectively. This is contrary to the previous good agreement between SEBS calculated R_n and G_0 at least for the AQUA dataset and the results should therefore be examined more closely. It can be seen in Table 12 that for every record H is equal to H_{wet}. Since SEBS constrains H to the range set by H_{wet}, and H_{dry}, H was calculated to be less than or equal to H_{wet} for every data record and H was therefore assigned the value of H_{wet}. Although the field validation site is in an irrigated apple orchard at almost complete canopy cover where it would be expected that the sensible heat flux would be tending towards the wet limit, it is unlikely that for every record the calculated heat flux would be exactly at the wet limit.

The sensible heat flux as measured in the field for each of the days of image capture is shown in Figure 31. Generally, the diurnal sensible heat flux can be seen to peak just after midday. Contrary to the soil heat flux trend where the flux was measured as significantly higher at TERRA overpass time than at AQUA overpass time, there is no such trend with the field measured sensible heat flux data.

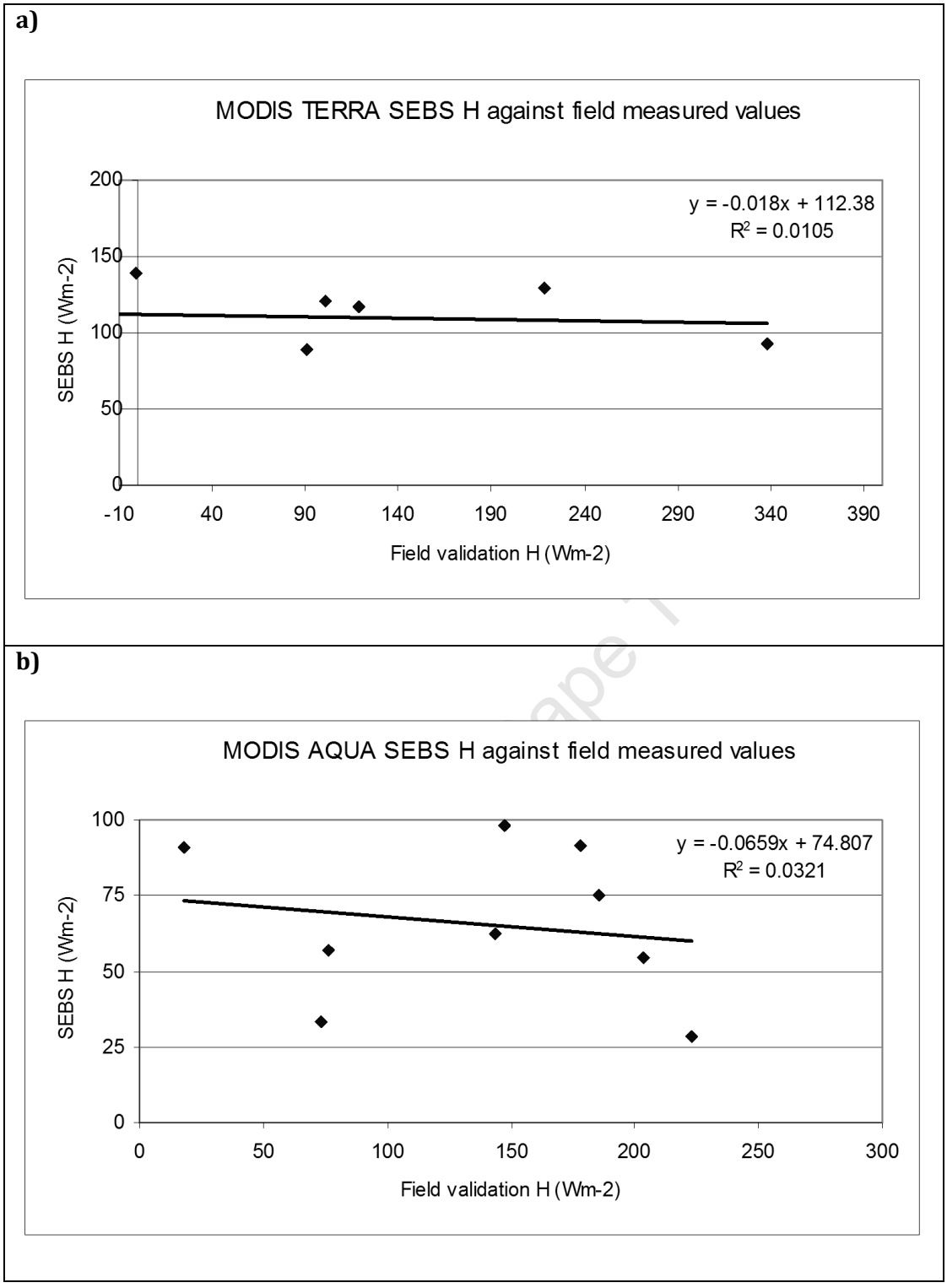

Figure 30: TERRA (a) & AQUA (b) SEBS sensible heat flux (H) against field measured values.

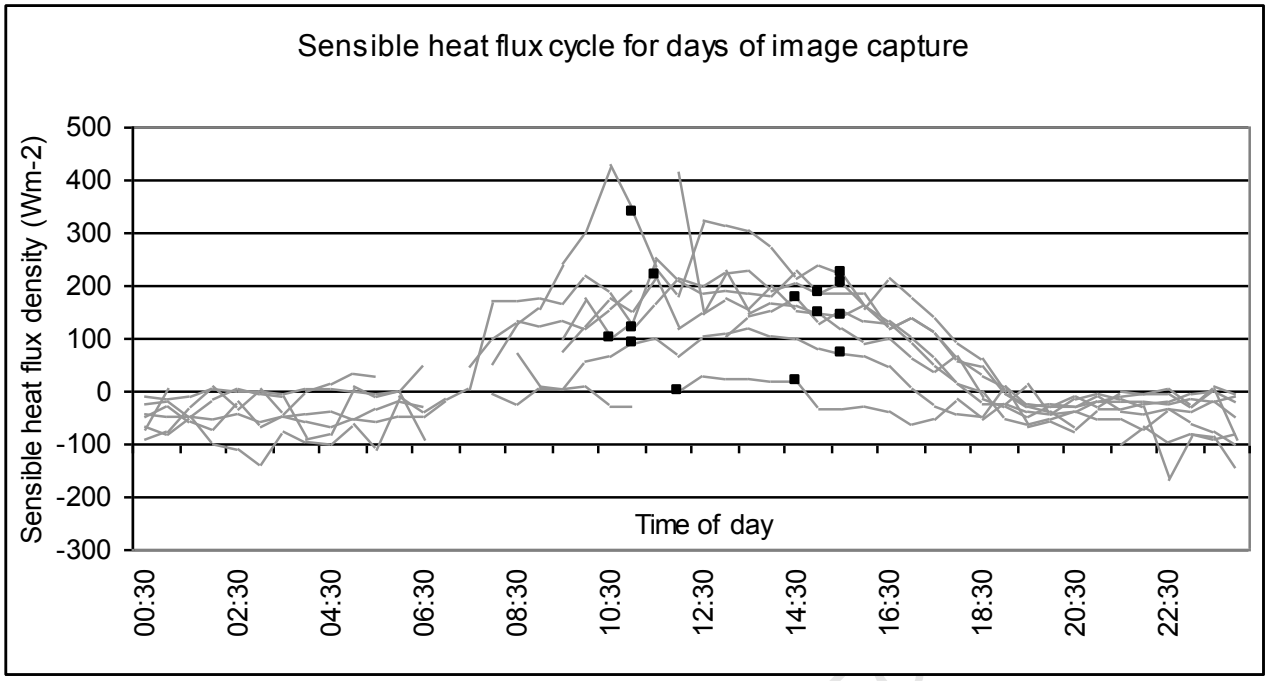

Figure 31: The sensible heat flux as measured in the field for days of image capture (grey lines) with the time of each satellite image capture shown as a black square.

Possible explanations for the sensible heat flux always being set at the wet limit will be addressed later (Chapter 6.3) however the consequences of this on further results will be briefly discussed here. At the wet limit, λE_{wet} = λE and substituting this in Equation [16], will always result in relative evaporation being equal to one in this scenario. Additionally, at the wet limit, the evaporative fraction will be higher since the numerator in Equation [17] is large in this scenario whereas the denominator will be unchanged. A high instantaneous evaporative fraction ultimately results in a high daily ET after the upscaling to the daily timeframe has taken place (Equation [18]).

It has been shown that the net radiation and the soil heat flux calculated in the SEBS model compare favourably with the field validation results, especially when the AQUA sensor is used. However, the SEBS calculated sensible heat flux is significantly higher than the field measured values. This error is propagated through the remaining calculations leading to a relative evaporation which always equals one and therefore an elevated evaporative fraction. This in turn leads to an overestimation in the daily evaporation.

5.3.4. LATENT HEAT FLUX

In the simplified energy balance equation (Equation [1]), the latent heat flux is solved as the residual of the equation. Therefore the accuracy of the latent heat flux is dependent upon the accuracy of the net radiation, soil heat flux and the sensible heat flux which precedes the calculation of the latent heat flux in the SEBS. Since it has been ascertained that the sensible heat flux is always at the wet limit and there is no correlation between the SEBS estimated values and the field measured values, there will be little value in validating the SEBS latent heat flux results. Rather, the causes of the uncertainties in the calculations of the preceding terms (R_n, G_0 and H) will be established in Chapter 7.

For the sake of completeness, the latent heat flux as measured in the field for each of the days of image capture is shown in Figure 31. As with the sensible heat flux, the diurnal latent heat flux can be seen to peak just after midday however the peak is more pronounced than in the case of the sensible heat flux.

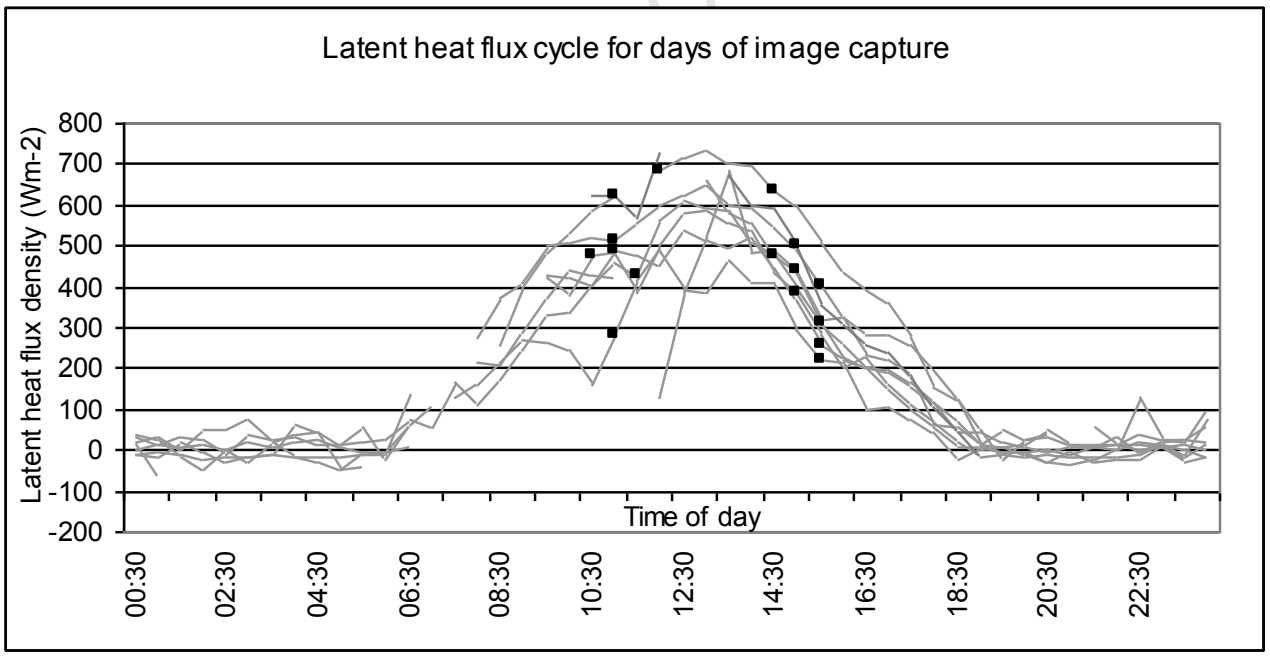

Figure 32: The latent heat flux as measured in the field for days of image capture (grey lines) with the time of each satellite image capture shown as a black square.

5.4. SUMMARY OF RESULTS

In summary, the results have shown that:

1) Despite the uncertainties found in the T_0 and albedo which are used in the calculation of net radiation, the SEBS calculated R_n compared favourably with the field measured data for both the TERRA and the AQUA data, with the results from AQUA being better than the TERRA results with r^2 being 0.89 and 0.72 respectively.
2) The results of the SEBS calculated soil heat flux from the AQUA dataset have a higher correlation ($r^2 = 0.62$) than the results from the TERRA dataset ($r^2 = 0.13$), probably due to the view angle (and thus viewed fractional vegetation cover) at AQUA overpass time.
3) .The SEBS calculated sensible heat flux is significantly higher than the field measured values. This error is propagated through the remaining calculations leading to a relative evaporation which always equals one and therefore an elevated evaporative fraction. This in turn leads to an overestimation in the daily evaporation.

The structure of the remainder of the thesis is now outlined to enable the reader to follow the direction of the proceeding text. Model uncertainties (excluding roughness parameters) particular to the study area are explored in Chapter 6. Adaptations to processing methods which are expected to lead to improved results are described and applied to a new study area in Chapter 7. Finally in Chapter 8, changes to the methodology are applied back to the Mouton's Valley field validation site.

6. MODEL UNCERTAINTIES

The pressure on water resources in South Africa creates a need for water resource managers to have accurate information on all aspects of water resource occurrence and use. To quantify the various components involved in calculating water use by means of field-based observations would be a difficult and time consuming process, providing only point-based measurements at a specific point in time. This problem is compounded when one considers that several measurements over time would be needed to accurately measure or monitor water use. To address these problems, Gibson *et al*. (2009) investigated the usefulness and applicability of remote sensing technologies as a tool for water resource assessment and specifically for the quantification of water use at farm level. Their approach relied on a simplified equation in which each component of the water balance equation was calculated for a hydrological year using mostly remote sensing techniques or products where possible.

To derive the remote sensing datasets for input into water balance equations, several complex models were applied to the input data. Although all of the components quantified by remote sensing data were subject to uncertainties and limitations, Gibson *et al.* (2009) were alerted to the possibility of uncertainties through the calculation of *ET*. The calculation of *ET* revealed that the total annual *ET* calculated using the Surface Energy Balance System (SEBS) model for the study area exceeded the total rainfall for the same area and time period. Although it may be possible for annual actual evapotranspiration to exceed annual precipitation in certain instances, such as where large scale irrigation from groundwater resources is practised, in this particular study, it is believed that actual evapotranspiration was overestimated. Since irrigated agriculture forms a small portion of the catchment (2.4%) in comparison to natural vegetation (29.7%) and dryland agricultural (66.5%), the higher actual evapotranspiration than precipitation at catchment scale cannot be ascribed to evaporative losses due to irrigation. As a consequence, the origins of uncertainties with regard to the accuracy of the final results were explored using the estimation of *ET* as an example.

The derivation of *ET* is a complex process requiring several sources of input data and numerous processing steps to derive intermediate output products. The intermediate products are then combined through additional processing algorithms to derive the final daily *ET* product. The SEBS model is available as part of the open source freeware ILWIS (available at www.52north.org), therefore it can be

used by practitioners with remote sensing knowledge who may not necessarily have the micrometeorological expertise to develop a model themselves to estimate *ET*. Whilst the open-source format of SEBS is very useful and can speed up the research process, there are some instances where specialist knowledge is required to implement the model correctly to derive the most accurate results. Furthermore, the complexity of the SEBS model together with the inherent uncertainty in using remote sensing derived products as input implies that a large number of sources of uncertainty may exist and should be properly understood.

This chapter attempts to highlight some of the uncertainties encountered when using the SEBS model in a heterogeneous area in South Africa. Several authors have addressed issues related to sensitivity of the SEBS model to various input parameters (most notably Van der Kwast *et al*., 2009). This paper differs in that it focuses on the pre-packaged version of SEBS in ILWIS and the sensitivity of SEBS to some parameters over which the user has some control when using this version of the model, so informed choices can be made at various stages in the processing chain, in order to limit the introduction of unnecessary uncertainties. Furthermore, in this paper the sensitivities of SEBS to input parameters is related to daily *ET* rather than energy flux results since this is of interest to water managers and other users. This chapter will describe some of the uncertainties introduced by the sensitivity of the SEBS model to a) land surface temperature and air temperature gradient, b) the choice of fractional vegetation formula, c) displacement height and the height at which wind speed is measured, and d) study area heterogeneity.

6.1. STUDY AREA

The study area, situated in the Piketberg region in the Western Cape Province of South Africa (Figure 33), encompasses a quaternary catchment (G10K) in which commercial agriculture plays an important role. The area experiences winter rainfall (May to October), has a diverse topography and is drained by the perennial Berg River which enters the Atlantic Ocean at Velddrif on the West Coast.

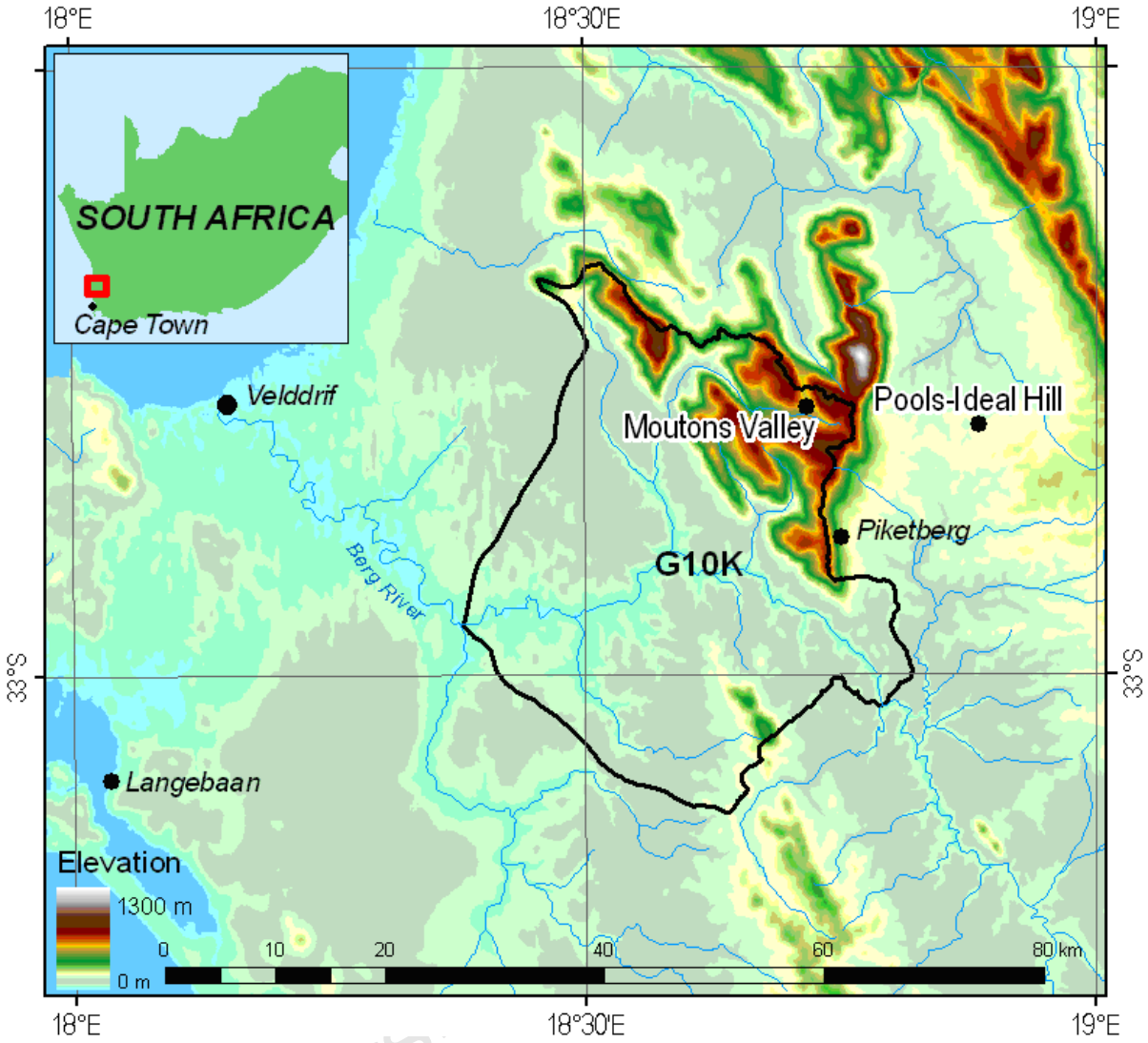

Figure 33: Orientation map showing the G10K catchment, the Mouton's Valley field validation site and the weather station Piketberg: Pools-Ideal Hill (shown as Pools-Ideal Hill) situated in a dryland agricultural area which was used for experimental purposes.

The climate in the area is varied with the western part of the catchment experiencing a maritime Mediterranean climate whilst the eastern part is considered to have a continental influence. The varying climate has an influence on the land use in the area with low-lying areas being dominated by dryland agriculture (predominantly wheat fields). In addition, temporary commercial irrigated agriculture (potatoes) under centre pivot irrigation as well as pockets of natural vegetation, described as shrublands and low fynbos, are found. The elevated area towards the northeast of the catchment is dominated by natural vegetation in the form of low- and high-fynbos with reported alien vegetation infestations. Cultivated irrigated lands in the form of deciduous and citrus fruit tree orchards are also found, although to a lesser extent.

Due to limited financial resources, field validation could not be conducted at multiple sites or for the entire hydrological year for which the water balance components were calculated. Therefore energy flux results presented in this research correspond to the specific field validation site (hereafter referred to as Mouton's Valley site) and period. In addition, an automatic weather station installed in a dryland agricultural area (hereafter referred to as Piketberg: Pools-Ideal Hill site) was used to compare results between land covers. However, there was no validation data available for this site.

6.2. MATERIALS AND METHODS

The Surface Energy Balance System (SEBS) is a model proposed by Su (2002) for the estimation of atmospheric turbulent fluxes and evaporative fraction using satellite earth observation data in combination with meteorological information. The SEBS model is used to estimate daily actual *ET* from remotely sensed and meteorological data by calculating the energy required for water to change phase from liquid to gas (Equation [1]). The complete formulation of the SEBS model is given in Chapter 2.3. A simplified sequence illustrating the processing in SEBS is given in Table 13.

Table 13: Sequence of SEBS processing (adapted from Su *et al*., 2008).

INPUTS		**OUTPUTS**
Incoming shortwave radiation (SW↓), land surface temperature (θ_0), albedo (α), air temperature (θ_a), land surface emissivity (εa)	→	Net radiation (R_n)
Fractional vegetation cover (fc), α, R_n	→	Land surface emissivity (εa), Soil heat flux (G_0) Sensible heat flux (H_{dry})
R_n, G_0	→	Sensible heat at the dry limit (H_{dry})
Horizontal wind speed (U), T_0, T_a, Leaf Area Index (LAI), Roughness length for momentum transfer (Z_{om}), fc	→	Frictional velocity (u*), Monin-Obukhov length (L), Sensible heat flux (H), Excess resistance to heat transfer (kB^{-1}), Roughness length for heat transfer (Z_{oh})
Specific humidity (es), R_n, G_0, u*, Z_{oh}	→	Wet-limit stability length (L_{wet}), Sensible heat flux at the wet limit (H_{wet})
H_{dry}, H_{wet}, H	→	Relative evaporation (Λr)
H_{wet}, Rn, G_0	→	Evaporation at the wet limit (λE_{wet})
λE_{wet}, Λr , R_n, G_0	→	Evaporative fraction (Λ)
Λ, Daily radiation (R_{n24}), Daily soil heat flux (G_{24})	→	E_{daily}

According to Su (2006), it is possible to estimate the latent heat flux as a residual after the sensible heat flux has been derived. However, because the sensible heat flux is not constrained by the available energy but is determined solely by surface temperature and the meteorological conditions at the reference height, there is an associated uncertainty in the derived latent heat flux and therefore also in the evaporative fraction. However, in SEBS this uncertainty is limited by considering the energy balance at the limiting cases since the actual sensible heat flux is constrained to the range set by the sensible heat flux at the wet limit (derived from a combination equation), and the sensible heat flux at the dry limit (set by the available energy).

According to formulations by Su (2002), the relative evaporation is derived from the sensible heat flux and the sensible heat flux calculated at the wet and dry limits. The relative evaporation (Equation [16]) is, in turn, used together with R_n, G_0 and the latent heat flux at the wet limit to estimate the evaporative fraction (Equation 17]). In SEBS it is assumed that the daily value of evaporative fraction is approximately equal to the instantaneous value, and from this, the daily evaporation is given in Equation [18]. The daily net radiation flux is given in Equation [19].It can be seen from Equations [18] and [19] that aside from evaporative fraction itself, albedo is the sole remote sensing derived variable used in the upscaling from instantaneous evaporative to daily *ET*.

For the purpose of calculating *ET* in this research, MODIS TERRA and AQUA data (MOD021KM _ Level 1B Calibrated Radiances – 1 km: Collection 5) were used. MODIS images are captured daily or every second day and therefore it is possible, in South Africa, to obtain a good coverage throughout the year. MOD02 and MYD02 data were selected for the field validation period. Single date (28 February 2008) ASTER level 1B - Registered Radiance at the Sensor, and ASTER level 2 – AST08 Surface Kinetic Temperature, were used to compare the results of the higher resolution sensor to those of the same date coarser resolution MODIS sensor. The required meteorological data (air temperature, wind speed, radiation, sunshine duration) can be obtained directly from an automatic weather station (AWS) or indirectly (air pressure, specific humidity) using empirical formulae and data from the AWS. Weather data from the Mouton's Valley and the ARC-ISCW, Piketberg: Pools-Ideal Hill AWSs were used.

6.3. UNCERTAINTIES IN EVAPOTRANSPIRATION ESTIMATES WITH SEBS

Overgaard *et al.* (2006) put forward the argument that there is a mismatch between the scale for which the theory behind developed models is assumed valid (typically point scale), and the scale of the typical application. For this reason, the parameters in physically-based models are in reality conceptual, and that even when mean parameters are available, the highly non-linear behaviour of most land-surface models cannot be expected to simulate the mean response of a particular area (Overgaard *et al*., 2006). Furthermore, the complex interaction of different sources of uncertainty in the modelling process means that a good model driven by poor input data will not necessarily produce acceptable results (Beven, 2008) and trying to separate the different sources of error is difficult since they interact in complex non-linear ways (Beven, 2006).

Further, the analysis of remote sensing and GIS products usually results in maps of discrete or continuous variables (Dungan *et al*., 2002), which can be associated with several sources of error or uncertainty. These include: (1) errors or uncertainties associated with the specific remote sensing data obtained; (2) errors or uncertainties introduced with the processing and analysis of image and field data; (3) errors or uncertainties associated with the specific model; and (4) errors or uncertainties associated with positional aspects (including image resolution). Wang *et al.* (2005) identify additional sources of errors including sampling and measurement error of ground truth data, errors of spectral values and radiometric calibration of images, errors from the leap from spectral measurements to interpretation of a categorical variable, modelling errors due to misunderstanding the relationship between spectral and thematic variables, and errors from GIS operations.

Errors and sensitivities in the derivation of *ET* for this study were identified as (but are by no means limited to): (1) land surface and air temperature gradient; (2) the choice of fractional vegetation cover formula; (3) zero plane displacement height and the height of wind speed measurement in relation to displacement height; and (4) study area heterogeneity.

6.3.1. LAND SURFACE AND AIR TEMPERATURE GRADIENT

The calculation of *ET* using the SEBS model relies on two temperature sources: air temperature (T_a) and land surface temperature (T_0). Su (2002) reported on the sensitivity of sensible heat flux to the gradient between land surface temperature and air temperature hourly and Badola (2009) reported that of all remotely sensed input parameters, SEBS was most sensitive to change in ($T_0 - T_a$). T_0 plays a role in the determination of net radiation (*Rn*) (Table 13) and therefore soil heat flux (G_0), but its main contribution (together with the aerodynamic resistance) is in the calculation of the sensible heat flux.

To quantify the uncertainty associated with T_0 estimates for the field validation site, the T_0 retrieved from MODIS data was compared with the Meteosat SEVIRI T_0 data product (SEVIRI/Meteosat LST Product: LSA-4 (MLST) Product version 7.2) corresponding to the same time of image acquisition. The motivation for using Meteosat SEVIRI T_0 data was to try to set a realistic uncertainty range in T_0 in this particular heterogeneous environment. It was found that there were differences of up to 10 K between MODIS T_0 and SEVIRI T_0 with SEVIRI T_0 being consistently higher than MODIS T_0 which is in agreement with the findings by Madeira *et al*. (2005). This large range in T_0 can be ascribed to the topographically rough nature of the terrain in the vicinity of the field validation site.

In addition to the SEBS model sensitivity to T_0, the near-surface air temperature (T_a), as measured by weather stations) has a direct influence on the evaporation process and inaccuracies in measurements can lead to distorted reference *ET* measurements and actual *ET* estimates. For this reason, accuracy in air temperature measurements is needed at the weather stations themselves. Additionally, the heterogeneity of the study area implies that spatially distributed air temperature across the study area is needed. This is because the spatial variations of surface characteristics (including topography and land cover) have a large influence on the near-surface weather conditions (Voogt, 2006). Increasing the accuracy of air temperature inputs will increase the likelihood of accurate *ET* estimates.

The sensitivity of daily *ET* calculated by SEBS to $\Delta(T_0 - T_a)$ for the Mouton's Valley site was assessed by varying T_0 by up to 10 K around the estimated T_0 and keeping the T_a constant. The results (FIGURE 34 34) indicated that for the Mouton's Valley site (where the estimated T_0 is 301 K, the estimated T_a is 293 K and $T_0 - T_a$ equals 8 K), daily *ET* can vary by up to 1.5 mm in this 10 K $\Delta(T_0 - T_a)$ range. Adjusting

T_a around a 10 K range, to create the same Δ($T_0 - T_a$) as when T_0 was adjusted, results in a very similar daily ET range. SEBS limits evapotranspiration by setting a wet and a dry-limit. At the Mouton's Valley site, at $T_0 - T_a < 7.4$ K, the sensible heat flux is at the wet-limit. At the wet limit, the equation used to calculate the sensible heat flux (Equation [4]) is given in Su (2002) which differs from the sensible heat flux equations which are used when the wet-limit has not been reached (Equations [6], [7] and [8]) (Su, 2002).

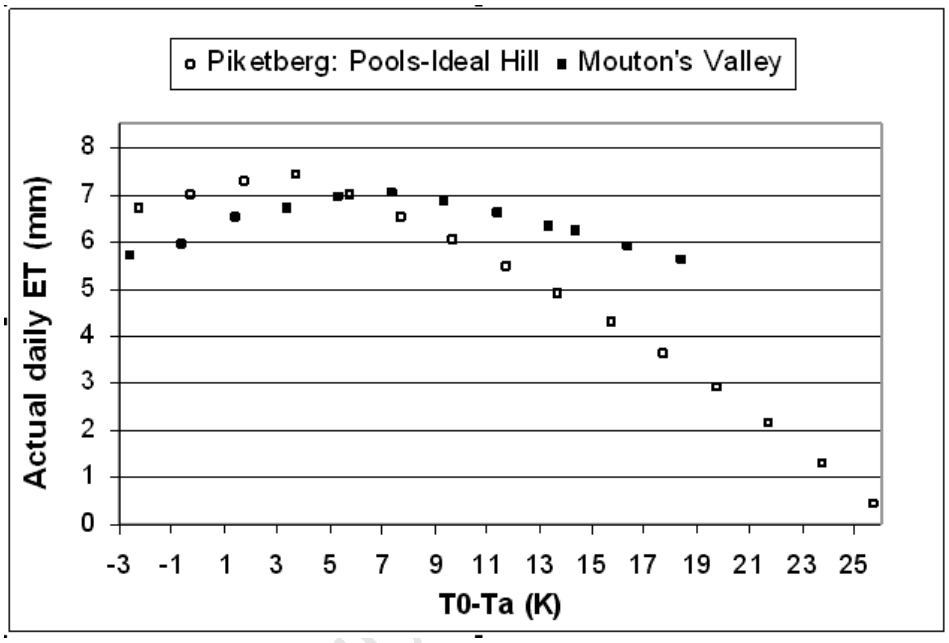

Figure 34: Sensitivity of SEBS-estimated daily ET to Δ($T_0 - T_a$) the Mouton's Valley field validation site and the Piketberg: Pools-Ideal Hill site.

In Equation [4], with decreasing $T_0 - T_a$, the denominator is decreased by the decrease in the Δ (the rate of change of saturation vapour pressure with temperature) and therefore the sensible heat flux at the wet limit increases resulting in a decrease in the latent heat flux, a decrease in the evaporative fraction and a decrease in the daily evapotranspiration. This is the reason for the decrease in daily actual evapotranspiration with $T_0 - T_a$ once the wet-limit has been reached.

Where the wet-limit has not been reached, Equations [6], [7] and [8] are used in the determination of the sensible heat flux. In Equation (8), with decreasing $T_0 - T_a$, there will be decreasing sensible heat flux estimation, resulting in increasing latent heat flux and therefore increasing daily actual

evapotranspiration. This explains why the daily actual evapotranspiration increases with decreasing T_0 - T_a until the wet-limit is reached. At the wet-limit Equation [4] is used and the daily evapotranspiration decreases with decreasing T_0 - T_a due to decreasing saturation vapour pressure.

The modelling of the sensitivity of ET to T_0 in a dryland agriculture environment at Piketberg: Pools-Ideal Hill (where the estimated T_0 is 311 K, the measured T_a is 295 K and $T_0 - T_a$ is 16 K) is also shown in Figure 34. It can be seen that the sensitivity of daily ET to $\Delta(T_0 - T_a)$ is greater than the Mouton's Valley site with a range of 7 mm across the same $\Delta(T_0 - T_a)$ where T_0 is increased and decreased by 10 K. In the case of the Piketberg: Pools-Ideal Hill site, the wet-limit is not reached when using similar T_0 - T_a values as is used for the Mouton's Valley scenario. This is possibly due to the calculated lower roughness lengths of the Piketberg: Pools-Ideal Hill site (in combination with different atmospheric conditions) when compared with the Mouton's Valley site, resulting in a higher sensible heat flux for the same $T_0 - T_a$ as observed at the Mouton's Valley site. In the selected T_0 - T_a range (10 K), the sensible heat flux is not forced to the wet limit. However when T_0 - T_a is lowered further, the wet-limit drop off in evapotranspiration (which occurs at T_0 - T_a ~3 K in this particular instance) is reached.

It can therefore be said that the sensitivity of daily ET to $\Delta(T_0 - T_a)$ is dependent on the land cover being studied and may also be dependent on the calculated $(T_0 - T_a)$ itself. It should, however, be noted that the uncertainty related to T_0 in the dryland agricultural area is almost certainly lower than the 10 K range found at the Mouton's Valley site since the dryland agricultural at Piketberg: Pools-Ideal Hill is topographically flat and relatively homogeneous. However, it is useful to note the differences in sensitivity to $\Delta(T_0 - T_a)$ on the same day, for two land covers in close proximity to each other, therefore re-emphasizing the care that should be taken (particularly regarding the accuracy of input data) when using SEBS in a heterogeneous environment.

Furthermore, the calculated sensitivity of the sensible heat flux at the Piketberg: Pools-Ideal Hill site to $\Delta(T_0 - T_a)$ was found to be in close agreement with the sensitivity of ΔH=10•$\Delta(T_0 - T_a)$ reported by Su (2002) for cotton, when the wet limit has not been reached. At the wet-limit, the sensitivity of the sensible heat flux to $\Delta(T_0 - T_a)$ was found to be ΔH=-8.32•$\Delta(T_0 - T_a)$. For the Mouton's Valley site, it was found that calculated sensitivity of the sensible heat flux to $\Delta(T_0 - T_a)$, is ΔH = -8.68•$\Delta(T_0 - T_a)$ where the wet limit has been reached and of ΔH = 6.09•$\Delta(T_0 - T_a)$ where the wet limit has not been reached. It can

therefore be seen that the sensitivity of H (and therefore daily ET) to $\Delta(T_0 - T_a)$ is dependent on the land cover type, T_0, and whether the wet limit has been reached.

The uncertainties in the interpolation of T_a together with the uncertainties related to T_0 estimates create ambiguity with regard to the accuracy of the results. This is particularly prohibitive since these parameters are used in the initial stages of SEBS model implementation, meaning that erroneous input data would be translated through the entire processing sequence and eventually be reflected in the final calculation of actual ET.

6.3.2. FRACTIONAL VEGETATION COVER

Fractional vegetation cover (f_c) and its complement are used in the calculation of the roughness length for heat transfer (Su *et al.*, 2005) which, in turn, is used in the calculation of the sensible heat flux. In addition, f_c is used in the estimation of the soil heat flux (Su, 2002) and in the preprocessing stages to assign surface emissivity values (Sobrino & El Kharraz, 2003) which are used to derive land surface temperature. Fractional vegetation cover is a user defined input into the pre-packaged version of SEBS in ILWIS and different formulations of f_c are intentionally utilized in SEBS for different purposes. Therefore, the effect of the choice of formula, and its calibration, on resulting ET should be noted.

Several methods for the calculation of f_c are described in the literature. These methods generally make use of leaf area index (*LAI)* (Choudhury, 1987, cited in French *et al*., 2003) as input or require pixel *NDVI* together with a minimum and maximum *NDVI* value (Carlson & Ripley, 1997; Gutman & Ignatov, 1998). These minimum and maximum *NDVI* values are either constant (Sobrino & El Kharraz, 2003) or can be derived directly from the scene or from a time series.

For example, if fractional vegetation cover is calculated according to the formula for vegetation proportion (Sobrino & El Kharraz, 2003) (Equation [25]). In contrast with $NDVI_{min}$ and $NDVI_{max}$ values as defined by Sobrino & El Kharraz (2003), Figure 35 shows the distribution of *NDVI* values across the entire study area for a winter wet season and summer dry season scene. It can be seen that the range of

0.2 to 0.5 is frequently exceeded within this study area, particularly in the winter wet season. The distribution of *NDVI* in this study area is therefore scene and season dependent.

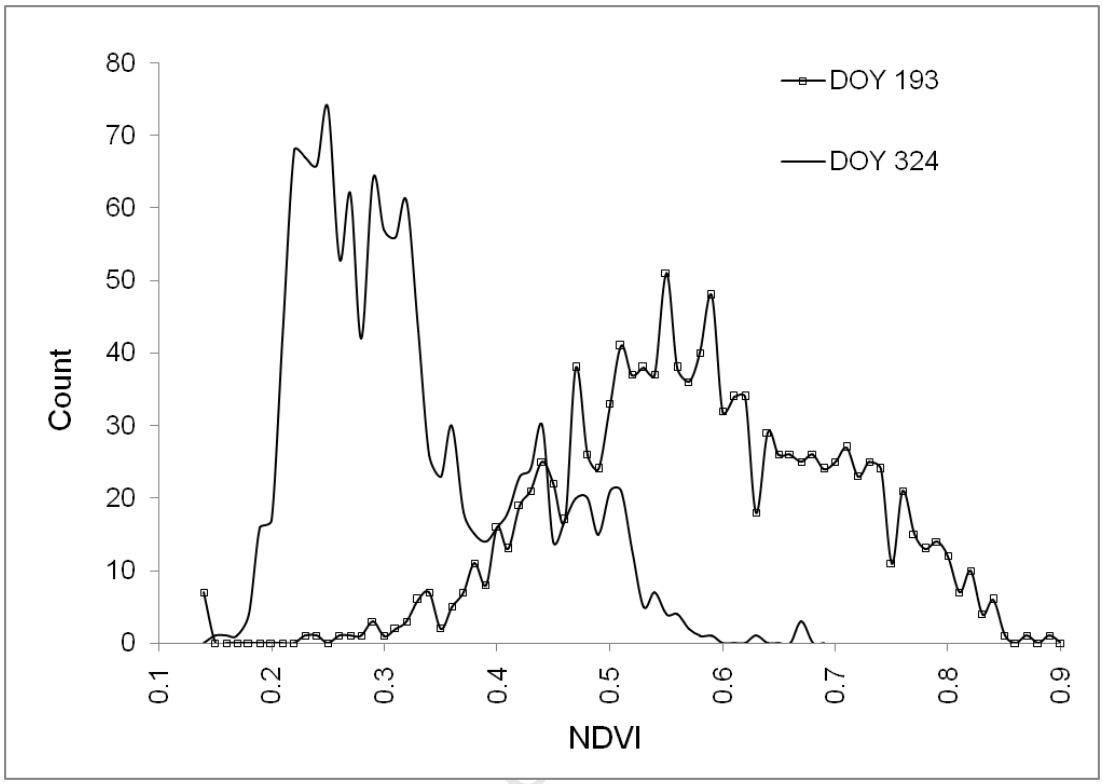

Figure 35: *NDVI* distribution for the study area for a winter wet season scene (DOY 193) and a summer dry season scene (DOY 324).

At *NDVI* of 0.5 and higher, maximum vegetation cover is assumed and f_c = 1. The assumption is therefore that the soil is completely shaded, and based on the soil heat flux equation (Su, 2002), the soil heat flux is only a function of net radiation and fractional vegetation cover, equalling 5 % of net radiation. In contrast, the field validation data at TERRA overpass indicate a relatively high soil heat flux (approximately 12 – 16 % of net radiation) since the bare soil underneath the trees receives direct radiation as a result of the solar zenith and azimuth angle in combination with the orientation of the tree rows. At AQUA overpass, when the soil of the field validation site is shaded (effectively mimicking a vegetated pixel), there is a much better agreement between field validation (approximately 3 – 15 % of net radiation) and the SEBS results (approximately 5 % of net radiation) for soil heat flux.

The fractional vegetation cover calculation can be tested using the field validation data at Mouton's Valley and by rearranging the soil heat flux equation (Equation [3]):

$$f_c = -\left[\frac{\frac{G_0}{R_n} - \Gamma_c}{\Gamma_s - \Gamma_c}\right] - 1 \qquad [30]$$

Where Γc (0.05) (Monteith, 1973 in Su, 2002) and Γs (0.315) (Kustas and Daughtry, 1989 in Su, 2002) are the soil heat flux ratios for full vegetation canopy and for bare soil respectively. Solving Equation [30] by substituting the field measured G_0 values, fractional vegetation cover is calculated to range from 0.58 – 0.73 at TERRA overpass and at AQUA overpass from 0.67 – 1. If this is taken to be a true reflection of fractional vegetation cover of the apple orchard at image acquisition time, the NDVI minimum and maximum values should be adjusted as a fractional vegetation cover of 1 is not a realistic result especially at TERRA acquisition time.

Considering f_c calculated above, the need for calibrating *NDVI* by defining an appropriate $NDVI_{max}$ for the study area is apparent. Substituting this f_c and the corresponding *NDVI* for the Mouton's Valley site for each MODIS TERRA and AQUA acquisition and keeping the $NDVI_{min}$ = 0.2 as suggested by Sobrino & El Kharraz (2003) in Equation [25] results in an average $NDVI_{max}$ = 0.65, which is more appropriate for the study area during the field validation period.

The benefits of using a set minimum and maximum *NDVI* should be weighed up against using scene-specific estimates especially for scenes which do not contain a full range of vegetation cover as this will skew the results of the fractional vegetation calculation. The sensitivity of daily *ET* to choice of f_c formula and the calibration of $NDVI_{min}$ and $NDVI_{max}$ are shown in Figure 36 for the Mouton's Valley site. The curve in Figure 36 was created by repeatedly varying f_c and recomputing daily *ET*. The points on the curve show that for the same pixel, a different formula would produce a different f_c result: it can be seen that in this instance, the calculated daily *ET* can vary by up to 0.7 mm depending on the f_c input.

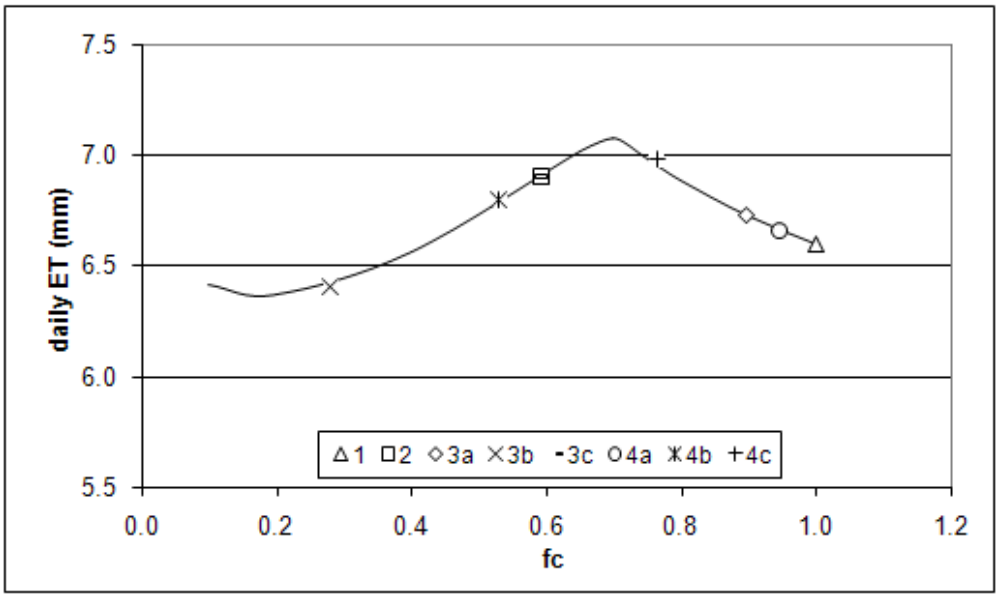

1	Fixed NDVI max (0.5) and min (0.2) (Sobrino & El Kharraz, 2003))
2	LAI dependent (Choudhury, 1987, cited in French et al., 2003)
3a	Scene dependent NDVI max (0.563) and min (0.207) (Carlson & Ripley, 1997)
3b	Time series derived NDVI max (0.863) and min (0.184) (Carlson & Ripley, 1997)
3c	Study area derived NDVI max (0.65) and min (0.2) (Carlson & Ripley, 1997)
4a	Scene dependent NDVI max (0.563) and min (0.207) (Gutman & Ignatov, 1998)
4b	Time series derived NDVI max (0.863) and min (0.184) (Gutman & Ignatov, 1998)
4c	Study area derived NDVI max (0.65) and min (0.2) (Gutman & Ignatov, 1998)

Note: where fc is calculated to be greater than 1, then fc is taken to be equal to 1

Figure 36: Sensitivity of SEBS-estimated ET to a range in fractional vegetation cover input values for the apple orchard field validation site. f_c values resulting from specific formulae and methods are indicated.

From the results it can be concluded that if it is possible to obtain field data in order to derive an appropriate *NDVI* minimum and maximum value, the formula by Carlson & Ripley (1997) can be used. Alternatively the formula by Choudhury (1987) cited in French *et al*. (2003) using *LAI* as input may be used as it gives the same result as displayed in Figure 36.

Fractional vegetation cover should be calculated outside of SEBS and care should be taken in the choice of formula as the variation in ET as a function of f_c has been demonstrated.

6.3.3. ZERO PLANE DISPLACEMENT HEIGHT

The objective of this section is to highlight that the type of weather station and the reference height at which wind speed is measured is critical to the correct implementation of the SEBS model particularly in tall canopies.

Zero plane displacement height (d_0) values are used in combination with the reference height at which wind speed is measured (z) in the process of determining the sensible heat flux (H). d_0 can be obtained from the literature or can be empirically derived from the remote sensing vegetation inputs *via* the calculation of roughness length (the methodology adopted by Su, 2002; Timmermans *et al*., 2005; and Van der Kwast *et al*., 2009). Alternatively the combination approach of Jia *et al*. (2009) can be used. Using the empirical model, $NDVI$ and $NDVI_{max}$ are used to determine roughness length for momentum transfer (z_{0m}) with the method described by Su & Jacobs (2001) as reported in Hailegiorgis (2006). Next, the vegetation height is calculated from z_{0m} followed by d_0 using the method of Brutsaert (1982) as reported in Hailegiorgis (2006).

In South Africa, the installation of automatic agrometeorological weather stations complies with standards set by the World Meteorological Organisation except in the height measurement of wind speed and direction. South African agrometeorological standards state that wind speed and wind direction are measured at 2 m above the surface (ARC-ISCW, 2010) in contrast to the South African Weather Service (SAWS) which measures wind speed and direction at 10 m above the surface.

A problem arises when using data from agrometeorological weather stations in canopies of 3 m or higher (where $d_0 \geq 2$), as is the case with orchards in the study area. To derive the sensible heat flux (Su, 2002) the calculation of $z - d_0$ is required, where z is the reference height at which wind speed is measured (2 m, in the case of an agrometeorological weather station). When measuring wind speed at 2 m, and solving for H using the equations defined by Su (2002) and given in Equations [6], [7] and [8], a situation arises where $z \leq d_0$, and the ln of a negative number needs to be solved.

In this study, the average canopy height at the Mouton's Valley site was reported to be 3.2 m in the apple orchard (Jarmain & Mengistu, 2011) and therefore d_0 > 2 m so the condition where $z \leq d_0$ is reached using agrometeorological weather stations. The alternative would be to use weather data from the SAWS which would allow for the sensible heat flux to be calculated for much higher canopies than for the above scenario. However, it is agrometeorological weather stations which are installed in agricultural areas where this and other studies of this nature take place. Should only agrometeorological weather station data be available, the upscaling of the available meteorological data to a higher reference height should be investigated based on radiosonde observations (Ershadi, 2010).

The effect on d_0 in high canopies is shown by using the Mouton's Valley site as an example, and testing for the sensitivity of daily *ET* to d_0 (Figure 37) At approximately d_0 = 1.8 m, a rapid decrease in daily *ET* estimation is noted as d_0 approaches 2 m. It can be surmised therefore (although this should be tested in different environments and under different meteorological conditions) that when using wind speed measured at 2 m above the surface, the SEBS model should not be used in canopies of 2.7 m and higher as it is at this point that the model becomes highly sensitive to changes in d_0.

The uncertainty in the calculation of the sensible heat flux introduced when the displacement height approaches the height of wind speed measurement should be carefully considered and addressed since errors in the calculation of the sensible heat flux will be propagated through the model and will eventually influence the final *ET* calculation as demonstrated in this study.

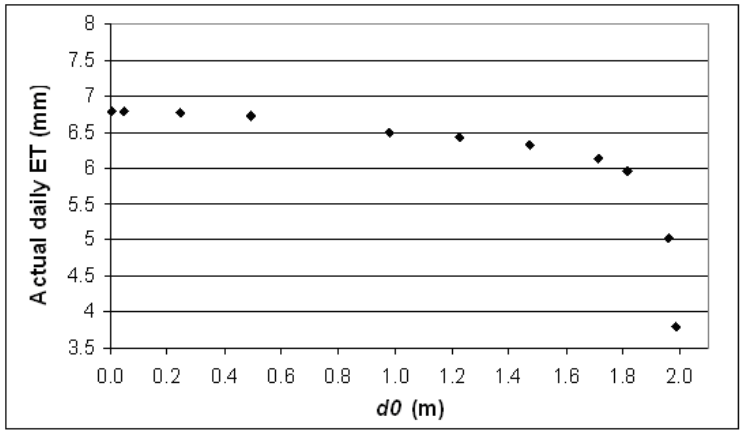

Figure 37: Sensitivity of SEBS-estimated *ET* to d_0 for the Mouton's Valley field validation site when wind speed is measured at 2m.

6.3.4. HETEROGENEITY OF THE STUDY AREA

Heterogeneity as related to the concept of the spatial variability of a landscape plays an important role in the application of remote sensing data to the calculation of *ET*, especially in the selection of the spatial resolution of the particular sensor. Various studies have shown that, for complex heterogeneous landscapes, there is lower confidence in variables derived using low resolution sensor data (Moran *et al*., 1997; Kustas *et al*., 2004; Garrigues *et al.*, 2006; McCabe & Wood, 2006; Li *et al.*, 2006; Li *et al*., 2008; Lakhankar *et al*., 2009) as intra-pixel spatial heterogeneity is lost due to the integration of the radiometric signal.

The effect of heterogeneity on SEBS derived *ET* can be illustrated by comparing the results from a single date (28 February 2008) ASTER image at 90 m resolution with the results of the same date MODIS image at 1 km resolution for the Mouton's Valley site and for the Piketberg: Pools-Ideal Hill site in Figure 38. When the SEBS model was run on the ASTER image, it was apparent that the albedo estimation for both the homogeneous and heterogeneous sites was unrealistically low when compared with literature values. When the albedo calculation was carried out on the ASTER image which had not been atmospherically corrected, the albedo values more closely matched literature values. Since the ASTER and MODIS sensors are on board the same platform (TERRA) and the images were captured simultaneously and therefore under exactly the same atmospheric conditions with identical sensor and solar zenith angles, the SEBS model was rerun on the MODIS and ASTER data without applying atmospheric correction, in order to remove any bias that this low albedo may be introducing in the ASTER results. This approach is justified since the results are used for comparative purposes only and results are not being assessed relative to field values or images from other dates. The uncorrected images were only used in this section to analyze the impact of heterogeneity and all other results reported on in this chapter are derived from images that have been atmospherically corrected.

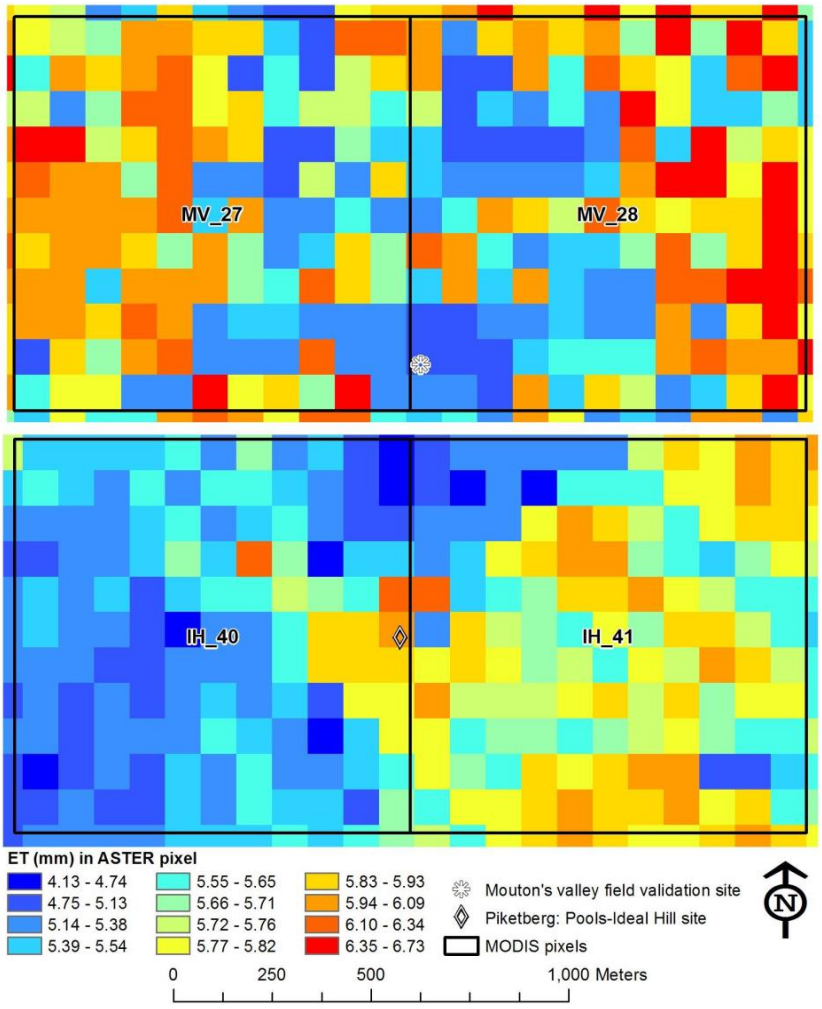

Figure 38: SEBS derived *ET* from ASTER data shown in the context of two MODIS pixels for both the Mouton's Valley site (above) and the Piketberg: Pools-Ideal Hill site (below).

Since both the Mouton's Valley site and the Piketberg:Pools-Ideal Hill site are located close to a pixel boundary, the results of two adjacent MODIS pixels are presented and labelled MV_27 and MV_28 for the Mouton's Valley site and IH_40 and IH_41 for the Piketberg:Pools-Ideal Hill site. In Table 14 the mean and standard deviations of digital elevation model (DEM) from the Shuttle Radar Topography Mission (SRTM), *NDVI* and T_0 at ASTER resolution (90m) for the selected MODIS pixels at each site are shown. The standard deviations of elevation (*DEM)*, *NDVI* and T_0 indicate that at ASTER resolution, the Mouton's Valley site is more heterogeneous than the Piketberg:Pools-Ideal Hill site.

Table 14: Heterogeneity of Mouton's Valley field validation site vs. Piketberg: Pools-Ideal Hill site illustrated by mean and standard deviation of DEM, *NDVI* and T_0.

	MODIS		ASTER	
Parameters	**Pixel**	**Value**	**Mean**	**Std Dev**
DEM	MV_27	641 mamsl	556.98 mamsl	39.67
	MV_28	641 mamsl	550.87 mamsl	52.26
	IH_40	187 mamsl	159.14 mamsl	3.56
	IH_41	179 mamsl	166.57 mamsl	6.48
NDVI	MV_27	0.38	0.39	0.16
	MV_28	0.38	0.45	0.16
	IH_40	0.18	0.13	0.04
	IH_41	0.16	0.11	0.01
T_0	MV_27	300.58 K	301.39 K	2.62
	MV_28	300.59 K	298.00 K	1.47
	IH_40	310.42 K	310.23 K	1.04
	IH_41	311.32 K	309.23 K	0.71

Table 15 and Table 16 show that the R_n estimation is lower when using MODIS than when using ASTER in both the homogeneous and heterogeneous sites. In both the more heterogeneous and homogeneous area, the energy partitioning (the percentage of R_n allocated to G_0, H and LE) remains similar regardless of the resolution of the pixel. However a bigger variation in the more heterogeneous area is observed. For the Piketberg:Pools-Ideal Hill site, G_0, H and LE allocation is the same regardless of the resolution of the calculation. At the Mouton's Valley site (Table 16), the ASTER results show lower allocation of energy to G_0 and a higher allocation of energy to H when compared to the MODIS results. Energy allocation to LE is marginally higher at ASTER resolution than at MODIS resolution.

For the Piketberg:Pools-Ideal Hill site (Table 16), the ET estimated from ASTER and averaged for each of the MODIS pixels is 5.4 mm and 5.7 mm and with standard deviations of 0.34 and 0.26 for IH_40 and IH_41 respectively (Fig. 10). The ET estimated from MODIS for IH_40 and IH_41 are 6.3 mm and 6.1 mm respectively. For the Mouton's Valley site (Table 15), the ET estimated from ASTER and averaged for each of the MODIS pixel is 5.7 mm and 5.8 mm and with standard deviations of 0.36 and 0.46 for MV_27

and MV_28 respectively. The *ET* estimated from MODIS for both MV_27 and MV_28 is 6.4 mm. At both the more heterogeneous Mouton's Valley site and the more homogeneous Piketberg: Pools-Ideal Hill site, the *ET* calculated from the ASTER scene and averaged to the MODIS pixel resolution is less than the MODIS derived *ET* for the same pixels.

Table 15: Comparison of energy partitioning in MODIS pixels for more heterogeneous Mouton's Valley field validation site: mean ASTER value per pixel vs. MODIS pixel value.

	MODIS	**ASTER**		**Energy partitioning**	
Parameter	**pixel**	**Mean**	**Std Dev**	**MODIS**	**ASTER**
Fc	0.20 0.20	0.29 0.43	0.37 0.41		
evaporative fraction	0.91 0.91	0.88 0.87	0.05 0.06		
G0	137.30 137.28	113.96 103.60	45.99 56.94	26.20% 26.20%	23.68% 20.26%
H	36.24 36.35	43.52 53.40	22.35 30.15	6.92% 6.94%	9.05% 10.44%
LE	350.49 350.34	323.68 354.28	43.19 36.81	66.88% 66.86%	67.27% 69.29%
Rn	524.03 523.97	481.17 511.28	21.90 18.80		
ET daily	6.38 6.37	5.72 5.75	0.36 0.46		

Since the difference in the evaporative fraction results (as borne out by the energy partitioning) is marginal using different pixel resolutions, it would be expected that there should be agreement between the daily *ET* results at both resolutions. However, since this is not the case, the difference in daily *ET* results can be ascribed to the upscaling of evaporative fraction to daily *ET*. At the heterogeneous site, even though the results from ASTER do detect more variability in the energy partitioning, the evaporative fraction results indicate that the significance of this variation is rather minimal when comparing the higher resolution results to the lower resolution results. More significant

Table 16: Comparison of energy partitioning in MODIS pixel for more homogeneous Piketberg: Pools-Ideal Hill site: mean ASTER value per pixel vs. MODIS pixel value.

	MODIS	**ASTER**		**Energy partitioning**	
Parameter	**pixel**	**Mean**	**Std Dev**	**MODIS**	**ASTER**
fc	0.00 0.00	0.00 0.00	0.00 0.00		
evaporative fraction	0.85 0.85	0.84 0.87	0.04 0.02		
G0	121.77 118.91	106.51 112.86	5.44 4.38	31.50% 31.50%	31.30% 31.39%
H	39.05 39.25	37.52 32.73	10.94 5.70	10.10% 10.40%	11.03% 9.10%
LE	225.75 219.34	196.26 213.91	14.23 10.25	58.40% 58.10%	57.67% 59.50%
Rn	386.57 377.50	340.30 359.50	15.84 11.38		
ET daily	6.25 6.09	5.35 5.71	0.34 0.26		

appears to be the higher daily *ET* results from MODIS than ASTER indicating uncertainty in the upscaling of evaporative fraction to daily *ET*. This suggests that, for this particular example, landscape heterogeneity is not the dominating factor at energy partitioning level whereas the resolution of the sensor does appear to play a role in the upscaling from instantaneous to daily *ET* through the use of albedo (Equations [18] and [19]). Since atmospheric correction was not carried out on the images and the sample size was small, general conclusions cannot be made, although the results do point towards the importance of accurate albedo estimations for the upscaling of evaporative fraction to daily *ET* and that landscape heterogeneity may play a role at this level rather than at energy partitioning level.

The complexities associated with the derivation of *ET* and the uncertainties described in this chapter imply that potential errors will be introduced at various stages of *ET* derivation. These errors are related to error production and error propagation as defined by Veregin (1989). Error production refers to a situation where errors in output products are attributed mainly to the specific operations applied to the data, thereby producing errors in the output products while no errors were present in the original data used as input. On the other hand, error propagation refers to the process where potentially erroneous input data is passed through certain processing sequences and errors accumulate in output products. In the case of deriving *ET*, errors will be compounded if intermediate error-bearing output products are used in additional processing sequenced to derive the final result.

The opportunity for error production is introduced when it is considered that the SEBS model is complex in itself as it consists of three tools (Su, 2006), namely:

- a set of tools to determine physical parameters of the land surface;
- an extended model to derive roughness length for heat transfer; and
- a model to determine evaporative fraction on the basis of the energy balance.

An example of error production was illustrated in the case of deriving fractional vegetation cover using ill-defined *NDVI* limits. An error in the calculation of fractional vegetation cover would be propagated to soil and sensible heat flux calculations. This in turn will be propagated to the calculation of the latent heat flux and therefore *ET*. Prior to adjusting for the study area, *ET* was set at the wet limit, although this was not the case after $NDVI_{max}$ was adjusted. In the absence of known suitable *NDVI* maximum and minimum values *a priori,* a fractional vegetation cover formula, such as proposed by Choudhury (1987) cited by French *et al*. (2003), which makes use of *LAI* rather than NDVI may be used.

The opportunity for error propagation is introduced at the initial stages of *ET* derivation when it is considered that remote sensing data together with standard meteorological data are required by the SEBS model. Due to uncertainties associated with remote sensing and the interpolation of meteorological data, potential errors will propagate throughout the processing sequence. An additional

opportunity for error propagation is introduced when considering land surface temperature, air temperature and their gradient ($T_0 - T_a$) since T_0 values derived from two different sources differed by up to 10 K for the field validation site. The sensitivity of SEBS to $T_0 - T_a$ appears to vary between land covers and the sensitivity may be dependent on the estimated T_0 value itself. This implies that an error in the input data would propagate through the model and cause uncertainty in the final derivation of *ET*. However, the range in uncertainty cannot be modelled as it appears to vary between land cover types. Furthermore, the use of air temperature from weather stations interpolated across a study area introduces more opportunities for error propagation, especially in a heterogeneous environment where T_a may vary over a short distance dependent on *inter alia* land cover. This will be compounded in areas with limited weather station coverage in a heterogeneous environment due to the influence of topography on near-surface weather conditions.

From the data presented here it can be seen that the study area comprises a spatially diverse landscape with a high level of heterogeneity. In order to successfully estimate *ET* and capture the full range of variability in fluxes, the choice of spatial resolution of remote sensing data is crucial. Kustas *et al*. (2004) and Li *et al*. (2006) found that when the spatial resolution exceeds 500 m, mixed pixels containing large contrasts in surface temperature and vegetation cover could cause significant errors (Li *et al.*, 2008). Flores *et al*. (2009) also demonstrated the impact of topographic heterogeneity on near-surface soil temperature. McCabe & Wood (2006) found that MODIS has limited capacity in capturing the spatial variability in fluxes at field level but estimates for the spatial average flux at large scales may be accurate (McCabe & Wood, 2006). The results presented here differ from those reported in the listed literature in that it was found that although the absolute values for the various energy fluxes differ from MODIS to ASTER, the proportional partitioning of energy compared well between the MODIS and ASTER results at both the more homogeneous site and the more heterogeneous site. However, it is in the upscaling of evaporative fraction to daily *ET* where the uncertainty appears to be introduced when working at varying resolutions. The sensitivity of the SEBS model to albedo with a focus specifically on the upscaling of evaporative fraction to daily *ET* is lacking in the literature as often the sensitivities to input parameters are determined by assessing the sensible heat flux results (such as Badola, 2009; Van der Kwast *et al*., 2009). Mariotto & Gutschick (2010) proposed that since most vegetation canopies are non-Lambertian reflectors, the assumption of a horizontally homogeneous Lambertian surface reflecting energy equally in all directions affects the calculations of albedo and vegetation index. They show that if the spatial variation of non-Lambertian reflectance can be formulated, the accuracy of the estimation and discrimination of *ET* among different land cover types

can be improved. This is particularly true in a heterogeneous environment. It is possible that the assumption of Lambertian reflectance in a heterogeneous environment may be the reason for lower than anticipated albedo values at ASTER resolution.

The zero plane displacement height (and therefore the height of the canopy) has been highlighted as being an important factor to consider in combination with the reference height at which the wind speed is measured. It was shown in Figure 37 that as the displacement height tends to the reference height at which wind speed is measured, there is a rapid drop-off in *ET* estimates. Since wind speed is routinely measured at 2, 5 and 10m above the surface, when using these models in taller canopies, the user should ensure use of a weather station measuring wind speed at 10 m above the surface. By implication, the same models will not be suitable for use in canopies of taller than 15 m.

In this chapter, the sensitivities of SEBS estimated daily *ET* to various parameters have been shown. The sensitivities have always been related back to daily *ET* rather than the sensible heat flux since it is the daily *ET* which is of interest to water managers and other users of the results of the SEBS model. Generalizations regarding the magnitude of errors produced by uncertainties in the input data have not been made as the dependence on study area and the interaction of various input parameters in the model was not the objective of this study. However, it has been shown that users should consider which input parameters can be calculated outside of the prepackaged version of SEBS and a decision as to which is the most appropriate methodology should be taken.

6.5. CONCLUDING REMARKS

The results presented here can be used to improve on the project by Gibson *et al*. (2009) to determine the usefulness and applicability of using remote sensing technologies as a tool for resource assessment and determination of water use. Although promising, uncertainties in estimating the various parameters were encountered. These uncertainties could broadly be classified as 1) errors in input data, 2) uncertainties related to spatial heterogeneity of the study area and resolution of input data, and 3) processing errors resulting in either error production or error propagation or both.

In this chapter some of these uncertainties are described by using the example of the derivation of evapotranspiration using the SEBS model. Uncertainty related to input data was demonstrated through investigating problems related to land surface and air temperature as well as in the derivation of displacement height. Uncertainty related to the heterogeneity of the study area in terms of land cover and topography in relation to the spatial resolution of input data was also demonstrated. Finally, uncertainty in data processing was demonstrated using the case of determining fractional vegetation cover as example. These uncertainties and potential errors are compounded when considering that applying the SEBS model for calculating *ET* is a complex process, requiring several image processing sequences that are combined to produce the final result. This may lead to a situation where errors may be propagated and compounded through the processing chain, eventually affecting the final output product.

The various uncertainties and potential errors of propagation and production are associated with the accuracy of the final output product. Ideally, sources of uncertainty will need to be identified and the accumulation and propagation of errors will need to be modelled. This will enable the quantification of error or uncertainty originating either from source data or through processing errors. Simultaneous multi-parameter sensitivity analysis of inputs which are used in the SEBS model would help in determining to which parameters the SEBS model is most sensitive and under which conditions these sensitivities are the most pronounced. This would begin to address the uncertainties highlighted in this research and may lead to greater confidence in using SEBS generated *ET* results.

Although illustrating uncertainty using *ET* as an example, the derivation of all the components of the water balance equation using remote sensing data was influenced by similar uncertainties and the actual water consumption of individual agricultural fields could not be calculated. However, methodologies untested in South Africa were applied to the study area with many challenges encountered at both a data and skills capacity level. If the uncertainties and limitations encountered in the course of the research project are considered and acted upon it may be possible that at least parts of the methodology may be relevant at a later stage for water use determination.

In conclusion, users of the pre-packaged version of SEBS in ILWIS are offered the following advice:

1. Since SEBS is sensitive to the T_0 - T_a gradient, care should be taken when estimating T_0 in a topographically diverse area as retrievals are less accurate in this setting. In particular, SEBS should not be used in mountainous areas with coarse resolution sensors since the heterogeneity of the T_0 cannot be captured at the appropriate scale. Furthermore, the sensitivity to $T_0 - T_a$ is also dependent on whether the wet-limit has been reached.

2. Care should be taken when selecting a fractional vegetation cover formula as this should be appropriate for the study area, especially if *NDVI* min and max values need to be defined. In particular, it is advised that if a *LAI* product is available at the appropriate scale, that it be used to estimate fractional vegetation cover according to the formula by Choudhury (1987).

3. The reference height of the weather station should be considered in relation to the canopy height of the study area. In an area where field crops with a low canopy height predominate, the use of an agrometeorological weather station is appropriate. However, where tree crops and natural vegetation with a canopy height exceeding 2.7 m are found, weather stations which measure wind speed at 10 m are probably more appropriate.

4. The scale at which the evapotranspiration results are required must be considered in relation to the choice of sensor and therefore pixel resolution and the heterogeneity of the study area. When working at a catchment scale a coarse resolution sensor may be appropriate for energy partitioning, whereas, for farm or field scale results a higher pixel resolution will be required to detect inter-field or inter-farm variations. The influence of albedo on the accurate upscaling of evaporative fraction to daily *ET* should be considered and this may also be a function of landscape heterogeneity.

7. ACCOUNTING FOR MODEL UNCERTAINTIES

From the conclusions drawn in Chapter 6, implementing the recommended changes to the methodology and validating the results in the Moutons Valley validation site would have little value for the following reasons: 1) The topography of the field validation site lends itself to uncertainties in T_0 and T_a due to the close proximity of the mountain on either side of the field validation site. 2) The reference height at which wind speed is measured cannot be changed retrospectively for the field validation period. 3) The heterogeneity in the environs of the field validation site implies that the results may be valid at catchment scale but at field or farm scale, the MODIS pixel resolution is not suitable. 4) The short field campaign period required that all available MODIS images be selected and processed to achieve the maximum number of SEBS derived energy flux results for comparison with the field validation results. Therefore single MODIS images were used rather than 8-day or 16-day products and atmospheric correction is required for these daily products and at times, high solar and sensor zenith angles are inevitable.

However, the research would not be complete without testing the advice given in Chapter 6 to users of the prepackaged SEBS model. Since some of the proposed changes would be impossible to apply to the Moutons Valley validation site retrospectively, a new study area was selected. The changes to the methodology are described in Chapter 7.1 with some analysis and discussion given around each of these modifications. In Chapter 7.2, the results of having adapted the methodology in a new study area are presented along with a discussion.

The attention to ensuring the highest accuracy and suitability of input data involved: the preselection of a homogeneous catchment at MODIS pixel resolution, use of an already atmospherically corrected MODIS data product, the adjustment of the *NDVI* maximum value for use in the fractional vegetation cover formula, the use of a South Africa Weather Services weather station data to measure the wind speed at 10m rather than at 2m, the use of literature values and a land cover map to assign roughness length and displacement height estimates and finally the use of both TERRA and AQUA images to determine the impact of land surface air temperature gradient and time of day at which the satellite image was captured. The selection process for the two quaternary catchments (Gibson *et al*., 2011) considered the homogeneity of quaternary catchments and the availability of data to ensure the most

homogenous catchments with the necessary data required. The remaining considerations and adaptations to the previously presented methodology (Chapter 4) are now explained and some of the results presented.

Quaternary catchment P10A is located immediately to the north-west of Grahamstown (Figure 39). It is a 'pear shaped' catchment with a total area of 125.6 km^2. It comprises undulating topography with valleys that are quite deeply incised in places. The topographical elevation in the catchment ranges from 487 mamsl to 806 mamsl. The annual average rainfall is 466 mm/a. The rainfall in the area is lowest in the winter months of June and July. It receives the lowest rainfall (~16 mm/month) in July and the highest (~57 mm/month) in March (October is also a high rainfall month). The monthly distribution of average daily maximum temperatures shows that the average midday temperatures for Grahamstown range from 18.9°C in July to 26.8°C in February. The region is coldest during July when the temperature drops to 5.6°C on average during the night.

The land cover which most commonly occurs in catchment P10A is 'Thicket, Bushland, Bush Clumps, High Fynbos', followed by 'Shrubland and Low Fynbos' (Van den Berg *et al.*, 2008). These two classes make up 97.2 % of the entire catchment.

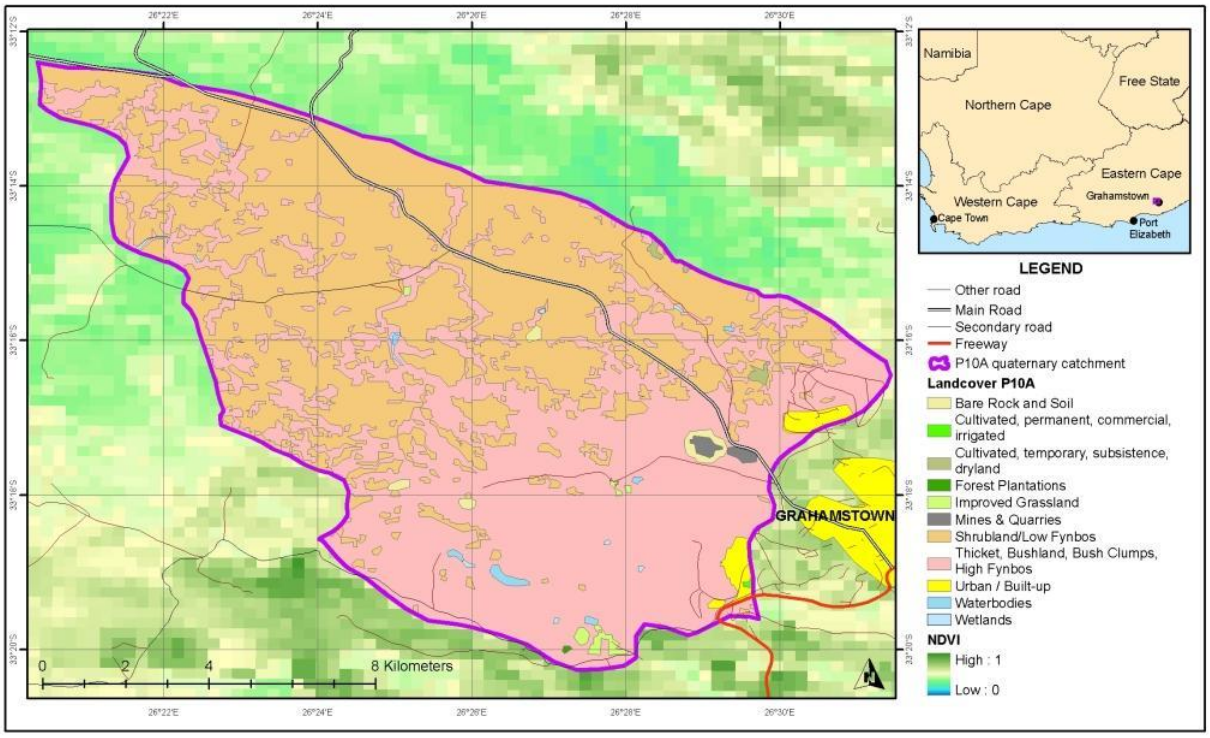

Figure 39: P10A study area.

7.1. ADAPTING THE METHODOLOGY

The methodology presented in Chapter 4 was modified and applied to the P10A catchment over the period July 2006 to June 2007. The aspects are discussed are: atmospheric effect (Chapter 7.1.1), fractional vegetation cover (Chapter 7.1.2), reference height (Chapter 7.1.3), land surface and air temperature gradient (Chapter 7.1.4) and roughness lengths (Chapter 7.1.5).

7.1.1. ATMOSPHERIC EFFECTS

The accurate retrieval of surface reflectance and temperature is very important in deriving land surface biophysical parameters and in the determination of fluxes. In mapping the surface physical properties the surface information is highly affected by atmospheric components (scattering by aerosols and absorption by gases, such as oxygen, water vapour and ozone) and their magnitude (Hailegiorgis, 2006). The simplified method for atmospheric correction (SMAC) proposed by Rahman & Dedieu (1994) has been programmed into the prepackaged SEBS model in ILWIS to correct for the effects of the atmosphere on MODIS visible, near infrared and shortwave infrared data. SMAC is a radiative transfer model and therefore requires a description of the components in the atmospheric profile in order to correct for these effects.

Each of the reflective bands (bands 1-5 & 7) is atmospherically corrected using SMAC. Due to many pixels of missing data in the MODIS atmospheric products over the Gibson *et al.* (2009) study area, mean values were used to correct for the entire study area leading to some doubt as to the accuracy of the method. To negate the need for atmospherically correcting MODIS level 1B images as was the approach of Gibson *et al.* (2009), the MCD 43 - Surface Reflectance BRDF/Albedo Product – specifically MCD43A4 was used. The models used in creating this product best describe the differences in radiation due to the scattering (anisotropy) of each pixel and rely on multi-date, atmospherically corrected, cloud-cleared input data measured over 16-day periods. Both Terra and Aqua data are used in the generation of this product, providing the highest probability for quality input data (http://modis-land.gsfc.nasa.gov/brdf.htm). This corrected data can then be used for the calculation of all input parameters derived from the MODIS reflective bands on the assumption that parameters such as

albedo, *NDVI* and fractional vegetation cover generally do not significantly change over a 16-day period. Although this assumption may not always hold true especially after rainfall events following a prolonged dry period, at an annual time scale, phenological changes are probably adequately captured.

To minimize the influence of the atmosphere on the MODIS radiative bands which are used to derive land surface temperature, the day of year which was predominantly used in each catchment for the MCD43A4 can be considered. The MODIS data products select the best quality data in the 16-day period to estimate the reflectance products. The assumption is therefore made that on that particular day, factors such as atmospheric effects (including the presence or absence of clouds) and solar and sensor zenith angles are most favourable and the best quality thermal infrared data will also be available.

The atmospheric transmissivity on a particular day can also be considered. Atmospheric transmissivity (also known as the clearness index) is the ratio of global solar radiation at ground level to extra-terrestrial solar radiation. An example of the top of atmosphere (TOA) radiation versus the shortwave radiation which reaches the land surface is shown in Figure 40 where it can be seen that the TOA radiation is a perfect sinusoidal curve whereas the surface shortwave radiation is erratic as it is influenced by atmospheric particles and cloud cover. The atmospheric transmissivity should be calculated at image capture time for selected images by dividing the solar radiation measured at the appropriate weather station by the calculated extra-terrestrial solar radiation from date, latitude and time of day using the formula given in Allen *et al.* (1998). Images with the highest atmospheric transmissivity should be selected for further analysis.

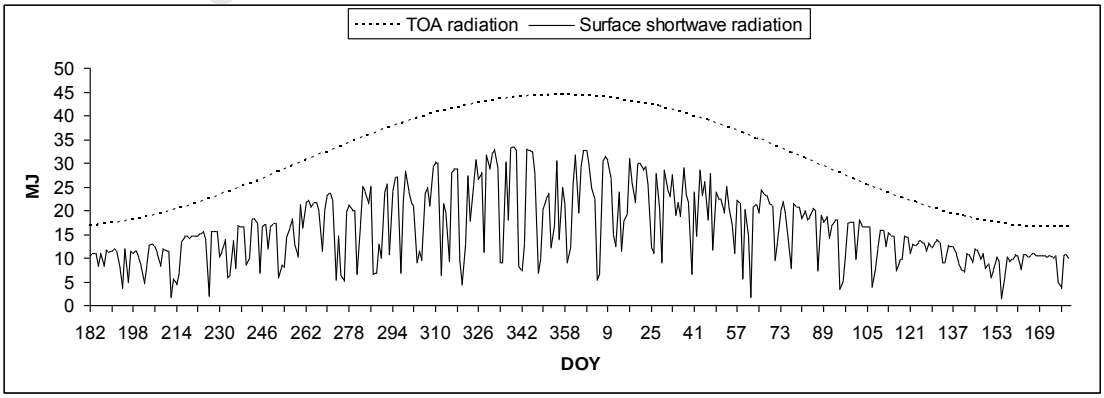

Figure 40: An example of top of atmosphere radiation versus surface shortwave radiation at the same location .

7.1.2. FRACTIONAL VEGETATION COVER

Fractional vegetation cover (f_c) is a user defined input into the pre-packaged version of SEBS in ILWIS and different formulations of f_c are used in SEBS for different purposes. Fractional vegetation cover and its complement are used in the calculation of the roughness length for heat transfer (Su *et al.*, 2005) which, in turn, is used in the calculation of the sensible heat flux. In addition, f_c is used in the estimation of the soil heat flux (Su, 2002).

It has already been stated that care should be taken when selecting fractional vegetation cover formula as this should be appropriate for the study area, especially if *NDVI* minimum and maximum values need to be defined. For the P10A catchment, the formula by Carlson & Ripley (1997) was used with a scene specific $NDVI_{max}$ value defined. The *NDVI* maximum values over the study period were analyzed and the 98th percentile value of $NDVI_{max}$ (0.756) was assigned (Gibson *et al.*, 2011).

In Chapter 6.3.2, several methods for the calculation of f_c which are described in the literature are highlighted.. These methods generally make use of *LAI* (Choudhury, 1987) as input or require pixel *NDVI* together with a minimum and maximum *NDVI* (Carlson & Ripley, 1997; Gutman & Ignatov, 1998). These minimum and maximum NDVI are either constant (Sobrino & El Kharraz, 2003) or can be derived directly from the scene or from a time series. For example, if fractional vegetation cover is calculated according to the formula for vegetation proportion (Sobrino & El Kharraz, 2003), then NDVI minimum is defined to be 0.2 and NDVI maximum is 0.5, where pixels with NDVI values of 0.5 or higher are considered to be fully vegetated and pixels with values of 0.2 or lower to be bare soil. The values between NDVI minimum and maximum represent the mixed vegetation cover with differing degrees of sparse vegetation.

It was earlier (Chapter 6.3.2) concluded that if it is possible to obtain field data in order to derive an appropriate NDVI maximum value, the formula by Carlson & Ripley (1997) can be used. Alternatively the formula by Choudhury (1987) using *LAI* as input may be used.

For P10A catchment the formula by Carlson & Ripley (1997) was used with NDVI minimum and maximum being derived from a time series analysis of NDVI values for the study area during the study period.

Showing the effect of utilizing the *LAI* approach to estimate f_c against the method using appropriately selected $NDVI_{max}$, Gibson *et al*. (2011) show the effect on the calculated sensible heat flux and the sensible heat flux at the wet and dry limits of using the two approaches (Figure 41). It can be seen that when using the *LAI* approach, the calculated sensible heat flux (H) is higher by 0-20 W.m^{-2}. The calculated sensible heat flux at the dry limit (H_{dry}) is higher by 10-30 W.m^{-2} and the sensible heat flux at the wet limit (H_{wet}) is generally lower by –10 - –20 W.m^{-2}. The changes in H_{wet} and H_{dry} are due to the influence of fractional vegetation cover on the soil heat flux (G_0) alone, whereas the change in H is due to the use of fractional vegetation cover (and its complement) in the calculation of roughness length for heat transfer (Su, 2002). In this particular example, it is therefore shown that using ill-defined $NDVI_{max}$ to estimate fractional vegetation resulted in a lowering of the sensible heat flux which would contribute to overestimations of *ET* (Gibson *et al*., 2011).

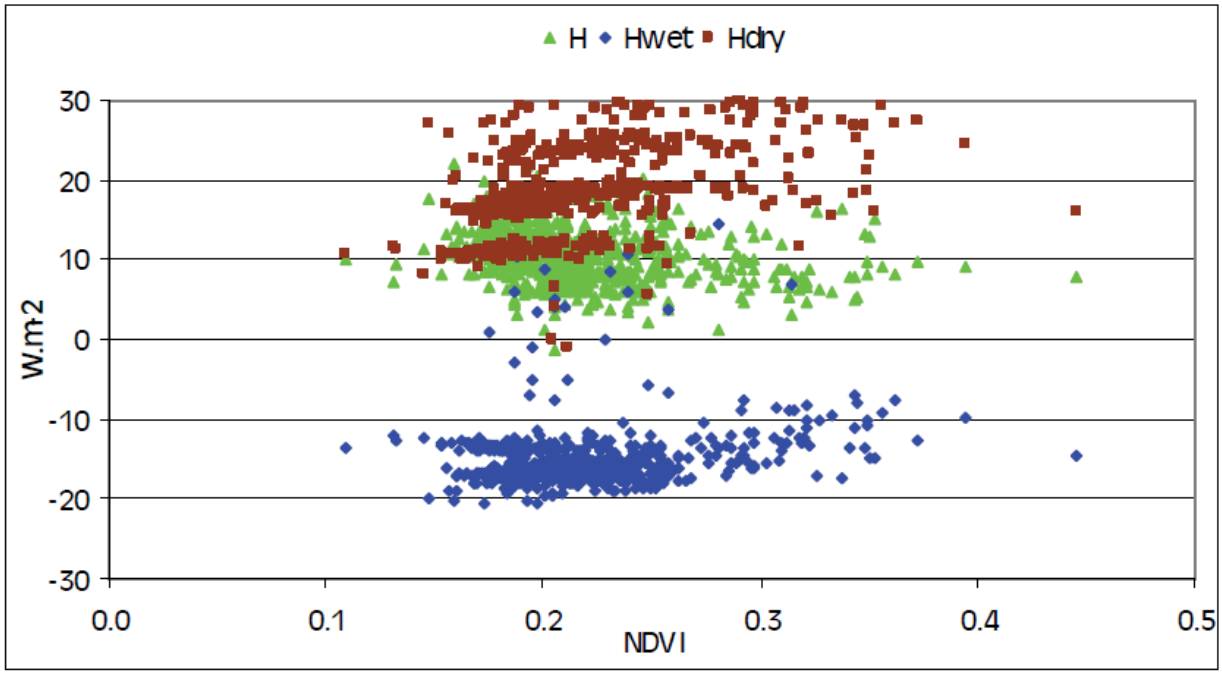

Figure 41 Difference in sensible heat flux results when using the *LAI* or *NDVI* approach to calculate the fractional vegetation cover. The results obtained with using the *NDVI* approach are subtracted from the results obtained with the LAI approach (Gibson *et al*., 2011).

To contextualize this, it should be stated that this calculation was done for a January image where the net radiation is over 600 $W.m^{-2}$. Therefore 0 – 20 $W.m^{-2}$ differences in the sensible heat flux only accounts for a very small difference in the overall energy balance. Therefore although the calculation of fractional vegetation cover either through the choice of $NDVI_{max}$ or through the *LAI* approach should be chosen appropriately (as it is important to reduce all sources of uncertainty from the modelling), the effect of using one method rather than the other was shown not to be the major source of underestimation of the sensible heat flux, in this research.

7.1.3. REFERENCE HEIGHT

The sensitivity of the SEBS model to the reference height at which wind speed is measured, particularly in areas with tall canopies, has been discussed (Chapter 6.3.3). For tall vegetation the 2 m reference height from ARC-ISCW weather stations may not suitable. For this reason SAWS weather station data was used since wind speed is measured at 10 m above the surface and it may be more appropriate in study areas which include tall canopies.

7.1.4. LAND SURFACE AND AIR TEMPERATURE GRADIENT

The calculation of *ET* using the SEBS model relies on two temperature sources: air temperature (T_a) and land surface temperature (T_0). Su (2002) reported on the sensitivity of sensible heat flux to the gradient between land surface temperature and air temperature and Badola (2009) reported that of all remotely sensed input parameters, SEBS was most sensitive to change in T_0-T_a. T_0 plays a role in the determination of net radiation and therefore soil heat flux, but its main contribution (together with the aerodynamic resistance) is in the calculation of the sensible heat flux.

It can be seen from Equations [4] and [5] that at the wet and dry limits, the land surface and air temperature gradient is not considered in the calculation of the sensible heat flux. For this reason, T_0-T_a does not play a role in the calculation of *ET* if the wet or dry limits have been reached. However, T_0-T_a is used to determine whether or not the limits are reached (Equations [6], [7] and [8]) and therefore should not be completely discounted in these instances. The sensitivity of the sensible heat flux $\Delta(T_0\text{-}T_a)$

for two different environments was calculated in Chapter 6.3.1 and it was concluded that the sensitivity of H (and therefore daily *ET*) to $\Delta(T_0\text{-}T_a)$ is dependent not only T_0 but also on the land cover type (and therefore associated roughness parameters), and whether the wet limit has been reached. It can be seen in Figure 34 that in two different environments, the sensitivity of SEBS calculated daily *ET* is dependent on both the land cover and $T_0\text{-}T_a$. For each scenario in Figure 34, the wet limit occurs at the apex of the respective curve. Where the wet limit has been reached, the daily *ET* increases with increasing $T_0\text{-}T_a$; however, where the wet limit has not been reached, the daily *ET* decreases with increasing $T_0\text{-}T_a$. It was concluded that SEBS should not be used in mountainous areas or topographically diverse areas as T_0 retrievals are less accurate in this setting and particularly with coarse resolution sensors since the heterogeneity of the T_0 cannot be captured at the appropriate scale. Topographical analysis of potential study areas should be done to minimize the uncertainties that inaccurate T_0 calculations will contribute to the *ET* results.

However, should the uncertainties associated with $T_0\text{-}T_a$ be reduced and $T_0\text{-}T_a$ is assumed to be correct, H has been shown to be sensitive to fluctuations in this term especially in unstable conditions and in the transition phase where $T_0\text{-}T_a$ moves from negative to positive and back again (Su, 2002). According to Su (2002), this sensitivity is suspected to be caused by the current stability correction functions used in SEBS not adequately describing this transition. This was found to be particularly true in the shrubs and grasslands experiments and more accurate results for agricultural areas were found (Su, 2002). In the similarity theory used in the formulation of the sensible heat flux (Equations [6], [7] and [8]), steady state and horizontally homogeneous conditions are assumed (Gellens-Meulenberghs, 2000) which may not always be good descriptors of natural vegetation and topography in South Africa. It should also be noted that many of the agrometeorological theories and formulae were developed for agricultural crops and not for natural vegetation and perhaps additional parameterization should be considered for those land uses which fall outside of agricultural crops.

Furthermore, since the lag effect of the heating of land differs to the heating of the air and therefore $T_0\text{-}T_a$, the time of day of image acquisition may be important and the choice of satellite sensor (such as TERRA which captures images in the morning versus AQUA which captures images in the afternoon) should be considered in this context. Further considerations are the superior functioning of the AQUA MODIS over the TERRA MODIS sensor. The difference in launch dates allowed for some improvements to be made to the AQUA instrument. Xiong *et al*. (2002b) report on the differences between AQUA and

TERRA signal-to-noise ratios (SNR) and on-orbit noise equivalent temperature differences. The reported results on both these parameters are that AQUA performs better than TERRA; however, TERRA is performing within the prelaunch standards (with the exception of band 7).

Since the aim of this research was to minimize uncertainties as far as possible, the selection of homogeneous catchments (particularly with respect to topography but also considering land cover), should minimize the uncertainties associated with T_0 estimation in the chosen catchments. For this reason P10A was chosen as being homogeneous (Gibson *et al*, 2011). To minimize the uncertainties for the thermal bands, data from the AQUA sensor was used for the majority of the processing, however, TERRA data was also used for comparative purposes and to indicate the influence of the time of day on *ET* results due to differing meteorological conditions and differing T_0-T_a due to the differential heating of the land surface and the air.

It has already been stated that T_0-T_a is used in the calculation of the sensible heat flux and it should be noted once again that *H* is inversely related to *ET*. As the energy allocated to heating the air increases, so the energy available to evaporate water decreases. This in turn leads to a decrease in evaporative fraction and a decrease in *ET*. The effect of using TERRA data versus using AQUA data is illustrated in Figure 42. It can be seen that when using TERRA data which is captured in the morning, T_0-T_a is lower than T_0-T_a calculated using AQUA data which is captured in the afternoon. It can also be seen by the negative slope of the TERRA results in Figure 42 that the sensible heat flux is always calculated to be at the wet limit when using TERRA data. An indication of the wet limit having been reached is the decrease in sensible heat flux with increase in T_0-T_a whereas the positive slope indicates that the wet limit has not been reached and *H* is calculated using combination equations (Equations [6], [7] and [8]). It appears that at TERRA overpass, the transition phase where T_0-T_a moves from negative to positive is not complete, unstable conditions exist and the stability correction functions in SEBS are not suitable.

Paradoxically, the fact that the wet limit has been reached does not necessarily mean that the daily estimated *ET* calculated from using TERRA data will be higher than the AQUA results due to the inverse relationship between *H* and *ET* and the fact that AQUA results are generally close to the wet limit and therefore clustered around the wet limit transition.

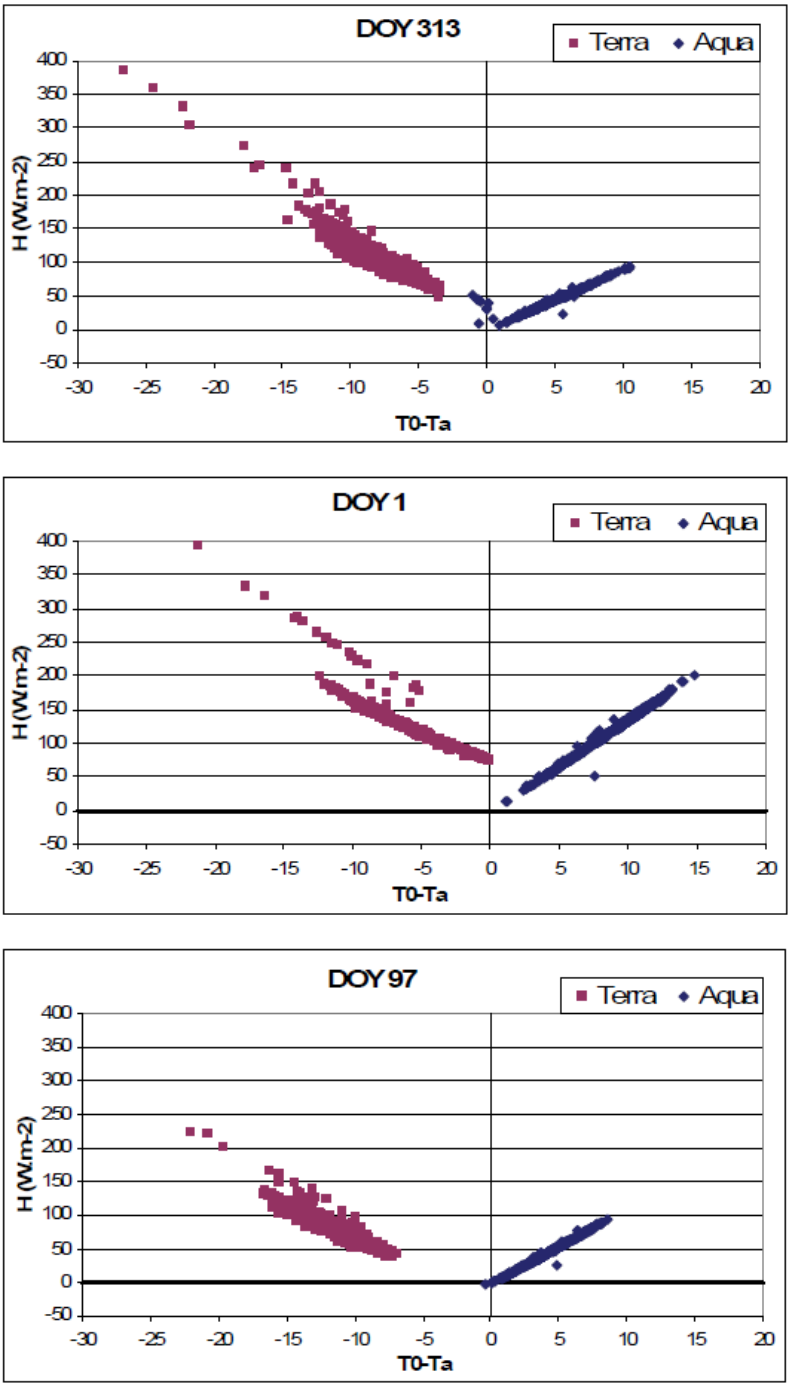

Figure 42: Sensible heat flux calculated using TERRA and AQUA data on the same day plotted against T_0-T_a.

These results have very important implications for selecting suitable satellite imagery for a remote sensing energy based *ET* estimation (particularly with respect to the time of day of image capture) and further research is required on this topic.

According to Allen *et al* (2010), in a paper on the status and continuing challenges in operational remote sensing of *ET*, errors in surface temperature (T_0) retrievals from many satellite systems can range from 3 – 5K. This is due to uncertainty in atmospheric conditions, surface emissivity, view angle, and shadowing. Allen *et al.* (2010) report that Hook and Prata (2001) suggested that T_0 retrievals from modern satellites could be as accurate as 0.5K. However since surface temperature gradients used in energy balance models are often in the order of 1 to 5K Allen *et al* (2010) state that even this amount of error together with large uncertainties in the air temperature measurements, makes the use of models based on differences in absolute estimates of surface and air temperature cumbersome.

7.1.5. ROUGHNESS LENGTHS

The roughness length for momentum transfer, or momentum roughness (z_{0m}), is an important parameter for the wind profile calculations contained within Equations [7] and [8] and also for the calculation of roughness length for heat transfer, or heat roughness (z_{0h}) (Equation [12]). The earth's surface is usually rough and for a rough surface, z_{0m} is taken to equal the surface roughness length (z_0) (Brutsaert, 1982).

Roughness length (z_0) is a measure of the aerodynamic roughness of a surface and is related to but not equal to the height of the roughness elements. Many studies have been conducted to relate z_0 with measurable characteristics of the surface and the simplest and most obvious method is to relate it to the mean height of the roughness obstacles (h_0) (Brutsaert, 1982). Studies relating z_0 to h_0 report h_0 / z_0 of between 7.35 and 8 (Brutsaert, 1982). In reality, the matter is not as simple as relating height of obstacles to roughness height since h_0 / z_0 is a fairly complicated function of other surface characteristics too (Brutsaert, 1982). z_0 is also a function of the shape and density distribution of the roughness elements. For example, a grassy plain has a lower roughness than an area with many trees and buildings (Kipp & Zonen, 2005) and an additional term, zero plane displacement height (d_0) is defined as the height above the ground at which zero wind speed is achieved due to friction caused by roughness elements. In Figure 43 it can be seen that the height of the roughness obstacles is identical in both images and if a simple h_0 / z_0 were to be used, the z_0 value would be identical for both images. However, the distribution and density of the roughness elements have a profound influence on roughness length.

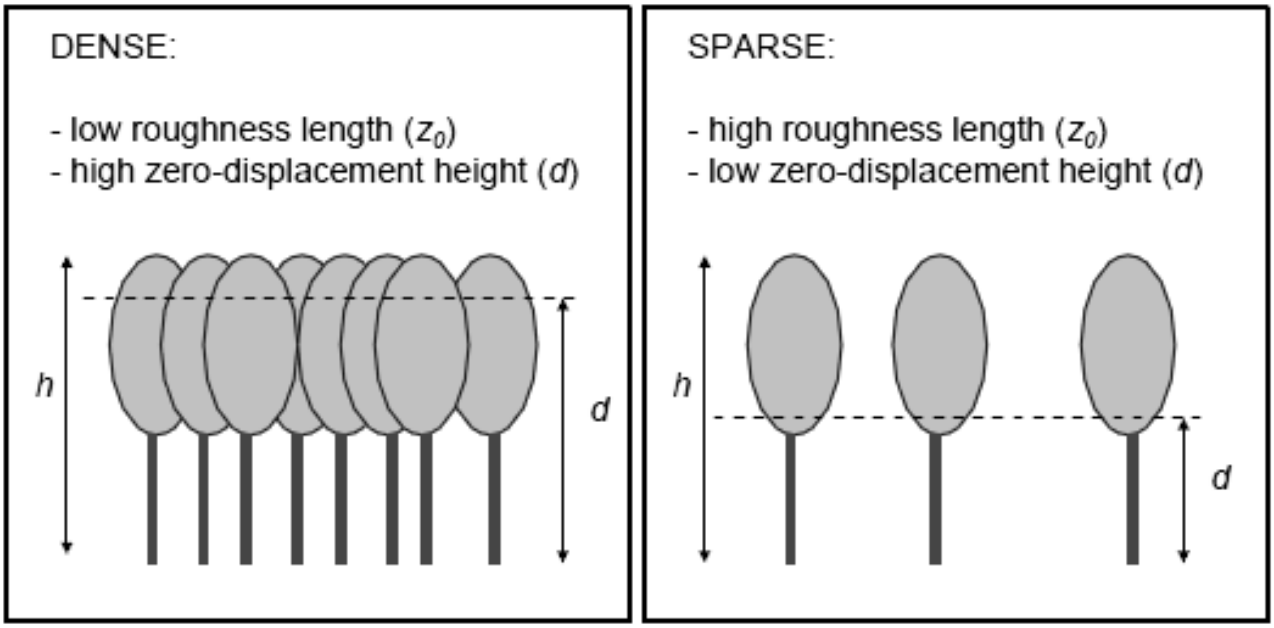

Figure 43: Dependence of roughness length and displacement height on height and density of roughness elements (e.g. trees) (Kipp & Zonen, 2005).

It can be seen that the determination of z_0 is a complex problem yet despite the difficulties presented, the commonly accepted approach is to use a ratio relating the obstacle height to roughness length. It can be deduced intuitively that the accuracy of z_0, when applying a ratio approach, to remote sensing data will be dependent on both the spatial resolution of the remote sensing data and the heterogeneity of the landscape under study. For example, a large dense homogeneous stand of an agricultural crop will have an accurate z_0 calculation even at coarse image resolution; however, in a fragmented landscape a less homogenous land cover, such as savannah, will have larger uncertainties attached to the z_0 calculation at a coarse resolution and a higher resolution will be required. This is problematic when using coarse resolution imagery such as MODIS to estimate z_0.

For this research three dates were used for the analysis, day of year (DOY) 185 & 217 of 2006 and DOY 017 of 2007. These dates were selected to illustrate three scenarios: where *H* is not at the wet-limit (DOY 017), where *H* is close to the wet limit (DOY 217) and where *H* is at the wet-limit (DOY 185).

To derive land cover z_0 values, the National Land Cover 2000 map (Van den Berg *et al*, 2008) was used as a basis. By using high resolution SPOT imagery, the NLC 2000 map was modified through visual interpretation to delineate land covers on the basis of roughness characteristics. Roughness lengths and displacement heights were assigned to each new land cover class using literature values for similar land

covers. The footprint of the MODIS pixel was then overlaid on the land cover map and the land cover class covering the largest area within each MODIS pixel was assigned to each MODIS pixel. This process can be seen in Figure 44. It must be noted that this process is highly subjective and there are some flaws in selecting a roughness parameter for a pixel purely based on the majority land cover within the pixel. This highlights the influence of the resolution of the satellite imagery and the heterogeneity of the landscape on SEBS results.

Land cover labelled Shrubland (South) can more accurately be described as grassland (Figure 44a). A z_0 value from Table 17 of 0.034 m corresponding to the z_0 value for grass was assigned. Land cover labelled Shrubland (North) as shown in (Figure 44b was assigned a value of 0.0408 m from Table 17, a value assigned to heather. Thickets and bush clumps ((Figure 44c) were found mostly in the central portion of the catchment and were assigned a z_0 value of 0.2 m for 1 – 2 m high vegetation (Brutsaert, 1982).

Table 17: Land use classes in the PELCOM land use database and associated z_0 values adapted from Su (2006).

LAND USE CLASS	**Z_{0M} (M)**
Fresh water, salt water	*0.0002*
Bare soil in built-up areas, bare soil in natural areas	*0.0012*
Main roads and railways	*0.0035*
Grass in built-up area	*0.0334*
Grass	*0.0340*
Heather, other open spaces in natural areas	*0.0408*
Potatoes, Beets, other crops, bulbs	*0.0639*
Greenhouses	*0.4066*
Cereal, maize	*0.4966*
Built-up area in rural area, buildings in rural areas	*0.5488*
Orchards	*0.6065*
Continuous urban area	*1.1058*
Deciduous forest, coniferous forest, deciduous and coniferous forest in urban area, built-up area with dense forest	*1.2214*

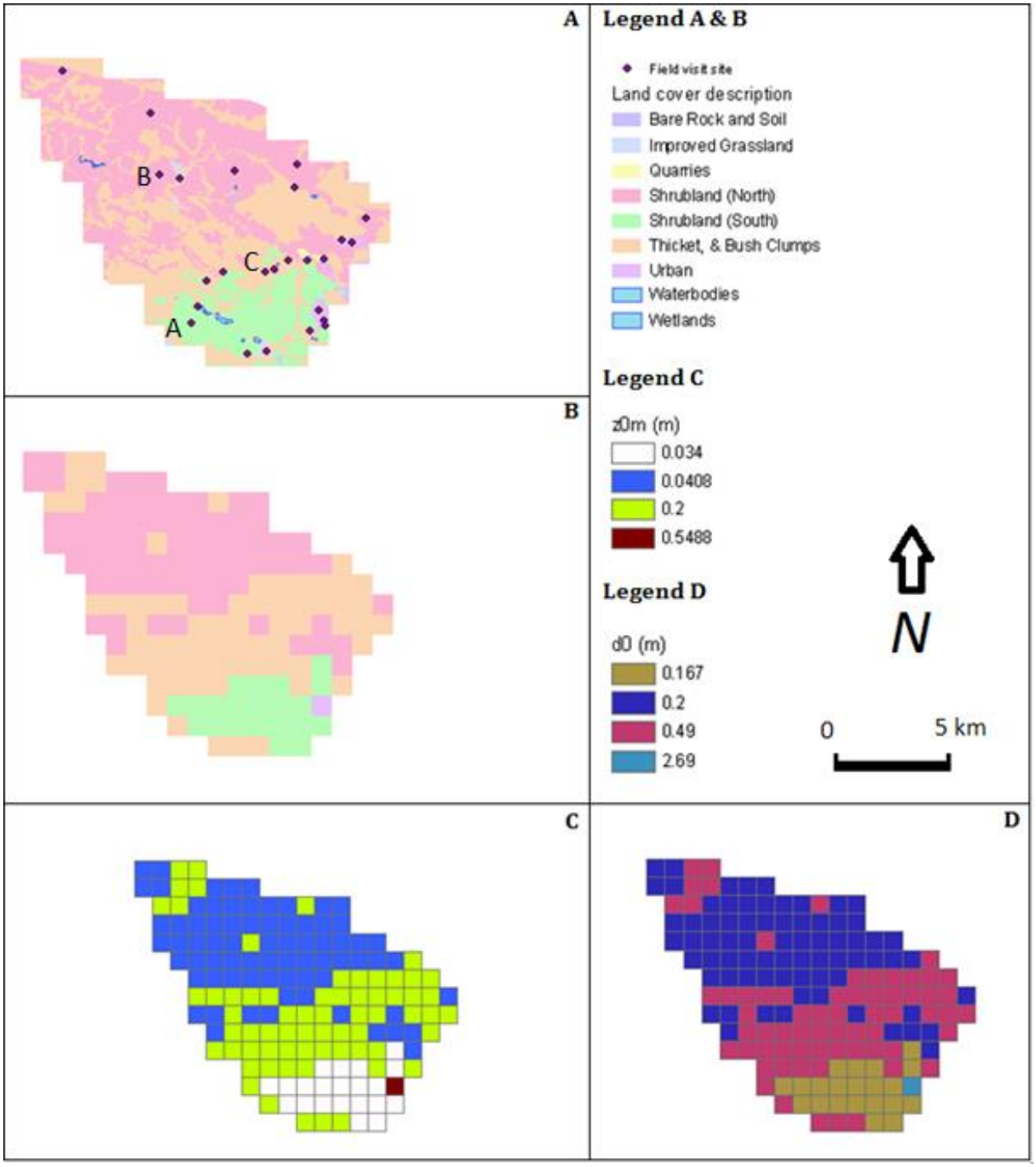

Figure 44: The process of allocating z_0 and d_0 values in the P10A catchment (plus 1 km buffer) a. Modified land cover map, b. land cover by MODIS pixel, c. Allocated roughness lengths and d. Zero plane displacement heights. Note that the labels A, B, and C on Figure 44a indicate the locations at which photographs in Figure 45 are taken.

A: z_0 = 0.034 m

B: z_0 = 0.0408 m

C: z_0 = 0.2 m

Figure 45: Land covers and assigned z_0 values from the literature. a: Shrubland (South) more accurately described as grassland. b: Shrubland (North) and c: Thickets and bush clumps.

The SEBS model was run using both these methods for deriving z_0 values keeping all other input parameters unchanged. It is particularly important to note that the roughness length is used together with T_0 in the calculation of H (Equations [6] – [8]). The combined effect of uncertainties in T_0, together with inaccuracies in z_0 leads to compounded inaccuracies in the calculation of H and therefore ET.

It is believed that the overestimation in ET in SEBS is caused by the sensitivity of H to $T_0 - T_a$ and z_{0m}, both separately and in combination, particularly at high $T_0 - T_a$ and z_{0m}. This is illustrated in Figure 46 where three z_0 values are assigned homogenously across the P10A catchment and the SEBS model runs for each of these z_0 values keeping all other input parameters unchanged.

Three different dates are selected to show the sensitivities at high $T_0 - T_a$ (Figure 46a), $T_0 - T_a$ close to zero (Figure 46b) and negative $T_0 - T_a$ (Figure 46c). It can be seen in Figure 46a that the sensible heat flux is most sensitive to high z_0 values at high $T_0 - T_a$ values. As z_0 and $T_0 - T_a$ decrease, so too does the sensitivity of H to these values (Figure 46b). In Figure 46c where H approaches the wet limit, the slope changes and the sensitivity to $T_0 - T_a$ and z_0 is less predictable. This is due to the fact that at the wet limit $T_0 - T_a$ and z_0 are not used as direct inputs into the calculation of H since Equation [4] is used for this calculation. It can therefore be said that at low $T_0 - T_a$, the importance of a correct z_0 is less critical than at a high $T_0 - T_a$ where the accuracy of z_0 is very important, particularly in areas with high roughness lengths, generally corresponding to taller vegetation. Similarly, Gokmen *et al.* (2012) state that $T_0 - T_a$ is the driving force for the sensible heat transfer. However, for low $T_0 - T_a$, H becomes less sensitive to the magnitude of aerodynamic factors. This gives weight to the observation that the underestimation of H in SEBS is caused by the sensitivity of H to $T_0 - T_a$ and z_{0m}, both separately and in combination, particularly at high $T_0 - T_a$ and z_{0m}.

The calculation of H, which in turn is used to determine the latent heat flux and ultimately daily evapotranspiration estimation, has been reported to be sensitive to aerodynamic roughness lengths (z_{0m} and z_{0h}) (Lin, 2006). In the SEBS model, two methods for determining z_0 are proposed: z_0 can be obtained from the literature or can be empirically derived from the remote sensing vegetation inputs. If z_0 is derived from remote sensing vegetation inputs, the normalized difference vegetation index (*NDVI*) is used (Equation [11]. Next the obstacle height (or vegetation height) (h_0) is calculated from the roughness height for momentum transfer (Equation [9]) followed by the zero plane displacement height (Brutsaert, 1982) (Equation [10]).

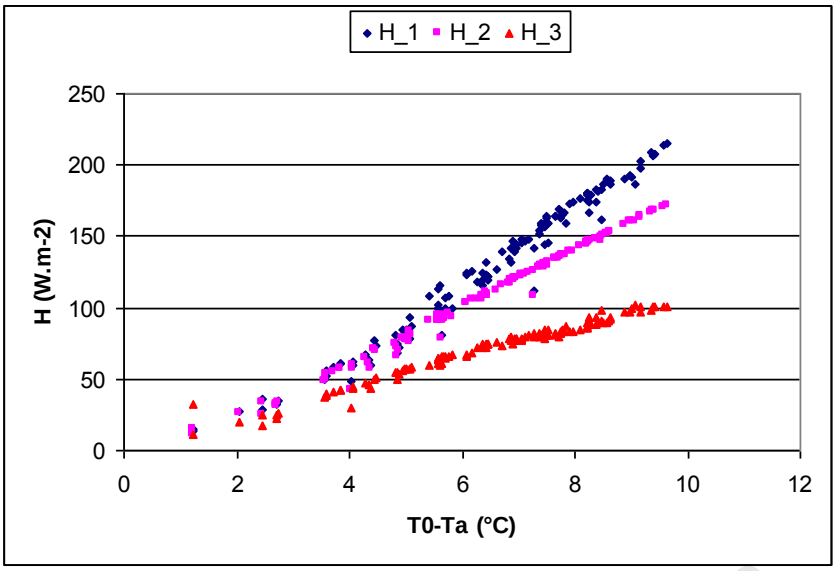

a)

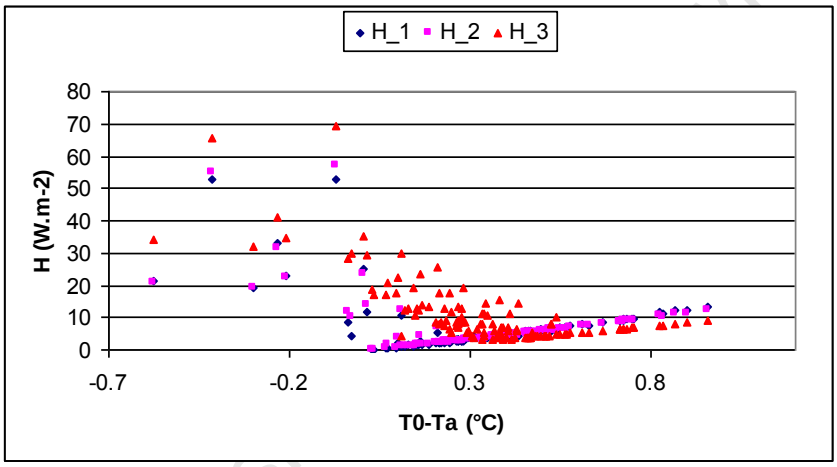

b)

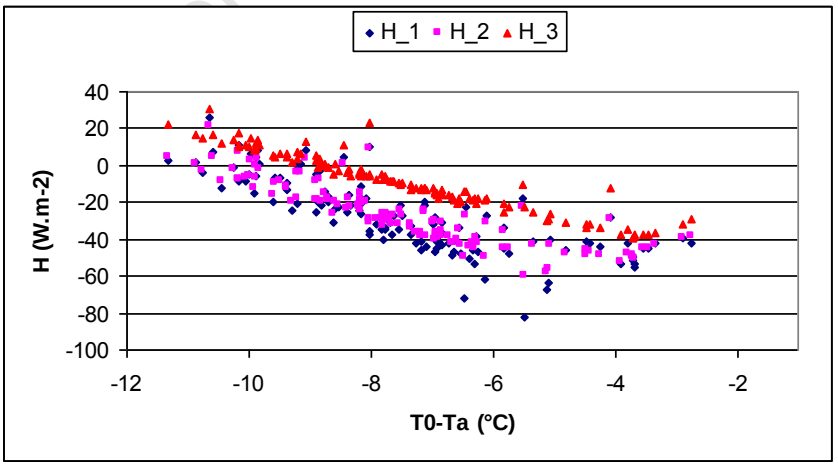

c)

Figure 46: Sensitivity of sensible heat flux to z_0 and T_0 - T_a across the entire P10A catchment. H_1: z_0 is set to 1m; H_2, z_0 is set to 0.5m; and H_3, z_0 is set to 0.1m. a) Summer scene DOY 017: sensitivity of H to z_0 increases with increasing T_0 - T_a. b) Winter scene, DOY 217: sensitivity of H to z_0 is non-linear around T_0 - T_a =0. c) Winter scene, DOY 185: the slope is negative in this instance indicating that the wet limit has been reached at low T_0 - T_a.

It is apparent that if Equations [9] - [11] are used to calculate z_0 and d_0, then areas which have a low *NDVI* will be assigned a low roughness length, a low canopy height and a low displacement height. Although this assumption may generally hold true in certain irrigated agricultural regions, it does not allow for the case of semi-arid environments where shrubs and fynbos type vegetation have a low *NDVI* during the hot dry summer but the canopy height does not follow a seasonal curve in the way that *NDVI* does. In this scenario, the roughness length, canopy height and displacement height are independent of *NDVI* and should not vary as much as *NDVI* throughout the year.

An alternative method for obtaining roughness length is using look-up tables such as the Pan-European Land Use and Land Cover Monitoring (PELCOM) land use database with associated z_0 values (Su, 2006). It can be seen in Table 17 that not all land covers in South Africa are contained within this type of database so a large amount of guesswork is required to match South African land covers to existing databases. Additionally, the phenological stage of the vegetation is not reflected here which will be particularly important for land covers where the height of the vegetation changes dramatically during the course of a growing season.

It is postulated that should it be possible to obtain a more accurate measure of z_0 which can be used as input into the SEBS model, then the calculation of the *H* will be more accurate in turn leading to a more accurate *ET* value rather than reported overestimations (Gibson *et al*, 2009; Gibson *et al*, 2011).

The z_0 values generated from *NDVI* are compared with the literature assigned z_0 values for DOY 185, 217 and 017 in Figure 47. In the southern portion of the catchment where literature assigned z_0 values are low (0.034 m), the *NDVI* derived values significantly exceed the literature values for each selected DOY and a clear seasonal influence is not apparent. It is possible that the small number of pixels in this class did not allow for a trend to develop. The greenness of the vegetation is apparent in Figure 45a even though at that particular time of year the vegetation was short. The greenness of the vegetation implies that the *NDVI* will be high and the z_0 derived from *NDVI* would not be expected to return realistic z_0 values.

For the northern portion of the catchment where the very low shrubland occurs and a z_0 value of 0.0408 m was assigned, there is once again a higher z_0 value returned for the *NDVI* values for each of the selected DOY. A clearer seasonal trend can be discerned here with the summer scenes returning lower

NDVI derived z_0 values from the summer scene than the winter scene, implying that the vegetation is less green in the summer scene than in the winter scene. Conversely for the thickets and bush clumps class, the *NDVI* derived z_0 values were lower than the literature assigned values. In this class a clear seasonal trend could be observed with the summer scene returning lower z_0 values than the winter scenes. This is not believed to be a true reflection of reality since there is probably little seasonal vegetation variation within this class.

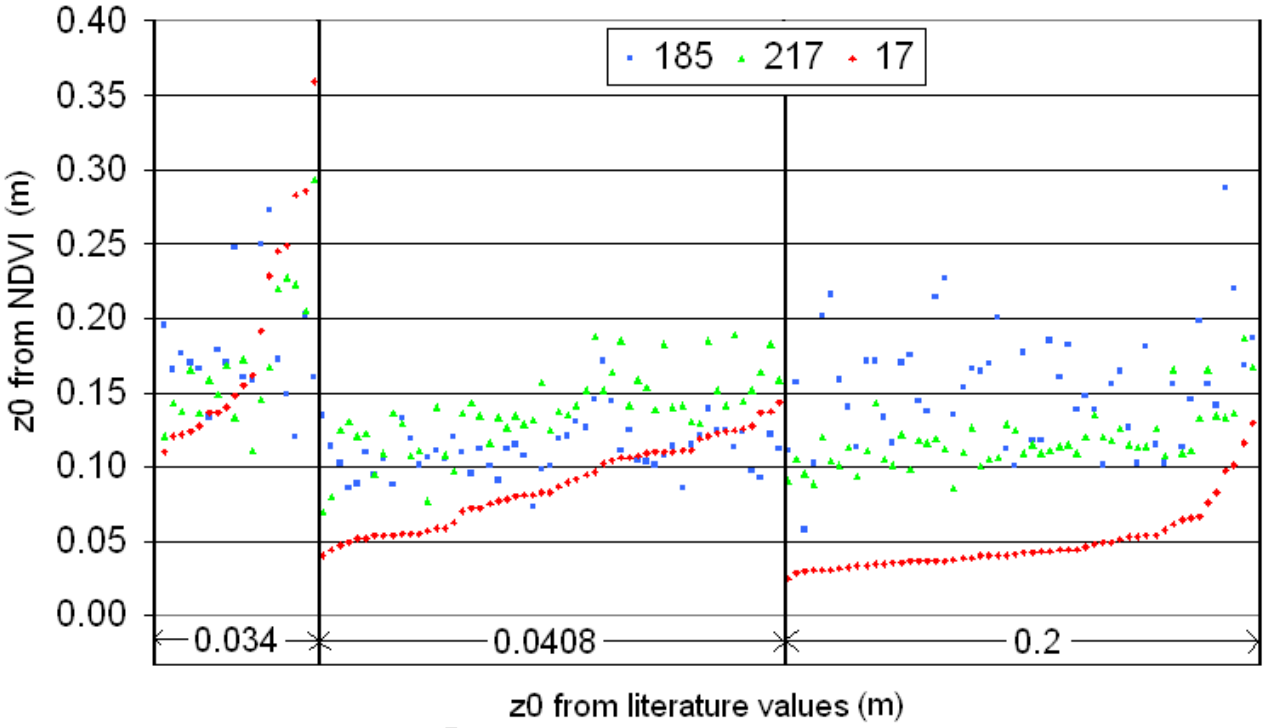

Figure 47: Comparison of z_0 literature values to z_0 values from *NDVI* for DOY 185, 217 and 017.

It can be seen in Figure 48 that the two different methods of calculating z_0 produced differing H results, and both *NDVI* derived values and literature values for z_0 reproduced the trends shown in Figure 42. Furthermore the influence of T_0 - T_a and the impact on whether the wet limit has been reached is again apparent by the curve. The results from the *NDVI* derived values are more clustered than the results from literature values which are more scattered. The clustered *NDVI* derived results are probably as a result of the well-known inverse correlation between *NDVI* and T_0 (Agam *et al*, 2007).

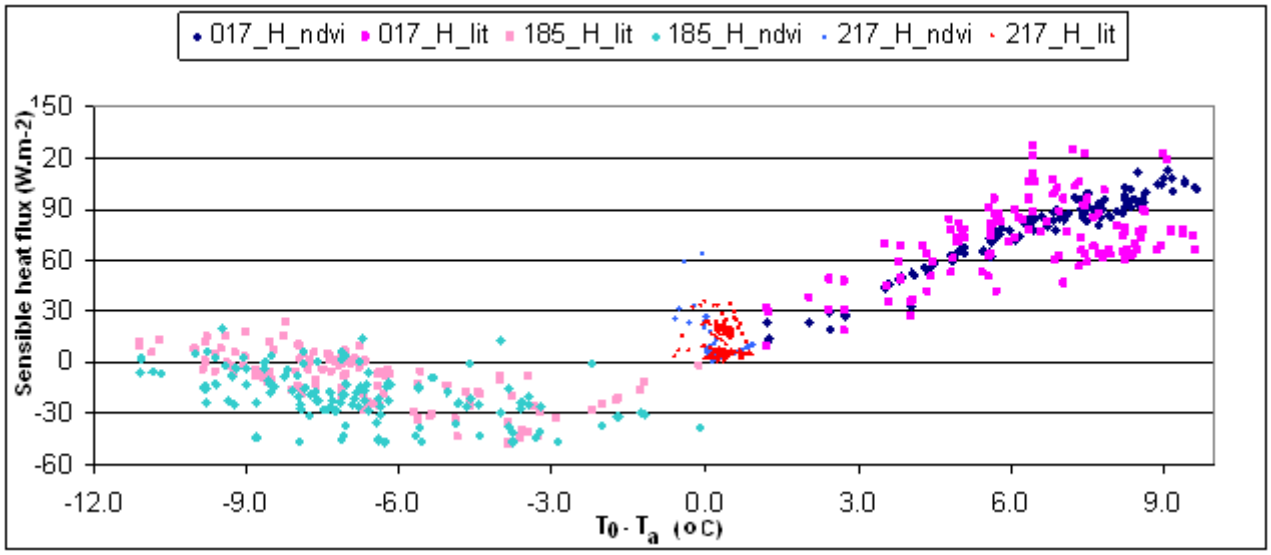

Figure 48: Comparison of z_0 literature values to z_0 values derived from *NDVI* for *H* results plotted against T_0 - T_a for DOY 185, 217 and 017.

Apparent from the results is that although there are differences in estimated *H* when different methods for estimating z_0 are used, *H* remains low for both winter (DOY 185 & 217) and summer (DOY 017) scenes. This implies that the *ET* estimate will be high for each of the days represented in this research. Although the SEBS model has been shown to be sensitive to z_0 (particularly in combination with T_0 - T_a), the results from this research showed no significant changes in the calculation of *H* when two different methodologies were used for z_0 determination.

7.2. RESULTS AND DISCUSSION

This component of the research was an iterative process as the importance of addressing some of the items above was only discovered through selecting images, running the model, analyzing the results and then adapting the methodology and input data. Due to the iterative nature and the volume of data involved, it is very difficult (and not particularly helpful) to present the results of all iterations but rather to present results after all the adaptations to input data, image selection, as described in Chapter 7.1 had been made.

The catchment average daily *ET* results from the SEBS model are shown in Figure 49 plotted against reference *ET*. It can be seen that the SEBS model results in *ET* which is consistently at, or higher than, than reference ET_0. This is true for both the AQUA and TERRA data. Despite all the modifications to increase accuracies, the sensible heat flux remains low with the resulting *ET* being close to reference evaporation.

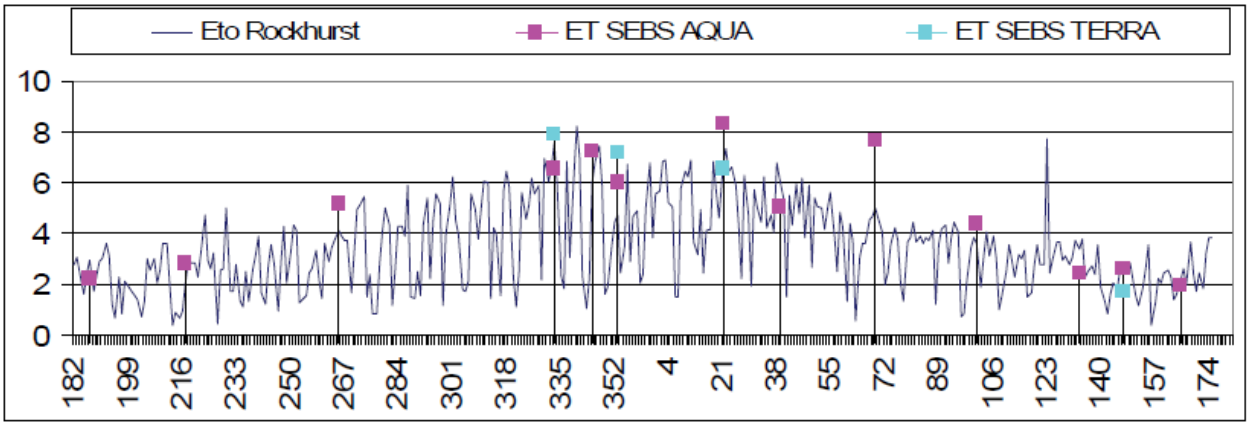

Figure 49: Catchment average *ET* calculated for P10A using the SEBS model with AQUA and TERRA data and plotted against ET_0 calculated from the Rockhurst weather station for the study period (July 2006-June2007)

In Figure 50 and Figure 51, the SEBS *ET* and SEBS evaporative fraction AQUA results are plotted against T_0-T_a for individual pixels. The range in estimated *ET* in the catchment for each selected day throughout the study period can be seen.

From the results it can be seen that in SEBS:

1. A high *ET* is caused by a high evaporative fraction.
2. A high evaporative fraction is caused by energy being partitioned to the latent heat flux rather than the sensible heat flux.
3. Since the SEBS model solves the latent heat flux as the residual of the energy balance, the calculation of a low sensible heat flux is the most contributing factor to high *ET* in SEBS.

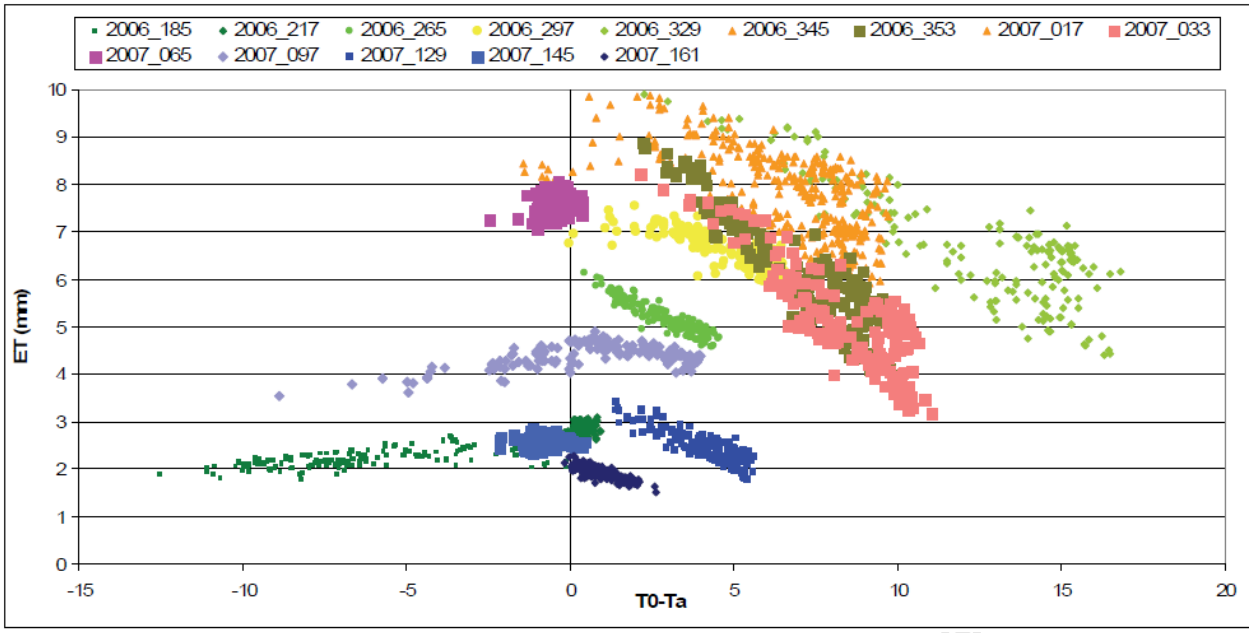

Figure 50: AQUA SEBS *ET* results for each date processed for the P10A catchment plotted against T_0 - T_a.

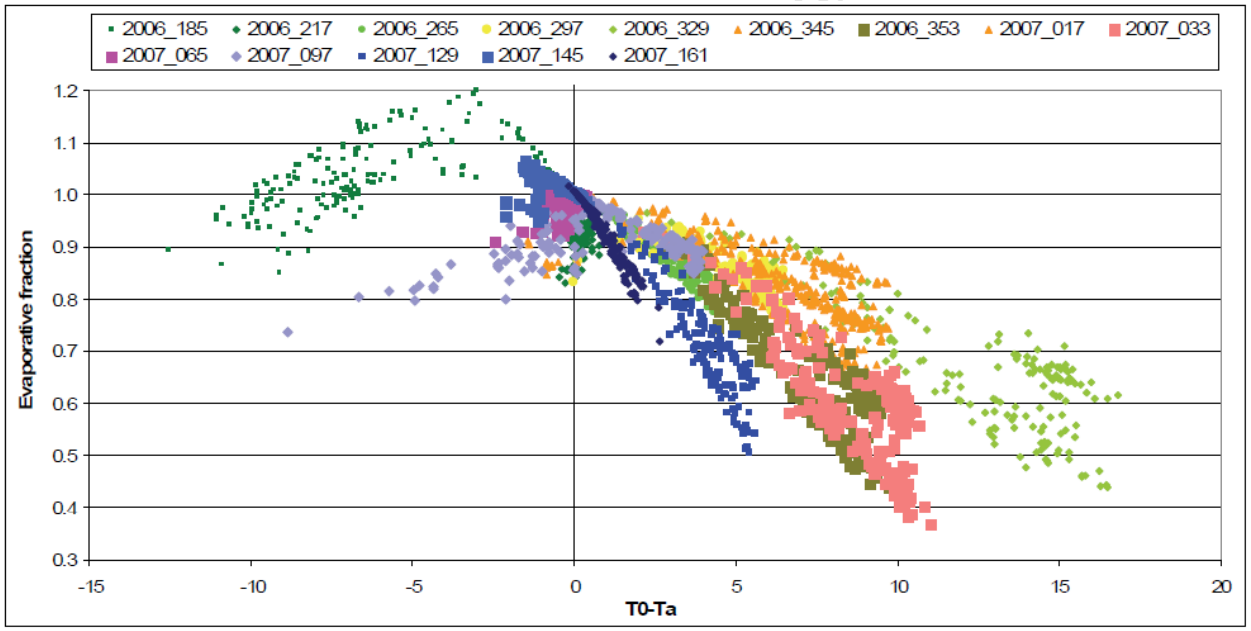

Figure 51: AQUA SEBS evaporative fraction results for each date processed for the P10A catchment plotted against T_0 - T_a.

Cleugh *et al.* (2007) in Allen *et al.* (2010) summarize challenges in using near surface temperature gradients (T_0 - T_a) based on absolute estimates of T_0 and T_a. Contributing to confidence in T_0 - T_a estimation are uncertainties and biases to error in T_0 and T_a themselves, uncertainties in surface emissivity, and differences between radiometrically derived T_0 and the aerodynamically equivalent T_0.

The sensitivity of H to T_0 - T_a and z_0 has already been discussed. Figure 51 shows the evaporative fraction results for each AQUA scene plotted against T_0 - T_a. It can be seen that in the case of T_0 - T_a greater than zero, as T_0 - T_a increases, the evaporative fraction decreases. This is in line with the sensitivity of H to T_0 - T_a as illustrated earlier in Chapter 7.1.4. Also apparent from Figure 51 is that on no occasion does the evaporative fraction fall below 0.3 and the majority of the pixels fall above 0.7 (median 0.876). This leads to the conclusion that regardless of the accuracy of the input data (excluding image resolution) or the environment, these results indicate that the SEBS model remains unable to allocate sufficient energy to the sensible heat flux in order to arrive at realistic ET estimates when compared to ET_0 across the year (Figure 49).

According to Jia *et al*. (2003), the traditional aerodynamic resistance (between source height and the reference height) is usually estimated on the basis of surface-layer similarity theory. However, when using remotely sensed thermal infrared measurements in such traditional single-source formulation, the assumption is generally made that the radiometric surface temperature measured by a radiometer is equivalent to aerodynamic surface temperature. This approximation is applied to heterogeneous land surface by adding an excess resistance to the traditional aerodynamic resistance commonly expressed under the form of a non-dimensional parameter (kB^{-1}). However, when using remotely sensed thermal infrared imagery, the radiometric surface temperature measured by the sensor is assumed to equal the aerodynamic surface temperature input into models. The purpose of the kB^{-1} term is to account for relating H to radiometric surface temperature rather than H to aerodynamic surface temperature (Jia *et al*., 2003) and if an appropriate value for kB^{-1} can be determined, then H can be accurately estimated using radiometric surface temperature.

Finally, Beven (1979) undertook a sensitivity analysis of the Penman-Monteith equation where he states that his most important conclusion is that the sensitivity of Penman-Monteith estimates of actual evapotranspiration to different input parameters is more dependent on the values of the aerodynamic and canopy resistance parameters that introduce the influence of vegetation type into the equation, than on climatic difference between sites. Further to this, he states that all the input variables exhibit high daytime sensitivity coefficients during a summer period when evapotranspiration rates are high. Since the Penman-Monteith equation is used in the establishment of both the sensitive heat flux at the wet limit and the sensible heat flux itself, it is possible that the same sensitivities reported by Beven (1979) may be of importance here particularly since these parameters are being estimated for a heterogeneous landscape and are input into the model at MODIS resolution.

8. APPLICATION OF ADJUSTED METHODOLOGY BACK TO MOUTON'S VALLEY FIELD VALIDATION SITE

The sensitivity of the SEBS model to various input parameters has been demonstrated. The sensitivity to choice of fractional vegetation cover, displacement height (in relation to reference height), albedo (as it relates to heterogeneity and the upscaling to daily ET) and $T_0 - T_a$ was revealed for the Moutons Valley study site where the field validation took place. The sensitivity of the SEBS model to aerodynamic roughness parameters in combination with $T_0 - T_a$ was demonstrated in the P10A catchment in the Eastern Cape.

8.1. RESULTS

Although it was previously stated that the adaptation of the methodology will add little value to the results of the Moutons Valley field validation site, the influence of selecting the correct $NDVI_{max}$ on the fractional vegetation cover and how this impacts finally on SEBS calculated energy fluxes and daily ET is important. The method is therefore re-applied to the Moutons Valley validation site for the field validation period, keeping all variables unchanged with the exception of the fractional vegetation cover. The results of these adaptations are given for TERRA results only (Table 18).

It can be seen that by using a higher $NDVI_{max}$ value the fractional vegetation cover may be more realistic at MODIS pixel resolution where there is mixed land cover and not only apple orchard at full cover (since it will be equal to less than 1), the resulting soil heat flux is higher, and the sensible heat flux and sensible heat flux at the wet limit are lower. Since net radiation is not affected by the f_c calculation, in Equation [17] in the calculation of the evaporative fraction, an increase in G_0 will imply a lower amount of energy potentially available for evaporation. The lower H when using the higher $NDVI_{max}$, leads to the lower denominator in Equation [17] resulting in a higher evaporative fraction which in turn leads to a higher daily ET. Given that it has already been shown that the daily ET estimated using the SEBS model is significantly higher than the field measurements, an increase in daily ET with a lower fractional vegetation cover is therefore exacerbating the overestimation of daily ET (Figure 52). It is therefore shown that in this particular instance, that by improving the accuracy of the input data, the accuracy of the final results decreases.

Table 18: SEBS TERRA results comparison by increasing $NDVI_{max}$ from 0.5 to 0.65 in f_c calculation (Equation 17]).

DOY	NDVI	$NDVI_{max}$	f_c	G_0	H	H_{wet}	λE	EF	ET_{daily}
315	0.54	0.65	0.57	102	68	24	461	0.87	6.8
		0.5	1	32	92	92	507	0.85	6.6
320	0.6	0.65	0.79	127	76	76	586	0.88	7.6
		0.5	1	38	130	130	590	0.82	6.6
321	0.59	0.65	0.75	110	54	54	518	0.91	7.5
		0.5	1	34	120	120	528	0.81	6.7
322	0.53	0.65	0.54	104	52	45	491	0.9	7.2
		0.5	1	32	117	117	498	0.81	6.4
323	0.63	0.65	0.91	129	128	128	541	0.81	6.9
		0.5	1	40	192	192	565	0.75	6.4
324	0.56	0.65	0.64	109	25	22	540	0.96	8.2
		0.5	1	34	89	89	551	0.86	7.4
325	0.57	0.65	0.68	133	71	71	622	0.89	8.4
		0.5	1	41	139	139	645	0.82	7.7
326	0.58	0.65	0.71	102	48	11	484	0.91	7.4
		0.5	1	32	84	84	519	0.86	7

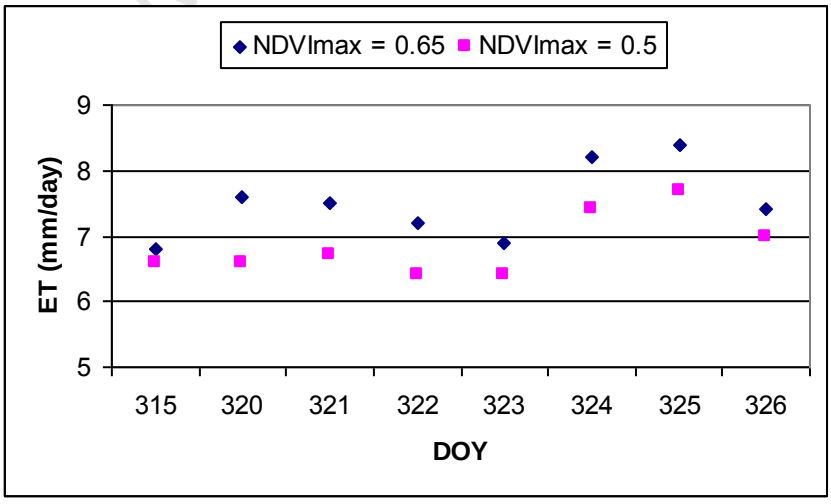

Figure 52: Impact of $NDVI_{max}$ value in the f_c calculation in daily ET estimation in SEBS for TERRA data.

In Table 19, the z_{0m}, h_0 and d_0 for each image calculated from *NDVI* and $NDVI_{max}$ (maximum scene *NDVI*) are shown. It can be seen that on average, the values for z_{0m}, h_0 and d_0 are higher when calculated from the AQUA data than from the TERRA data.

Table 19: z_{0m}, h_0 and d_0 for each image calculated from *NDVI* and $NDVI_{max}$.

DOY	SENSOR	NDVI	$NDVI_{max}$	z_{0m}	h_0	d_0
315	TERRA	0.54	0.66	0.30	2.24	1.49
	AQUA	0.53	0.65	0.30	2.24	1.49
319	AQUA	0.6	0.68	0.37	2.71	1.80
320	TERRA	0.6	0.68	0.37	2.74	1.82
	AQUA	0.63	0.71	0.38	2.81	1.87
321	TERRA	0.59	0.69	0.34	2.50	1.67
	AQUA	0.59	0.75	0.28	2.06	1.37
322	TERRA	0.53	0.70	0.26	1.89	1.26
	AQUA	0.57	0.63	0.40	2.93	1.96
323	TERRA	0.63	0.66	0.44	3.26	2.17
	AQUA	0.62	0.68	0.40	2.94	1.96
324	TERRA	0.56	0.67	0.33	2.41	1.61
	AQUA	0.6	0.65	0.42	3.11	2.07
325	TERRA	0.57	0.69	0.31	2.31	1.54
	AQUA	0.63	0.66	0.44	3.26	2.17
326	TERRA	0.58	0.66	0.37	2.75	1.83
	AQUA	0.53	0.65	0.31	2.24	1.50
average result				0.36	2.61	1.74
average TERRA result				0.34	2.51	1.67
average AQUA result				0.37	2.70	1.80

Keeping all other parameters the same, the SEBS model was run for the MODIS TERRA images only using the *NDVI* method to derive the aerodynamic parameters and was then repeated using a literature value of z_{0m} = 0.6 which is the value given for orchards in the PELCOM table (Table 17). The adjustment to fractional vegetation cover was made using the $NDVI_{max}$ of 0.65 as suggested earlier. The sensitivity to z_{0m} at the Moutons Valley site is now shown. The results of the SEBS calculated energy fluxes for each of these scenarios are shown in Table 20 compared with the field validation values.

Table 20: SEBS MODIS TERRA results for the *NDVI* method to estimated z_{0m} and the literature value for z_{0m} (0.6) compared with field validation results (using adjusted $NDVI_{max}$ in fractional vegetation cover formula).

DOY	T0 - Ta	Source	R_n	G_0	H_{dry}	H	H_{wet}	λE	Λ	Λ_r	ET_{daily}
315	8.5	NDVI derived z0 values	631	102	529	68	24	461	0.87	0.91	6.8
		Literature z0 values	631	102	529	310	-227	219	0.41	0.29	3.3
		Field measurements	520	85	#	339	#	278	0.45	#	4.1
320	2.2	NDVI derived z0 values	789	127	662	76	76	586	0.88	1	7.6
		Literature z0 values	789	127	662	49	-200	613	0.93	0.71	8
		Field measurements	764	121	#	218	#	425	0.66	#	5.2
321	4.1	NDVI derived z0 values	682	110	572	54	54	518	0.91	1	7.5
		Literature z0 values	682	110	572	111	-196	461	0.81		6.6
		Field measurements	673	97	#	101	#	476	0.82	#	5
322	6.3	NDVI derived z0 values	647	104	542	52	45	491	0.9	0.99	7.2
		Literature z0 values	647	104	542	212	-203	330	0.61	0.44	4.8
		Field measurements	712	102	#	119	#	492	0.81	#	5
323	-0.4	NDVI derived z0 values	797	129	668	128	128	541	0.81	1	6.9
		Literature z0 values	797	129	668	-4	-262	672	1	0.7	8.6
		Field measurements	775	105	#	#	#	#	#	#	4.7
324	4.1	NDVI derived z0 values	674	109	565	25	22	540	0.96	0.99	8.2
		Literature z0 values	674	109	565	111	-263	454	0.8	0.6	6.9
		Field measurements	719	114	#	91	#	514	0.85	#	7.1
325	-2.4	NDVI derived z0 values	826	133	692	71	71	622	0.89	1	8.4
		Literature z0 values	826	133	692	41.7	41.7	651	0.94	1	8.8
		Field measurements	794	111	#	-1	#	684	#	#	7.3
326	6.1	NDVI derived z0 values	635	102	532	48	11	484	0.91	0.93	7.4
		Literature z0 values	635	102	532	197	-246	336	0.63	0.43	5.1
		Field measurements	726	117	#	-11	#	620	1.02	#	#

In conclusion, despite adaptations to the methodology, when it was applied back to the Mouton's Valley validation site, the SEBS estimated *ET* remains above the field measured values. It can be seen in Figure 53, that regardless of interventions, the SEBS results largely remain outside accepted accuracy parameters.

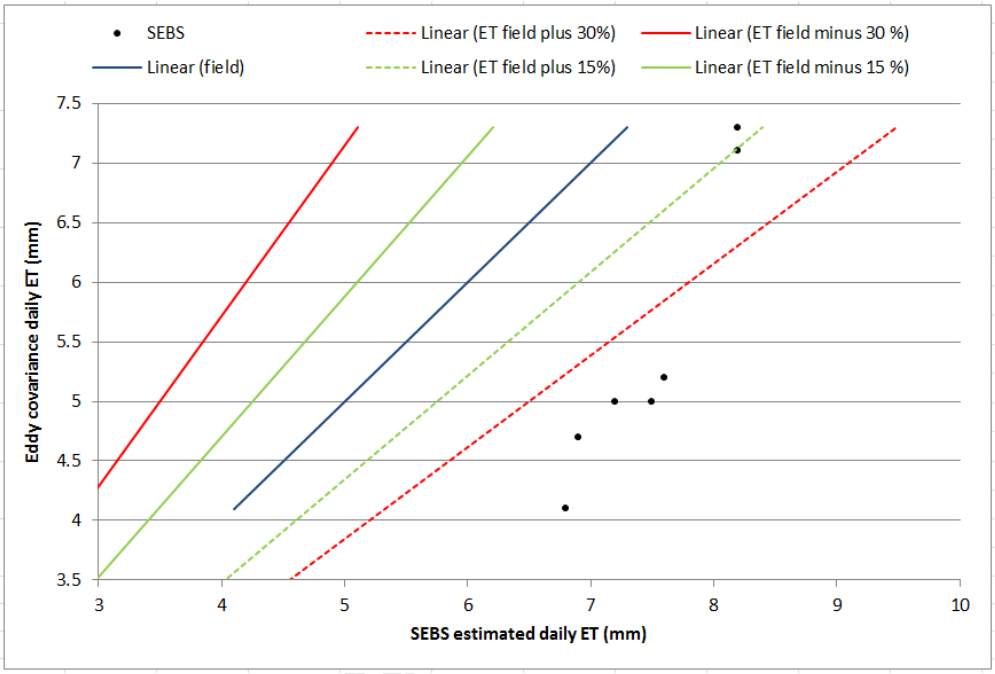

Figure 53: SEBS *ET*, after the methodology was adapted, plotted against field measured *ET*. Note: only TERRA results were processed.

8.2. DISCUSSION

The sensitivity of the sensible heat flux to z_{0m} can be seen in Table 20 where the calculated daily *ET* can vary by up to 3.5 mm (for DOY 315) depending on the selected aerodynamic values. This is significant as this equates to 80% of the field measured value when using the z_{0m} value taken from literature and 166% of the field measured value when using the *NDVI* derived z_{0m} value. Also apparent is that when using the *NDVI* method to derive z_{0m}, the sensible heat flux is at, or close to the wet limit. Contrary to this, when using the literature value for z_{0m}, the wet limit is reached on only one occasion (DOY 325). It was shown in Table 20 that the *NDVI* method to derive z_{0m} always results in a value lower than the

literature value of 0.6 m. In Figure 54, the daily *ET* for each method to derive z_{0m} and the field validation value is plotted against $T_0 - T_a$. Here it can be seen that when using a literature value for z_{0m}, the daily *ET* decreases with increasing $T_0 - T_a$ with a total range in daily *ET* of 5.5 mm per day. When using the *NDVI* method, the daily *ET* does not reflect the same fluctuation with change in $T_0 - T_a$ and a total range of 1.6 mm is seen. Furthermore, the *NDVI* method tracks the field validation values better than when using a fixed literature value for z_{0m}. The increasing sensitivity of daily *ET* (via *H*) with increasing $T_0 - T_a$ to the selected aerodynamic values is apparent with the exception being where $T_0 - T_a$ is negative. When using the wet-limit equation (Equation [5]), the sensible heat flux decreases with increasing $T_0 - T_a$ resulting in increasing *ET* with increasing $T_0 - T_a$. The downward trend in daily *ET* with $T_0 - T_a$ is therefore more apparent with the literature z_{0m} values since there is consistent use of Equations [6] - [8] whereas with the *NDVI* derived method, the wet limit is reached on many occasions thereby eliminating the downward trend in *ET* with increasing $T_0 - T_a$. This leads to the conclusion that the SEBS model is sensitive to $T_0 - T_a$ in combination with z_{0m}.

Should the uncertainties associated with $T_0 - T_a$ be reduced and $T_0 - T_a$ is assumed to be correct, *H* has been shown to be sensitive to fluctuations in this term especially in unstable conditions and in the transition phase where $T_0 - T_a$ moves from negative to positive and back again (Su, 2002). According to Su (2002), this sensitivity is suspected to be caused by the current stability correction functions used in SEBS not adequately describing this transition. This was found to be particularly true in the shrubs and grasslands experiments and more accurate results for agricultural areas were found (Su, 2002). The lag effect of the heating of land differs to the heating of the air and therefore $T_0 - T_a$, and the time of day of image acquisition may be important and the choice of satellite sensor (such as TERRA which captures images in the morning versus AQUA which captures images in the afternoon) should be considered in this context. Further, Beven (1979) documents the diurnal variation in canopy resistance illustrating that differing land covers have different diurnal ranges and since it has been shown that the SEBS model is sensitive to $T_0 - T_a$ in combination with vegetation parameters, this challenges the assumption of a constant evaporative fraction which is used in remote sensing energy balance models for the upscaling of instantaneous energy fluxes to daily *ET*.

In a recent publication, Lu *et al.* (2012) have reported a significant overestimation of the evaporative fraction (and hence *ET*) using the SEBS model. This is the first set of authors apart from Gibson *et al.* (2009), (2011) to report such a large overestimation of ET using SEBS. According to Lu *et al*. (2012),

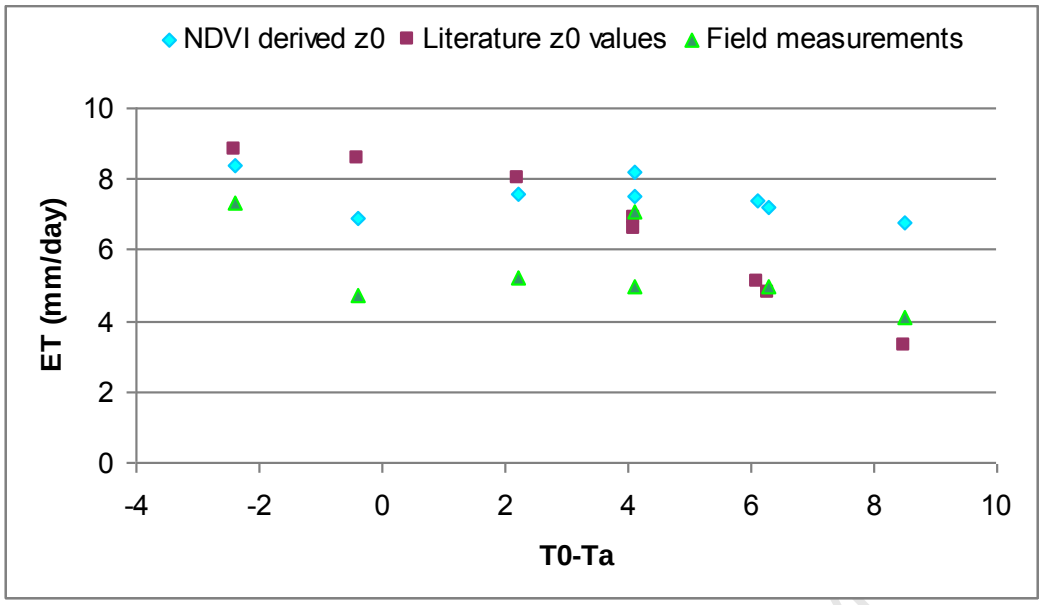

Figure 54: Daily ET calculated using $NDVI$ derived z_{0m}, a literature value for z_{0m} and the field validation value, plotted against $T_0 - T_a$.

SEBS underestimates sensible heat flux, and the underestimation of surface available energy also contributes to the overestimation of the evaporative fraction. Lu *et al.* (2012) report that the evaporative fraction is overestimated by more than 0.5. Given that the evaporative fraction is an index ranging from 0 – 1, an overestimation of this magnitude is significant. Lu *et al*. (2012) ascribe the overestimation of evaporative fraction to: lack of energy balance closure in field validation methods, the underestimation of R_n-G_0, the heterogeneity of the study area and the empirical determination of the aerodynamic parameters.

After stating that the SEBS model underestimates the sensible heat flux in particular for sparsely vegetated, semiarid, regions, because of an underestimation of sensible heat flux for these areas, Gokmen *et al*. (2012) propose an explicit integration of soil moisture information as a water stress index through a modified definition of kB^{-1}. This is motivatied by the vertical distribution of the sources of sensible heat which changes considerably under increasing levels of water stress and needs to be accounted for in the model. Gokmen *et al*. (2012) state that they explicitly take into account that water stress will increase the roughness length for heat transfer (z_{0h}) and assuming that z_{0m} stays the same, from Equation [12] and [13] it can be seen that kB^{-1} will be reduced. This is explained through stomatal control which is more efficient for the top layers of the canopy where the aerodynamic resistance is at a minimum. Therefore under non-water stress conditions, top leaves have more vigour and higher

stomatal conductance values. Top leaves therefore have a higher potential water loss rate than leaves lower down the canopy indicating that stomata exert increasingly greater control over water use from the bottom to the top of the canopy. Therefore under water-stressed conditions stomata of leaves will close the closer to the top of the canopy they are found. There will be an associated increase in T_0 toward the top of the canopy since the available energy is higher near the top. Finally, lower canopy layers are expected to have less fluctuation in $T_0 - T_a$, which means that as plant water stress increases the source of heat will increasingly move towards the top of the canopy, thereby increasing z_{0h} and reducing kB^{-1}.

This is illustrated in Figure 55. In Figure 55a, it can be seen that in non-water stressed environments, the $T_0 - T_a$ will remain relatively stable from the soil surface to the top of canopy. The water loss potential of the leaves increases towards the top of the canopy as does stomatal conductance and plant vigour. This results in the roughness length for heat transfer remaining low, kB^{-1} being high and a resulting low sensible heat flux. In the water stressed scenario in Figure 55b, it can be seen that $T_0 - T_a$ increases towards the top of the canopy, resulting in water stress. Increased stomatal control towards the top of the canopy occurs due to the environmental stress imposed on the plant. As a result, the roughness height for heat transfer is high although the roughness of the surface between the water stressed and non-water stressed scenario remains constant. In order to account for a high roughness length for heat transfer in the water stressed scenario, Gokmen *et al*. (2012) propose the adjustment of kB^{-1}.

In the formulation of the water stress index by Gokmen *et al*. (2012), and in the testing and field validation of the method, field measured values were used to integrate the soil moisture into the calculation of *H*. However, Gokmen *et al*. (2012) took this a step further by using passive microwave measurements of soil moisture to achieve operational application of the mapping of daily *ET*. This may represent an improvement to the SEBS model changing it conceptually from a one layer-source model to a multilayer source model (where the soil surface is considered separately to the vegetation) through the spatial parameterization of the soil moisture through passive remote sensing.

a)

b)

Figure 55: Explanation for underestimation of *H* in SEBS. a) Non-water stressed environment, b) Water stressed environment.

9. CONCLUSIONS AND RECOMMENDATIONS

In Chapter 9.1, a summary of the research findings is presented. In Chapter 9.2, proposed explanations for the overestimation of *ET*, despite the many adjustments to the methodology, are put forward. Final conclusions and recommendations are made in Chapter 9.3 with particular application to the South African environment

9.1. SUMMARY OF RESEARCH

The broad aim of this research was to implement the pre-packaged SEBS model in ILWIS in the South African environment with MODIS TERRA and AQUA data. As a pre-packaged software is accessible to remote sensing practitioners who may not have specific energy balance expertize, it is important for the pre-packaged version of SEBS to be tested before large scale roll-out (for operational, research or monitoring purposes) is implemented (Chapter 1.1). Therefore the aim (Chapter 1.2) was to compare, analyse and validate the results with field measured eddy covariance data, elucidate model sensitivities and make recommendations on the future use of the pre-packaged SEBS model.

The specific objectives were given as, for the field validation site, to:

1. Apply the pre-packaged SEBS model in ILWIS.
2. Compare and analyse results obtained from daily MODIS TERRA (MOD 02) and MODIS AQUA (MYD 02) data for:

    a. the calculated remotely sensed parameters (albedo, vegetation parameters, emissivity and land surface temperature) which are required as input into the SEBS model;

    b. the energy balance and evapotranspiration calculations using the pre-packaged SEBS model in ILWIS;

3. Validate the energy balance and evapotranspiration results with field measured data;

4. Analyse and explain the results and identify potential sources of error or model sensitivities.

It had been initially anticipated that ASTER imagery corresponding to the field validation period would be available for the study area. However due to difficulties with field equipment and the presence of cloud, only one ASTER image was available. Since there would be little value in using a single ASTER image, only MODIS data was used. The resolution of the MODIS imagery in relation to the field validation site resulted in a mixed pixel effect leading to some difficulties in assessing the validity of the validation process. Nevertheless, the SEBS model was applied, the various modules of the algorithm were unpacked and explained, and the sensitivities to various inputs were explored.

In fulfillment of Objective 1, the remote sensing parameters which were calculated using the pre-packaged SEBS model in ILWIS and then used in the estimation of the surface energy fluxes were presented in Chapter 5. The results (Objective 2a) for albedo were low when compared with literature values and may be due to inadequacies in the data used in the atmospheric correction process. Various factors were investigated to ascertain the major influences on the albedo calculation and it was found that the solar zenith angle played the biggest role in the albedo calculation. The *NDVI* calculation typically yields lower results for TERRA data than with AQUA data, however no trend could be detected. T_0 was almost always calculated as being higher in the afternoon than in the morning. However there appears to be a high uncertainty associated with this calculation when compared with the T_0 obtained from MSG/SEVERI.

The results of the energy flux calculations were mixed. SEBS calculated daily *ET* was higher than field measured values (Objective 2b) implying an overestimation of *ET* using the SEBS model. When analysing the results of the individual energy fluxes it was found that despite the uncertainties associated with T_0 and albedo which are used in the calculation of net radiation, the SEBS calculated R_n compared favourably with the field measured data for both the TERRA and the AQUA data with the AQUA results being superior to the TERRA results. The soil heat flux result corresponded better to the field validation results for the AQUA results than the TERRA results with the TERRA results underestimating the soil heat flux when compared with the field validation results.. This was due to the

structure and orientation of the orchard in relation to the sensor view angle allowing an f_c of lower than one whereas if viewed at nadir, an f_c of equal to one would be more appropriate for the orchard.

The results for the sensible heat flux showed no agreement between the SEBS calculated values and the field measured values for both the TERRA and AQUA results. Furthermore, for every data record, the sensible heat flux was calculated to be at the wet limit. Since the sensible heat flux is always at the wet limit, $\lambda E_{wet} = \lambda E$ and therefore relative evaporation is always equal to one, therefore the evaporative fraction is higher leading to a high daily ET calculation. The overestimation of daily ET can therefore be ascribed to the underestimation of the sensible heat flux.

The sensitivity of SEBS to parameters over which the user has some control when using this version of the model, was explored in Chapter 6 (Objective 4). It was shown that SEBS is sensitive to land surface temperature and air temperature gradient and the magnitude of this sensitivity depended on the land cover and whether or not the wet-limit had been reached. The choice of fractional vegetation cover formula was shown to influence the daily ET results by up to 0.7 mm. It was shown that the height of the vegetation canopy should be considered in relation to the weather station reference height to avoid the sensible heat flux from becoming unsolvable due to a negative ln calculation. Finally the study area was shown to be heterogeneous although the resolution at which fluxes were calculated did not significantly impact on energy partitioning results. The differences in the upscaling from evaporative fraction to daily ET at varying resolutions observed implies that the heterogeneity may play the biggest role in the upscaling and the influence of albedo on this calculation should be studied.

In using different resolution satellite imagery (ASTER and MODIS) it was shown that landscape heterogeneity is not the dominating factor at energy partitioning level whereas the resolution of the sensor does appear to play a role in the upscaling from instantaneous to daily ET through the use of albedo. These results point towards the importance of accurate albedo estimations for the upscaling of evaporative fraction to daily ET and that, in SEBS, landscape heterogeneity may play a role at this level rather than at energy partitioning level.

Four points of advice were presented for users of the pre-packaged SEBS model:

1) Since SEBS is sensitive to the T_0 - T_a gradient, care should be taken when estimating T_0 in a topographically diverse area as retrievals are less accurate in this setting. In particular, SEBS should not be used in mountainous areas with coarse resolution sensors since the heterogeneity of the T_0 cannot be captured at the appropriate scale. Furthermore, the sensitivity to $T_0 - T_a$ is also dependent on whether the wet-limit has been reached.

2) Care should be taken when selecting a fractional vegetation cover formula as this should be appropriate for the study area, especially if *NDVI* min and max values need to be defined. In particular, it is advised that if a *LAI* product is available at the appropriate scale, that it be used to estimate fractional vegetation cover according to the formula by Choudhary (1987).

3) The reference height of the weather station should be considered in relation to the canopy height of the study area. In an area where field crops with a low canopy height predominate, the use of an agrometeorological weather station is appropriate. However, where tree crops and natural vegetation with a canopy height exceeding 2.7 m are found, weather stations which measure wind speed at 10 m are probably more appropriate.

4) The scale at which the evapotranspiration results are required must be considered in relation to the choice of sensor and therefore pixel resolution and the heterogeneity of the study area. When working at a catchment scale a coarse resolution sensor may be appropriate for energy partitioning whereas, for farm or field scale results a higher pixel resolution will be required to detect inter-field or inter-farm variations. The influence of albedo on the accurate upscaling of evaporative fraction to daily *ET* should be considered and this may also be a function of landscape heterogeneity.

From the model sensitivities and uncertainties raised and the four points of advice given above, implementing the recommended changes to the methodology and validating the results in the Moutons Valley study area would have little value. For this reason, a separate research project at quaternary catchment scale (Chapter 7) for the P10A catchment near Grahamstown in the Eastern Cape, acting on these points of advice, was presented. The attention to ensuring the highest accuracy and suitability of input data involved: the pre-selection of a homogeneous catchment at MODIS pixel resolution, use of an

already atmospherically corrected MODIS data product, the adjustment of the *NDVI* maximum value for use in the fractional vegetation cover formula, the use of a South Africa Weather Services weather station data to measure the wind speed at 10 m rather than at 2 m, the use of literature values and a land cover map to assign roughness length and displacement height estimates and finally the use of both TERRA and AQUA images to determine the impact of land surface air temperature gradient and time of day at which the satellite image was captured.

Further in Chapter 7, the sensitivity of the SEBS model to the roughness length was presented in the P10A catchment. In the SEBS model, two methods for determining z_0 are possible: z_0 can be obtained from the literature or can be empirically derived from the remote sensing vegetation inputs. It was postulated that should it be possible to obtain a more accurate measure of z_0 which can be used as input into the SEBS model, then the calculation of the H will be more accurate, in turn leading to a more accurate ET value rather than reported overestimations. The results in P10A illustrated that although the SEBS model was shown to be sensitive to z_0 (particularly in combination with T_0 - T_a), no significant changes in the calculation of H was found when two different methodologies were used for z_0 determination.

Finally, parameters which could be changed for the study area and which may have an impact on the energy flux results were made (Chapter 8). The two changes made were in the choice of $NDVI_{max}$ (and therefore the calculation of fractional vegetation cover) and z_{0m}. The SEBS energy flux results were compared with the field validation data. It was shown that by using a higher $NDVI_{max}$ value the fractional vegetation cover may be more realistic at MODIS pixel resolution where there is mixed land cover. Despite the more realistic soil heat flux results, the sensible heat flux is in fact calculated to be lower when using this adjusted $NDVI_{max}$ and therefore the overestimation of daily ET with the SEBS model is exacerbated. The sensitivity of the sensible heat flux to z_{0m} was shown and the calculated daily ET can vary by up to 3.5 mm depending on the selected aerodynamic values. The NDVI method to derive z_{0m}, resulted in the sensible heat flux being at, or close to the wet limit. Contrary to this, when using the literature value for z_{0m}, the wet limit was reached on only one occasion. Finally the SEBS model was shown once again to be sensitive to $T_0 - T_a$ in combination with z_{0m}.

9.2. PROPOSED EXPLANATIONS FOR THE OVERESTIMATION OF *ET*

Despite much attention being given to the accuracy of the remote sensing input parameters in this research, the SEBS model consistently underestimated the sensible heat flux resulting in an overestimation of the daily *ET*.

In the SEBS formulation publication (Su, 2002), an extended model for the determination of the roughness length for heat transfer is described. However, according to Timmermans *et al*. (2011), the roughness height for heat transfer is only valid for short vegetation. The SEBS model has been shown to be sensitive to z_{0m}. Errors in the estimation of z_{0m} will be propagated through to the calculation of z_{0h}. z_{0m} and z_{0h} are used together with $T_0 - T_a$ to estimate the sensible heat flux. Furthermore, the sensitivity of calculations for the roughness height for heat transfer has been shown to be more sensitive in sparse canopies (Su *et al*., 2001), which is a landscape descriptor very appropriate to the South African environment.

McCabe & Wood (2006) found that at field scale, SEBS energy flux values calculated using ASTER are not regularly within 10% of values calculated using MODIS, but at a catchment scale, results for ASTER, Landsat and MODIS are within 10% of each other. In another study, aggregating input data was found to result in an underestimation of *ET* with the aggregated result being 15% lower than that obtained at original image resolution (Ershadi *et al.*, 2013). Contrary to this, the results presented in this thesis indicate that the partitioning of the energy balance is not affected by the image resolution (Chapter 6.3.4). However in the upscaling of evaporative fraction to daily *ET*, the albedo affected the daily *ET* result.

Further, subpixel heterogeneity at MODIS resolution has been shown by Li *et al*. (2008) to impact on the accuracy of surface flux estimates. Scaling techniques can address some of these issues but aggregation rules for scaling will differ depending on the environment (Kalma *et al*., 2008). Furthermore, applying models to large areas is hindered by the lack of high resolution ground measurements (i.e. meteorological observations), therefore despite the possibility of obtaining higher spatial resolutions of

satellite images, the spatial resolution of other input data into models remains a limitation (Kalma *et al*., 2008).

In complex environments, it is not possible to describe the remote sensing derived input parameters (*NDVI*, f_c, z_{0m}, T_0) at the correct level of accuracy and spatial resolution required for the accurate estimation of the sensible heat flux. The method used in this research to determine roughness length for momentum transfer was limited by the availability of data at appropriate scale, and aggregation rules for mixed pixels such as those proposed by Shuttleworth *et al*. (1997) were not considered in this research. The uncertainty in the T_0 observations (Kalma *et al*., 2008) combined with the uncertainties introduced in the roughness length estimates, results in error production and propagation through to the sensible heat flux. Therefore, in complex environments, an accurate daily *ET* is unlikely due to:

1. the inadequate spatial resolution and precision of remote sensing derived input parameters,
2. the sensitivity of the SEBS model to aerodynamic and temperature parameters (largely derived from remote sensing data),
3. the assumptions made at a micrometeorological level in the calculation of kB^{-1} , and
4. the uncertainties associated with the stability functions in the calculation of the sensible heat flux (Gellens-Meulenberghs, 2005).

Supporting the finding that the SEBS model is unable to allocate enough energy to the sensible heat flux, Lu *et al.* (2012) report a significant overestimation of the evaporative fraction using the SEBS model. The overestimation of evaporative fraction is ascribed to heterogeneous study areas and the empirical determination of the aerodynamic parameters. Gokmen *et al.* (2012) report on the underestimation of the SEBS derived sensible heat flux, particularly in sparsely vegetated, semiarid regions. Gokmen *et al*. (2012) propose an integration of soil moisture information as a water stress index for these regions. This will modify kB^{-1} in order to correct for an underestimation of the sensible heat flux.

The Australian example has shown that an aerodynamic resistance-surface energy balance approach failed because small errors in the surface temperature resulted in large errors in the sensible heat flux (Cleugh *et al*., 2007). An alternative approach of setting a fixed daily value for leaf-level stomatal conductance to calculate *ET* has been proposed (Cleugh *et al*., 2007). Similar to the approach being

implemented in South Africa by Palmer & Weiderman (2011), *ET* is calculated from a combination of leaf area index (derived from MODIS) and potential evapotranspiration (from meteorological data).

The following statement by Overgaard *et al*. (2006) summarizes in essence the findings of this thesis: "The more of the physical processes involved in the generation of land-surface fluxes we can parameterise, the more likely it is that we can predict the behaviour of the land surface under different conditions. This is, of course, only true if we can measure or realistically estimate all parameters in such detailed models, preferably at the scale of application." This statement was made in a discussion as to the choice of land-surface flux model, particularly whether a simple model is more desirable than a complex model.

Overgaard *et al.* (2006) refer to Raupach & Finnigan (1988) who stated that the choice of model in any given situation is a trade-off between the desirable but incompatible traits of realism and simplicity. Overgaard *et al*. (2006) argue that realism is desirable from the point of view that realistically structured, and consequently very detailed models, will provide realistic results. On the other hand, simplicity is desirable from the point of view that simple models will require fewer parameters, which will extend the applicability of the model outside the intensely monitored experimental areas (Overgaard *et al.*, 2006).

Parsimony is often mentioned in the question of what physics to include and loosely put, a parsimonious model includes just enough elements to explain: not more, but not less either (Kleinhans *et al*., 2010). The dilemma of model selection and the choice between parsimonious and complex physically based models is also a challenge for researchers tackling the remote sensing estimation of *ET*. In the view of Savenije (2009), scientists should realize that all models are wrong and if this is accepted (to a greater or lesser extent), then with a close enough examination, it will always be possible to find some observations that will not be matched by model predictions (Beven, 2008). Furthermore, there may be multiple models that perform within some limits of acceptability (Beven, 2008). The role of the scientist is therefore to understand where models are wrong, and especially why they are wrong. This is the process of scientific discovery (Savenije, 2009) which will allow for the formulation of alternative and possibly better models.

The results of this research have shown that using the SEBS model as it is currently programmed in ILWIS, did not yield accurate daily evaporation results when compared with the field validation data for this particular study. Some limitations in the field validation approach are noted, such as measurements of *LAI* and irrigation not being taken and the mixed pixel effect due to the size of the apple orchard in relation to a MODIS pixel. Despite adaptations to the methodology to address model sensitivities there was not a significant improvement in the daily *ET* results. The recent paper by Gokmen *et al*. (2012) highlights shortcomings in the original SEBS model. However, the new parameterization which may contribute towards improved results with the modified SEBS model, adds to the complexities of the model. Thus the potential for further uncertainties and sensitivities to the new parameters would need to be investigated.

The complexity of the SEBS model and its assumptions at micrometeorological level, make the realistic estimation of energy fluxes improbable at field and catchment scale. Due to the complexity of the model with many input parameters, numerous errors may be introduced and propagated through the model. The model is sensitive to remote sensing parameters which ideally should be estimated at high spatial resolution. However, satellite imagery at a daily timescale is captured at a coarse spatial resolution. Therefore, it is difficult to deduce, at an appropriate spatial scale, the input parameters to which the model is sensitive.

Finally, the SEBS model is available as part of the open-source freeware ILWIS and can therefore be freely used by remote sensing practitioners without micrometeorological expertise. However, it is necessary for the user to have a good understanding of micrometeorological concepts in order to understand model sensitivities and to assess the accuracy of the results.

9.3. RECOMMENDATIONS

Whilst the original motivation for this research was to estimate water use of crops in order to determine the legal compliance of water users to water use legislation, there are many other potential applications for a spatial representation of *ET*. A particular drive should be towards the implementation of an operational system of managing water resources such as has been implemented in Australia

(albeit in an experimental phase to date). As in Australia, the selection of a suitable method for estimating *ET* from remote sensing should consider the accuracy of the method but pragmatism dictates that computational load and robustness, reliability of data sources, and the degree of automation achievable should be considered (Glenn *et al*., 2011).

The attraction of the SEBS model has been that it is available as part of the open-source freeware ILWIS and can be used "off the shelf" without detailed micrometeorological expertise required. Should this research have shown that accurate results could be obtained from using this version of the SEBS model, then the wide scale use of the model may have been recommended in South Africa. It could be advised that topographic roughness and aggregating data for a mixed pixel effect be incorporated into the methodology before making a final recommendation for or against the use of the SEBS model. However given the heterogeneity and sparse canopy cover of much of the South African landscape, and the further complexities that this would introduce to the methodology, higher accuracies are not anticipated and therefore adapting the methodology further is not recommended.

Whilst other authors using the SEBS model in previous studies have reported *ET* estimates within an acceptable range, this was not found to be the case in the two study areas presented in this research. Because of this discrepancy, it is recommended that should further research be carried out on the SEBS model in South Africa, it should be limited to agricultural areas where accurate vegetation parameters can be obtained, where high resolution imagery with low sensor zenith angles is available and where canopy cover is complete.

It is recommended that the research effort in estimating actual *ET* for vast tracts of natural vegetation, rangeland and dryland agriculture in South African be directed in two avenues. Firstly, the development and/or improvement of existing parsimonious models should be explored. Secondly the validation of the recently released MODIS evapotranspiration data product, MOD16 (http://modis.gsfc.nasa.gov/data/dataprod/dataproducts.php?MOD_NUMBER=16), should be addressed as a matter of urgency. Both these methods bypass the use of thermal imagery. This is advantageous given the reported sensitivities of the SEBS model to $T_0 - T_a$ coupled with associated uncertainties in the T_0 estimation. For high spatial resolution water use efficiency and crop water use studies, the SEBAL model appears to be delivering acceptable levels of accuracy however the lack of

local capacity development is of concern and should be addressed since the data processing is carried out in the Netherlands without advancing the knowledge of South African scientists.

The use of more parsimonious models such as the model reported by Palmer & Weiderman (2011) should not be overlooked. This is of particular importance given the spatial resolution restrictions of the available satellite imagery together with the complexity of the landscape which characterises much of South Africa. Furthermore, it is a vegetation index coupled with meteorological data (Guerschman *et al*., 2009) which has been found to be the best performing method in Australia and given the parallels drawn between the two countries, lessons from Australia should be applied in South Africa. Finally, this represents an opportunity for skill development and capacity building for South African scientists.

Concurrent to this, research is required, as a matter of priority, into the validation of the recently released MODIS evapotranspiration data product, MOD16 developed by Mu *et al*. (2011), in the South African environment. Since it is anticipated that MOD16 will generate considerable interest in South Africa, it is important that the accuracy of the product is ascertained across South African conditions in order to determine the potential constraints and possible errors of the *ET* estimates. To date, the MOD16 data have not been validated locally. Scientists wishing to employ the data in modelling activities are thus unable to determine any confidence intervals or indeed accuracies of the data.

Although the SEBS model was found to produce overestimates of *ET* when implemented as described in the methodology of this research, many valuable lessons have been learnt through the course of this research. Perhaps the most valuable lesson has been around the difficulties in applying complex models to heterogeneous environments. However, the use of the SEBS model to estimate water use in forested areas has not yet been tested in South Africa. This remains an avenue for future research.

A final recommendation would be to consider research funding for a heterogeneity mapping project for South Africa to update similar research by Tanser & Palmer (1999). The purpose of such a dataset would be to allow for the selection of the appropriate level of complexity of models based on a priori knowledge on the complexity of the landscape under study.

Despite the overestimations of *ET* using the methodology described in this research, the recommendations which have arisen from the research determine that the research project has been successful in that the South African research agenda into remote sensing estimation of *ET* can be said to have been significantly advanced as a result.

10. REFERENCES

Adreen W, 2011. 'Towards environmental flows: comparing water law in four countries', available at URL: http://www.globalwaterforum.org/2011/06/01/towards-environmental-flows-comparing-water-law-in-four-countries/, date accessed 8 Sept 2011.

Agam N, Kustas WP, Anderson MC, Li F & Neale CMU, 2007. 'A vegetation index based technique for spatial sharpening of thermal imagery', *Remote Sensing of Environment*, vol. 107, no. 4, pp. 545-558.

Ahmad M, Bastiaanssen WGM & Feddes RA, 2005. 'A new technique to estimate net groundwater use across large irrigated areas by combining remote sensing and water balance approaches, Rechna Doab, Pakistan', *Hydrogeology Journal,* vol.13, pp.653-664.

Allen RG, Pereira LS, Raes D & Smith M, 1998. 'Crop evapotranspiration: guidelines for computing crop water requirements' *FAO Irrigation and Drainage Paper 56*, Rome, 300 pp.

Allen RG, Tasumi M, Morse A, Trezza R, Wright JL, Bastiaanssen W, Kramber W, Lorite I, & Robison CW, 2007. 'Satellite-Based Energy Balance for Mapping Evapotranspiration with Internalized Calibration (METRIC)—Applications', *Journal of Irrigation and Drainage Engineering*, vol. 133, no. 4, pp. 395-407.

Allen RG, Hendrickx J, Bastiaanssen W, Kjaersgaard J, Irmak A & Huntington J, 2010. 'Status and continuing challenges in operational remote sensing of ET'. In*: Proceedings of: 5th National Decennial Irrigation Conference*, December 5 - 8, 2010, Phoenix, Arizona.

Alvarez JAG, 2007. 'Effects of land cover changes on the water balance of the Palo Verde Wetland, Costa Rica', M.Sc. thesis, International Institute for Geo-information Science and Earth Observation, The Netherlands.

ARC-ISCW, 2010. Technical manual for the AgroClimatology Weather Station Network. ARC-ISCW internal report, Agricultural Research Council-Institute for Soil, Climate and Water, South Africa, Report No. GW/A/2008/60, 2010.

Badola A, 2009. 'Validation of Surface Energy Balance System (SEBS) over forest land cover and sensitivity analysis of the model', M.Sc. thesis, International Institute for Geo-information Science and Earth Observation, The Netherlands.

Bandara KMPS, 2006. **'**Assessing irrigation performance by using remote sensing', Ph.D. thesis, International Institute for Geo-information Science and Earth Observation, The Netherlands.

Baret F, Clevers JGPW, Stevens MD, 1995. 'The robustness of canopy gap fraction estimations from red and near-infrared reflectances: A comparison of approaches'. *Remote Sensing of Environment*, vol 54, pp 141 – 151.

Bastiaanssen WGM, Menenti M, Feddes RA & Holtslag AAM, 1998. 'The Surface Energy Balance Algorithm for Land (SEBAL): Part 1 formulation', *Journal of Hydrology*, vol. 212 , no.213, pp.198-212.

Bastiaanssen WGM, Chavez RG, Alsulamain A & Ahmad M, 2006. 'Estimation of groundwater extraction on irrigated lands in arid zones from thermal infrared satellites'. *Unpublished report* 16pp.

Bastiaanssen WGM & Bos MG, 1999. 'Irrigation performance indicators based on remotely sensed data: a review of literature', *Irrigation and Drainage Systems,* vol. 13, no. 4, pp. 291-311.

Batatia H & Bessaih N, 2009. 'Satellite land surface temperature for Sarawak area', Geospatial World, available at URL: http://www.geospatialworld.net/index.php?option=com_content&view=article&id=15188%3Asatellite-land-surface-temperature-for-sarawak-area&catid=123%3Aenvironment-overview, date accessed 12 May 2011.

Batelaan O & De Smedt F, 2001. 'WetSpass: a flexible, GIS based, distributed recharge methodology for regional groundwater modelling'. In: Gehrels, H., Peters, J., Hoehn, E., Jensen, K., Leibundgut, C., Griffioen, J., Webb, B. & Zaadnoordijk, W-J. (eds). Impact of Human Activity on Groundwater Dynamics. IAHS Publ. no. 269, Wallingford UK, pp.11-17.

Beven K, 1979. 'A sensitivity analysis of the Penman-Monteith actual evapotranspiration estimates', *Journal of Hydrology*, vol. 44, pp. 169 – 190.

Beven K, 2006. 'On undermining the science?', *Hydrological Processes,* vol. 20, pp. 3141-3146.

Beven K, 2008. 'On doing better hydrological science', *Hydrological Processes,*vol. 22, pp. 3549-3553.

Blight GE, 2002. 'Measuring evaporation from soil surfaces for environmental and geotechnical purposes', *Water SA*, vol. 28, no. 4, pp. 381-394.

Brutsaert W, 1982. '*Evaporation into the atmosphere'*, Reidel, Dordrecht, The Netherlands.

Burger D (ed), 2003. '*South African Yearbook 2002/3*', Published by Government Communications (GCIS).

Burger D (ed), 2005. '*South African Yearbook 2004/5*', Published by Government Communications (GCIS).

Burger D (ed), 2011. '*South African Yearbook 2010/11*', Published by Government Communications (GCIS).

Carlson TN & Ripley DA, 1997. 'On the Relation between NDVI, Fractional Vegetation Cover, and Leaf Area Index', *Remote Sensing of Environment*, vol. 62, no. 3, pp. 241-252.

Carrer D, Roujean JL & Meurey C, 2010. 'Comparing Operational MSG/SEVIRI Land Surface Albedo Products From Land SAF With Ground Measurements and MODIS', *IEEE Transactions on Geoscience and Remote Sensing*, vol. 48, no. 4, pp 1714-1728.

Cleugh HA, Leuning R, Mu QZ & Running SW, 2007. 'Regional evaporation estimates from flux tower and MODIS satellite data', *Remote Sensing of Environment*, vol. 106, no. 3, pp. 285-304.

Courault D, Seguin B & Olioso A, 2005. 'Review on estimation of evapotranspiration from remote sensing data: From empirical to numerical modeling approaches', *Irrigation and Drainage Systems*, vol. 19, pp. 223-249.

Dungan JL, Kao D & Pang A, 2002. 'The uncertainty visualization problem in remote sensing analysis', in: *Proceedings of International Geoscience & Remote Sensing*, Toronto, Canada, June 2, 2002, pp. 729-731.

Ershadi A, 2010. 'Land-atmosphere interactions from canopy to troposphere', M.Sc. thesis, International Institute for Geo-information Science and Earth Observation, The Netherlands, 2010.

Ershadi A, McCabe, Evans & Walker JP, 2013. 'Effects of spatial aggregation on the multi-scale estimation of evapotranspiration', *Remote Sensing of Environment,* vol. 131, pp. 51–62.

Flores AN, Ivanov VY, Entekhabi D & Bras RL, 2009. 'Impact of hillslope-scale organization of topography, soil moisture, soil temperature, and vegetation on modelling surface microwave radiation emission', *IEEE Transactions on Geoscience and Remote Sensing*, vol. 47, no. 8, pp 2557-2571.

French AN, Schmugge TJ, Kustas WP, Brubaker KL & Prueger J, 2003. 'Surface energy fluxes over El Reno, Oklahoma, using high-resolution remotely sensed data', *Water Resources Research*, vol. 39, no. 6, pp. 1164-1176.

Garrigues S, Allard D, Baret F & Weiss M, 2006. 'Quantifying spatial heterogeneity at the landscape scale using variogram models', *Remote Sensing of Environment*, vol. 103, no. 1, pp. 81-96.

Gebreyesus MG, 2009. 'Validation of RS approaches to model surface characteristics in hydrology: a case study in Guareña Aquifer, Salamanca, Spain', M.Sc. thesis, International Institute for Geo-information Science and Earth Observation, The Netherlands.

Gellens-Meulenberghs F, 2000. 'Evapotranspiration and surface heat fluxes over Belgium: outcome and perspectives', *Agronomie*, vol. 20, no. 8, pp. 857-868.

Gellens-Meulenberghs F, 2005. 'Sensitivity Tests of an Energy Balance Model to Choice of Stability Functions and Measurement Accuracy', *Boundary Layer Meteorology*, vol. 115, no. 3, pp. 453-471.

Gibson LA, Münch Z, Engelbrecht J, Petersen N & Conrad JE, 2009. 'Remote sensing as a tool towards resource assessment and determination of the legal compliance of surface and groundwater use', Research Report 1960/1/09, Water Research Commission, Pretoria, South Africa.

Gibson LA, Münch Z, Carstens M & Conrad JE, 2011. 'Remote sensing evapotranspiration (SEBS) evaluation using water balance', Consultancy Report K8/929/1. Water Research Commission, Pretoria, South Africa.

Glenn EP, Doody TM, Guerschman JP, Huete AR, King EA, McVicar TR, Van Dijk AIJM, Van Niel TG, Yebra M & Zhang YQ, 2011. 'Actual Evapotranspiration Estimation by Ground and Remote Sensing Methods: The Australian Experience', *Hydrological Processes*, vol. 25, no. 26, pp. 4103 – 4116.

Gokmen M, Vekerdy Z, Verhoef A, Verhoef W, Batelaan O & van der Tol C, 2012. 'Integration of soil moisture in SEBS for improving evapotranspiration estimation under water stress conditions *', Remote Sensing of Environment*, vol. 121 , pp. 261–274.

Gowda PH, Chavez JL, Colaizzi PD, Evett SR, Howell TA, & Tolk JA, 2007. 'Remote sensing based energy balance algorithms for mapping ET: current status and future challenges', *Transactions of the American Society of Agricultural and Biological Engineers*, vol. 50, no. 5, pp.1639-1644.

Gowda PH, Chavez JL, Colaizzi PD, Evett SR, Howell TA & Tolk JA, 2008. 'ET mapping for agricultural water management: present status and challenges', *Irrigation Science*, vol. 26, pp. 223-237.

Guerschman JP, Van Dijk AIJM, Mattersdorf G, Beringer J, Hutley LB, Leuning R, Pipunic RC & Sherman BS, 2009. 'Scaling of potential evapotranspiration with MODIS data reproduces flux observations and catchment water balance observations across Australia', *Journal of Hydrology*, vol. 369, no 1-2, pp. 107-119.

Gutman G & Ignatov A, 1998. 'The derivation of the green vegetation fraction from NOAA/AVHRR data for use in numerical weather prediction models', *International Journal of Remote Sensing*, vol. 19, no. 8, pp. 1533-1543.

Hailegiorgis WS, 2006. 'Remote sensing analysis of summer time evapotranspiration using SEBS algorithm: a case study in Regge and Dinklel, The Netherlands', M.Sc. thesis, International Institute for Geo-information Science and Earth Observation, The Netherlands.

Hellegers PJGJ, Jansen HC & Bastiaanssen WGM, 2011. 'An interactive water indicator assessment tool to support land use planning', *Irrigation and Drainage* (DOI: 10.1002/ird.641).

Jackson R.D, Reginato RJ & Idso SB, 1977. 'Wheat canopy temperature: a practical tool for evaluating water requirements', *Water Resources Research 13*, 651-656.

Jarmain C, Mengitsu M, Jewitt GPW, Kongo V & Bastiaanssen W, 2009. 'A methodology for near-real time spatial estimation of evaporation', Research Report 1751-1-09, Water Research Commission, Pretoria, South Africa.

Jarmain C & Mengistu MG, 2011. 'Validating energy fluxes estimated using the surface energy balance system (SEBS) model for a small catchment', WRC Consultancy Report K8/824, Water Research Commission, Pretoria, South Africa.

Jarmain C, Klaasse A, Basson FC, Meininger W, Wilmink S & Bastiaanssen W, 2011a. 'Developing an operational remote sensing system for monitoring of efficient crop water and nitrogen use of grapes', Western Cape Province, Final report to the Western Cape Provincial Department of Agriculture.

Jarmain C, Singels A, Obando E, Paraskevopoulos A & Mthembu I, 2011b. 'Water use efficiency of irrigated agricultural crops determined with satellite imagery', Progress Report. K5/2079//4. Water Research Commission, Pretoria.

Jarmain C, Singels A, Obando E, P Paraskevopoulos A, Olivier F, Münch Z, van der Merwe B, Walker S, van der Laan M, Messehazion M, Savage M, Pretorius C, Annandale J & Everson C, 2013. 'Water use efficiency of irrigated agricultural crops determined with satellite imagery'. K5/2079//4. Deliverable 6, Water use efficiency Report 2012/13. Water Research Commission, Pretoria.

Jarmain C & Klaasse A, 2012. 'Fruitlook: An operational service to improved crop water and nitrogen management in grapes and other deciduous fruit trees using satellite technology for the season of 2011-12', Progress Report, Western Cape Provincial Department of Agriculture.

Jarmain C & Meijninger WL, 2012. 'Assessing the impact of Invasive Alien Plants on South African water resources using remote sensing techniques'. IAHS publication no. 352, pp. 388-392.

Jha MK & Chowdary VM, 2006. 'Challenges of using remote sensing and GIS in developing nations', *Hydrogeology Journal*, vol. 15, no. 1, pp. 197-200.

Jia L, Su Z, van den Hurk B, Menenti M, Moene HAR, Baselga Yrisarry JJ, Ibanez M & Cuesta A, 2003. 'Estimation of sensible heat flux using the Surface Energy Balance System (SEBS) and ATSR measurements', *Physics and Chemistry of the Earth*, vol. 28, no.1-3, pp. 75-88.

Jia L, Xi G, Liu S, Huang C, Yan Y, & Liu G,.2009. 'Regional estimation of daily to annual regional evapotranspiration with MODIS data in the Yellow River Delta wetland'. *Hydrology and Earth System Sciences*, vol. 13, no. 10, pp 1775 - 1787.

JPL, 2009. SWIR- ASTER User Advisory. [online]. Available at URL:http://asterweb.jpl.nasa.gov/swir-alert.asp [Accessed 30 March 2009]

Kalma JD, McVicar TR & McCabe MF, 2008. 'Estimating Land Surface Evaporation: A Review of Methods Using Remotely Sensed Surface Temperature Data', *Surveys in Geophysics*, vol. 29, no. 4-5, pp. 421-469.

Kaur R, Srinivasan R, Mishra K, Dutta D, Prasad D & Bansal G, 2003. 'Assessment of a SWAT model for soil and water management in India', *Land Use and Water Resources Research*, vol. 3, pp. 1-7.

Kipp & Zonen, 2005. 'Large Aperture Scintillometer instruction manual', Delft, Holland.

Klaasse A, Bastiaanssen W, Jarmain C & Roux A, 2008. 'Water use efficiency of table and wine grapes in Western Cape, South Africa', WaterWatch report, Wageningen, the Netherlands, 68 pp.

Klaasse A, Jarmain C, Roux A, Becu O & Ginati A, 2011. 'GrapeLook: space based services to improve water use efficiency of vineyards in South Africa'. Proceedings of: *62nd International Astronautical Congress*, 3-7 October 2011, Cape Town.

Kleinhans MG, Bierkens MFP & van der Perk M, 2010. 'On the use of laboratory experimentation: "Hydrologists, bring out shovels and garden hoses and hit the dirt"', *Hydrology and Earth System Science, HESS Opinions*, vol. 14, no. 2, pp. 369–382.

Kongo VM & Jewitt GPW, 2006. 'Preliminary investigation of catchment hydrology in response to agricultural water use innovations: A case study of the Potshini catchment – South Africa', *Physics and Chemistry of the Earth*, vol. 31, no. 15-16, pp. 976-987.

Kustas WP, Li F, Jackson TJ, Prueger JH, MacPherson JI & Wolde M, 2004. 'Effects of remote sensing pixel resolution on modelled energy flux variability of croplands in Iowa', *Remote Sensing of Environment*, vol. 92, no. 4, pp. 534-547.

Lakhankar T, Ghedira H, Temimi M, Azar AE & Khanbilvardi R, 2009. 'Effect of land cover heterogeneity on soil moisture retrieval using active microwave remote sensing data', *Remote Sensing*, vol. 1, no. 2, pp. 80-91.

Leuning R, Zhang YQ, Rajaud A, Cleugh H & Tu K, 2008. 'A simple surface conductance model to estimate regional evaporation using MODIS leaf area index and the Penman-Monteith equation', *Water Resources Research*, vol. 44, 10419.

Li Z, Jia L, Su Z, Wan Z & Zhang R, 2003. 'A new approach for retrieving precipitable water from ATSR2 split-window channel data over land area', *International Journal of Remote Sensing*, vol. 24, no. 24, pp. 5095-5117.

Li Z, Yu G, Li Q, Fu Y & Li Y, 2006. 'Effect of spatial variation on areal evapotranspiration simulation in Haibei, Tibet plateau, China', *International Journal of Remote Sensing*, vol.27, no. 16, pp. 3487-3498.

Li F, Kustas WP, Anderson MC, Prueger JH & Scott RL, 2008. 'Effect of remote sensing spatial resolution on interpreting tower-based flux observations', *Remote Sensing of Environment*, vol. 112, no. 2, pp. 337-349.

Liang S, 2001. 'Narrowband to Broadband Conversions of land surface albedo I: Algorithms', *Remote Sensing of the Environment*, vol. 76, no. 2, pp. 213-238.

Lin W, 2006. 'Satellite based regional scale evapotranspiration in the Hebei Plain, Northeastern China', M.Sc. thesis, International Institute for Geo-information Science and Earth Observation, The Netherlands.

Lin W, van de Velde R & Su Z, 2008. 'Satellite based regional-scale evapotranspiration in the Hebei Plain, Northeastern China', in: *Proceedings of Dragon 1 Programme Final Results 2004–2007*, 21– 25 April 2008, Beijing, China.

Lu J, Li Z-L, Tang R, Tang B-H, Wu H, Yang F, Labed F & Zhou G, 2012. 'Evaluating the SEBS-estimated evaporative fraction from MODIS data for a complex underlying surface', *Hydrological Processes*, doi: 10.1002/hyp.9440.

Madeira C, Dash P, Olesen F & Trigo I, 2005. 'Intercomparison of Meteosat-8 derived LST with MODIS and AATSR similar products', in: Proceedings of *2005 EUMETSAT Meteorological Satellite Conference*, 19 - 23. September 2005, Dubrovnik, Croatia.

Mao K, Qin Z, Shi J & Gong P, 2005. 'A practical split window algorithm for retrieving land-surface temperature from MODIS data', *International Journal of Remote Sensing*, vol.26, no. 15, pp. 3181-3204.

Mariotto I & Gutschick VP, 2010. 'Non-lambertian corrected albedo and vegetation index for estimating land evapotranspiration in a heterogeneous semi-arid landscape', *Remote Sensing*, vol. 2, no. 4, pp. 926-938.

Mather P, 1999. 'Computer Processing of Remotely Sensed Images: An Introduction', Wiley, Chichester.

McCabe MF & Wood EF, 2006. 'Scale influences on the remote estimation of evapotranspiration using multiple satellite sensors', *Remote Sensing of Environment*, vol. 105, no. 4, pp. 271-285.

McCabe MF, Wood EF, Wójcik R, Pan M, Sheffield J, Gao H & Su H, 2008. 'Hydrological consistency using multi-sensor remote sensing data for water and energy cycle studies', *Remote Sensing of Environment*, vol. 112, no. 2, pp. 430-444.

Melesse AM, Oberg J, Nangia V, Beeri O & Baumgartner D, 2006. 'Spatiotemporal dynamics of evapotranspiration at the Glacial Ridge prairie restoration in northwestern Minnesota', *Hydrological Processes*, vol. 20, no. 7, pp. 1451-1464.

Menenti M & Choudhury BJ, 1993. 'Parameterization of land surface evapotranspiration using a location dependent potential evapotranspiration and surface temperature range'. In: Proceedings of *Exchange Processes at the Land Surface for a Range of Space and Time Scales*, 13-16 July 1993, Yokohama, Japan.

Moran MS, Clarke TR, Inoue Y & Vidal A, 1994. 'Estimating crop water deficit using the relation between surface-air temperature and spectral vegetation index', *Remote Sensing of Environment,* vol. 49, no. 2, pp. 246–263.

Moran MS, Humes KS & Pinter PJ, 1997. 'The scaling characteristics of remotely-sensed variables for sparsely-vegetated heterogeneous landscapes', *Journal of Hydrology*, vol. 190, no. 3-4, pp. 337-362.

Mu Q, Heinsch FA, Zhao M & Running SW, 2007. 'Development of a global evapotranspiration algorithm based on MODIS and global meteorology data', *Remote Sensing of Environment,* vol. 111, no. 4, pp. 519-536.

Mu QZ, Zhao MS & Running SW, 2011. 'Improvements to a MODIS global terrestrial evapotranspiration algorithm', *Remote Sensing of Environment*, vol. 115, pp. 1781-1800.

Münch *Z,* Conrad, JE, Gibson LA, Palmer AR & Hughes D, 2013. 'Satellite earth observation as a tool to conceptualize hydrogeological fluxes in the Sandveld, South Africa', *Hydrogeology Journal*, vol. 21(5), pp 1053-1070.

NASA Earth Science Enterprise, Earth Science Applications Directorate, University of South Carolina Affiliated Research Center, 2005. '*Remote Sensing Crop Type for Sustainable Development by the Department of Water Affairs & Forestry, Republic of South Africa',* Project by Department of Water Affairs & Forestry Pretoria, South Africa and NASA Affiliated Research Center, University of South Carolina.

NASA, 2007. Advanced Spaceborne Thermal Emission and Reflectance Radiometer. [online]. Available at: http://asterweb.jpl.nasa.gov/schedule.asp. [Accessed 23 October 2007]

Overgaard J, Rosbjerg D & Butts MB, 2006. 'Land-surface modelling in hydrological perspective – a

review', *Biogeosciences*, vol. 3, no. 2, pp. 229-241.

Palmer AR & Weideman CI, 2011. 'Exploring trends in evapotranspiration in the KNP: towards a water use efficiency model for rangeland production in semi-arid savannas', In: Proceedings of *IXth International Rangeland Congress*, 2-8 April 2011, Rosario, Argentina.

Pan M, Wood EF, Wójcik R & McCabe MF, 2008. 'Estimation of regional terrestrial water cycle using multi-sensor remote sensing observations and data assimilation', *Remote Sensing of Environment,* vol. 112, no. 4, pp. 1282–1294.

Petropoulos G, Carlson TN, Wooster MJ & Islam S, 2009. 'A review of Ts/VI remote sensing based methods for the retrieval of land surface energy fluxes and soil surface moisture', *Progress in Physical Geography,* vol. 33, no. 2, pp. 224–250.

Rahman H & Dedieu G, 1994. 'SMAC: a simplified method for the atmospheric correction of satellite measurements in the solar spectrum', *International Journal of Remote Sensing*, vol. 15, no. 1, pp. 123-143.

Roerink GJ, Su Z & Menenti M, 2000. 'S-SEBI: A simple remote sensing algorithm to estimate the surface energy balance', *Physics and Chemistry of the Earth (B)*, vol, *25*, no. 2, pp.147-157.

Rwasoka DT, Gumindoga W & Gwenzi J, 2011. 'Estimation of actual evapotranspiration using the Surface Energy Balance System (SEBS) algorthim in the Upper Manyame catchment in Zimbabwe', *Physics and Chemistry of the Earth, vol* 36, pp. 736–746.

Santhi C, Muttiah RS, Arnold JG & Srinivasan R, 2005. 'A GIS–based regional planning tool for irrigation demand assessment and savings using SWAT', *Transactions of the American Society of Agricultural Engineers*, vol. 48, no. 1,, pp. 137–147.

Savage MJ, Everson CS, Odhiambo GO, Mengistu MG & Jarmain C, 2004. 'Theory and practice of evaporation measurement, with special focus on SLS as an operational tool for the estimation of spatially-averaged evaporation', Research Report 1335/1/04, Water Research Commission, Pretoria, South Africa.

Savenije HHG, 2009. '"The art of hydrology"', *Hydrology and Earth System Science, HESS Opinions*, vol. 13, no. 2, pp. 157–161.

Schmugge TJ, Kustas WP, Ritchie JC, Jackson TJ, & Rango A, 2002. 'Remote sensing in hydrology', *Advances in Water Resources,* vol. 25, no. 8-12. pp. 1367-1385.

Shuttleworth WJ, Yang ZL & Arain MA, 1997.' Aggregation rules for surface parameters in global models', *Hydrology and Earth System Science*, vol 1, no. 2, pp. 217-226.

Sinclair S & Pegram GGS, 2010. 'A comparison of ASCAT and modelled soil moisture over South Africa, using TOPKAPI in land surface mode', *Hydrology and Earth System Sciences,* vol. 14, no. 4, pp. 613-626.

Sobrino JA & Raissouni N, 2000. 'Toward remote sensing methods for land cover dynamic monitoring: Application to Morocco', *International Journal of Remote Sensing*, vol. 21, no. 2, pp. 353 – 366.

Sobrino JA & El Kharraz J, 2003. 'Surface temperature and water vapour retrieval from MODIS data', *International Journal of Remote Sensing,* vol. 24, no. 24, pp. 5161-5182.

Sobrino JA, Gómez M, Jiménez-Muñoz JC & Olioso A, 2007. 'Application of a simple algorithm to estimate daily evapotranspiration from NOAA–AVHRR images for the Iberian Peninsula', *Remote Sensing of Environment,* vol. 110, no. 2, pp. 139–148.

Su Z, Schmugge TJ, Kustas WP & Massman WJ, 2001. 'An evaluation of two models for estimation of the roughness height for heat transfer between the land surface and the atmosphere', *Journal of Applied Meteorology*, vol. 40, no. , pp. 1933-1951.

Su Z, 2002. 'The surface energy balance system (SEBS) for estimation of turbulent heat fluxes', *Hydrology and Earth System Sciences*, vol. 6, no. 1, pp. 85-99.

Su Z & Roerink GJ (eds), 2004. 'Drought Risk Reduction', Alterra-rapport 1135, Wageningen, The Netherlands.

Su H. McCabe MF & Wood EF, 2005. 'Modeling Evapotranspiration during SMACEX: Comparing Two Approaches for Local- and Regional-Scale Prediction', *Journal of Hydrometeorology*, vol. 6, no. 6, 910-922.

Su Z, 2006. 'An introduction to the surface energy balance system (SEBS)', Lecture notes, ESA TIGER Capacity Building Facility 1st Training Course on "Advanced optical remote sensing", 22-25 November 2006, Cape Town, South Africa.

Su Z, Wang L & Parodi GN, 2008. 'SEBS for ILWIS Open Source: A Practical Tool for Surface Energy Balance Estimates from Remote Sensing Data, Surface Energy Balance Models of Agricultural Areas from Earth Observation Data', 13 March 2008, Lima, Perú.

Tanser FC & Palmer AR, 1999. 'The application of a remotely-sensed diversity index to monitor degradation patterns in a semi-arid heterogeneous, South African landscape', *Journal of Arid Environments*, vol. 43, no 4, pp. 477-484.

Tasumi M, Allen RG & Trezza R, 2008. 'At-surface reflectance and albedo from satellite for operational calculation of land surface energy balance', *Journal of Hydrologic Engineering*, vol. 13, no. 2, pp. 51-63.

Timmermans J, Van der Tol C, Verhoef A, Verhoef W, Su Z, van Helvoirt M & Wang L, 2011. 'Quantifying the uncertainty in estimates of surface- atmosphere fluxes through joint evaluation of the SEBS and SCOPE models', *Hydrology and Earth System Sciences Discussion*, vol. 8, no. 2, pp. 2861-2893.

Timmermans WJ, Van der Kwast J, Gieske ASM, Su Z, Olioso A, Jia L & Elbers J, 2005. 'Intercomparison of energy flux models using ASTER imagery at the SPARC 2004 site, Barrax, Spain', in: Proceedings of *the ESA WPP-250 : SPARC final workshop*, 4-5 July 2005, Enschede, The Netherlands.

Timmermans WJ, Kustas WP, Anderson MC & French AN, 2007. 'An intercomparison of the surface energy balance algorithm for land (SEBAL) and the two-source energy balance (TSEB) modeling schemes', *Remote Sensing of Environment*, vol. 108, no. 4, pp. 369-384.

Todini E & Ciarapica L, 2001. 'The TOPKAPI model. (Chapter 12). In: *Mathematical models of large watershed hydrology*, VP Singh *et al*. (Eds). Water Resources Publications, Littleton, Colorado, USA.

Toller GN & Isaacman A, 2002. 'MODIS Level 1B Product User's Guide'**,** Available at URL**:** http://mcst.gsfc.nasa.gov/uploads/files/M1054.pdf , date accessed: 16 May 2011.

USGS, 2007. SLC-off Products: Background. [online]. Available at URL: http://landsat.usgs.gov/data_products/slc_off_data_products/slc_off_background.php.[Accessed 23 October 2007]

Van den Berg EC, Plarre C, Van den Berg HM & Thompson MW, 2008. 'The South African National Land Cover 2000', Report GW/A/2008/86, Agricultural Research Council-Institute for Soil, Climate and Water, Pretoria, South Africa.

Van der Kwast J, Timmermans W, Gieske A, Su Z, Olioso A, Jia L, Elbers J, Karssenberg D & De Jong S, 2009. 'Evaluation of the Surface Energy Balance System (SEBS) applied to ASTER imagery with flux-measurements at the SPARC 2004 site (Barrax, Spain)', *Hydrology and Earth System Sciences*, vol. 13, no. 7, pp. 1337-1347.

Van der Tol C, Van der Tol S, Verhoef A, Su Z, Timmermans J, Houldcroft C & Gieske A, 2009. 'A Bayesian approach to estimate sensible and latent heat over vegetated land surface', *Hydrology and Earth System Sciences*, vol. 13, no. 6, pp. 749-758.

Veregin H, 1989. 'Error modelling for the map overlay operation', In: Goodchild MF & Gopal S. (eds), Accuracy of Spatial Databases, Taylor and Francis, London.

Verstraeten WW, Veroustraete F & Feyen J, 2008. 'Assessment of evapotranspiration and soil moisture content across different scales of observation', *Sensors,* vol 8, no. 1, pp. 70-117.

Voogt MP, 2006. 'Meteolook, a physically based regional distribution model for measured meteorological variables', MSc. Thesis TU Delft, The Netherlands. Abstract available at: http://www.citg.tudelft.nl/live/pagina.jsp?id=50e40a94-07c2-4ccc-a3e9-849c85ecbfd0&lang=en&binary=/doc/Voogt2006.pdf. Accessed 19 May 2011.

Wan Z, 2006. 'MODIS land surface temperature products users' guide', Available at: http://g.icess.ucsb.edu/modis/LstUsrGuide/MODIS_LST_products_Users_guide.pdf. Accessed 19 May 2011.

Wang G, Gerther GZ, Fang S & Anderson AB, 2005. 'A methodology for spatial uncertainty analysis of remote sensing and GIS products', *Photogrammetric Engineering & Remote Sensing*, vol. 17, no. 12, pp.1423-1432.

Wang K, Li Z & Cribb M, 2006. 'Estimation of evaporative fraction from a combination of day and night land surface temperatures and NDVI: A new method to determine the Priestley–Taylor parameter', *Remote Sensing of Environment*, vol. 102, no. 2-4, pp 293-305.

WE Consult, 2011. 'Operational Monitoring Product for Planning and Water Allocation in the International Incomati Basin (WATPLAN)'. Stakeholder analysis report. 53 pp.

Xin S, 2006. 'Regional evapotranspiration over the arid inland Heihe River Basin in northwest China', M.Sc. thesis, International Institute for Geo-information Science and Earth Observation, The Netherlands.

Xiong X, Chiang K, Guenther B & Barnes WL, 2002a. 'MODIS Reflective Solar Bands Calibration Algorithm and On-orbit Performance' , In: Proceedings of *SPIE — Optical Remote Sensing of the Atmosphere and Clouds III*, October 2002, Hangzhou, China.

Xiong X, Sun J, Esposito J, Guenther B & Barnes WL, 2002b. 'MODIS Thermal Emissive Bands Calibration Algorithm and On-orbit Performance' , In: Proceedings of *SPIE — Optical Remote Sensing of the Atmosphere and Clouds III*, October 2002, Hangzhou, China.

Zhang YQ, Chiew FHS, Zhang L, Leuning R, Cleugh HA. 2008. 'Estimating catchment evaporation and runoff using MODIS leaf area index and the Penman-Monteith equation', *Water Resources Research*, vol. 44: W10420

APPENDIX 1

The required MODIS data products, *MOD 02 level 1B calibrated radiances*, aggregated to 1km resolution and the *MOD 03 geolocation* files can be selected and ordered online at http://ladsweb.nascom.nasa.gov/data/search.html. Once an order is placed, the user is notified by e-mail and directed to an ftp site where the data can be downloaded.

The *MOD021KM-Level 1B calibrated radiances -1KM* data set contains calibrated and geolocated at-aperture radiances, in $W/(m^{-2}\mu m^{-1}sr)$, for 36 bands generated from MODIS Level 1A sensor counts (Toller & Isaacman, 2002) in Hierarchical Data Format (hdf), with an aggregated pixel resolution of 1000m. Also required are the *MOD 03-Geolocation* files corresponding to each MOD021KM file ordered. The geolocation file contains geodetic coordinates, ground elevation, and solar and satellite zenith and azimuth angle for each MODIS 1-km sample and should be ordered together with its corresponding Level 1B calibrated radiance as this is needed for further processing.

The MODIS instrument (Table A1 & Table A2) captures 36 spectral bands ranging in wavelength from 0.4 μm to 14.4 μm with a high radiometric sensitivity (12 bit) and provides very low out-of-band response. The resolution varies from two bands which are imaged at a nominal resolution of 250 m at nadir, five bands at 500 m, and the remaining 29 bands at 1 km.

It should be noted that although the instruments on board TERRA and AQUA are both MODIS sensors, the difference in launch dates allowed for some improvements to be made to the AQUA instrument. Xiong *et al*. (2002a) report on the reflective solar bands on-orbit calibration and give the signal-to-noise ratios (SNR) for each of the bands for TERRA and AQUA. TERRA MODIS which has been in orbit since 1999 initially used the A-side electronics and then B-side electronics. However, after the failure of the B-side power supply, the instrument reverted to the A-side electronics. For the shortwave infrared (SWIR) bands, the second A-side configuration (A-II) electronics are used. The signal-to-noise ratios (SNR) differ for each set of electronics (Xiong *et al*., 2002a). The SNR is given in Table A3 for each of the reflective bands used in this research for MODIS TERRA and AQUA along with the original specifications. For MODIS TERRA, only the SNR for the electronics used, is given. It is clear from Table

A3 that for all bands, the SNR for AQUA is superior to that of TERRA. It should also be noted that the SNR for TERRA band 7 is out of specification. This was determined pre-launch.

Xiong *et al*. (2002b) reported on the on-orbit calibration of the MODIS thermal emissive bands used primarily for surface temperature retrieval (bands 31 and 32, used in this research for land surface temperature retrieval). The results showed that bands 31 and 32 on both TERRA and AQUA are performing better than design requirements with on-orbit noise equivalent temperature differences of AQUA in band 32 being marginally superior to that of TERRA.

The MODIS Swath Tool (MST) can be downloaded from http://lpdaac.usgs.gov/landdaac/tools/mrtswath/index.asp. The MST is used to project the images to the appropriate map projection: Transverse Mercator, central meridian 19°, WGS84 datum. The MST is also used to subset the image so that the image processing time is reduced and processing of all images is carried out over the same geographical space (top left corner: -32.5°S, 18°E; bottom right corner: -33.25°S, 19°E). The MST is used to convert the selected bands - cropped by geographical area and transformed to the required map projection – to geoTIFF format. The output is eight geoTIFF files. In a similar process the Height, SensorZenith, SensorAzimuth, SolarZenith and SolarAzimuth hdf files are extracted from the MOD 03 geolocation file using the MST. Note that the geolocation data (SensorZenith, SensorAzimuth, SolarZenith and SolarAzimuth) originally contained within in the MOD 03 hdf files are scaled values and therefore must be corrected by the scale factor 0.01.

Toller & Isaacman (2002) details the calibration of digital number in MODIS Level 1B data. For each band, the reflectance/radiance scales and offsets are obtained from original hdf file. The freeware HDF Explorer can be used to do this and can be downloaded from: www.space-research.org/explorer_download.html.

Table A1: MODIS instrument specifications (http://modis.gsfc.nasa.gov/about/design.php).

Orbit:	705 km, 10:30 a.m. descending node (TERRA) or 1:30 p.m. ascending node (AQUA), sun-synchronous, near-polar, circular
Scan Rate:	20.3 rpm, cross track
Swath Dimensions:	2330 km (cross track) by 10 km (along track at nadir)
Telescope:	17.78 cm diam. off-axis, afocal (collimated), with intermediate field stop
Size:	1.0 x 1.6 x 1.0 m
Weight:	228.7 kg
Power:	162.5 W (single orbit average)
Data Rate:	10.6 Mbps (peak daytime); 6.1 Mbps (orbital average)
Quantization:	12 bits
Spatial Resolution:	250 m (bands 1-2) 500 m (bands 3-7) 1000 m (bands 8-36)
Design Life:	6 years

Table A2: MODIS data specifications (adapted from http://modis.gsfc.nasa.gov/about/design.php).

Band	**Bandwidth** (nm)	**Spectral Radiance** (W/m² sr⁻¹μm⁻¹)	**Required signal to noise ratio**
1	620 - 670	21.8	128
2	841 - 876	24.7	201
3	459 - 479	35.3	243
4	545 - 565	29.0	228
5	1230 - 1250	5.4	74
6	1628 - 1652	7.3	275
7	2105 - 2155	1.0	110
8	405 - 420	44.9	880
9	438 - 448	41.9	838
10	483 - 493	32.1	802
11	526 - 536	27.9	754
12	546 - 556	21.0	750
13	662 - 672	9.5	910
14	673 - 683	8.7	1087
15	743 - 753	10.2	586
16	862 - 877	6.2	516
17	890 - 920	10.0	167
18	931 - 941	3.6	57
19	915 - 965	15.0	250
Band	**Bandwidth** (μm)	**Spectral Radiance** (W/m² sr⁻¹μm⁻¹)	**Required noise-equivalent temperature difference**
20	3.660 - 3.840	0.45(300K)	0.05
21	3.929 - 3.989	2.38(335K)	2.00
22	3.929 - 3.989	0.67(300K)	0.07
23	4.020 - 4.080	0.79(300K)	0.07
24	4.433 - 4.498	0.17(250K)	0.25
25	4.482 - 4.549	0.59(275K)	0.25
26	1.360 - 1.390	6.00	150(SNR)
27	6.535 - 6.895	1.16(240K)	0.25
28	7.175 - 7.475	2.18(250K)	0.25
29	8.400 - 8.700	9.58(300K)	0.05
30	9.580 - 9.880	3.69(250K)	0.25
31	10.780 - 11.280	9.55(300K)	0.05
32	11.770 - 12.270	8.94(300K)	0.05
33	13.185 - 13.485	4.52(260K)	0.25
34	13.485 - 13.785	3.76(250K)	0.25
35	13.785 - 14.085	3.11(240K)	0.25
36	14.085 - 14.385	2.08(220K)	0.35

Table A3: MODIS reflective solar bands (RSB) key specifications (typical scene radiance, and SNR) with TERRA and AQUA MODIS on-orbit measured SNR (adapted from Xiong *et al*., 2002a).

Band	**SNR**	**SNR**	**SNR**	**SNR**
	Specifications	***TERRA (B)***	***TERRA (A-II)***	***AQUA (B)***
1	128	177		201
2	201	483		536
3	243	317		325
4	228	314		323
5	74		133	154
7	110		95	156

Table A4: MOD 02 and MYD 02 data used in this research.

Date		**Day of year and time (UT) of image capture**	**File name (.hdf)**
10-Nov-08	2008-315	08:50	MOD021KM.A2008315.0850.005.2008315184056
		13:10	MYD021KM.A2008315.1310.005.2008316161211
14-Nov-08	2008-319		No Terra data selected due to cloud cover over validation site
		12:45	MYD021KM.A2008319.1245.005.2008320172158
15-Nov-08	2008-320	09:10	MOD021KM.A2008320.0910.005.2008320195807
		13:30	MYD021KM.A2008320.1330.005.2008321191815
16-Nov-08	2008-321	08:15	MOD021KM.A2008321.0815.005.2008321203349
		12:35	MYD021KM.A2008321.1235.005.2008325065751
17-Nov-08	2008-322	08:55	MOD021KM.A2008322.0855.005.2008325020549
		13:15	MYD021KM.A2008322.1315.005.2008325074230
18-Nov-08	2008-323	09:40	MOD021KM.A2008323.0940.005.2008325023554
		12:20	MYD021KM.A2008323.1220.005.2008325030004
19-Nov-08	2008-324	08:45	MOD021KM.A2008324.0845.005.2008324231943
		13:05	MYD021KM.A2008324.1305.005.2008325192215
20-Nov-08	2008-325	09:25	MOD021KM.A2008325.0925.005.2008325215559
		12:10	MYD021KM.A2008325.1210.005.2008326174322
21-Nov-08	2008-326	08:30	MOD021KM.A2008326.0830.005.2008326174202
		12:50	MYD021KM.A2008326.1250.005.2008327190054